Hydration of Slag Cement

Theory, Modeling and Application

Wei Chen

HYDRATION OF SLAG CEMENT

Theory, Modeling and Application

Promotion committee

prof.dr. F. Eising	University of Twente, chairman
prof.dr.ir. J. Huétink	University of Twente, promotor
dr.ir. H.J.H. Brouwers	University of Twente, assistant-promotor
prof.dr. Z. Shui	Wuhan University of Technology
prof.dr.ir. J.C. Walraven	Technical University of Delft
prof.dr.ir. K. Van Breugel	Technical University of Delft
prof.dr.ir. S. Van der Zwaag	Technical University of Delft
dr. R.J. Van Eijk	Telematica Instituut
prof.dr.ir. R. Akkerman	University of Twente
prof.ir. D.G. Mans	University of Twente

ISBN 90-365-2437-7

Ph.D. Thesis, University of Twente, The Netherlands.

Cover design: Karien Dommerholt

Printed by PrintPartners Ipskamp BV, Enschede, The Netherlands.

Typeset with the LaTeX Documentation System.

Author email: chanweycn@hotmail.com

HYDRATION OF SLAG CEMENT

THEORY, MODELING AND APPLICATION

DISSERTATION

to obtain
the doctor's degree at the University of Twente,
on the authority of the rector magnificus,
prof.dr. W.H.M. Zijm,
on account of the decision of the graduation committee,
to be publicly defended
on Thursday 25 January 2007 at 15:00

by

Wei Chen
born on 3 August 1976
in Wuhan, China

This dissertation has been approved by the promotor

prof.dr.ir. J. Huétink

and the assistant-promotor

dr.ir. H.J.H. Brouwers

献给我的家人

To my family

Preface

This thesis comprises the work I have done during the past four years in The Netherlands. Doing a PhD is challenging for me both scientifically and in respect to the daily life. Fortunately, together with the help of a lot of people, companies and institutions, this thesis has been finished and published. People who contribute to this research with scientific guidance, financial support, spiritual encouragement or in many other ways merit sharing the accomplishment presented in this work and deserve my sincere thanks.

First, I am most grateful to my supervisor dr.ir. H.J.H. Brouwers who provided me with the opportunity to work in this group and guided me through the whole process. His efficient guidance, continuous encouragement and great patience constituent the most essential foundation of this thesis. His way of creative thinking, critical evaluating, optimistic foreseeing and his open mind are always the references with which I developed my research habits.

Furthermore, I am greatly indebted to prof.dr. Z. Shui (Wuhan University of Technology, China) who enlightened me with the possibility of doing my PhD in The Netherlands in 2002. The discussions during my visits to Wuhan and his visits to the Netherlands also helped me a lot.

I also appreciate very much the financial supports from the dr.ir. Cornelis Lely Foundation and the members of our user group who sponsored my research project and support continually our research activities. I am glad to see that this sponsor group has grown enormously in the past years, and I wish to mention and thank especially the four very first ones: Delta Marine Consultants (ir. W.J. Bouwmeester-Van den Bos), Public Works and Water Management, Ministry of Transport (ir. J.J.W. Gulikers), Jaartsveld Groen en Milieu (ir. S.J. Dijkmans) and SenterNovem Soil+ (dr. A. Honders).

Furthermore, I would like to thank my promotor prof.dr.ir. J. Huétink for his critical reading of this thesis and his willingness to act as my promotor. My thanks also go to prof.dr.ir. R. Akkerman for his reading of this thesis.

I would like to thank dr. R.J. Van Eijk (Telematics Institute, the Netherlands) for the fruitful discussions on CEMHYD3D, pore solution composition, and his permissions to reproduce the figures and graphs from his PhD thesis. Special thank goes to prof.dr. H. Pöllmann (University of Halle, Germany) for measuring the oxide compositions of materials, the comments on the XRD data and the discussion about the hydrotalcite. Prof.dr. H. Justnes (SINTEF, Norway) helped me with his experience of measuring the chemical shrinkage of cement paste. dr.ir. T.C. Bor (University of Twente, The Netherlands) helped me on the XRD analysis of the paste samples. ir. J.J.W. Gulikers corrected the numerous editorial errors in the draft of this thesis. Ing. G.H. Snellink and mr. J. Dogger helped me by maintaining good conditions in the lab and making appropriate experimental setups. Their help is greatly acknowledged.

I also wish to thank the other colleagues working in the CM&E Department. I would like to thank the chair leaders drs. G.M.G.M. van Lieshout and prof. ir. D.G. Mans for their support on the background. I thank especially my two *paranimfen* Dipl.-Ing. M. Hunger and Dipl.-Ing. G. Hüsken. Since they joined the group, we shared a lot of wonderful time when working in the lab, discussing during our "ConcreteCorner" meeting, traveling for conferences and enjoying the original Thüringer sausages. Of course, their critical reading of this thesis contributes to the quality a lot. I would like to thank also our two lovely secretaries, Yolanda and Graziana, for their daily help.

My sincere thanks go to my Chinese friends in Enschede as well. I enjoyed very much the time in the evening or during the weekends when we were cooking together, playing games,

traveling around, or simply chatting. Many of them deserve my special thanks because beside the wonderful hours we stayed together, they helped me with my research as well. An incomplete list includes: dr. L. Ren, dr. X. Dong, dr. Y. Xu, dr. Y. Huang, mr. Y. He, dr. S. Ran, dr. J. Xu, mr. C. Song, dr. J. Zhu, mr. J. Wu and ms. J. Song.

I owe the most to my family, especially to my parents and my wife, Wenbin. Without their supports, this thesis would not be possible for me. Every small success of me is attributed to them and every compliment from them always adds to my strength for my goals. I would like to thank especially my uncles and aunts as well. This thesis is actually a fruit out of their continuous guidance and encouragement since I was a small boy. They also take good care of my parents when I am away from them for such a long time.

陈伟
Wei Chen

Enschede
The Netherlands

Contents

Chapter 1

Introduction

1.1 Use of cement and concrete in construction

Concrete, by its definition, is a composite material composed by a binding medium within which are embedded particles or fragments of a relatively inert filler. The filler may be widely available natural or artificial, fine or coarse aggregates. The binding medium, which can harden to form a kind of adhesive glue, is called cement. The possible first use of concrete dates back to several thousand years ago when the Israeli people used the spontaneously combusted limestone and oil shale to form a natural deposit. Another typical example of the use of ancient concrete is the mix made by Romans at about 300 BC from slaked lime and a volcanic ash called pozzuolana. Admixtures were even used, like animal fat, milk and blood. The modern concrete age is generally considered to start from the patent of Joseph Aspdin in 1824, who invented the precursor of the most common binder used in modern concrete—the Portland cement.

Concrete is now the most commonly used construction material in the world. At least three advantages contribute to its wide application: (1) high durability, (2) relatively low cost (most of the materials can be obtained locally) and (3) can be formed into odd shapes. The broadening application field of concrete yields a growing demand of cement production, the principle binder in concrete. The world cement production amounts to about 2,220 million tons (MT) in the year 2005, about half being produced in China, and in the past 15 years, it has been doubled (Figure 1.1). Due to the economic booming in some developing countries, like China and India, it is expected that this trend of growth will continue in the coming decades.

The cement consumption in The Netherlands is relatively stable in the recent 15 years, with

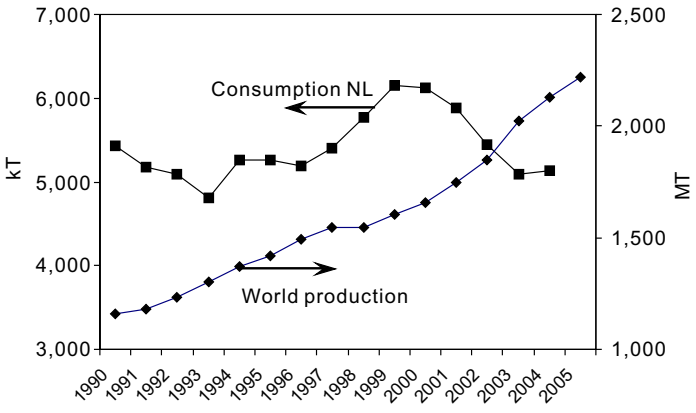

Figure 1.1: World cement production and cement consumption in The Netherlands. (a) world cement production, data source: U.S. Geological Survey (1996–2006); (b) cement consumption in the Netherlands, data source: Kramer (2006).

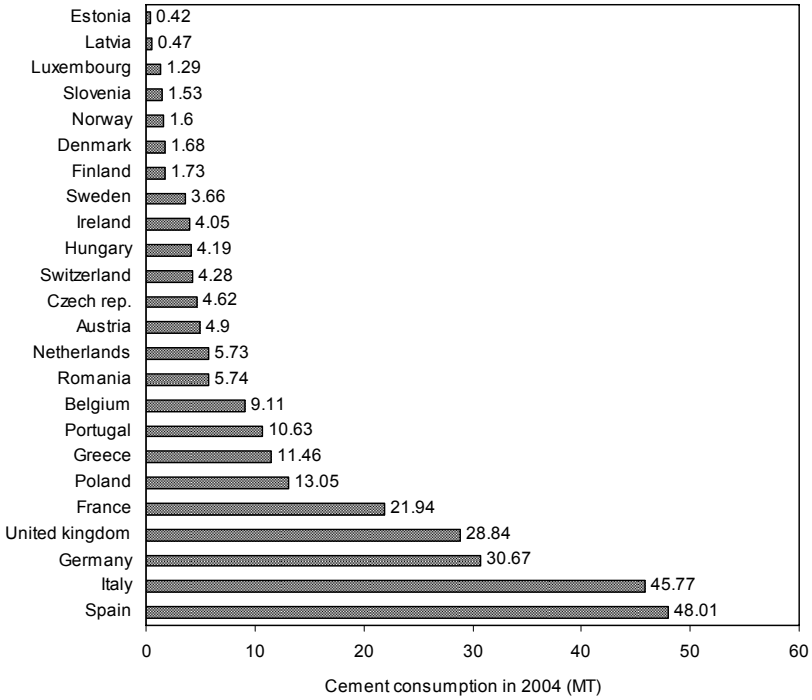

Figure 1.2: Cement consumption in some European countries in 2004, data source: Lacroux (2006).

the peak value of about 6,000 kT in 1999 and 2000 (Figure 1.1). Spain and Italy are the two biggest cement consumers in Europe, followed by Germany, U.K. and France (Figure 1.2).

However, there are still some disadvantages of concrete, which deserve special attentions: (1) it is characterized by its low tensile strength, easily cracking when it is subject to tension; (2) the on-site casting and forming process is time-consuming. The waiting period before the formwork can be removed impedes the rapid construction; (3) concrete has a high weight/strength ratio, limiting its application in large span structures; (4) concrete shows time-dependent volume changes, normally in the form of shrinkage and creep. Besides these inherent limitations of the material itself, the concrete production is also marked by its impacts on the environment and huge energy demand. For example, the production of one ton of Portland cement produces approximately 1.25 ton of CO_2, 0.5 ton contributed by the calcining of limestone and 0.75 ton by the energy demand.

One of the solutions for minimizing the environmental impacts of cement production is to use some supplementary cementitious materials (SCM) in concrete. These materials are normally by-products from other industries or natural materials, which may or may not be further processed for direct use in concrete. They are sometimes referred to as mineral admixtures. Some of these materials do not posses any binding capacities at all, and can only be used together with some other materials. This family of materials is sometimes called pozzolanic material. Other SCM might show cementitious properties themselves, like slag, in an appropriate environment.

1.2 Use of blastfurnace slag in cement

Blastfurnace slag is produced when iron ore is reduced by coke at about 1,350–1,550 °C in a blastfurnace. The molten iron, main product of a blastfurnace, is formed from the ore, while the other components form a liquid slag. When flowing to the bottom of the furnace, the liquid slag forms a layer above the molten iron due to the smaller density of slag. After being separated from the molten iron, the liquid slag is cooled down in the air or with water and is prepared for further use. Typically, about 220 to 370 kilograms of blastfurnace slag are produced per metric ton of pig iron. Lower grade ore results in more slag—sometimes as much as 1.0 to 1.2 tons of slag per ton of pig iron (Kalyoncu, 1998).

The liquid slag crystallizes if cooled slowly, and forms a glass if cooled rapidly. There are three main types of blastfurnace slag, categorized by the way of cooling it:

1. The granulated slag is produced by quenching the liquid slag with large amount of water to produce sand-like granulates. The granulates normally contain more than 95 percent of glass. Normally, they are ground to fine powder, called ground granulated blastfurnace slag (GGBFS).
2. The pelletized slag is produced by partially cooling the slag with water, and then flinging it into air. The pellets contain much less glass content if compared to the granulates, as low as 50 percent. Part of the pelletized slag is used as concrete aggregate and much is used in cement production as raw material as well.
3. The air-cooled slag is formed by allowing the slag to solidify slowly in air, and sometimes followed by accelerated cooling with a water spray. The air-cooled slag is hard and dense, being normally used for road bases, railway ballast, asphalt paving and concrete aggregate.

In this work, unless otherwise stated, the term “slag” is used to depict the granulated or pelletized blastfurnace slag.

Among the three types of blastfurnace slag, GGBFS is the most valuable one due to the cementitious properties it shows if mixed with lime, alkalis or Portland cement. For the same reason, it is often mixed with Portland cement to produce slag (blended) cement and marketed. According to the standard in the United States (ASTM C595-05) and in China (GB1344-1999), the slag content in the cement can be up to 70 percent (in mass), while in the European standard EN 197-1, the blended cement can contain as much as 95 percent of slag (in mass).

The slag cement is usually produced by feeding the Portland cement clinker together with the required proportion of dry granulated slag and added calcium sulfates into grinding mill. Separate grinding of Portland cement clinker and slag followed by blending is also used to produce slag cement.

The use of slag cement in construction practice has attracted much attention because slag as a by-product is often cheaper than Portland cement. Furthermore, concrete made from slag cement has also certain engineering advantages, such as low heat release, low permeability and good durability in aggressive environments (Glasser, 1991). Furthermore, since the slag is an industrial by-product, use of slag has many environmental advantages, such as low energy cost, use of secondary raw material and low pollutant gas emission. These advantages make it preferable to the conventional binders in practice.

Until the 1950’s, granulated slag was mainly used in the manufacture of Portland cements as raw feedstock to make cement clinker. In the 1950’s, slag cement became available in some countries as a separate product. The first granulation facility in America to make a separate slag cement product was established in the early 1980’s. Cement containing slag has been used in Europe for over 100 years.

In The Netherlands, more than 50 m/m% of the cement delivered on the market is CEM III, a cement made essentially from slag and a small proportion of clinker (Figure 1.3).

In this research, the term “slag cement” is always used to denote the cementitious materials

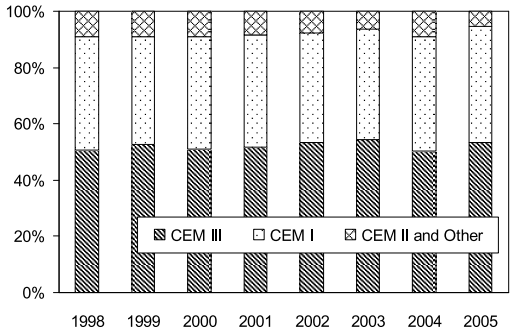

Figure 1.3: Cement consumption in The Netherlands (m/m% of types, data source: Kramer (2006)).

used in concrete and containing slag. Therefore, it can be either alkali-activated slag, or blended cement. Furthermore, the term "cement" is used for all the binders in concrete, including clinker, calcium sulfates, slag, fly ash, silica fume, etc. The term "Portland cement" refers to the mixture of ground clinker and calcium sulfates (anhydrite, hemihydrate and dihydrate).

1.3 Properties of GGBFS

1.3.1 Typical oxide composition

The major oxides in the GGBFS are lime (CaO), silica (SiO_2), alumina (Al_2O_3), magnesia (MgO) and some others (SO_3, FeO or Fe_2O_3, TiO_2, K_2O, Na_2O, etc.) in minor amounts. While the oxide composition of GGBFS can vary from one blastfurnace to another, the product from one blastfurnace remains relatively consistent. Compared to the typical oxide composition of clinker, GGBFS generally contains less lime, more silica, alumina and magnesia than clinker. Normal blastfurnace slag contains alkalines (Na^+, K^+) in a mild level, and if quenched with sea water, the alkali level could be relatively high. Chemical compositions of some blastfurnace slags produced in France and Luxembourg in 1980 are shown in Table 1.1.

1.3.2 Glass and crystalline minerals in slag

Slags suitable for cement production are almost completely glassy, while Portland cement clinkers are generally crystalline. The high glass content of slag and the metastable nature of the glass is an important source of activation energy during its hydration. However, a certain amount of crystalline mineral is still consequently encountered when analyzing the phase composition

Table 1.1: Chemical compositions of 27 blastfurnace slags produced in France and Luxembourg in 1980 (Taylor, 1997).

	Mean	Minimum	Maximum		Mean	Minimum	Maximum
Na_2O	0.39	0.25	0.50	TiO_2	0.55	0.49	0.65
MgO	5.99	3.63	8.66	MnO	0.64	0.34	1.31
Al_2O_3	13.29	10.26	16.01	FeO	1.24	0.29	9.32
SiO_2	33.48	31.96	37.29	S^{2-}	0.94	0.68	1.25
P_2O_5	0.13	0.00	0.34	F^-	0.16	0.06	0.31
SO_3	0.04	0.00	0.19	Cl^-	0.02	0.003	0.05
K_2O	0.70	0.44	0.98	Ign. Loss	0.42	0.00	1.04
CaO	42.24	37.92	44.38	Total	99.68		

of slags. Those crystalline minerals mainly include melilite, merwinite, bredigite and spinelle, all of which are much less reactive than the parent glass that they replace during crystallization (Glasser, 1991). Typical crystalline minerals found in slag are listed in Table 1.2. The amount of glass content in slag can be controlled in the production process.

The glass content in slag can be determined with optical microscopy and by the difference from quantitative X-Ray diffraction analysis (QXDA) determinations of crystalline minerals (Taylor, 1997). The QXDA procedure is considered to be more accurate than the light microscopy, except for a high glass content in which the crystalline peak intensities are too weak to measure (Hooton and Emery, 1983). Both methods sometimes fail if the crystalline region is below a certain size. Image analysis with a scanning electron microscope (SEM) can also be used.

The presence of small amounts of crystalline minerals does not influence the performance of slag significantly. In some cases, it is even beneficial for some properties of slag cement concrete like strength and durability. However, the presence of large amounts of crystalline minerals reduces the reactivity of slag greatly, which leads to poor performance of the slag.

1.3.3 Latent-hydraulic property

The slag is known for its latent-hydraulic property, i.e. it is reactive with water, but only at such a slow rate that it is normally mixed with other substances called activators, which can remarkably accelerate the reaction of slag. The most commonly used activators for GGBFS are sulfates, Portland cement, sodium silicate, calcium hydroxide, and in rare cases caustic soda (NaOH). A big portion of these activators contain alkali metal (e.g. Li, Na, K), thus they are called alkali activators. The composed materials made from GGBFS and alkali activators are denoted as alkali-activated slag (AAS). Typical AAS consists of GGBFS with 3.5–5.5 percent (in mass) of Na_2O_{eq} added, usually as caustic soda or water-glass. Increasing the dosage of activators accelerates the strength development and increases the 28d strength of the paste made from AAS (Narang and Chopra, 1983).

Some of the activators can be taken simply as catalyst of the slag reaction, because they are highly soluble and can hardly react with the oxides in slag to form solid products. A typical example is NaOH solution. Other activators might take part in the slag reaction in addition to its activation effect. For example, if sulfates are used, it can react with the aluminum and calcium in slag to form a solid hydration product—ettringite.

If the slag is activated with Portland cement or clinker, the mixture is called slag-blended cement. It is also simply called "blended cement" in this research since the slag-blended cement is the main research object. The two major constituents in blended cement, i.e. slag and clinker, are normally ground to comparable fineness, together or separately. However, they show remarkably different reaction rates. After being mixed with water, Portland cement in the blended cement

Table 1.2: Possible crystalline minerals in blastfurnace slags (Smolczyk, 1980)[§].

Main components		Minor components		Seldom observed	
Melilite	solid solution of	Dicalcium silicate	C_2S	Anorthite	CAS_2
Gehlenite	C_2AS	(α, α', β, γ)		Forsterite	M_2S
Akermanite	C_2MS_2	Monticellite	CMS	Enstatite	MS
Merwinite	C_3MS_2	Rankinite	C_3S_2	Perowskite	CT
Diopside	CMS_2	Pseudo-Wollastonite	CS	Spinelle	MA
Other Pyroxenes		Oldhamite	CaS		

[§]: Notation in cement chemistry is used, i.e. C = CaO, S = SiO_2, A = Al_2O_3, F = Fe_2O_3, $\overline{S}$ = SO_3 etc., see Appendix B.

starts to hydrate immediately. Meanwhile, a small amount of GGBFS reacts, probably due to the presence of calcium sulfates in cement. Then, the hydration of slag is greatly activated by alkalis and later by the calcium hydroxide (CH) released by the hydration of Portland cement. Generally, the slag hydration rate is far lower than that of clinker. For example, about 90–100 percent of the clinker hydrated in the blended cement pastes with a water/cement ratio of 0.5 after being cured at different temperatures for one year in the experiments of (Escalante-García and Sharp, 1998). At the same age, only about 50–70 percent of the slag has hydrated, as observed in the experiments (Battagin, 1992; Hinrichs and Odler, 1989; Luke and Glasser, 1988; Lumley et al., 1996).

1.4 Properties of slag cement concrete

Concrete made with slag cement normally has similar properties to that with Portland cement. However, obvious differences are still observed, most of them being beneficial to application and others on the contrary. A brief review about the properties of slag cement concrete is made here, with the major focuses on the comparison with concrete made from Portland cement.

1.4.1 Fresh properties

Normally, the paste volume in slag cement concrete is higher than in Portland cement concrete for the same cement content (in mass) due to the relatively lower density of slag (about 2.9 g/cm^3) than that of clinker (about 3.15 g/cm^3). The increased paste volume can normally improve the workability of concrete with low paste content or lack of fine particles in aggregate.

The setting time of blended cement is generally longer than that of Portland cement. As the proportions of slag increase in the blended cement or concrete the setting or stiffening time extends. An increase in slag content from 35 percent to 65 percent increases initial set by approximately 60 minutes. The delayed setting of blended cements allows concrete to be worked for longer periods. This is of benefit in avoiding the formation of cold joints in large pours and in hot weather concreting.

The bleeding capacity and bleeding rate of concrete is affected by the ratio of the surface area of solids to the unit volume of water. When slag is used as a cement replacement, these effects depend on the fineness of the slag compared to the Portland cement and the combined effect of the total cementitious material. If the slag is finer than the Portland cement, and substituted on an equal basis, bleeding is reduced. Conversely, if the slag is coarser, the rate of bleed increases. Blended cements containing slag and manufactured by the intergrinding process generally cause a reduction in bleeding tendency.

1.4.2 Strength development

The use of slag in cement is known to cause decreased early age strength compared to that of Portland cement concrete. However, the ultimate strength can increase with the addition of slag (Figure 1.4).

The strength development of slag cement concrete is more sensitive to the curing temperature than Portland cement concrete. Low temperature can remarkably retard the strength gain and cause problems when the early age strength is important (Dubovoy et al., 1986).

High fineness of slag cement increases the compressive strength, but the enhancement is much less prominent at early ages than that for Portland cement (Frigione, 1986). The compressive strength increases with increasing glass content in the slag as well, especially with regard to the later ages. However, slag with completely vitreous glass does not always lead to the highest strength. A low percentage of crystallization (3–5 percent in mass) was found to be beneficial to the compressive strength development (Figure 1.5(a)) (Frigione, 1986).

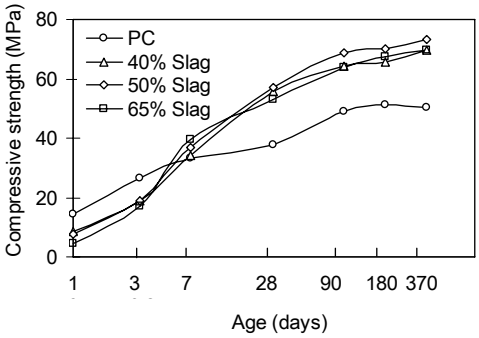

Figure 1.4: Compressive strength development of mortar cube samples containing various amounts of slags (Dubovoy et al., 1986).

1.4.3 Durability

The durability of concrete in a certain condition is one of its most important properties when exploring the application of a certain type of concrete. In this section, some durability aspects of concrete containing slag are discussed, including the alkali-silica reactivity, sulfate resistance, salt scaling, carbonation and ion diffusion.

Alkali-silica reactivity The partial replacement of Portland cement by GGBFS reduces the reaction between some siliceous components of concrete aggregates and the alkalis. Several factors contribute. First, normal GGBFS contains less alkali compared to Portland cement. Thus, a dilution effect takes place, reducing the total amount of alkali in concrete. Second, the slag in cement reacts at a remarkably lower rate, further reducing the total amount of alkalis released by the cement hydration. Third, the reaction products of slag with Portland cement clinker have higher potentials for binding alkalis (see Chapter 5). Thus, a large part of the alkali is immobilized in the solid products and the pH value of the pore solution is lower. High glass content in the slag reduces the expansion caused by alkali-silica reaction (ASR) (Frigione, 1986). Again, a low percentage of crystallization (about 7 percent in mass) increases the suppression effect compared to the slag of pure vitreous glass (Figure 1.5(b)).

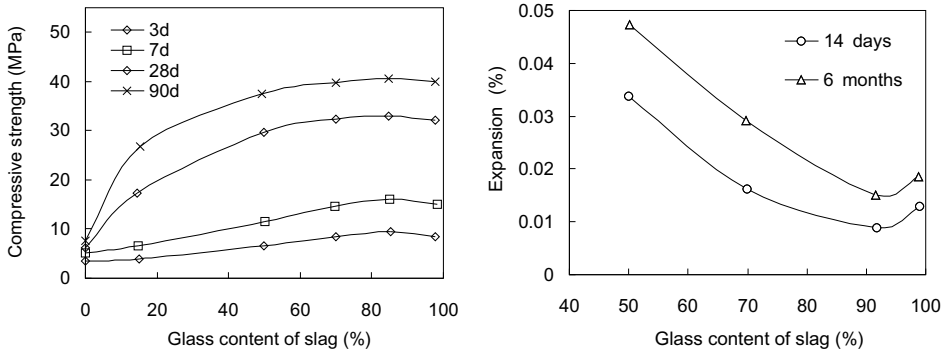

(a) Compressive strength (b) ASR expansion

Figure 1.5: Effect of glass content in slag on (a) the compressive strength development of mortars and (b) ASR expansion of concrete, after Frigione (1986).

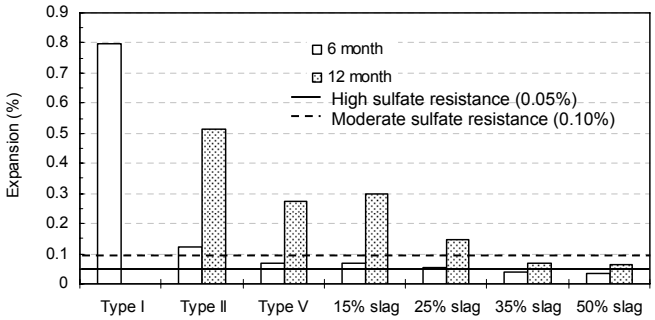

Figure 1.6: Expansion percentage of concrete made from different cements and with different slag replacement levels (data source: Slag Cement Association (2002)).

Sulfate resistance: The addition of slag into concrete reduces the risk of sulfate attack. 15 and 25 percent slag cement replacement can already achieve moderate sulfate resistance, and 35 and 50 percent can achieve high sulfate resistance, based on ASTM C989-05 six month expansion limits (Figure 1.6). Possible explanations for this effect include:

1. Slag does not contain C_3A, so its addition in concrete dilutes the total amount of C_3A in the system;
2. Slag cement concrete has low permeability, making it harder for sulfates to penetrate into concrete;
3. Slag reacts with $Ca(OH)_2$ to form calcium silicate hydrate (C-S-H) gel (see Chapter 4), thus decreasing the total amount of $Ca(OH)_2$ in the system, which is necessary in the case of sodium sulfate attack.

Salt scaling Concrete containing high contents of GGBFS are susceptible to salt scaling (the loss of surface layers of cement mortar during repeated freeze-thaw cycles and when de-icing salts are used). Due to this problem, the amount of slag in a Portland cement concrete is limited in some specifications.

Carbonation The carbonation resistance of concrete made from slag cement is affected by the environment and the slag content. Investigations of some field structures showed that concretes with 50 percent slag as replacement achieved resistance to carbonation similar to that of normal Portland cement concretes of equivalent mixture proportions. However, carbonation is greater in the high slag content (70 m/m%) cements, especially if the concrete is exposed to a dry environment (Osborne, 1999).

Ion diffusion Normal concrete made from slag cement shows denser microstructure as compared to Portland cement concrete if the same water/cement ratios are used. The ion diffusion rates in slag cement concrete are thus much lower than those in Portland cement concrete (Table 1.3). The low diffusion rates partially explains the good performance of slag cement concrete against ASR expansion and chloride ingression.

Another important feature of slag cement concrete is the low heat release of slag cement hydration. Since the heat release of slag reaction is slow and low compared to that of Portland cement, the risk of cracking due to the thermal gradient generated in massive concrete is minimized, which in turn improves the durability of concrete.

Table 1.3: Diffusion coefficients of Na^+, K^+ and Cl^- ions in hardened mortars made with Portland cement and slag cement (Daube and Bakker, 1986).

Diffused ion	Time (days)	w/c	Diffusion coefficient ($\times 10^{-8}$ cm^2/s)		Slag content of cement (m/m%)
			Portland cement	Blended cement	
Na^+	3	0.5	7.02	1.44	75
	14	0.5	2.38	0.1	75
	28	0.55	1.47	0.05	60
	28	0.6	3.18	0.05	60
	28	0.65	4.73	0.06	60
K^+	3	0.5	11.38	2.1	75
	14	0.5	3.58	0.21	75
	28	0.55	3.57	0.12	60
	28	0.6	6.21	0.23	60
	28	0.65	8.53	0.41	60
Cl^-	5	0.5	5.08	0.42	75
	103	0.5	2.96	0.04	75
	60	0.5	4.47	0.41	65

1.5 Hydration of slag cement

Although the slag cement concrete is already widely used in construction practice, there is still a strong request for researches on improving the use of slag in cement. Most knowledge in both the engineering practice and the scientific society about slag reaction is empirically obtained, based on which various national standards are formulated for guiding practice purpose. However, this body of knowledge is far from sufficient if compared to that of Portland cement and there is a big demand of the chemical knowledge underlying the slag reaction in cement. At least three aspects should be considered concerning the use of slag in concrete, based on which are practical suggestions for the production process and the field applications:

1. The reactivity of slag can vary from one slag to the other to a great extent. Not all the slags produced in various blastfurnaces are suitable for use in concrete. The applicability of given slags as construction materials is thus important in an economic respect, mainly depending on the reactivity of the slags. While the reactivity of slag can be adjusted in the iron production process, practical suggestions about the oxide composition and the processing methods are valuable;
2. The long-term properties of concrete made from slag cement is even more complex and important than that made from Portland cement because of the latent hydraulic nature of slag itself. It might take years for slag to achieve hydration degrees comparable to those of clinker phases;
3. The microstructure of cement paste—the gluey part in concrete—is altered when slag is used to replace the Portland cement. The changed microstructure has different properties, and thus changes the performance of concrete as well.

For a better understanding of the performance of slag in concrete and the possible improvement of its use, fundamental knowledge about its reaction and interaction with other constituents is important. It is known that the aggregates in concrete are generally inert in nature, rendering the paste and the interfacial transition zone (ITZ, the contact region between paste and aggregate) susceptible to improvement. This research is therefore focused on the development of paste structure containing slag. The microstructure development of the hydrating paste is chosen

as the topic because it is known to govern lots of properties of concrete, especially with respect to the durability considerations.

1.5.1 Chemistry of slag reaction

The chemistry of slag reaction involves the knowledge about the chemical reactions going on during the reaction process of slag, and some accompanied properties like heat release and volumetric changes. A few factors are important in microstructural considerations: the reaction rate, types of reaction products, their compositions, quantities and distribution. While the researches on these characteristics of hydrating Portland cement paste is quite abundant, researches on the slag cement reaction are much less. It is difficult to find some reliable theories which can derive the composition and quantities of reaction products from slag.

Furthermore, systematic considerations for the various factors influencing the slag reactivity in cement are not well developed, yet. While lots of efforts have been made to investigate the effect of oxide composition (Smolczyk, 1980), and fineness of slag on the hydration process, little care is taken to consider the pore solution composition in the hydrating pastes. In glass chemistry, it is a general knowledge that the corrosion rate of silicate glass depends highly on the alkalinity of the environment (Douglas and El-Shamy, 1967; El-Shamy et al., 1972; Mysen, 1988). Therefore, robust methods for predicting the alkali concentration in the pore solution of hydrating slag cement paste are valuable when evaluating the reactivity of slag in cement.

1.5.2 Microstructure

The microstructure of hydrating cement paste is altered when slag takes part in the reaction. These changes are responsible for the differences between the properties of Portland cement concrete and those of the slag cement concrete, which are discussed in the previous sections. Therefore, it is important to establish methods which can successfully represent the microstructure development of hydrating slag cement paste, and predict the accompanying properties.

1.5.3 Computer modeling

Although there are extensive experimental works on the hydration of slag cement considering different factors, efforts are normally made to clarify one or a few of them. To predict the properties using empirical knowledge can be even more difficult because the conditions under consideration normally cannot fit completely into the conditions used in experiments. In many national standards, the criteria for the applicability of one slag are often performance-related. In other words, a series of time-consuming and costly tests need to be conducted before one type of slag cement is applied in engineering.

The computer modeling of cement hydration yields the possibilities to bridge the gap between the objective overall performance of the material and the observed individual facts on it. A model, stated or defined as "a theoretical and mathematical representation that predicts experiments observations" (Jennings et al., 1996), is expected to predict results within, or beyond, the existing observations. Modeling work on the one hand can deepen the understanding of the material, and on the other hand, can extrapolate properties outside the available data. The ultimate goal of microstructural modeling is to predict the performance of cement-based materials throughout its service life.

While lots of efforts have been made on computer modeling of Portland cement hydration (Bentz, 2005; Van Breugel, 2004; Van Eijk, 2001), computer modeling of slag cement reaction is relatively scarce. At least three factors hinder the development: (a) the lack of knowledge about the chemistry of slag reaction; (b) the complexity involved with respect to the interaction between the two constituents in slag cement (slag and Portland cement); (c) the reactivity of slag in cement.

Computer models can be established if knowledge about these three factors are available. The simulation results can be used for further applications. For example, the reactivity of slag

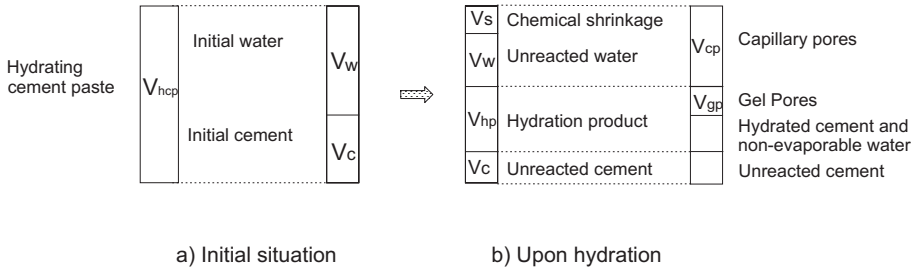

Figure 1.7: Schematic illustration of the chemical shrinkage of cement hydration.

can be derived from the slag hydration degree, which in turn can be used to evaluate the slag. The resultant microstructure, containing information about the anhydrous cement and products, can be used for predicting the long-term performance of concrete, such as strength, durability and volume changes.

1.6 Shrinkage of concrete

1.6.1 Shrinkage phenomena in practice

The hardening process of concrete is generally accompanied by its volume change, mostly in the form of shrinkage. In other words, a volume reduction is observed when the fresh mixture turns into a solid matrix. The extent of the reduction normally increases as the hardening process proceeds if no special measures are taken to mitigate it. There are several causes for the shrinkage of concrete in practice, most of them being associated with the state of water in it.

Water present in the initial mixture is partially combined in the solid formed due to the hydration reaction of cement. The remaining part may migrate in the micro- and meso-pores. Water exchange between concrete and the surrounding environment is also possible. Another probable source is the thermal consequence of the hydration reaction. The hydration of cement is a heat-releasing process. If not dispersed properly, heat can accumulate and induce volume changes of concrete due to the local temperature variations. Shrinkage caused by the temperature variations can be mitigated taking use of many measures developed in concrete technology.

The shrinkage caused by the water transformation in concrete can be classified into three categories:

1. **Chemical shrinkage** is the phenomenon in which the absolute volume of hydration products is less than the total volume of anhydrous cement and water before hydration (Tazawa, 1998) (Figure 1.7). It is an intrinsic property of the hydration reaction and can be monitored during the process. Actually, it is often used as a method to evaluate the degree of the cement hydration. The chemical shrinkage is often calculated as the volume reduction versus unit mass of the initial cement, or reacted cement.
2. **Autogenous shrinkage** is the macroscopic volume reduction of cementitious materials when cement hydrates after initial setting. It does not include the volume change due to loss or ingress of substances, temperature variation, the application of an external force and restraint (Tazawa, 1998). It is often induced by the self-desiccation that occurs during hydration under sealed or partially saturated conditions. As cement hydration proceeds, a dense microstructure of the matrix (paste, mortar or concrete) is obtained, which contributes to the main structural function of concrete, the strength. However, the dense structure also prevents the intrusion of external water into the structure for the reaction of cement. Hence, self-desiccation, a phenomenon describing the drop of internal relative

humidity and creation of empty pores within the cement paste, takes place. If these pores are not secondly filled with water, surface tension in the adsorption layer of water and the capillary forces due to the formation of meniscus are generated, which contracts the solid wall of pores and induces a volume reduction of the solid matrix. The chemical shrinkage increases the porosity of the paste and generates numerous menisci in the paste. Formation of menisci causes the drop of the internal relative humidity (RH), aggravating the autogenous shrinkage. The autogenous shrinkage can be expressed as the percentage of volume reduction "autogenous shrinkage ratio" or one dimensional length change "autogenous shrinkage strain".

3. **Drying shrinkage** is due to the loss of water from the concrete during environmental exposure. This phenomenon can lead to cracks in concrete elements if not properly accounted for during the design and construction procedure. Meanwhile, the drying shrinkage can be minimized by specifications of curing conditions for the construction (for example, sealing and wetting).

1.6.2 Problems induced by shrinkage

Shrinkage of concrete normally causes cracks in the micro or macro scale. It generates tensile stress in the paste (the principle gluey part of concrete) due to the internal or external restraint. If the tensile stress exceeds the maximum tensile stress capacity of concrete, cracking takes place. The cracks due to shrinkage can lead to reduced strength, decreased durability, problems with aesthetic appearance and even failure of elements. These cracks may serve as canals for substance transfer in the concrete, which is normally undesired. Deteriorative ingredients from the environment (such as chloride, sulfide and carbonates) might permeate into the concrete. Components in concrete can also be leached out via these canals, for example, portlandite. Thus, the deterioration of concrete is greatly accelerated if cracking takes place in it.

Among the three categories of shrinkage sources as defined in the preceding section, the chemical shrinkage and autogenous shrinkage deserve special attention because cracks as results of these two types of shrinkage develop uniformly throughout the concrete element and can lead to a complete dysfunction of the structure. Cracks due to drying shrinkage mainly occur on the surface of the element and afterward measures can be taken to fix it. It can also be simply prevented by appropriate curing of the structure. For a concrete prism fully restrained at both ends, cracks may develop at a shrinkage strain of around 200–250 με (= μm/m), not accounting for the creep effect of concrete. Under some conditions 200–250 με could occur at the age of 10 days at normal room temperature (25°C) and 50% relative humidity (Tazawa, 1998).

The problem of autogenous shrinkage should especially be considered for three groups of applications of concrete: high strength concrete, self-compacting concrete and massive concrete. In high strength concrete, very low water/binder ratios, ranging from 0.25 to 0.40, are used. The continuous hydration of the binder consumes the water, aggravating the self-desiccation process, which in turn increases the autogenous shrinkage. Furthermore, mineral admixtures are commonly used in high performance concrete, like silica fume and blastfurnace slag, refining the microstructure and increasing the autogenous shrinkage. Self-compacting concrete shows greater autogenous shrinkage than ordinary concrete with increasing powder content. Autogenous shrinkage of this type of concrete with a unit powder content of 500 kg/m^3 might be 100–400 με (Tazawa, 1998). In massive concrete, large amount of GGBFS is commonly used to suppress the temperature rise. However, the use of very fine slag is known to increase the autogenous shrinkage (Chan et al., 1998) as well, due to the large amount of C-S-H formed in the products (Domone, 2006) and refined pore structure.

1.6.3 Possible methods for mitigating shrinkage

As durability of concrete structures is gaining more and more interests in construction practice, improving the durability of concrete deserves special attention and several strategies to mitigate the chemical and autogenous shrinkage have been developed in the past decades (Bentz and Jensen, 2004). Some of these strategies use physical instrumentation, such as specific curing conditions, counteractive temperature change and structural restrains in the design of elements. Since these measures affect the reaction externally, they cannot radically eliminate the shrinkage, which is an intrinsic property of the hardening process itself. More efforts are made to change the concrete mixture composition, such as the binder type, aggregate content, and mineral additives. In these ways, the shrinkage can be mitigated by reducing the chemical shrinkage, changing the pore structure of concrete, decreasing the surface tension of the pore solution, providing additional water for hydration, or forming shrinkage resisting skeleton in the structure.

1.6.4 Shrinkage-compensating cement

Among the various ways of mitigating the shrinkage of concrete, using binders exhibiting expansive volume change are among the most effective ones. The idea of using shrinkage-compensating cement in concrete is to balance the shrinkage and to prevent cracking by using some processes exhibiting expansive potentials. In practice, the expansion is restrained by reinforcement; thus, a slight compressive stress is generated. This compressive stress is beneficial for counteracting the contraction of concrete in the subsequent drying process.

It is observed in practice that the formation of some hydration products in hardening cementitious system can yield an expansive effect on the external volume change. Typical examples of such products include ettringite, portlandite and brucite. Normally the formation of large quantities of such products should be avoided since the excessive expansion induced by their formations can also yield cracking in concrete, inducing the same problems as shrinkage. However, the formation of products with expansive potentials can also be used in a positive way, to compensate the shrinkage. For example, the growth of portlandite crystals clearly reduces the autogenous shrinkage of cement paste (Baroghel-Bouny et al., 2006). Following this routine, several types of shrinkage-compensating cement have been developed which hydrate to yield expansion capacities.

The shrinkage-compensating cement can be produced in two different ways: (1) by changing the recipe of the ingredients for making cement and the kiln conditions to form some expanding compounds. The American Type K cement falls into this group. (2) by adding some expanding admixture into Portland cement, which will hydrate to give the expansion capacities. This method has been widely used in Japan and China to produce shrinkage-compensating cement.

The method of adding expanding admixture into Portland cement has several advantages as listed below:

1. Its amount in concrete can be flexibly adjusted to control different expansion degrees.
2. The production process for concrete with this admixture is the same as normal concrete.
3. Different sources can be used, either ettringite-based or hydroxide-based, or a combination of both. The selection can be based on both economic considerations and the local availability.
4. Production of this admixture can take use of industrial by-products, like industrial gypsum, steel slag, fly ash etc, making it environmentally and economically more preferred.

Hence, this method is followed in this thesis to produce a mineral shrinkage-compensating admixture for use in cement-based mortar and concrete. It is made from some industrial by-products, which is expected to lower the cost of this product. Concrete made with this mineral shrinkage-compensating admixture is expected to be more durable compared to that made with some organic admixtures because all the ingredients are inorganic minerals.

The computer-based cement hydration model is used to design and predict the hydration of various ingredients in the new admixture, and the microstructure development of cement pastes containing this admixture. The properties of the simulated microstructure can be used to investigate the possible mechanism of expansion and to improve the performance of the admixture.

1.7 Outline of thesis

The work presented in this thesis involves fundamental knowledge in cement chemistry, new developments in computer science and practical experiences in concrete technology. Experiments reported in literature and executed in this thesis are used as supports to the theoretical derivations and models. These theories are further developed into a 3-D computer-based model ready for use in a scientific or industrial environment. Experimental results, presented in literature, obtained in the lab, or virtually simulated with the computer model, are used for validating or calibrating the solutions to the problems addressed.

It is always kept in mind that this research should not only contribute to fundamental knowledge about cement chemistry, but also bring chances for answering practical questions encountered in engineering and for developing new applications of slag in cement. Therefore, efforts are made always together with the newest fundamental chemical knowledge, and attention is also paid to the practical administrative and economical prospects.

The research framework of this thesis is presented in Figure 1.8. It is composed of 9 chapters, which are described in details below.

Chapter 2 of this thesis introduces some background knowledge of cement hydration and its computer modeling. Chemical and microstructural characteristics of hydrating Portland and slag cement paste are presented. This body of general knowledge is expected to provide the basis for understanding the prospective developments in this thesis. A few computer models for simulating the hydration process of Portland cement are introduced, with special emphasis on the computer model CEMHYD3D.

Chapter 3 of this thesis deals with the reaction of slag in AAS. The reaction of pure slag is investigated with observations in experiments presented in literature about the type of hydration products, their compositions, and accompanying properties in the reaction process. A stoichiometric approach is used to develop theoretical models that are able to predict both the compositions and the quantities of hydration products.

Chapter 4 of this thesis investigates the reaction of slag in blended cement. Interactions between the reaction of pure slag and those of clinker phases are investigated based on concepts like product equilibrium and CH consumption. The stoichiometric approach is used again for developing models that account for the degree of CH consumption and types of C-S-H formed.

Chapter 5 of this thesis is focused on the pore solution chemistry of hydrating cement paste. Methods for predicting the alkali concentrations in the pore solution of hydrating Portland and slag cement pastes are established. The methods are further used to predict the concentrations of other ions in the solution. The alkali concentrations predicted with these methods are used in computer modeling of slag cement hydration for determining the reactivity of slag in an alkaline environment.

Chapter 6 of this thesis concerns the computer modeling of Portland cement hydration. The 3-D computer model CEMHYD3D (*Van Eijk version*, Van Eijk (2001)) is taken over and extended with the newest development in cement chemistry and subsequently modified with considerations to the reaction mechanisms.

Chapter 7 of this thesis is about the computer modeling of slag cement hydration. Methods for predicting the reactivity of slag with respect to its oxide composition and the alkalinity of pore solution are proposed. The *Van Eijk version* of CEMHYD3D is extended for simulating the slag cement hydration taking use of the new theoretical models proposed in Chapter 3 and 4. The new CEMHYD3D is validated with experimental results from literature.

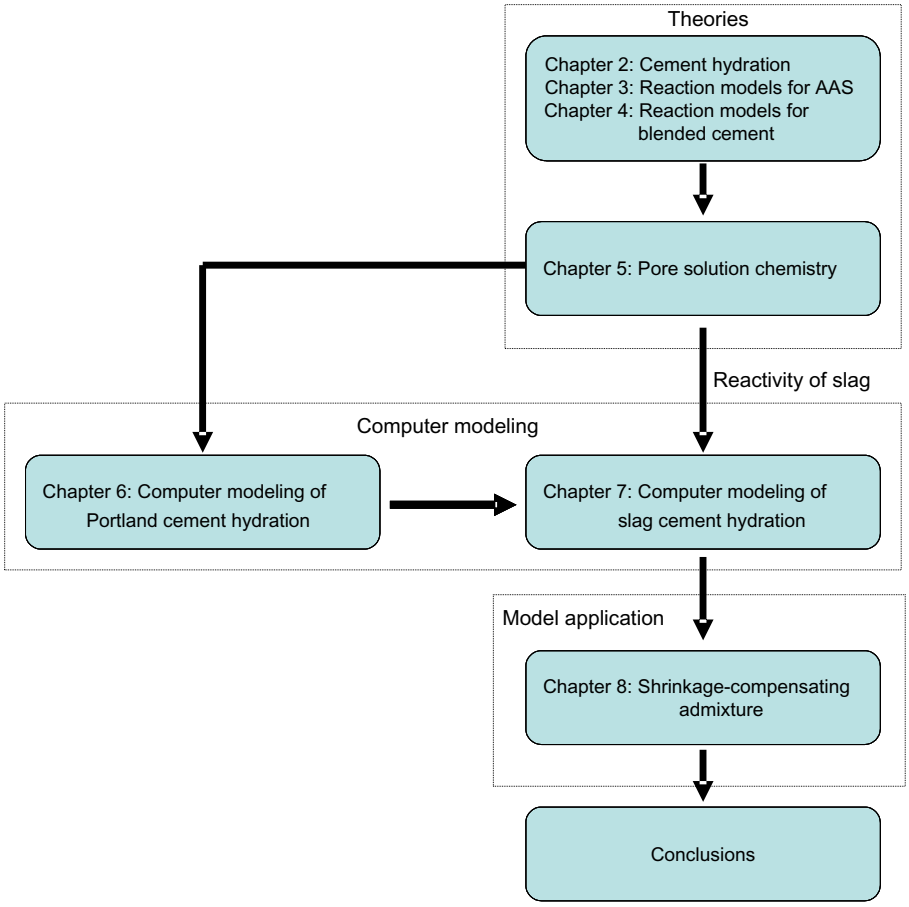

Figure 1.8: Framework of this thesis.

Chapter 8 of this thesis deals with the development of a shrinkage-compensating admixture for cement based on the gained insights on slag reaction chemistry and with the aid of the new computer model. The newly developed shrinkage-compensating admixture is tested in experiments. Virtual testing of the hydration process is executed with the new CEMHYD3D developed in Chapter 6 and 7.

Finally, conclusions of this research are drawn in Chapter 9 of this thesis. Furthermore, this chapter proposes some recommendations about the use of the theories, computer models and the new shrinkage-compensating admixture.

Chapter 2

Hydration and microstructure development of cement paste

2.1 Introduction

The reaction of cement in concrete is a complex process involving the interactions between the anhydrous solid compounds and water. The anhydrous compounds continuously disappear in the paste (the mixture of cement and water) accompanied by the consumption of water and formation of solid products. This process is called "*hydration*" (Taylor, 1985). The solid products are called "*hydration products*". The hydration of cement is a typical chemical process, i.e. a series of chemical reactions take place, causing phase transformation, substances redistribution, energy change, and physical consequences. The ultimate result of cement hydration is a solid, porous material possessing certain engineering properties like strength, shape stability and chemical encapsulation. This "stone-like" material often contains different phases like anhydrous reactants, hydration products, air voids, pore solution, and sometimes externally intruded substances. These phases are intermixed with each other, establishing a structure normally characterized in a very fine scale (in micrometer or nanometer). Hence, this structure is generally called "*microstructure*", and the time-dependent change of this microstructure as the result of the continuous hydration of cement is called "*microstructure development*".

The hydration of modern cement has been investigated continuously since the Portland cement was developed more than 150 years ago. A brief review about the historical development of Portland cement and the researches about it since the first patent for "Portland cement" can be found in the work by Blezard (1998). Comprehensive reviews about the recent developments in cement chemistry are presented in the works by Jennings et al. (1996), Taylor (1997), Van Breugel (1997), Hewlett (1998) and Mindess et al. (2003).

In this chapter, the chemistry of cement paste hydration at ambient temperature is introduced, with the specific focuses on the reaction of Portland cement and slag cement. The microstructure development of hydrating cement paste is discussed. Introductions about a few of the most widely used computer models for cement hydration are presented, one being used throughout this thesis and subject to enhancements and extensions in this thesis.

A few definitions are relevant when describing the hydration process of cement. A "*paste*" denotes the slurry containing cement powder and water, which is able to set and harden. It possesses some microstructure, which is changing due to the continuous cement hydration. The mass fraction of water to cement in the initial paste is called "*water/cement ratio*" (w/c). Typically, the w/c ranges from 0.3 to 0.6. Lower values are frequently encountered in high strength concrete nowadays. "*Curing*" denotes the physical treatment of the paste, i.e. the temperature at which the paste is kept and the moist exchange of the paste with the environment. "*Hardening*" means the stiffening process during which a remarkable physical strength of the paste is developed. The "*microstructure*" is the assembly of the different phases in the paste, for example, anhydrous cement, water, air voids and hydration products (Figure 1.7).

2.2 Hydration of Portland cement

Portland cement is the most common type of cement used in construction. It is made by heating a mixture of limestone, clay or other materials containing similar oxides to about 1450°C. The cooled product is called Portland cement clinker, which is then mixed with gypsum (together with some other forms of calcium sulfate as well) and ground into a very fine powder. Some other minor constituents are sometimes added, of which the amounts are different in various specifications.

2.2.1 Properties of Portland cement clinker

Geometrical properties

The properties of cement are influenced to a critical extent by its particle size distribution (PSD). The PSD becomes wider as the material becomes easier to grind, which is related to the packing density of the individual clinker mineral grains suspended in the clinker melt. It is commonly represented by the Rosin-Rammler distribution (Masuda et al., 2006). The Rosin-Rammler function is particularly suited to representing particles generated by grinding, milling and crushing operations. It is represented by two parameters (d_m and n_d) as:

$$R = 100 \exp\left[-\left(\frac{d}{d_m}\right)^{n_d}\right] \tag{2.1}$$

in which d is the particle size (μm), R is the retained fraction (m/m%) at size d, d_m is the mean particle size (μm, 36.79 m/m% of the material being of size greater than d_m), and n_d is a measure of the spread of particle sizes (bigger values corresponding to narrower distributions). The applicability of the Rosin-Rammler distribution function can be determined by curve fitting the actual sieve size data of particles of a sample. A least square regression analysis can be carried out to fit the data points and the correlation coefficient can be used to estimate the goodness of the fit. For open-circuit milling, the values of n_d obtained using an X-ray sedigraph are 0.99–1.07; for closed circuit milling, in which the fine material is separated and only the coarser material is further ground, n_d can be as high as 1.23–1.28 if the separation is efficient. Laser granulometry typically gives values of n_d lower by 0.15–0.20 (Taylor, 1997).

The experimental techniques employed for determining the PSD include sieving, sedimentation, using an Andreasen pipette or a sedimentation balance, the Coulter counter, the light extinction and scattering methods (Masuda et al., 2006), and image analysis. Using some automated methods for measuring PSD becomes popular in the past decades like the measurement of the low-angle scattering of light and laser granulometry.

Another important concept accounting for the geometric characteristics of cements is the fineness. It is one of the major factors influencing the rate of cement hydration. The fineness of cement is characterized by the surface area of the powder, measured by an air permeability method according to the standard EN 196–6, so called "Blaine fineness". The principle is to measure the resistance to air flow through a compact bed of cement powder. Normal Portland cements have surface areas in the range of 300–350 m^2/kg and the rapid-hardening Portland cement in the range of 400–550 m^2/kg. Another method commonly used is the Brunauer-Emmett-Teller (BET) gas adsorption method. It normally gives results two to three times higher than the air permeability method.

The specific surface area (SSA) can be calculated from a PSD curve as (Taylor, 1997):

$$S = 6 \times 10^3 \times F_s \times \sum f_d/(d \times \rho) \qquad (m^2/kg) \tag{2.2}$$

in which S is the calculated SSA (in m^2/kg), F_s is an empirical constant accounting for the different assumptions regarding the surface shape that are made implicitly or explicitly in the determination of PSD and the definition of SSA, f_d is the mass fraction of particles with the size

Table 2.1: Chemical composition and mass fractions of mineral phases in normal Portland cement clinker (Taylor, 1997).

Name	Formula	Mass fraction (m/m%)
Alite	C_3S	50–70
Belite	C_2S	15–30
Aluminate	C_3A	5–10
Ferrite	C_4AF	5–15

d (in μm), ρ is the density of the material (in g/cm^3).

Chemical composition

The most abundant oxides in Portland cement clinker are CaO, SiO_2, Al_2O_3, Fe_2O_3, with minor amounts of MgO, TiO_2, SO_3, Na_2O, K_2O and so on. Most of these oxides are contained in four major mineral phases, called alite, belite, aluminate and ferrite (Taylor, 1997). Chemical compositions of these four clinker phases and their normal mass fractions in Portland cement clinker are presented in Table 2.1.

It is noteworthy that none of these phases in commercial clinker is pure, i.e. they always contain some other ions besides the four major oxides C, S, A, and F. Furthermore, the A/F ratio in the ferrite is different from one clinker to another. Thus, the formula C_4AF is more likely an approximation to the real composition.

Besides these four clinker phases, some other minerals may also be present in clinker, including some alkali sulfates, free lime, periclase, etc.. Although these constituents exist in relatively small amounts, they may have some significant influences on the hydration process of clinker and the overall properties of concrete made from the Portland cement.

The elemental composition of clinker can be determined with X-Ray fluorescence (XRF), selective dissolution with ethylenediaminetetraacetic acid (EDTA) or atomic absorption spectrophotometry. The mineral composition is relatively more difficult to determine. Several methods are available, like light microscopy, electron-microscopy, X-Ray diffraction spectroscopy, X-Ray fluoresce (Taylor, 1997; Van Breugel, 1997). However, the results obtained with different methods may differ from each other to a markable extent.

A widely employed indirect method for determining the mineral composition of clinker is the Bogue's computation, with which the mass fractions of clinker phases are calculated as (Mindess et al., 2003):

$$x_{C_3S} = 4.07x_C - (7.60x_S + 6.72x_A + 1.43x_F + 2.85x_{\bar{S}}) \tag{2.3}$$

$$x_{C_2S} = 2.87x_S - 0.754x_{C_3S} \tag{2.4}$$

$$x_{C_3A} = 2.65x_A - 1.69x_F \tag{2.5}$$

$$x_{C_4AF} = 3.04x_F \tag{2.6}$$

in which x_C etc. are the mass fractions of component oxides C etc. in the cement and x_{C_3S} etc. are the mass fractions of corresponding phases. These equations are based on the understanding that chemical equilibrium is established at the clinkering temperature, and is maintained throughout the critical cooling period, and more importantly, the chemical compositions of the phase are the same as defined in their formulas. Errors may exist due to the formation of minor compounds and the formation of the solid solutions. Therefore, the Bogue composition is commonly referred to as the potential mineral composition.

2.2.2 Hydration

Immediately after the Portland cement is mixed with water, hydration starts. The newly mixed paste which shows a remarkable flowablility is called "fresh cement paste" and the subsequently result, a hardened paste possessing significant strength, is called "hardened cement paste".

The hydration of cement is a complex process, consisting of a series of individual chemical reactions that occur both simultaneously and successively. The process progresses spontaneously upon contact of the binder with water and is accompanied with heat release. The process is influenced by mainly factors below (Odler, 1998):

1. Phase composition of the cement and the presence of foreign ions within the crystalline lattices of the individual clinker phases;
2. Fineness of the cement, in particular its particle size distribution and specific surface;
3. Water to cement ratio;
4. Curing temperature;
5. Presence of chemical admixtures, i.e. chemical substances added in small amounts to modify the hydration rate and properties of the cement paste;
6. Presence of additives, i.e. materials interground with cement in large amounts, such as GGBFS or pulverized fly ash.

Chemical reaction

Due to the extreme complexity involved when considering the interactions, the hydration reactions of the clinker phases are often investigated separately and presented as the reaction of the individual phase. This way of presentation is taken over in this section, and all the phases are regarded pure, i.e. the effects of minor compounds and solid solution are not included.

The reaction of C_3S and C_2S can be written as:

$$C_3S + (3 + g - \hat{a})H_2O \rightarrow C_{\hat{a}}SH_g + (3 - \hat{a})CH \tag{2.7}$$

$$C_2S + (2 + g - \hat{a})H_2O \rightarrow C_{\hat{a}}SH_g + (2 - \hat{a})CH \tag{2.8}$$

in which $\hat{a}$ and g are the C/S and H/S ratios in C-S-H, respectively. The symbol for the water content in the hydration products g is consistently used in this thesis for the purpose of simplifying the expressions.

The hydration product C-S-H is an amorphous or nearly amorphous calcium silicate hydrate with the composition varying in a wide range. Published data on the C/S molar ratio of the C-S-H phase present in mature C_3S pastes hydrated at ambient temperature range between about 1.4 and 2.0. Values around 1.7–1.8 are generally accepted to be the probably most correct ones (Odler, 1998; Taylor, 1997).

C_3A can react with water rapidly, and thus the paste develops strength at very early ages. Therefore, calcium sulfates are added in commercial cements to regulate its reaction. The reaction of C_3A with the presence of gypsum and water to form ettringite (most likely the case in hydrating Portland cement paste) is written as:

$$C_3A + 3C\bar{S}H_2 + (g - 6)H \rightarrow C_6A\bar{S}_3H_g \tag{2.9}$$

When all the gypsum in the paste is consumed by the hydration of C_3A, the ettringite starts to decompose and react with C_3A to form monosulfate as:

$$2C_3A + C_6A\bar{S}_3H_{32} + (3g - 32)H \rightarrow 3C_4A\bar{S}H_g \tag{2.10}$$

If there is no calcium sulfate present for the formation of ettringite, the C_3A reacts with water to form a gel-like product at ordinary temperature. Later, this material transforms into hexagonal crystals corresponding to the phases C_2AH_8 and C_4AH_g. Thermodynamically, C_3AH_6 is the

only calcium aluminate hydrate stable at ambient temperature (Damidot and Glasser, 1995). Therefore, it is expected that the C_2AH_8 and C_4AH_g are converted ultimately into C_3AH_6. At temperatures above about 30°C or in pastes, conversion is rapid and sometime the AFm phases may not be observed; local temperature increase due to the strongly exothermic nature of the reaction probably has an important effect. Hence, the reaction of aluminate with water can be written accordingly as:

$$2C_3A + (8+g)H \rightarrow C_4AH_g + C_2AH_8 \tag{2.11}$$

$$C_4AH_g + C_2AH_8 \rightarrow 2C_3AH_6 + (g-4)H \tag{2.12}$$

Jupe et al. (1996) studied the reaction of C_3A at room temperature with water using rapid-energy dispersive diffraction. It is found that the C_3AH_6 does not begin to form until the intermediate phase, identified as C_2AH_8, reaches its maximum level; then as the intermediate decreases the rate of C_3A consumption increases slightly, feeding further the formation of C_3AH_6.

However, in the real cement paste, calcium hydroxide is formed from the hydration of calcium silicates, consequentially affecting the hydration of C_3A. With the presence of CH, C_4AH_g can form (Odler, 1998; Taylor, 1997). Recent work by Brouwers (2005) confirmed that the C_3A more likely reacts with CH and water at room temperature to form C_4AH_g. The reaction is written below as:

$$C_3A + CH + (g-1)H \rightarrow C_4AH_g \tag{2.13}$$

The hydration products of phases in the C_2(A,F) series are essentially similar to those formed from C_3A with A substituted by F under comparable conditions (Taylor, 1997). Therefore, its reaction is written as:

$$C_4AF + 3C\bar{S}H_2 + (g-2)H \rightarrow C_6A\bar{S}_3H_g + CH + FH_3 \tag{2.14}$$

$$2C_4AF + C_6A\bar{S}_3H_{32} + (3g-24)H \rightarrow 3C_4A\bar{S}H_g + 2CH + 2FH_3 \tag{2.15}$$

In the equations above, FH_3 is postulated to form. However, it is rarely detected in experiments and its formation is under doubt (Emanuelson and Hansen, 1997; Harchand et al., 1984). An Si-containing Fe-substituted hydrogarnet phase is believed to form with an approximate composition $C_6AFS_2H_8$ in the hydrated Portland cement paste. Its presence is proven by several studies (Brouwers, 2005; Copeland et al., 1960; Flint et al., 1941; Rodger and Groves, 1989; Taylor and Newbury, 1984). Hence, it is believed that the ferrite reacts with calcium silicates to form hydrogarnet in the form as (Brouwers, 2005) :

$$C_4AF + 2C_3S + (4+g)H \rightarrow C_6AFS_2H_g + 4CH \tag{2.16}$$

$$C_4AF + 2C_2S + (2+g)H \rightarrow C_6AFS_2H_g + 2CH \tag{2.17}$$

in which g is the water content in the hydrogarnet and depends on the hydration states (the drying condition that the paste is subject to, i.e. assembly of the temperature and RH).

Hydration kinetics

The hydration process of cement is exothermic, i.e. heat is released as the reaction progresses. This property is used in laboratories to monitor the hydration process by using a special calorimeter to record the rate of heat conduction needed to keep the temperature constant. The results are often presented as the calorimetric curve. A typical calorimetric curve for the hydration of Portland cement is presented in Figure 2.1. As can be seen, the hydration process are divided into five stages according to their different characteristics of heat release. The characteristics of these stages and their implications for concrete properties are included in Table 2.2.

The initial hydrolysis starts immediately after the cement is mixed with water. The part of alkalis in cement present as sulfates are dissolved into the solution. If the cement is rich in K, syngenite ($KC\bar{S}_2H$) can form in this stage, causing false set.

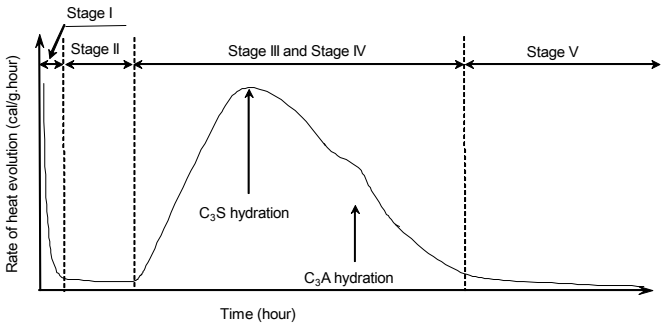

Figure 2.1: Rate of heat evolution during hydration of Portland cement, after Mindess and Young (1981).

The hydration process of Portland cement is marked by an obvious dormant period (Stage II in Figure 2.1). During the dormant period, which lasts typically for a few hours, the hydration progresses at a very low rate, and no significant strength is obtained. The amount of heat released by the cement hydration is also greatly reduced. This dormant period is important in concrete technology because during this period the concrete can be transported and shaped on the construction site.

An acceleration period follows the dormant period, during which the hydration progresses rapidly (Stage III). This period corresponds to the main exothermic peak in the curve in Figure 2.1. This period determines the final set of concrete, and the strength development at early ages.

After the acceleration period follows the deceleration and steady state period (Stage IV and V), during which the hydration rate is relatively slow. The strength of the concrete keeps increasing, and the heat release is much reduced compared to that of the acceleration period.

The causes of the dormant period and its transformation to the acceleration period are not quite clear. Several theories are proposed for this phenomenon, including the "impermeable hydrate layer theory", "electrical double layer theory", "nucleation of CH theory" and "nucleation of C-S-H theory". More details about these theories can be found in the work by Odler (1998).

Table 2.2: Stages of alite (C_3S) hydration, after Mindess and Young (1981).

Stage	Characteristics	Kinetics	Relative rate	Chemical process	Relevance to concrete properties
I	Initial hydrolysis	Chemical control	Rapid	Initial hydrolysis, dissolution of ions	
II	Dormant stage	Nucleation control	Slow	Continued dissolution of ions	Initial set
III	Acceleration	Chemical control	Rapid	Initial formation of hydration products	Final set and rate of initial hardening
IV	Deceleration	Chemical and diffusion control	Slow	Continued formation of hydration products	Rate of early strength gain
V	Steady state	Diffusion control	Slow	Slow formation of hydration products	Rate of later strength gain

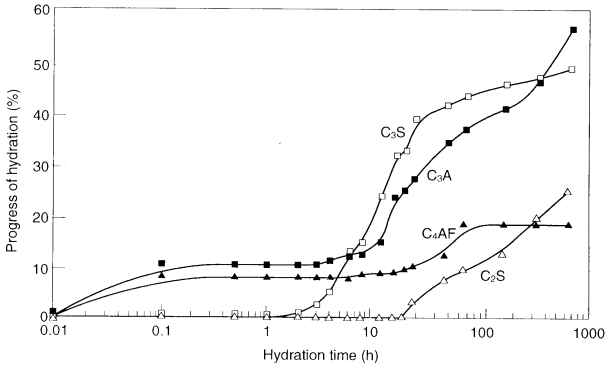

Figure 2.2: Hydration degree of clinker phases in Portland cement paste as a function of hydration time at ambient temperature, after Odler (1998).

Hydration degree

The hydration degree is the fraction of hydrated cement to that of the initial anhydrous cement in the paste. Typical curves representing the hydration degrees of clinker phases in a normal Portland cement pastes as a function of hydration time at ambient temperature are shown in Figure 2.2.

It can be seen that the hydration of C_3A and C_4AF starts immediately after the initial contact of cement with water. It is followed by a dormant period lasting for a few hours due to the presence of calcium sulfates. The initial reaction rate of C_3A is greatly affected by the amount and type of alkalis incorporated into the crystalline lattice. The C_3S and C_2S remain relatively inert at early ages. The hydration of C_3S starts at about 2 hours, and that of C_2S at about 30 hours. The hydration of C_3S and C_3A proceeds at comparable rates, which are obviously higher than those of C_2S and C_4AF.

It is noteworthy that in different cements those compounds hydrate at different rates due to the presence of impurities, conditions of cooling and grinding, and interaction with other compounds in cements. The reactivity of C_4AF may vary greatly depending on its A/F ratio.

2.2.3 Microstructure development

Hydration products

As a consequences of cement hydration, hydration products are formed continuously in the hydrating paste. Typical curves for the formation of hydration products in hydrating Portland cement pastes are shown in Figure 2.3.

The most abundant hydration product in Portland cement paste is C-S-H due to the large amount of alite and belite in the clinker. Its amount keeps increasing rapidly after the dormant period, firstly contributed mainly by the rapid hydration of alite and then by the belite hydration. The formation of CH corresponds well with the hydration of alite. Its amount increases sharply after the dormant period and the increment rate slows down when most of the alite has hydrated. The hydration of belite produces CH as well, but to a much less extent as compared to that of alite (see Eqs. (2.7) and (2.8)).

The rate of ettringite formation in hydrating Portland cement paste depends on the amounts and reactivities of both C_3A and C_4AF and the amount of calcium sulfates in the paste (Odler and Abdul-Maula, 1987). It proceeds more slowly in the presence of anhydrite than hemihydrate

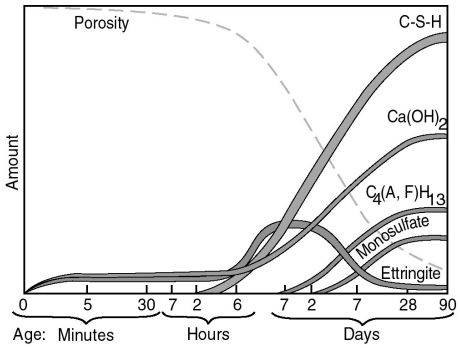

Figure 2.3: Formation of hydration products in Portland cement paste as a function of hydration time at ambient temperature, after Locher et al. (1976).

and dihydrate. If all the calcium sulfates are consumed and there is excessive C_3A or C_4AF in the paste, the ettringite is further converted into the monosulfate.

Microstructure

A schematic illustration of the microstructure development of hydrating Portland cement paste is shown in Figure 2.4. This illustration is mainly based on the observations with SEM or environmental scanning electron microscope (ESEM) images. The solid particles start to hydrate as suspensions in the solution. The hydration products are formed accompanied by the shrinkage of the anhydrous particles. They overlap with each other and build the solid skeleton, giving strength to the concrete.

Besides the solid compounds in the microstructure, another important phase is the pore space. Its volume is reduced continuously due to the increasing volume of solids. The pores are normally filled with water if the paste is cured in the saturated state. The pores in the paste can be classified into two categories according to their sizes: gel pores and capillary pores. It is important to note that the pores are normally highly irregular, therefore, the definition of pore size is rough.

A classification of pores is given by Mindess et al. (2003) as shown in Table 2.3. It is normally taken that the capillary pores are those remaining water-filled in saturated paste between the cement particles, and the gel pores are those existing in the hydration product C-S-H. The gel

Table 2.3: Classification of pores in hardened Portland cement paste, after Mindess et al. (2003).

Category	Size	Description	Effect on the concrete properties
Capillary pores	50 nm–10 μm	Macropores	Permeability, diffusivity
	10–50 nm	Large mesopores	Permeability in the absence of macropores, shrinkage above 80% RH
Gel pores	2.5–10 nm	Small mesopores	Shrinkage between 80% RH and 50% RH
	0.5–2.5 nm	Micropores	Shrinkage at all RH, creep
	Smaller than 0.5 nm	Interlayer spaces	

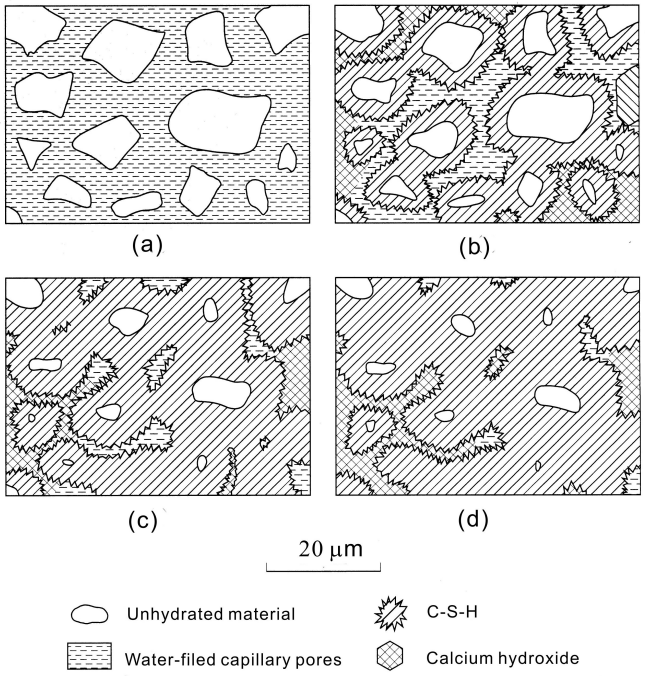

Figure 2.4: Schematic illustration of the microstructure development in hydrating Portland cement paste: (a) initial mix, (b) 7 days, (c) 28 days, (d) 90 days. After Mindess et al. (2003), calcium sulfoaluminates (ettringite and monosulfate in Figure 2.3) are included as parts of C-S-H.

porosity is regarded as a part of the C-S-H gel itself. However, this distinction should always be used with great care because of the complex shapes of pores. Furthermore, transformation of the pores from one category to the other can also take place, for example, due to the bulk shrinkage of paste, or formation of meniscus.

State of water

The initial water in the fresh paste is partially bound in the hydration products, and partially remains in the capillary pores. It can be roughly classified into three categories according to Powers (1960): capillary water, gel water and non-evaporable water.

The "non-evaporable" water is the retained water in the hydration products after drying the paste with the D-drying procedure (equilibrated with dry ice at -79°C, vapor pressure 0.5×10^{-3} mm Hg) (Powers, 1960). Heating the paste to a constant mass at 105°C in an atmosphere of uncontrolled humidity, but free of CO_2, reduces the retained water to the same extent (Taylor, 1997). The fraction of non-evaporable water to that in a fully hydrated paste is commonly used to determine the hydration degree of cement in the paste. It amounts to about 0.22–0.25 gram per gram of anhydrous cement for the complete hydration (Van Breugel, 1997) and its volume is reduced by about 28% (specific volume = 0.72 cm^3/g) compared to the free water (Brouwers, 2004b). The loss of non-evaporable water causes irreversible change of the hydration products and their decomposition.

Based on a large set of experimental data, Powers and Brownyard (1948) proposed the fol-

lowing equation for predicting the amount of non-evaporable water in fully hydrated Portland cement pastes as:

$$\frac{m_{nw}}{m^p} = 0.187x_{C_3S} + 0.158x_{C_2S} + 0.665x_{C_3A} + 0.213x_{C_4AF} \tag{2.18}$$

in which m_{nw} is the mass of non-evaporable water, m^p is the mass of hydrated Portland cement, x_{C_3S} etc. are the mass fractions of mineral C_3S etc. in Portland cement clinker.

The gel water is the part remaining in the gel pores in the hydration product, mainly C-S-H. It is removed when the paste is subject to D-drying. Thus, it is part of the "evaporable" water. Although the gel water can be removed from the paste, it exists in the gel pores as a part of the C-S-H and is not available for the hydration of other anhydrous cement. The gel water in hydrated cement pastes is compressed approximately 10% (in volume) as well (specific volume 0.9 cm^3/g). The amount of gel water in the hydrated Portland cement pastes can be predicted in a similar way to that for the non-evaporable water as (Brouwers, 2004b):

$$\frac{m_{gw}}{m^p} = 0.147x_{C_3S} + 0.216x_{C_2S} + 0.745x_{C_3A} + 0.258x_{C_4AF} + 0.261x_{C\bar{S}} \tag{2.19}$$

in which m_{gw} is the mass of gel water (in g). Note that Eq. (2.19) allows calcium sulfates in the cement.

The capillary water exists in the capillary pores, and is available for the hydration of cement. It is a part of the initial water present in the fresh paste and (if an external water supply is possible) a part of the imbibed water. The amount of capillary water may be insufficient to fill all the capillary pores in the paste; hence, some of the capillary pores become air voids and self-desiccation occurs.

Another concept frequently encountered in cement chemistry is the "chemically-bound water". It is regarded as the water chemically incorporated into the structure of hydration products, and cannot be removed without damaging the structure. This part of water includes the non-evaporable water, and part of the gel water. It can be approximately represented by the water retained in the paste at 11% RH, about 0.32 g per g hydrated cement (Taylor, 1987a).

The amount of water necessary for the complete hydration of Portland cement in the saturated state is about 0.42–0.44 g per g anhydrous cement (Taylor, 1997). This water includes the initial water in the starting fresh paste, and that imbibed from the environment (external water). If the paste is cured in a saturated state, i.e. external water is always available, the minimum w/c ratio for the complete hydration of Portland cement is about 0.38 (Powers and Brownyard, 1948), as the extra 0.06 g water per g cement is imbibed due to the chemical shrinkage; if the paste is sealed, the minimum w/c ratio is about 0.44.

Water retention

The actual amount of retained water in the hydration products depends on the hydration state of the paste (Schwiete and Ludwig, 1968; Taylor, 1997).

At room temperature, if the relative humidity remains higher than 88%, a hydrous form of the tetracalcium aluminum hydrate exists as C_4AH_{19}; at lower relative humidities, the stable form is C_4AH_{13}; at 22% RH the stable form reverts to C_4AH_{12} and at 11% RH to C_4AH_{11}; if dried at room temperature over P_2O_5 or heated to 120°C, it turns into C_4AH_7 (Schwiete and Ludwig, 1968).

In the saturated state and at room temperature, a supersaturated form of ettringite probably exists with the formula $C_6A\bar{S}_3H_{36}$ (Pöllmann, 2006; Pöllmann et al., 1989). Just below 80% RH, the stable form of ettringite is $C_6A\bar{S}_3H_{32}$ (Taylor, 1997), and if further heated to 100°C, a lower hydrate, namely $C_6A\bar{S}_3H_8$, is formed (Shimada and Young, 2001).

The water content in the hydrogarnet is stable compared to other hydration products, corre-

sponding to the formula $C_6AFS_2H_8$. However, it may also depend on the hydration state (Brouwers, 2005).

The water-binding capacity of the hydration product C-S-H is complex. C-S-H has a layer structure and comprises pores sizing in a wide range, which may be partially or completely filled with water. The total porosity is also influenced by the composition of C-S-H as well (Brouwers, 2004b). If dried at 105°C in a carbonation-free environment, for C-S-H with low C/S ratios (1.0-1.1), H/S ratios between 1–1.33 are measured (Steinour, 1944). In the mature C_3S paste in the D-dried state, H/S ratios in C-S-H ranging between 0.97-1.24 are measured with the C/S varying from 1.34 to 1.60 (Kantro et al., 1966), which is also measured in the experiment by Thomas et al. (2003). Therefore, it is taken in this thesis that the water retained in C-S-H at 105°C (or in the D-dried state) is equal to its C/S ratio ($\hat{a}$). Based on the work of Brouwers (2004b, 2005), at 80% RH, the H/S ratio in C-S-H can be expressed with $g = \hat{a} + 0.8$ and in the saturated state, the H/S ratio $g = \hat{a} + 1.5$.

Although the retained water in the hydration products might change in different hydration states and consequently their chemical formulas are altered, the expressions $C_{\hat{a}}SA_{\hat{b}}H_g$, M_5AH_{13}, $C_6AFS_2H_8$, $C_6A\bar{S}_3H_{32}$, C_4AH_{13} and C_2ASH_8 are used to denote the hydration products C-S-H, hydrotalcite, hydrogarnet, ettringite, tetracalcium aluminate hydrate and strätlingite, respectively, for the reason of simplification. Their different water contents are accounted for when physical and chemical properties of the hydration products are concerned, such as the water retention by the hydration products and the chemical shrinkage.

2.3 Hydration of slag cement

2.3.1 Alkali-activated slag

Alkali-activated slags as binders in concrete were first introduced in the former USSR in 1957 by Glukhovsky (1959). It is made from GGBFS and alkali-activators, the most commonly used ones being listed below (Glukhovsky, 1980; Shi and Day, 1995):

1. Caustic alkalis, MOH;
2. Non-silicate weak acid salts, M_2CO_3, M_2SO_3, M_3PO_4, MF, etc.;
3. Silicates, $M_2O{\cdot}nSiO_2$;
4. Aluminates, $M_2O{\cdot}nAl_2O_3$;
5. Aluminosilicates, $M_2O{\cdot}Al_2O_3{\cdot}(2\text{-}6)SiO_2$;
6. Non-silicate strong acid salts, M_2SO_4.

in which M is the alkali metal Na or K.

Hydration kinetics

The hydration kinetics of AAS is influenced by the nature of activators and their concentrations. Shi and Day (1995) concluded from the experimental results with a conduction calorimeter that three types of reaction kinetics can be distinguished, shown in Figure 2.5. The five stages similar to those of Portland cement hydration are recognized, indicated in the figure as well. Type A corresponded to cases when the slag is activated with Na_2HPO_4. A first peak is observed, due to the initial dissolution of slag. However, no further peaks exist, and the paste does not set and harden. Type B is observed when the slag is activated with NaOH. It is very similar to the reaction kinetics of Portland cement, and the five stages are clearly decerned. Type C is observed with Na_2SO_3, Na_2CO_3, Na_3PO_4 and NaF solutions as activator. Two peaks exist before the dormant period.

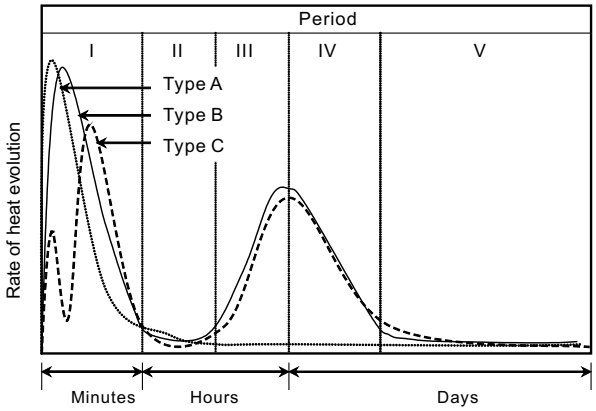

Figure 2.5: Three types of reaction kinetics of AAS, after Shi and Day (1995).

Hydration products

Similar to Portland cement hydration, C-S-H is the most abundant product in hardened AAS pastes (Richardson and Groves, 1992; Schilling et al., 1994; Wang and Scrivener, 1995). The C/S ratio (in moles) in C-S-H is generally close to that of the anhydrous slag. It is much lower than the C/S ratio in C-S-H from the normal Portland cement hydration. C-S-H is characterized by its high aluminum content. The A/S ratio in it can be as high as 0.1, indicating a high degree of aluminum substitution for silicon in its structure.

Furthermore, an M-A rich phase is commonly found in both AAS and the slag-blended cement pastes, generally referred to as the natural mineral hydrotalcite—$M_6A\bar{C}H_{12}$. The hydrotalcite is intimately mixed with C-S-H, making it hard to discern. The M/A ratio in it varies from 3.8 to 8.7 (Taylor, 1997). Harrisson et al. (1987) found a phase with an M/A ratio of 5.3 in the slag-blended cement paste and deduced it as a member of the hydrotalcite family. Richardson and Groves (1992) found an M-A rich phases as part of the "inner product" and envisaged it a hydrotalcite phase with an M/A ratio of 4.8. With X-Ray microanalysis, Wang and Scrivener (1995) found a hydrotalcite phase with an M/A ratio of 4.4 dispersed through the C-S-H. In the study of Gollop and Taylor (1996a), an M/A ratio of 4 in the hydrotalcite is found in the hardened slag-blended cement paste.

Allmann (1970) derived a layer ions structure by introducing trivalent ions into brucite-like layers with water molecules and a balancing anion in the interlayer sites. Specifically for the hydrotalcite phases, the structure can be attained based on layers of the type $[Mg_{1-x}Al_x(OH)_2]^{x-}$, where x ranges between 0.2 and 0.4. The balancing anion can be OH^-, Cl^- or CO_3^{2-} et al. In the same literature several M/A ratios of hydrotalcite observed in previous researches are included, with values ranging from 4 to 6.

XRD and differential thermal analysis (DTA) evidences indicate that there are some AFm phases existing in the paste. They are identified as the tetracalcium aluminate hydrate (C_4AH_{13}) (Wang and Scrivener 95)) or strätlingite (C_2ASH_8) (Richardson et al., 1994) or both (Narang and Chopra, 1983; Shi and Day, 1995) whereas in some AAS pastes neither is found (Richardson and Groves, 1992). The tetracalcium aluminum hydrate is most likely formed from glasses rich in lime and poor in alumina (Locher, 1960). Strätlingite is formed primarily from glasses rich in aluminum or poor in magnesium.

If gypsum is added as the activator, commonly together with CH, ettringite is found in AAS pastes while no trace of monosulfate is detected (Narang and Chopra, 1983). Gollop and Taylor

(1996b) studied hardened pastes of five slag-blended cements with different mass proportions of slag and Portland cement. Ettringite is found in all samples. Monosulfate is observed in four blends after one week, while with increasing age its amount decreased. The reason for the decrease can be that monosulfate is easily carbonated in the presence of CO_3^{2-}, Ca^{2+} and OH^- to form ettringite and hemicarbonate or finally mono-carbonate (Taylor, 1997). Therefore, in this thesis, ettringite is taken as the only sulfate-containing product from the slag hydration.

Poorly crystalline particles rich in iron and aluminum are found in AAS pastes, possibly being a form of calcium-deficient hydrogarnet (Richardson and Groves, 1992). According to the researches on Portland cement and fly ash reactions (Rodger and Groves, 1989; Schwiete and Ludwig, 1968; Taylor and Newbury, 1984), iron oxide in slags probably reacts into a hydrogarnet phase with the approximate composition $C_6AFS_2H_8$. CH in significant amount is rarely detected in AAS pastes. Even if it may form with some slag high in C, it may react further with C-S-H to increase its C/S ratio or with A to form the AFm phases from a long-term point of view.

Summarizing, the main hydration products in mature AAS pastes comprise C-S-H, hydrotalcite, an Fe-rich hydrogarnet phase, ettringite and AFm phases (C_4AH_{13} or C_2ASH_8). Since the reported M/A ratio in the hydrotalcite varies between 3.8 and 8.7, in this thesis, an M/A ratio of 5 is assumed. This value is also suggested by Taylor (1997) and is also close to those measured in experiments (Harrisson et al., 1987; Richardson and Groves, 1992; Wang and Scrivener, 1995). Therefore, the main hydration products of AAS include C-S-H, M_5AH_{13}, $C_6AFS_2H_8$, $C_6A\bar{S}_3H_{32}$, C_4AH_{13} and C_2ASH_8. The formula of C-S-H is denoted as $C_{\hat{a}}SA_{\hat{b}}H_g$ in which $\hat{a}$, $\hat{b}$ and g are the C/S, A/S and H/S ratios in the C-S-H, respectively.

Water molecules in the interlayer sites of the hydrotalcite-like phase can be removed reversibly without destroying its double layer structure (Allmann, 1970). Therefore, the water retention capacity of the hydrotalcite can also depend on the hydration state. The hydrotalcite has similar layer thickness to that of the AFm phases, so it may also have the same dehydration characterizations as them. Therefore, it is reasonable by assuming that the hydrotalcite has the same dehydration characterizations as the tetracalcium aluminate hydrate. At room temperature and at 35% RH a stable form of the strätlingite (C_2ASH_8) exists (Taylor, 1997).

Microstructure

The hardened AAS pastes are characterized by its fine pore structure compared to that of hardened Portland cement paste. The hydration products contain more gel pores and the pastes contain fewer capillary pores for the same w/b ratios (Brough and Atkinson, 2002; Häkkinen, 1993; Wang, 2000). Thus, it has low permeability. Coarse CH or AFt crystals are seldom observed in mature AAS pastes. Typical SEM and BSE images for hydrated AAS paste after one day are shown in Figure 2.6. The C-S-H is formed in the pore space originally occupied by the alkali solution (Gruskovnjak et al., 2006; Jiang et al., 1997). The hydrotalcite formed in the pastes is always closely mixed with C-S-H.

The microstructure development of hydrating AAS pastes is dominated by the rapid changes at early ages, and the slow development later. This corresponds well with the rapid setting of concrete made from AAS, and the slow strength gain at later ages.

2.3.2 Slag-blended cement

The hydration of slag-blended cement is more complex than that of Portland cement because the two constituents hydrate simultaneously and interfere with each other. Slag is activated by the alkalis and CH produced by the Portland cement hydration, and consumes a large amount of CH as well.

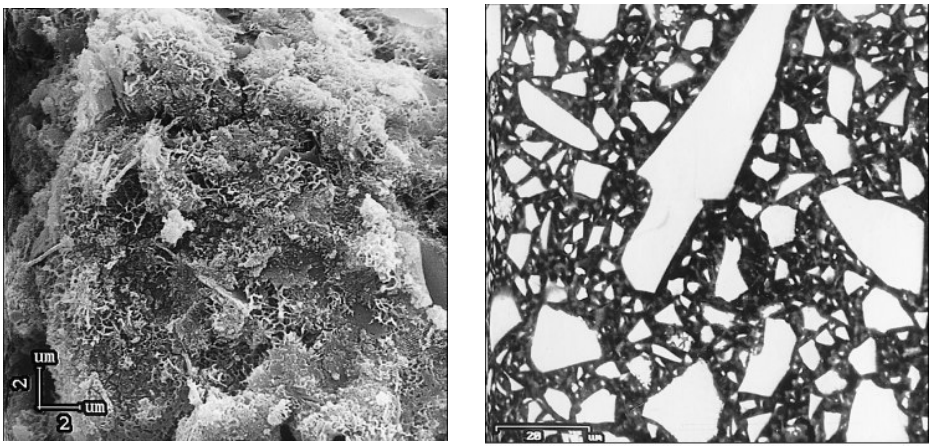

(a) SEM image (b) BSE image

Figure 2.6: Typical SEM (a) and BSE (b) images of hydrated AAS paste after one day, w/b = 0.25, T = 20°C, after Wang (2000).

Hydration rate of slag

The hydration rate of slag in blended cement is comparable to that of C_2S in Portland cement paste (Taylor, 1997). However, it can differ greatly from one slag to another due to the different reactivity of slag. The reactivity of slag depends on some factors like the oxide composition, presence of crystalline minerals, glass structure, pH values of the activation solutions and so on. An extensive discussion about the reactivity of slag is presented in Section 7.2. The activation energy of slag reaction in cement is about 50–59 kJ/mol (Fernández-Jimenéz and Puertas, 1997), higher than that of Portland cement (about 40 kJ/mol). Therefore, the reaction of slag is more sensitive to the curing temperature than that of Portland cement.

Typical curves for the hydration degree of slag in blended cement as a function of hydration time and with different slag proportions are presented in Figure 2.7. Similar to the AAS, the slag reaction proceeds rapidly during the early ages. At later ages, the reaction rate slows down.

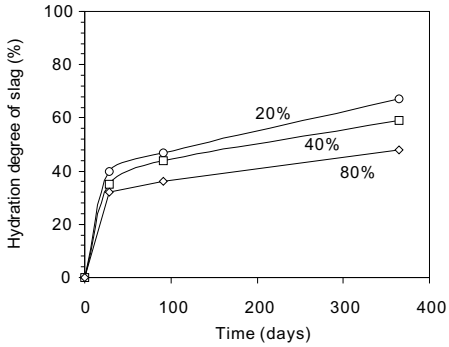

Figure 2.7: Hydration degree of slag in blended cement paste with different slag proportions in cement, w/c = 0.5, T = 20°C, determined with the EDTA method, after Schäfer (2004).

However, the increment of the degree is still higher than that of Portland cement, probably due to the large amount of anhydrous slag in the cement. Therefore, at later ages concrete made from slag cement may still show a significant strength gain due to the continuous hydration of slag. The other long-term properties may change with time for the same reason. Higher slag proportions in the cement result in lower hydration degrees.

Hydration products

Hydration products in the slag-blended cement paste comprise those products from both Portland cement and slag hydrations except that the amount of CH formed by the Portland cement hydration is influenced by the slag hydration (Pietersen and Bijen, 1994; Regourd, 1980; Richardson and Groves, 1992). C-S-H is the most abundant product in blended cement pastes. Its C/S ratio (in moles) is generally lower than that in the Portland cement paste. However, the C/S ratio in C-S-H is still higher than the C/S ratio in the pure slag (about 1.0–1.1), indicating additional calcium demand by the slag hydration. This calcium demand is supplied either by the CH formed by the Portland cement hydration (Hill and Sharp, 2003), or by the lower C/S ratio in the C-S-H (Harrisson et al., 1987). In this respect, the CH produced by the hydration of Portland cement acts not only as an activator or catalyst to the slag hydration, but also as a reactant.

No significant difference is found among the C/S and A/S ratios in the C-S-H gels in the "inner products" of both calcium silicates and slag, and all the "outer products" (Richardson and Groves, 1992), similar to the observations in Portland cement pastes with (Duchesne and Bérubé, 1995) or without supplementary materials (Groves et al., 1986; Richardson and Groves, 1992). This unimodel distribution is probably due to a compositional equilibrium of C-S-H in the inner and outer products.

The curing time is found to have a minor influence on the compositions of C-S-H. However, the slag proportions in the cement have a dominant influence. With increasing slag proportions in the cement, the C/S ratio in C-S-H decreases and the A/S ratio increases. C-S-H from the hydration of pure slags has a C/S ratio close to that of anhydrous slag (Richardson and Groves, 1992).

Microstructure

The microstructure of slag-blended cement paste is marked by its low permeability, due to the dense structure caused by the relatively large amount of C-S-H formed in the products. The amounts of CH are obviously more reduced than the values considering merely the dilution effect of slag (Regourd, 1980). The morphology of C-S-H is different from that of C-S-H in Portland cement pastes as well, more foil-like and less fibrillar.

The porosity and pore size distribution of hardened slag-blended cement paste are different from those of Portland cement paste. At early ages, the porosities of the former are comparable to that of the latter. At later ages, when the slag has reacted, the volume of pores in the 3–5 nm size range becomes larger (Uchikawa, 1986). Furthermore, the pores in hardened slag cement paste are more discontinuous and thin-walled (Feldman, 1986).

A schematic illustration of the spatial distributions of hydration products around slag particles is presented in Figure 2.8. The figure is based on the experiments with glassy discs zebra-coated with gold, which can mark the position of the original slag surface (Tanaka and Totani, 1983). These discs are embedded in Portland cement paste. The cross-section of glassy discs is then observed with SEM. The slag surface is found to be first covered by hydration products of Portland cement hydration, then attacked by Ca^{2+} ions from the supersaturated solution, producing the "inner hydrated layer". The subsequent dissolution of Ca^{2+} and Al^{3+} ions from slag leaves a skeleton of hydrated layers. The mobility of Mg^{2+} is restricted and hence higher concentrations in the skeleton hydrate are observed than those in the inner product and the anhydrous slag.

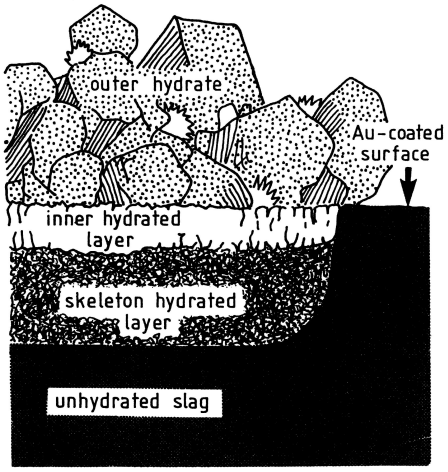

Figure 2.8: Distribution of slag hydration products in hydrating blended cement paste, after Tanaka and Totani (1983).

2.4 Computer modeling of Portland cement hydration

Several models for microstructure development have been developed in different groups using microstructural observations in experiments. Among them Powers's model is perhaps the first to depict the microstructure of cement-based materials (Powers and Brownyard, 1948). This model (depicted in Figure 1.7) enables the calculation about the volume fraction of phases in hardened cement pastes, and can be used to derive the chemical reaction going on in the cement paste (Brouwers, 2004b, 2005).

Later, benefiting from the rapid development in computer science, computer-based models are proposed, including the Jennings and Johnson's model (Jennings and Johnson, 1986), the DUCOM model developed in Japan (Maekawa et al., 1996), the NIST model by Bentz and Garboczi (Bentz and Garboczi, 1991), a kinetic model named HYMOSTRUC at the Delft University in The Netherlands (Van Breugel, 1997) and Navi and Pignat's model (Navi and Pignat, 1996). The formation of the microstructure is modeled explicitly. Together with the microstructure development, the hydration degree of cement, defined as the rate of cement hydration, is modeled as well.

Factors influencing the process such as w/c ratios, curing temperature, PSD of cement and sealed/saturated conditions are considered in most models. Properties pertaining to the hydration process are predicted, for example, the heat evolvement, chemical shrinkage, and porosity. Combined with further knowledge on mass and gas transport in the microstructure, and their interactions, the model can be used to model some long-term properties like durability, permeability and volume changes. Comprehensive reviews about the modeling of cement-based materials hydration can be found in the works of Jennings et al. (1996), Van Eijk (2001) and Van Breugel (2004).

In this section, the computer models HYMOSTRUC and the Navi and Pignat's model are introduced. The 3-D computer model CEMHYD3D is described in Section 2.5.

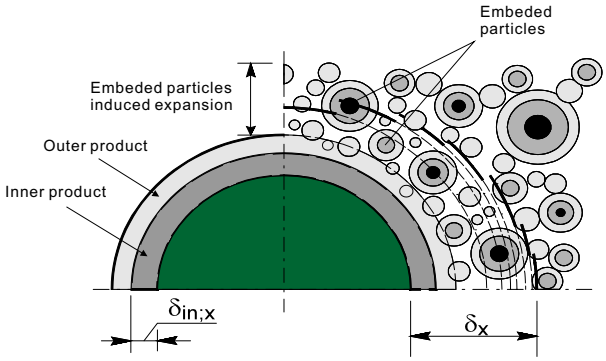

Figure 2.9: Principles of the computer-based 3-D cement hydration model HYMOSTRUC, after Van Breugel (1997).

2.4.1 HYMOSTRUC

The computer-based 3-D computer model HYMOSTRUC is developed at the Technical University of Delft in The Netherlands. The name is an acronym for HYdration, MOrphology and STRUCture formation. The model is developed for simulating the reaction process and the formation of the microstructure of hydrating Portland cement paste. The model accounts for the PSD and chemical composition of cement, the w/c ratio of the paste, and the curing condition. Cement particles are modeled as digitized spheres randomly distributed in a 3-D cube called "cell". The hydration process is modeled as the continuous growth of these particles. The anhydrous cement part keeps shrinking, representing the gradual reaction, and the porous shell around the cement is formed. The spheres keep growing, overlapping with each other, forming big clusters (Figure 2.9). As the hydration proceeds, the spheres become more and more connected and consequently the initial fresh paste turns into solid porous hardened paste. The simulation is executed on a time basis. The time increment reads:

$$\Delta t_{j+1} = t_{j+1} - t_j \tag{2.20}$$

The progress of the hydration is considered as the penetration depth, which is computed as:

$$\Delta\delta_{in;x,j+1} = \frac{K_i(\cdot)\cdot F_1(\cdot)\cdot [F_2(\cdot)]^{\lambda_h}\cdot \Omega_1(\cdot)\cdot \Omega_2(\cdot)\cdot \Omega_3(\cdot)}{\{(\delta_{x,j})^{\lambda_h}\}^{\beta_h}}\cdot \Delta t_{j+1} \tag{2.21}$$

in which:

- K_i: A rate constant depending on the rate controlling mechanism, cement composition and the hydration degree. $i = 0$ if it is a phase-boundary reaction and $i = 1$ if it is a diffusion-controlled reaction.
- F_1, F_2: Factors accounting for the effects of temperature.
- $\Omega_1, \Omega_2, \Omega_3$: Factors accounting for the water withdraw effect, water shortage in the system, and the amount of water in the hydrating mass, respectively.
- λ_h: Factor depending on the rate controlling mechanism; $\lambda_h = 0$ if it is a phase-boundary reaction and $\lambda_h = 1$ if it is a diffusion-controlled reaction.
- β_h: An empirical constant.
- δ_x: Total thickness of product layer of particle at the end of time step Δt_j.

The factors $F_1, F_2, \Omega_1, \Omega_2, \Omega_3$ are functions of the temperature, hydration degree, water content,

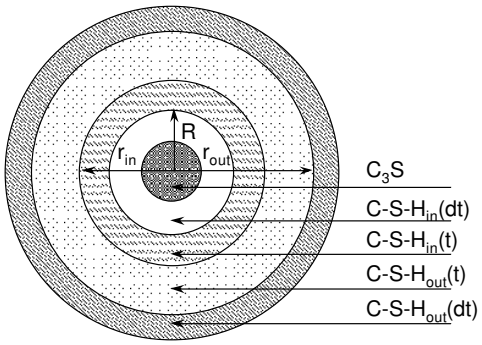

Figure 2.10: Illustration of one hydrating C_3S particle at time t, after Navi and Pignat (1996).

particle size, and the C_3S content in the cement. Methods for determining these factors are given in the work of Van Breugel (1997).

The cement hydration model HYMOSTRUC uses fundamental knowledge about the cement hydration, accounts for the different hydration mechanisms and kinetics during the hydration process, and thus has a very solid chemical background. The model parameters can be explained explicitly, and hence can be calibrated with numerous experimental data about cement hydration.

2.4.2 Navi's model

Navi and Pignat (1996) developed a 3-D computer model for simulating the hydration and microstructure development of C_3S pastes classified as "Integrated Particle Kinetics Model". The hydrated C_3S turns into products C-S-H and CH. The C-S-H grows inward or outward from the original particle edge, classified as "inner" and "outer" C-S-H accordingly. CH crystals are produced outside the outer products in the pore space. When one cm^3 C_3S dissolves, it produces 1.7 cm^3 C-S-H and 0.61 cm^3 CH. This part of C-S-H is further divided into two parts: 1 cm^3 inner C-S-H and 0.7 cm^3 outer C-S-H (Figure 2.10). Therefore, there is always a relation between the rate of C-S-H growth inward and that outward. Methods are proposed to determine the growth rate of inner C-S-H, which can in turn determine the rate of C_3S dissolution as well.

Similar to the HYMOSTRUC, the size of the particles keeps increasing, and they start to overlap with each other. If there is an overlap, the contact surface is calculated. The contact area is used to calibrate the reaction rate considering the effects of overlapping and shortage of water in the system.

2.5 CEMHYD3D: a 3-D computer-based cement hydration model

2.5.1 Introduction

Amongst the various computer models ever proposed for cement hydration, CEMHYD3D is believed to be one of the most advanced and well-known ones (Van Breugel, 2004) due to at least three advantages: (a) it uses the fundamental knowledge about hydration reactions and hydration products in the hydrating system; (b) the algorithm used, namely cellular automation (CA) rule, is very flexible. New knowledge can be implemented into the computer model by adding and changing corresponding modules; (c) the system is represented with a digitized microstructure; hence, microstructural characteristics can be easily evaluated, e.g. volume fraction of phases, percolation properties, contact areas between different phases (Van Eijk, 2001).

CEMHYD3D is a pixel-based digital model that uses pixels to represent the phases in the hardening paste/concrete. Each pixel is assigned to a phase, which is susceptible to move and

transforms into another phase. A procedure, named hydration cycle and consisting of dissolution, diffusion, reaction, and precipitation processes, is followed to simulate the gradual growth of grains and disappearance of reactants. Results of the simulation such as hydration degree, phase distribution, porosity and phase connectivity can be used to predict the material performance of hardened cement paste under investigation. Good accordance between the model predictions and experimental results, such as hydration degree, strength development and heat evolvement, are found (Van Eijk, 2001). Furthermore, the computer model is extended for simulating the pore solution composition of hydrating Portland cement paste (Van Eijk, 2001).

2.5.2 A brief history

The computer model CEMHYD3D was originally developed in NIST by Bentz and Garboczi (1991) to represent the hydration process of Portland cement two-dimensionally. It was later developed into a 3-D computer model and the reactions of other cementitious materials, like fly ash and silica fume, were incorporated (Bentz, 1997). In 1996, the basic principles of CEMHYD3D were taken over by Van Eijk (2001) and were further developed in The Netherlands. Thereafter, parallel developments proceeds both at the NIST and in The Netherlands. The newest developments on CEMHYD3D in NIST can be found in the works by Bentz (Bentz, 2000, 2005, 2006).

In The Netherlands, Van Eijk (2001) developed the CEMHYD3D into a personal computer based software. Routines were built to simulate the influence of contaminants on the cement hydration, and modules for predicting the pore solution compositions of hydrating Portland cement paste. The methods of model inputs and outputs are also modified, which saves much user time. Van Eijk (2001) also calibrated the model with two Dutch cements CEM I 32.5R and 52.5R.

In this thesis, if not otherwise stated, the model CEMHYD3D developed by Van Eijk is used, named "*Van Eijk's Model*", or the "*Van Eijk version*" of CEMHYD3D, instead of the CEMHYD3D developed in NIST.

2.5.3 Principles

The simulation starts with a microstructure representing the freshly-mixed paste, and proceeds by using some cellular automation and random walk algorithms. Reaction and precipitation processes are simulated by using knowledge available on cement hydration. The properties of the hydration process and the paste are calculated based on the phase change in the matrix and physical or chemical characteristics of the evolving microstructure. These properties are compared to the measurements in experiments for validating the model, and for calibrating the simulation. A flow diagram summarizing the primary procedures of the simulation is given in Figure 2.11. Note that the heat of hydration is also calculated from the 3-D cement hydration model, and is used to predict the temperature rise of the system if cured in an adiabatic condition. The temperature rise affects the hydration rate of reactants in the computer model. This interactive correlation is represented in Figure 2.11 by the left-right arrow.

Regenerating the initial microstructure

The model starts with an initial 3-D microstructure reconstructed from information of the cement powder such as the distribution of clinker phases (via SEM images) and PSD of cement. The hydrating cement paste is represented by a 3-D cube divided into a certain number of cubic pixels. The cement particles are built within the box using these pixels in an approximately spherical shape, namely "digitized particles". The rib size of one pixel is called "system resolution" (ℓ), which can be adjusted to different physical sizes. For a typical plant cement, most of the particles have sizes below 90 μm. Therefore, the dimension of the simulated microstructure is often set to be $100\times100\times100$ μm^3, and preferably $200\times200\times200$ μm^3. The pixel size ℓ for the microstructure is normally set to be 0.5 or 1 μm. Principally, bigger system dimension and smaller pixel size yields more representative structures. However, they are limited by the computation power available. If the system resolution is one μm, a one-μm particle is represented by one pixel. An

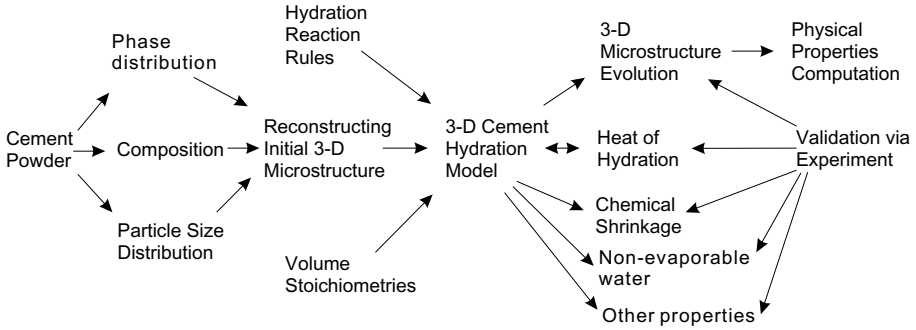

Figure 2.11: A flow diagram summarizing the primary procedures of the simulation (modified from Bentz (1995)).

example for the digitized particles of size 3 ℓ is shown in Figure 2.12, which contains 19 pixels (Van Eijk, 2001). Particles of other sizes are built in a similar way by placing the pixels in the best possible particle-forming positions. The properties of digitized particles with different sizes are shown in Table 2.4.

In Table 2.4, the properties of digitized particles are compared with those of spheres as well. It can be seen that for small particles with size $d = 1\ell - 3\ell$, the volume and surface area of digitized particles (column 2 and 3) are remarkably larger than those of the spheres (column 6 and 7); while for larger particles the digitized ones and spheres have identical volumes (see the ratios in column 9). The surface areas of the digitized particles are always larger than those of the spheres (column 10). For big particles ($d > 5\ell$), the shape factors (defined as the ratio between the product of surface area and size of particle and its volume, see Table 2.4) of digitized particles are very close to 9, which is obviously higher than that of the sphere. Larger shape factors for cement particles are reasonable considering the angular nature of the cement particles itself (Van Eijk, 2001). The ratio of shape factors between the digitized particles and spheres for big particles are very close to 1.5. This value is in good agreement with the conclusions of Reschke (2000), who derived values of 1.50, 1.52, and 1.53 for three different CEM I 32.5R cements.

An initial microstructure is generated preserving the correct particle size distribution and phase distributions making use of periodic boundaries. First, the volume of solid is calculated from the water/cement ratio by using the average density of the solid phases. Then, the number of digitized particles of each size is calculated from the particle size distributions of cement, inert and additives, and their mass fractions and densities. A routine for calculating the exact number

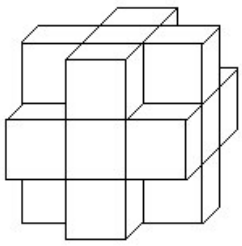

Figure 2.12: Digitized 3 ℓ particle in CEMHYD3D, after Van Eijk (2001).

of particles of each size is given by Van Eijk (2001). Third, the digitized particles are placed randomly in the box in the sequence from the largest to the smallest with periodic boundaries. The periodic boundaries are used to eliminate the sparsity effect due to the presence of boundaries (Figure 2.13).

Special attention should be taken when calculating the number of particles with the size 1 ℓ–3 ℓ because of the different volumes of the digitized particles and spheres. The number should always be divided by the ratios in column 10 in Table 2.4 to preserve the correct volume fractions. For example, if 100 ***spherical particles*** with the diameter 1 ℓ should be generated, which are determined from the PSD of cement (total volume 52 ℓ^3), 52 ***digitized particles*** of size 1 ℓ are put into the microstructure. Thus, the total volume for a 1 ℓ particle is correctly 52 ℓ^3 instead of 100 ℓ^3.

A careful comparison of the SSA by Van Eijk (2001) shows a good agreement of the SSA values among the measured ones, the calculated ones using the Rosin-Rammler curve and the values of the digitized particles systems (see Table 2.5).

The presence of aggregate, whose size is often an order of magnitude higher than the cement particle sizes, is simulated by putting an inert plane in the box before the particles are placed. In this way, wall effects of the aggregates are simulated. After placing all the particles into the box, an initial microstructure representing the particles positions and distributions is obtained.

With the composed particle structure, distribution of phases in the microstructure is simulated by assigning one phase to each solid pixel. In the *Van Eijk's Model*, many phases of reactants can be simulated, listed in Table 2.6, together with their physical properties. Computational techniques have been developed by Bentz (1997) to characterize the multi-phase spatial structure of the anhydrous cement and create a 3-D representation which reliably represents the phase volume

Table 2.4: Properties of digitized particles used in CEMHYD3D.

Digitized particle				Sphere				Digitized particle/sphere ratio		
1	2	3	4	5	6	7	8	9	10	11
Size	Volume	Surface area	Shape factor ♮	Size	Volume	Surface area	Shape factor ♮	Volume	Surface area	Shape factor
(d, ℓ)	(V, ℓ^3)	(S, ℓ^2)	(φ)	(d, ℓ)	(V, ℓ^3)	(S, ℓ^2)	(φ)			F_s
1	1	6	6	1	0.524	3.142	6	1.91	1.91	1.00
3	19	54	8.53	3	14.14	28.27	6	1.34	1.91	1.42
5	81	126	7.78	5	65.45	78.54	6	1.24	1.60	1.30
7	179	222	8.68	7	179.6	153.9	6	1.00	1.44	1.45
9	389	414	9.58	9	381.7	254.5	6	1.02	1.63	1.60
11	739	582	8.66	11	696.9	380.1	6	1.06	1.53	1.44
13	1,189	822	8.99	13	1,150	530.9	6	1.03	1.55	1.50
15	1,791	1,062	8.89	15	1,767	706.9	6	1.01	1.50	1.48
17	2,553	1,350	8.99	17	2,572	907.9	6	0.99	1.49	1.50
19	3,695	1,758	9.04	19	3,591	1,134	6	1.03	1.55	1.51
21	4,945	2,094	8.89	21	4,849	1,385	6	1.02	1.51	1.48
23	6,403	2,526	9.07	23	6,371	1,662	6	1.01	1.52	1.51
25	8,217	2,934	8.93	25	8,181	1,963	6	1.00	1.49	1.49
27	10,395	3,462	8.99	27	10,306	2,290	6	1.01	1.51	1.50
29	12,893	3,990	8.97	29	12,770	2,642	6	1.01	1.51	1.50
31	15,515	4,494	8.98	31	15,599	3,019	6	0.99	1.49	1.50
33	18,853	5,166	9.04	33	18,817	3,421	6	1.00	1.51	1.51
35	22,575	5,838	9.05	35	22,449	3,848	6	1.01	1.52	1.51
37	26,745	6,510	9.01	37	26,522	4,301	6	1.01	1.51	1.50
39	31,103	7,206	9.04	39	31,059	4,778	6	1.00	1.51	1.51

♮: $\varphi = S \cdot d / V$

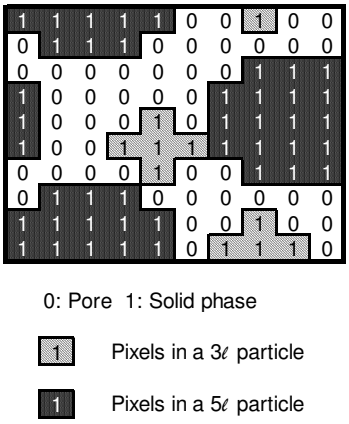

Figure 2.13: 2-D schematic illustration of an initial microstructure in CEMHYD3D with periodic boundary conditions for a 2-D system with size 10 $\ell \times 10\ \ell$.

fractions, phase surface area fractions, and phase autocorrelation structure. These characteristics are based on image analysis of two-dimensional images of the initial cement powder. They are further used to assign one phase to each solid pixel obeying a series of rules (Bentz, 1997). After this assignment, an initial microstructure preserving the right PSD of particles and distribution of phases is obtained.

While the 2-D SEM images and detailed information are not available for some cements under simulation, to assign the phases to the pixels is difficult using the autocorrelation method. In this case, a random distribution method is used. The phases are assigned randomly to the pixels preserving the appropriate volume fractions, resulting in a homogeneous phase distribution. It appeared that the randomly assigned phases and those based on 2-D images resulted in almost identical simulation results (Van Eijk, 2001).

Executing the simulation

Hydration of the initial microstructure is simulated in an iterative process consisting of discrete cycles as illustrated schematically for a two-dimensional system in Figure 2.14.

Each cycle consists of three processes: dissolution, diffusion and reaction. Basically, the

Table 2.5: Calculated and measured specific surface areas of three different cements (SSA, in m^2/kg, after Van Eijk (2001)).

	CEM I 32.5 R	CEM I 42.5 R	CEM I 52.5 R
Measured Blaine surface	270	420	550
Calculated SSA (Rosin-Rammler PSD, $\varphi = 6.8$)	257	371	499
Calculated SSA (Rosin-Rammler PSD, $\varphi = 6$)	227	328	441
Calculated SSA (Digitized PSD)	271	367	456

Table 2.6: Properties of phases used in CEMHYD3D (*Van Eijk's Model*, after Van Eijk (2001)).

Name	Density (ρ, g/cm^3)	Molar volume (ω, cm^3/mol)	Molar mass (M, g/mol)	Heat of formation (kJ/mol)	Dissolution probability
C_3S	3.21	71	228	-2,928	0.027
C_2S	3.28	52	171	-2,312	0.005
C_3A	3.03	89.1	270	-3,588	0.027
C_4AF	3.73	128	477	-5,090	0.003
$C\bar{S}H_2$	2.32	74.2	172	-2,023	0.0017
$C\bar{S}H_{0.5}$	2.73	53.2	145	-1,575	0.005
$C\bar{S}$	2.61	52.2	136	-1,425	0.001
$C_{1.7}SH_{4.0}$	2.12	108	229	-3,283	
$C_{1.1}SH_{3.9}$	1.69	101.8	172	-2,299	
CH	2.24	33.1	74	-986	
$C_6A\bar{S}_3H_{32}$	1.7	735	1250	-17,539	
$C_4A\bar{S}H_{12}$	1.99	313	623	-8,778	
C_3AH_6	2.52	150	378	-5,548	
FH_3	3	69.8	209	-824	
S	2.2	27	59	-908	
H	1	18	18	-286	

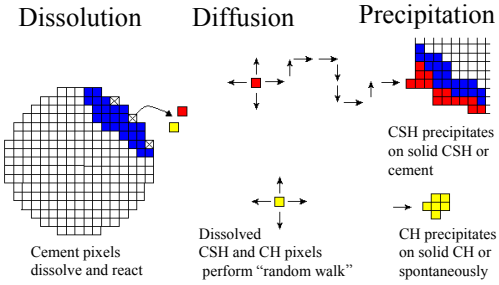

Figure 2.14: 2-D illustration of dissolution, diffusion and reaction steps for C_3S reaction in the *Van Eijk version* of CEMHYD3D. Blue = C_3S, Red = C-S-H and yellow = CH, after Van Eijk (2001).

phases dissolve from the surface of the cement particles, diffuse in the space available up to a certain number of steps, and react into hydration products due to nucleation or collision with other phases. The three processes are discussed in details below.

Dissolution The dissolution step is executed by scanning the entire 3-D microstructure for identifying all reactant phases which are soluble and enabling those pixels to dissolve if certain conditions are met. A dissolution probability is introduced beforehand in the model for defining the likelihood of each phase to dissolve. The reactant phases (such as C_3S, C_2S, C_3A, C_4AF, gypsum) have different dissolution probabilities (see Table 2.6) so that they dissolve at different rates. In this way the reaction kinetics of different phases are taken into account. All solid

Table 2.7: Default values of $\Pi^0_{j,nuc}$ and $[I]_{j,max}$ used in the *Van Eijk's Model*.

Diffusing species	$\Pi^0_{j,nuc}$	$[I]_{j,max}$
CH	0.01	9000
C_3A	0.0002	100000
FH_3	0.2	2500

pixels in contact with the water are marked as being capable of dissolution. In a second scan all marked pixels take a one-step random walk and if three requirements are met, i.e. (a) this step is into porosity, (b) the phase of the pixel is currently soluble and (c) a randomly chosen number is higher than the dissolution probability of this phase, the dissolution is allowed. When dissolution takes place, the solid pixel is converted to one or more diffusing pixels, preserving the appropriate volume equations. It is noteworthy that during this dissolution step, actually the reactions of some phases are already accounted for because the corresponding products are added as diffusing species, instead of one diffusing phase of the reactant. For example, when one pixel of C_3S dissolves, it converts into diffusing C-S-H and diffusing CH, which are the hydration products of C_3S. Therefore, C_3S has already reacted in this step.

After the scan, the number of dissolved pixels of each reactant is counted, and the corresponding diffusing species are added randomly in the water-filled spaces (porosity). The correct volume stoichiometry of the reactions is preserved statistically. For example, if 100 pixels of C_3S dissolve in a cycle, 152 diffusing C-S-H pixels and 61 diffusing CH pixels are added.

Diffusion After the correct numbers of diffusing species have been created, each of these diffusing pixels executes a random walk in the available water. For one step, the pixel moves into one of the neighboring porosity pixels. A large number of diffusing steps are executed, for example, 500 steps. During the diffusion process, three possibilities for the changes of the pixels are provided, including nucleation, precipitation and reaction. The diffusion directions are random, if only the pixel to occupy is porosity. After a number of diffusion steps, most of the diffusing species turn into solid products.

Nucleation of a diffusing pixel takes place for some species, including diffusing FH_3, CH, and ettringite. They convert to corresponding solid products at the current location. The likelihood for the species to nucleate is called "nucleation probability", which is exponentially proportional to the number of diffusing species remaining in the microstructure as (Bentz, 1997):

$$\Pi^i_{j,nuc} = \Pi^0_{j,nuc} \cdot (1 - e^{-\frac{[I]^i_j}{[I]_{j,max}}}) \tag{2.22}$$

in which $\Pi^i_{j,nuc}$ is the probability of nucleation for specie j at cycle i, $\Pi^0_{j,nuc}$ is the maximum probability of nucleation, $[I]^i_j$ is the number of diffusing pixels of specie j in the system in cycle i, and $[I]_{j,max}$ is a scale factor for specie j. By varying $\Pi^0_{j,nuc}$ and $[I]_{j,max}$, the number and crystal size of the solid products during the hydration can be controlled. This functional form gives a nucleation probability that will decay rapidly as $[I]^i_j$ becomes much less so that few new crystals will form late in the hydration (Figure 2.15). The values for $\Pi^0_{j,nuc}$ and $[I]_{j,max}$ are determined by the user as system inputs, or follow the default values, which are listed in Table 2.7.

Precipitation takes place if the diffusing pixel collides with the predesignated solid species. For example, a diffusing CH pixel precipitates if it collides with solid CH. During the precipitation process, the gradual growth of solid products in the microstructure is simulated.

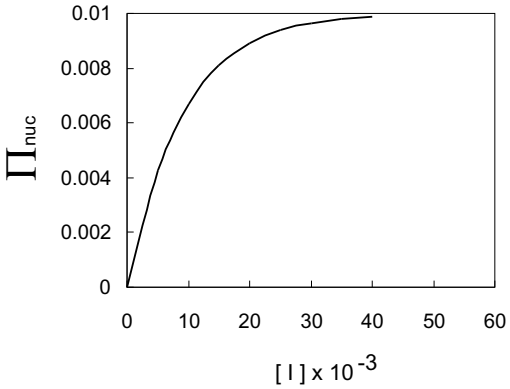

Figure 2.15: Change of Π_{nuc} as a function of the number of the diffusing species (after Eq. (2.22), $\Pi^0_{j,nuc} = 0.01$, $[I]_{j,max} = 9000$).

Reaction Reactions obeying a series of rules take place if the diffusing species collide with other solid/diffusing species. The possibility of the chemical reaction depends on the nature of the two species colliding. The pixels convert into solid products preserving the right volume stoichiometry. The pozzolanic reaction is simulated by a reaction between the diffusing CH and S, yielding pozzolanic C-S-H. Note that in the *Van Eijk's Model*, there are also possibilities for the nucleation of diffusing C_3A, following the same expression as Eq. (2.22). However, the nucleated C_3A turns into solid product C_3AH_6. Therefore, this procedure is marked by its reaction between C_3A and water, instead of the nucleation behavior of the pixel. It is thus considered as the reaction of diffusing C_3A.

The corresponding reaction equations on a volume basis can be determined from the numbers of moles that are given in the reaction equations and the molar volumes of compounds. To obtain a reaction in terms of pixels these volumes have to be normalized using the volume of the main original compound in that reaction.

A summary of the rules for phase changes considered in the model can be found in the work of Van Eijk (2001). The reactions taking place during dissolution and reaction process are listed as:

$$\begin{array}{cccccc} C_3S & + & 5.3H & \rightarrow & C_{1.7}SH_4 & + & 1.3CH \\ 1 & & 1.34 & & 1.52 & & 0.61 \end{array} \tag{2.23}$$

$$\begin{array}{cccccc} C_2S & + & 4.3H & \rightarrow & C_{1.7}SH_4 & + & 0.3CH \\ 1 & & 1.49 & & 2.08 & & 0.19 \end{array} \tag{2.24}$$

$$\begin{array}{cccc} C_3A & + & 6H & \rightarrow & C_3AH_6 \\ 1 & & 1.21 & & 1.69 \end{array} \tag{2.25}$$

$$\begin{array}{cccccc} C_3A & + & 3C\bar{S}H_2 & + & 26H & \rightarrow & C_6A\bar{S}H_{32} \\ 0.4 & & 1 & & 2.1 & & 3.30 \end{array} \tag{2.26}$$

$$\begin{array}{cccccc} 2C_3A & + & C_6\bar{S}_3H_{32} & + & 4H & \rightarrow & 3C_4A\bar{S}H_{12} \\ 0.24 & & 1 & & 0.10 & & 1.28 \end{array} \tag{2.27}$$

$$\begin{array}{ccccccc} C_4AF & + & 10H & \rightarrow & C_3AH_6 & + & CH + FH_3 \\ 1 & & 1.41 & & 1.17 & & 0.26 \quad 0.55 \end{array} \tag{2.28}$$

$$C_4AF + 3C\bar{S}H_2 + 30H \rightarrow C_6A\bar{S}_3H_{32} + CH + FH_3 \quad (2.29)$$
$$0.58 \quad 1 \quad 0.25 \quad 3.30 \quad 0.15 \quad 0.31$$

$$2C_4AF + C_6A\bar{S}_3H_{32} + 12H \rightarrow 3C_4A\bar{S}H_{12} + 2CH + 2FH_3 \quad (2.30)$$
$$0.35 \quad 1 \quad 0.29 \quad 1.28 \quad 0.09 \quad 0.19$$

$$1.1CH + S \rightarrow C_{1.1}SH_{3.9} + 2.8H \quad (2.31)$$
$$1.35 \quad 1 \quad 3.77 \quad 1.87$$

$$C_{1.7}SH_4 + 0.5H \rightarrow C_{1.1}SH_{3.9} + 0.6CH \quad (2.32)$$
$$1 \quad 0.08 \quad 0.94 \quad 0.18$$

The numbers below each reaction equation show the reaction stoichiometries on a volume basis, which are calculated from the properties listed in Table 2.6. Again the stoichiometries in all the reaction equations above are implemented on a statistical basis. For example, when 1 pixel of diffusing C_3A nucleates, the pixel immediately turns into solid C_3AH_6 and the possibility for the adjacent water to turn into solid C_3AH_6 is 0.69 (=1.69-1). In other words, if the randomly generated number is smaller than 0.69, the adjacent water pixel is changed into a solid C_3AH_6 pixel.

The hydration products comprise both chemically and physically bound water. The moles of water in each reaction do not take part in the reaction step directly but are calculated based on their fractions in the products.

After each hydration cycle, a new microstructure is obtained. The composition of this simulated microstructure is known and microstructural properties can be determined from it. Because the model keeps track of all reactions that have taken place, hydration related properties can be calculated, such as the hydration degree, amount of combined water, heat development and chemical shrinkage. It is noteworthy that the heat development influences the hydration process of cement in an ambient or adiabatic environment.

2.5.4 Model output

As the advantage of a digitalized model, CEMHYD3D represents the hydrating microstructure in a digitized way. Thus, the amount of hydration products and remaining reactants can easily be calculated. Other features including the connectivity and distribution of phases can also be evaluated. Therefore, properties of hydration, such as hydration degree, chemical shrinkage, combined and free water, and the heat release, can be computed. A typical representation of anhydrous and hydrated microstructure is presented in Figure 2.16.

The hydration degree of the clinker phase is computed using the number of the initial and remaining pixels as:

$$\alpha_j^i = \frac{[I]_j^0 - [I]_j^i}{[I]_j^0} \quad (2.33)$$

in which α_j^i is the hydration degree of phase j in cycle i, $[I]_j^0$ is the number of pixels in the initial microstructure, $[I]_j^i$ is the number of remaining pixels of phase j in cycle i. The overall hydration degree of the cement is calculated from the total numbers of initial and remaining cement pixels on a volume basis, which is further converted into the degree on a mass basis by using the densities of phases.

The current temperature of the paste at each hydration cycle is calculated using the enthalpy change of complete hydration for clinker phases (Table 2.8). A more comprehensive review about the enthalpy change of complete hydration of major clinker phases is given by Van Breugel (1997), in which the values are very close to those in Table 2.8. Note that when calculating the enthalpy changes the w/c ratio of the paste and the temperature should be accounted for

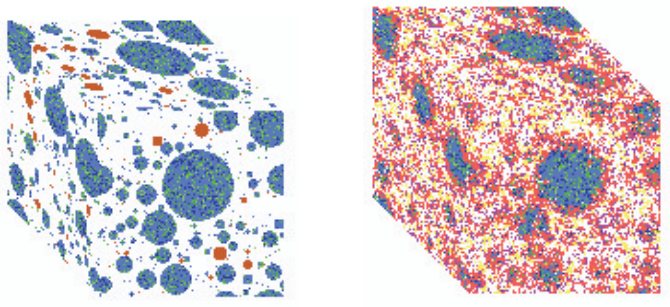

(a) Initial microstructure (b) Hydrated microstructure

Figure 2.16: Initial (a) and hydrated (b) microstructure after 500 cycles, based on 100· 100· 100 pixels in a 3-D box, blue = cement, brown = gypsum, red = C-S-H, yellow = CH, white = water, w/c = 0.5, CEM 32.5R, reproduced from Van Eijk (2001).

Table 2.8: Enthalpy change of complete hydration for major clinker phases (after Taylor (1997), w/c = 0.4 and T = 21°C).

Phase	Enthalpy (kJ/kg)
C_3S	517
C_2S	262
C_3A	1,144
C_4AF	418

due to their effects on the nature of the reaction (Copeland et al., 1960). The involvement of other reactants deserves attention because of the different products. For example, C_3A can both react with gypsum to form ettringite (Eq. (2.26)) and continues reacting with ettringite to form monosulfate (Eq. (2.27)). These two reactions give different enthalpy changes.

2.5.5 Reaction kinetics and induction time

The progress of clinker hydration is commonly classified into five stages, namely pre-induction period, induction (dormant) period, acceleration period, deceleration period and steady state period (see 2.1). This classification to a large extent is arbitrary because the kinetics of the reaction of individual phases is quite different from each other. For example, the reaction of C_2S with water shows an obvious dormant period, while the reaction of C_3A alone with water progresses rapidly. If gypsum is added intentionally to regulate the reaction speed of C_3A, it is significantly impeded, resulting in an obvious dormant period as well. Even so, the reactions of C_3A in real cement pastes still proceed more rapidly than those of C_3S and C_2S (Hewlett, 1998).

An induction time, a parameter given by the user, is used to simulate the burst of reaction after the pre-induction and induction periods (Bentz, 1997). It is taken valid for all clinker phases. Value of this parameter should be adjusted according to some experimental measurements. It is used in turn to make long-term predictions of the cement hydration.

A further attempt to model the induction period of cement hydration is to correlate the early-time dissolution probabilities for all of the cement clinker phases (C_3S, C_2S, C_3A and C_4AF) to the square of the amount of C-S-H that has formed (Bentz, 2000). As the C-S-H volume

fraction increases, the calculated dissolution probabilities cannot exceed the base dissolution probabilities (P^0, set beforehand empirically in the program). For pure C_3S hydration, a linear correlation between the dissolution probability and the square of the C-S-H quantity is found, while for cement, a better agreement to early time heat release is obtained using a parabolic instead of a linear proportionality (Bentz, 2000).

The model is operated on a cycle basis and no time dependent factors are hence taken into account, so the model results are not ready for use in a real time consideration. In order to relate the time-dependent microstructure and the corresponding material properties to real time, the calculation cycles are related to the real time by using a quadratic relation given by Bentz (1997) and based on the parabolic hydration kinetics:

$$t = B \cdot (cycles)^2 \tag{2.34}$$

in which t is the real time (in hour); B is the time conversion factor (in hour/cycle^2) and "cycles" are the number of executed calculation or model cycles.

The kinetic equation has been calibrated for U.S. CCRL, French Montalieu Portland cement (Bentz, 1997) and for two Dutch cements ENCI CEM I 32.5 and CEM I 52.5 (Van Eijk, 2001). This is done by using different experimental techniques to measure the hydration degree in real hydrating systems and relating the results to the degree of hydration given by the model. The determined values for "B" range from 0.3×10^{-3} to 1.7×10^{-3} hour/cycles^2.

2.5.6 Model applications

The model has been confirmed to be a useful tool in designing cement recipes because one can easily vary the w/c ratios, the amount and the PSD of cement and additives. Furthermore, the simulation can be performed assuming different environmental conditions such as variable temperatures and water saturated or sealed curing. These possibilities have been used to investigate temperature rise in silica fume pastes (Bentz et al., 1998) and the relation between cement PSD, w/c ratio and achievable degree of hydration and strength (Bentz et al., 1999; Bentz and Haecker, 1999). Studying the percolation and permeability aspects is possible because the obtained digital microstructure gives a 3-D representation of porosity and hydration products. Information about percolation and permeability can be obtained by looking at interconnectivity between one phase (pores or C-S-H) throughout the structure. From this information, one can predict relative diffusivities and leaching properties (Bentz and Garboczi, 1992; Van Eijk and Brouwers, 1998).

Princigallo et al. (2003) used CEMHYD3D to simulate the hydration kinetics of cement, porosity of the cement paste, percolation of solid phases and effect of particle size on the degree of hydration. Good agreements between the experimental measurements and the model predictions are found. Marchand et al. (2001) used CEMHYD3D to investigate the influence of calcium hydroxide dissolution in water on the transport properties of hydrated cement systems. The results of the numerical simulations are in good agreement with data of calcium leaching experiments performed in deionized water. Brouwers and Van Eijk (2003) used the model outputs of CEMHYD3D to predict the alkali concentration in the pore fluid in hydrating cement paste. Information of hydration degree of cement and amount of free water is obtained from the model. This concept of alkali release, decrease of pore solution volume and sorption by C-S-H is further incorporated into the computer model. Van Eijk and Brouwers (2001) used CEMHYD3D to investigate the long-term effects of contaminants in solidified waste on cement hydration by numerically simulating cement hydration and precipitation/dissolution of metal salts on the surface of cement grains. The composition of pore solution composition is predicted. The strength development predicted by the model is found to agree qualitatively with experimental results found in literature. The computer model is useful in predicting the strength and leaching resistance of solidified products and developing solidification recipes based on cement.

Chapter 3

Reaction models for alkali-activated slag[1]

3.1 Introduction

The chemistry of slag reaction in cement is much less well understood than the Portland cement hydration, although continuous efforts have been made since its application in construction. The lack of fundamental knowledge on the reaction of slag obstructs the explanations for the phenomena observed in experiments and practice, and impedes its further application in construction. Therefore, theories on the reaction of slag in cement are valuable, especially when applying new advancements in cement chemistry to slag cement, for example, computer modeling and long-term property prediction.

In this chapter, theoretical models are proposed for the reaction of AAS, which is taken to be the reaction of pure slag. These models can quantify the hydration products and determine their compositions. Together with the physical properties of the hydration products, the models can predict some microstructural characteristics of hydrating AAS pastes, such as chemical shrinkage, water binding and porosity. These properties are important when evaluating long-term performance of slag cement paste.

Models established in this chapter are validated with a number of experiments on AAS selected from literature. The models are further applied to calculate the water retention by the hydration products of AAS and sequentially to derive its hydration equation. Chemical shrinkage of the AAS paste in different hydration states is predicted. Methods for predicting the phase distributions on a volume basis in the hardened AAS pastes are proposed. The knowledge obtained in this chapter is also used in Chapter 4 of this research, in which reaction models for the slag-blended cement are developed.

3.2 Hydration models

Three reaction models for quantifying the hydration products and determining the composition of the main hydration product (C-S-H) are proposed based on stoichiometric calculations between the initial material (in glass) and the hydration products, i.e. the quantitative relationship between the reactants and the hydration products. These models consider different degrees of aluminum substitution for silicon in C-S-H. In this chapter, the oxides contained in the crystalline minerals are subtracted from the total oxides because they are not hydraulic, so that only the oxides in glass form are reactive. These oxides are assumed to be the only reactive part of the slag, which will hydrate congruently, and the crystalline minerals are considered inert during the hydration process of slag.

Two assumptions are introduced into the models:

1. Slag grain is a homogeneous mixture of all oxides; only the oxides in the glass are reactive (i.e. oxides in the crystalline minerals are inert).
2. All oxides in the glass react congruently to a number of hydration products which are selected based on the observations in experiments in literature.

[1] Parts of this chapter were published elsewhere (Chen and Brouwers, 2007a).

.

Table 3.1: Molar balance of oxides in hydration products of AAS.

Hydration product	Formula	Quantity	Molar balance								
			C	S	A	M	$\bar{S}$	F	H (105°C)	H (80% RH)	H (100% RH)
C-S-H	$C_{\hat{a}}SA_{\hat{b}}H_g$	n_{C-S-H}	$\hat{a}$	1	$\hat{b}$				$\hat{a}$	$\hat{a}+0.8$	$\hat{a}+1.5$
Hydrotalcite	M_5AH_{13}	n_{HT}			1	5			7♮	13♮	19♮
Hydrogarnet	$C_6AFS_2H_8$	n_{HG}	6	2	1			1	8	8	8
Ettringite	$C_6A\bar{S}_3H_{32}$	n_{AFt}	6		1		3		8	32	36
Strätlingite	C_2ASH_8	n_{ST}	2	1	1				8	8	8
Tetracalcium aluminate hydrate	C_4AH_{13}	n_{AH}	4		1				7	13	19

♮:Estimated value assuming the hydrotalcite and the tetracalcium aluminate hydrate have the same water binding characteristics, see text.

The moles of oxides from the glass part of slag can be calculated as:

$$n_i^{sl} = \frac{m_i^{sl}}{M_i} = \frac{m^{sl} \cdot [x_i^{sl} - \sum_j (x_j^{cr} \cdot x_{i,j}^{cr})]}{M_i} \tag{3.1}$$

in which n_i^{sl} is the moles of oxide i in the glass part of slag, m_i^{sl} is the mass of oxide i in the glass, M_i is the molar mass of oxide i, m^{sl} is the mass of slag, x_i^{sl} is the mass fraction of oxide i in slag, x_j^{cr} is the mass fraction of crystalline mineral j in the slag and $x_{i,j}^{cr}$ is the mass fraction of oxide i in the crystalline mineral j. If the crystalline minerals in the slag are not identified, they are taken to be merwinite (C_3MS_2) since it is the most common one observed in slag (Smolczyk, 1980). The value of $x_{i,j}^{cr}$ can be calculated from the chemical formula of the mineral. For example, the crystalline mineral merwinite (C_3MS_2) contains 51.2 m/m% C, 12.2 m/m% M and 36.6 m/m% S.

Among the selected hydration products (C-S-H, M_5AH_{13}, $C_6AFS_2H_8$, $C_6A\bar{S}_3H_{32}$, C_4AH_{13} and C_2ASH_8), hydrotalcite is the only magnesium-containing phase and all M reacts into it. Similarly, all iron oxide reacts into the hydrogarnet phase and all sulfates into ettringite.

Based on the chemical formula of each hydration product (Table 3.1), molar balances of major oxides in the product are readily determined. Water contents of the hydration products in different hydration states are also included in Table 3.1 based on the discussions in the previous section.

Using the molar balance of each oxide between the initial material and the hydration products, Eqs. (3.2)–(3.7) are established:

$$\hat{a} \cdot n_{C-S-H} + 6n_{HG} + 4n_{AH} + 2n_{ST} = n_C^{sl} \tag{3.2}$$

$$n_{C-S-H} + 2n_{HG} + n_{ST} = n_S^{sl} \tag{3.3}$$

$$\hat{b} \cdot n_{C-S-H} + n_{HT} + 4n_{HG} + n_{AFt} + n_{AH} + n_{ST} = n_A^{sl} \tag{3.4}$$

$$3n_{AFt} = n_{\bar{S}}^{sl} \tag{3.5}$$

$$5n_{HT} = n_M^{sl} \tag{3.6}$$

$$n_{HG} = n_F^{sl} \tag{3.7}$$

in which n_{C-S-H}, n_{HT}, n_{HG}, n_{AFt}, n_{AH} and n_{ST} are moles of the hydration product C-S-H, hydrotalcite, hydrogarnet, ettringite, tetracalcium aluminate hydrate and strätlingite, respectively; n_C^{sl},

n_S^{sl}, n_A^{sl}, n_M^{sl}, $n_{\bar{S}}^{sl}$, and n_F^{sl} are moles of the oxides contained in the glass content of slags, calculated with Eq. (3.1).

Based on Eqs. (3.5)–(3.7), the quantities of the hydrotalcite phase, ettringite and the hydrogarnet phases readily follow that:

$$n_{AFt} = \frac{n_{\bar{S}}^{sl}}{3} \tag{3.8}$$

$$n_{HT} = \frac{n_M^{sl}}{5} \tag{3.9}$$

$$n_{HG} = n_F^{sl} \tag{3.10}$$

Substituting n_{AFt}, n_{HT} and n_{HG} from Eqs. (3.8)–(3.10) into Eqs. (3.2)–(3.4) yields:

$$\hat{a} \cdot n_{C-S-H} + 4n_{AH} + 2n_{ST} = n_C^{sl} - 2n_{\bar{S}}^{sl} - 6n_F^{sl} = n_C' \tag{3.11}$$

$$n_{C-S-H} + n_{ST} = n_S' \tag{3.12}$$

$$\hat{b} \cdot n_{C-S-H} + n_{AH} + n_{ST} = n_A^{sl} - \frac{n_{\bar{S}}^{sl}}{3} - \frac{n_M^{sl}}{5} - n_F^{sl} = n_A' \tag{3.13}$$

in which n_C', n_S' and n_A' practically represent the quantities of C, S and A available for the hydration products C-S-H and the AFm phases (C_4AH_{13} and C_2ASH_8). By eliminating n_{C-S-H} from Eqs. (3.11)–(3.13), following equations are obtained:

$$4n_{AH} + (2 - \hat{a}) \cdot n_{ST} = n_C' - \hat{a} \cdot n_S' \tag{3.14}$$

$$n_{AH} + (1 - \hat{b}) \cdot n_{ST} = n_A' - \hat{b} \cdot n_S' \tag{3.15}$$

Solving Eqs. (3.14) and (3.15) simultaneously gives:

$$n_{AH} = \frac{(1-\hat{b})n_C' - (\hat{a} - 2\hat{b})n_S' - (2-\hat{a})n_A'}{\hat{a} - 4\hat{b} + 2} \tag{3.16}$$

$$n_{ST} = \frac{-n_C' + (\hat{a} - 4\hat{b})n_S' + 4n_A'}{\hat{a} - 4\hat{b} + 2} \tag{3.17}$$

Substituting n_{AH} and n_{ST} from Eqs. (3.16) and (3.17) into Eq. (3.11), n_{C-S-H} now reads:

$$n_{C-S-H} = \frac{n_C' - 2n_S' - 4n_A'}{\hat{a} - 4\hat{b} + 2} \tag{3.18}$$

In the system above (Eqs. (3.16)–(3.18)), there are five unknowns and three equations. Therefore, extra conditions are needed to solve the system. As the C_4AH_{13} and C_2ASH_8 are rarely both found in the mature AAS pastes in experiments, their formations are considered alternatively, corresponding to different cases in the models. Furthermore, variable degrees of A substitution in C-S-H are considered.

Richardson et al. (1994) found a linear increase of A/C ratios with S/C ratios in single-phase C-S-H. A general model is proposed for the structure of the substituted C-S-H, in which aluminum substitutes for silicon in the bridging tetrahedral of the structure. This model is later confirmed by Wang and Scrivener (2003) by using Nuclear magnetic resonance (NMR) technique. In a more recent work of Richardson (1999), based on the observations in a series of slag-blended cement pastes, a general relationship for the A/C and S/C ratios in the C-S-H is proposed as:

$$S/C = 0.4277 + 4.732 \cdot A/C \tag{3.19}$$

First, a model, designated **Model 1**, is proposed, in which no aluminum substitution for silicon in C-S-H is considered. This model is a simplified one because the A substitution for S most likely takes place in AAS pastes. Then, the aluminum substitution in C-S-H is accounted for. The molar balances of C, S and A in C-S-H are prescribed by the relation proposed by Richardson (1999) (Eq. (3.19)). Accordingly, another model, designated **Model 2**, is proposed. For some slags no AFm phases are formed in their hydration products. Hence, the third model, designated **Model 3**, is proposed. The C/S and A/S ratios in the hydration product C-S-H are taken to be free in this model. In all three models proposed, the quantities of the hydrotalcite phase, ettringite and the hydrogarnet phase always follow from Eqs. (3.8), (3.9) and (3.10), respectively.

3.2.1 Model 1: No aluminum substitution in C-S-H

In this simplified model, no A substitution for S in C-S-H is considered. Hence, $\hat{b} = 0$ in Eqs. (3.11)–(3.13). The quantities of C_4AH_{13}, C_2ASH_8 and C-S-H are now calculated from Eqs. (3.16)–(3.18) as:

$$n_{AH} = \frac{n'_C - \hat{a} \cdot n'_S - (2-\hat{a}) n'_A}{\hat{a}+2} \tag{3.20}$$

$$n_{ST} = \frac{-n'_C + \hat{a} \cdot n'_S + 4n'_A}{\hat{a}+2} \tag{3.21}$$

$$n_{C-S-H} = \frac{n'_C + 2n'_S - 4n'_A}{\hat{a}+2} \tag{3.22}$$

The system contains three equations (Eqs. (3.20)–(3.22)) and four unknowns (n_{AH}, n_{ST}, n_{C-S-H} and $\hat{a}$). In the following discussion, two cases are distinguished, depending on the formation of either C_4AH_{13} or C_2ASH_8.

First, the case pertaining to the formation of C_4AH_{13} is investigated, namely **Case 1**. Since no strätlingite is formed, $n_{ST} = 0$. From Eq. (3.21), it follows that:

$$-n'_C + \hat{a} \cdot n'_S + 4n'_A = 0 \tag{3.23}$$

Now, the C/S ratio ($\hat{a}$) reads:

$$\hat{a} = \frac{n'_C - 4n'_A}{n'_S} \tag{3.24}$$

Using the C/S ratio calculated from Eq. (3.24), n_{C-S-H} and n_{AH} are calculated as:

$$n_{C-S-H} = n'_S \tag{3.25}$$

$$n_{AH} = n'_A \tag{3.26}$$

It is shown in Eqs. (3.26) and (3.25) that the quantities of C_4AH_{13} and C-S-H are readily determined by the available A and S contents from the slags.

Then, as the second case, namely **Case 2**, the formation of C_2ASH_8 is considered and C_4AH_{13} is excluded from the hydration products, indicating $n_{AH} = 0$. Based on Eq. (3.20), the following equation is derived:

$$n'_C - \hat{a} \cdot n'_S - (2-\hat{a}) n'_A = 0 \tag{3.27}$$

Now, the C/S ratio ($\hat{a}$) reads:

$$\hat{a} = \frac{n'_C - 2n'_A}{n'_S - n'_A} \tag{3.28}$$

Similarly, substituting $\hat{a}$ into Eqs. (3.21) and (3.22) gives n_{ST} and n_{C-S-H} as:

$$n_{C-S-H} = n'_C - n'_A \tag{3.29}$$

$$n_{ST} = n'_A \tag{3.30}$$

In this model, for both cases the quantity of the AFm phase (C_4AH_{13} or C_2ASH_8) equals the amount of the available A from the slags. No aluminum substitution for silicon is considered to take place in C-S-H. Therefore, there is more A available for the formation of the AFm phases, which consumes C. Therefore, less C is available for the formation of C-S-H and the predicted C/S ratio is lower than the real ratio in C-S-H.

3.2.2 Model 2: Coupled relation between C/S and A/S ratios in C-S-H

As observed in experiments on the reaction of AAS, A enters the hydration product C-S-H and substitutes for S in the bridging tetrahedra of the dreierkette structure. So, incorporating the A substitution for S in C-S-H is important for modeling the reaction of AAS. In this model, the C/S ratio ($\hat{a}$) and A/S ratio ($\hat{b}$) in the C-S-H are coupled by the relation proposed by Richardson (Eq. (3.19)). The relation is further written as:

$$\hat{b} = (1 - 0.4277\hat{a})/4.732 \tag{3.31}$$

Similarly, two cases are considered, corresponding to the formation of C_4AH_{13} or C_2ASH_8, respectively.

First, **Case 1**, the case pertaining to the formation of C_4AH_{13}, is considered, indicating $n_{ST} = 0$. Thus, from Equation (3.21) the following equation is obtained:

$$-n'_C + (\hat{a} - 4\hat{b})n'_S + 4n'_A = 0 \tag{3.32}$$

By solving Eqs. (3.19) and (3.32) simultaneously, the C/S ratio is calculated as:

$$\hat{a} = \frac{n'_C + 0.85n'_S - 4n'_A}{1.36n'_S} \tag{3.33}$$

The A/S ratio is calculated from Eq. (3.19) as:

$$\hat{b} = \frac{-0.43n'_C + 0.99n'_S + 1.72n'_A}{7.54n'_S} \tag{3.34}$$

In this case, the quantity of C-S-H follows from Eq. (3.12) with $n_{ST} = 0$. n_{AH} is solved from Eq. (3.15) as:

$$n_{AH} = n'_A - \hat{b} \cdot n'_S \tag{3.35}$$

Because $n_{AH} \geqslant 0$ is valid for all slags, the following inequality is yielded:

$$\hat{b} \leqslant \frac{n'_A}{n'_S} \tag{3.36}$$

Substituting Eq. (3.34) into inequality (3.36) gives the condition for the formation of C_4AH_{13} as:

$$5.82n^{sl}_A + 0.43n^{sl}_C \geqslant 0.99n^{sl}_S + 1.164n^{sl}_M + 6.42n^{sl}_F + 2.8n^{sl}_{\overline{S}} \tag{3.37}$$

Inequality (3.37) is converted into the mass fraction of oxides in the slag by using the molar mass of C, S, A, M, $\overline{S}$ and F (Appendix B), yielding:

$$x_A + 0.13x_C \geqslant 0.29x_S + 0.51x_M + 0.70x_F + 0.61x_{\overline{S}} \tag{3.38}$$

Increasing the mass fractions of oxides on the left side has a positive influence on the formation of C_4AH_{13}; for the right side negative influence is expected. Hence, a conclusion can be drawn from inequality (3.38) that the AFm phase is likely formed in the hydration products from slags rich in C and A, or poor in S, M, F or $\overline{S}$.

Case 2 considers the formation of C_2ASH_8 and excludes C_4AH_{13} from the hydration products, indicating $n_{AH} = 0$. Again from Eq. (3.20) it follows:

$$(1-\hat{b})n'_C - (\hat{a}-2\hat{b})n'_S - (2-\hat{a})n'_A = 0 \tag{3.39}$$

Together with Eq. (3.19), the C/S ratio ($\hat{a}$) can be solved as:

$$\hat{a} = \frac{n'_C + 0.53n'_S - 2.53n'_A}{-0.11n'_C + 1.5n'_S - 1.27n'_A} \tag{3.40}$$

Again, the A/S ratio ($\hat{b}$) can be calculated from Eqs. (3.19) and (3.40) as:

$$\hat{b} = 0.21 + \frac{0.09(n'_C + 0.53n'_S - 2.53n'_A}{-0.11n'_C + 1.5n'_S - 1.27n'_A} \tag{3.41}$$

The quantity of C_2ASH_8 is calculated from Eq. (3.17) as:

$$n_{ST} = \frac{n'_A - \hat{b}\cdot n'_S}{1-\hat{b}} \tag{3.42}$$

The quantity of C-S-H follows from Eq. (3.18). Similar to Case 1, since strätlingite is formed, $n_{ST} \geqslant 0$. Substituting Eq. (3.42) into the inequality yields the same inequality as (3.36).

Inequality (3.36) indicates that the aluminum substitution degree in C-S-H is limited to a certain degree. This degree depends on the mineral composition of the slag, or more precisely, by the available A and S from the slag to form C-S-H and the AFm phases. This conclusion on the limit of the aluminum substitution degree in C-S-H is in line with the observation of Wang and Scrivener (2003). They found that silicon ions are occupying some of the bridging tetrahedral of the dreierkette structure in C-S-H. The aluminum substitution degree is limited due to the amount of aluminum available instead of any intrinsic limits. The authors concluded that the aluminum content from slags is firstly combined with magnesium in the hydrotalcite or potentially with calcium in the AFm phase rather than entering the C-S-H phase and increasing its A/C ratio.

Therefore, the aluminum substitution degree as coupled by Eq. (3.19) is the highest state of substitution. It should be used if the slag is relatively rich in C and A, or poor in the other oxides. If the maximum substitution degree is obtained, the remaining A combines with C (and S in the case of C_2ASH_8) to form the AFm phase. The actual substitution degree is thus determined by the amount of aluminum available. If the degree of aluminum substitution is overestimated (for example, in Eq. (3.19)) and exceeds the limit as prescribed by inequality (3.36), a negative value for the quantity of the AFm phase is yielded in this model. In this case, the third model—Model 3—should be used for modeling the slag reaction.

3.2.3 Model 3: No AFm phases in hydration products

Preliminary calculations using Model 2 show that for some slags the quantity of AFm phases (C_4AH_{13} or C_2ASH_8) may result in negative values, indicating the invalidity of Model 2 for these slags. The explanation for these negative values is that the oxide composition of the slag does not satisfy the inequality (3.38). In such cases, an alternative model is put forward, namely Model 3.

As observed in some hardened AAS pastes, neither C_4AH_{13} nor C_2ASH_8 is found (Richardson and Groves, 1992), indicating that neither of them is formed. Therefore, Model 3 is proposed,

Table 3.2: Oxide compositions of four slags selected from literature (m/m%)[§].

Oxide	Slag 1[a]	Slag 2[b]	Slag 3[c]	Slag 4[d]
C	41.7	40.2	41.45	37.7
S	37.2	35.5	35.5	37.0
A	11.0	12.6	12.15	8.4
M	7.74	9	8.34	10.8
$\overline{\text{S}}$	3.68	0	0.18	0.10
F	0.38	0.6	1.01	2.6
N	0.64	0	0.58	-
K	0.55	0	0.64	-
Total	102.89	97.9	99.85	96.6

[§]: All oxides are in the glass form;
[a]: Taken from Richardson and Groves (1992);
[b]: Taken from Wang and Scrivener (1995);
[c]: Taken from Brough and Atkinson (2002);
[d]: Taken from Häkkinen (1993).

in which the aluminum substitution for silicon in C-S-H is taken into account and no AFm phases are formed. The C/S and A/S ratios in C-S-H are no longer coupled by Eq. (3.19) and are taken to be free. Because no AFm phases are formed, $n_{AH} = 0$ and $n_{ST} = 0$. Now solving Eqs. (3.23) and (3.39) simultaneously gives the C/S ratio ($\hat{a}$) and A/S ratio ($\hat{b}$) in C-S-H as:

$$\hat{a} = \frac{n'_C}{n'_S} \tag{3.43}$$

$$\hat{b} = \frac{n'_A}{n'_S} \tag{3.44}$$

The quantity of C-S-H follows from Eq. (3.18).

On the one hand, the results derived from Model 3 are positive for all slags, thus there are no preconditions for this model about the oxide composition of slag. On the other hand, with some slags the A substitution degree (A/S) might exceed the maximum degree that follows from the Eq. (3.19). In such cases, Model 2 is used.

To conclude, Model 2 is always recommended to model the hydration of slags under investigation. If it is not applicable, most likely for slags poor in C and A, or rich in S, M, F or $\overline{\text{S}}$, Model 3 is recommended and used. The choice of models can be made beforehand based on Eq. (3.37).

3.3 Validations

To evaluate the proposed models, three slags are taken from literature, which are tested employing different techniques (Brough and Atkinson, 2002; Richardson and Groves, 1992; Wang and Scrivener, 1995). The oxide compositions of these slags are listed in Table 3.2. In Table 3.2, another slag besides the three slags is included too because it will be used in the simulations in Section 3.4.3. The oxides in the selected hydration products, i.e. S, C, A, M, $\overline{\text{S}}$ and F, are normalized to a total percentage of 100% (Table 3.3). The molar mass of each slag is also included, which is defined as:

$$M^{sl} = \sum (y_i \cdot M_i) \tag{3.45}$$

in y_i is the molar fraction of oxides i in the slag, calculated as:

$$y_i = \frac{\frac{x_i}{M_i}}{\sum(\frac{x_i}{M_i})} \tag{3.46}$$

It can be seen that the molar mass of each slag takes the value between M_C and M_S since C and S are the most abundant oxides in the glass content of slags (see Table 3.3). The C/S and A/S ratios (in moles) in the glass content of the anhydrous slags are included in Table 3.3 as well. No crystalline minerals in significant amounts are detected in all three slags, so all the oxides are in the glass form and are reactive.

Slag 1 is taken from the work of Richardson and Groves (1992), in which techniques of transmission electron microscopy (TEM) combined with electron microprobe analysis (EMPA) are used to analyze the hydration products of slag-blended cement with different slag proportions. C-S-H is found to be the most dominant product in both the "inner product" and the "outer product". The inner product of slag grains contained C-S-H of the same composition as the outer product C-S-H. It is closely mixed with an M-A rich hydrotalcite phase. Data for slag-blended cements with different slag proportions (from 0 to 100 m/m%) are collected in the experiments, while only those with the water-activated slag paste are used in this chapter since they represent the results of the pure slag reaction. The C/S ratio in C-S-H measured after 14 months hydration (w/b = 0.4, T = 20°C) is 1.18 and the A/S ratio in it is 0.11. No AFm phases are found in the pure GGBFS system although they are detected in the blended cement pastes.

Slag 2 is taken from the work of Wang and Scrivener (1995). SEM and backscattered electron (BSE) analysis combined with energy dispersive X-ray (EDX) microanalysis together with XRD is used in this research. The slag is activated with 4M NaOH solution or 2M water-glass solution with a liquid/solid ratio of 0.25 and cured at 20±2 °C or 80 °C. C-S-H is the main hydration product regardless of the activator used. Hydrotalcite is formed as well in the AAS paste. C_4AH_{13} is observed while no C_2ASH_8 is found. The A/C ratio in the C-S-H is 0.08 at the age of 1 day and increases slightly to 0.10 after 1 year curing.

Slag 3 is taken from the work of Brough and Atkinson (2002). Hydration products of slags activated with water glass or potassium hydroxide (KOH) solution are analyzed by using SEM equipped with EDX and ^{29}Si magic angle spinning nuclear magnetic resonance (MAS NMR) together with XRD. The NMR results show long-chain substituted C-S-H. The C/S ratio in C-

Table 3.3: Oxide compositions in the glass content of three slags from Table 3.2 together with their molar fractions and molar mass. Only the six selected oxides are included, after being scaled to 100%.

Oxide	Slag 1		Slag 2		Slag 3		M
	m/m%	mol%	m/m%	mol%	m/m%	mol%	
C	41	43.5	41.2	43.3	42	44.4	56.1
S	36.6	36.2	36.2	35.6	36	35.5	60.1
A	10.8	6.3	12.9	7.4	12.3	7.2	102
M	7.6	11.2	9.2	13.5	8.5	12.4	40.3
$\overline{S}$	3.6	2.7	0	0	0.2	0.1	80.1
F	0.4	0.1	0.5	0.2	1	0.4	159.6
Total	100	100	100	100	100	100	-
C/S	1.12	1.2	1.14	1.22	1.17	1.25	-
A/S	0.26	0.15	0.31	0.17	0.29	0.16	-
M^{sl}	59.46		59.01		59.27		-

Table 3.4: Quantities of hydration products of AAS and C/S ratio in C-S-H predicted with Model 1 and the measured C/S ratios in different experiments.

Hydration	Slag 1 (mol %)		Slag 2 (mol %)		Slag 3 (mol %)	
product	Case 1	Case 2	Case 1	Case 2	Case 1	Case 2
$C_{\hat{a}}SA_{\hat{b}}H$	85.06	83.91	82.55	80.46	82.91	80.98
M_5AH_{13}	5.32	5.73	6.31	7.06	5.94	6.61
$C_6AFS_2H_8$	0.33	0.36	0.44	0.5	0.91	1.01
$C_6A\overline{S}_3H_{32}$	2.12	2.28	0	0	0.11	0.12
C_4AH_{13}	7.17	0	10.7	0	10.13	0
C_2ASH_8	0	7.72	0	11.98	0	11.28
Total	100	100	100	100	100	100
C/S ($\hat{a}$)	0.7	0.95	0.68	1.08	0.72	1.09
C/S Exp.	1.18[a]		1.2[b]		1.1[c]	
A/S Exp.	0.112[a]		0.12[b]		0.125[c]	

[a]: By Richardson and Groves (1992);
[b]: By Wang and Scrivener (1995);
[c]: By Brough and Atkinson (2002);

S-H is highly variable if activated with water glass, and is about 1.1 if activated with KOH solution. Here, only the data obtained in hardened paste activated with KOH solution are used because silicon is introduced into the system when the water glass is used as activator. The A/S ratio measured in the KOH-activated slag is 0.125 at 1 year. Hydrotalcite is formed in the inner product with an M/A ratio of 5.6. C_4AH_{13} or a similar phase is found in small quantities in the KOH-activated paste.

In Table 3.2 and 3.3, another slag, namely Slag 4, is also included, which is taken from the study of Häkkinen (1993). This slag is

In the works above, the oxide compositions of slags are all given in mass fractions. They are firstly converted into mole fractions as Eq. (3.46).

First, Model 1 is applied to all three slags. The quantities of the hydration products (in molar percentages) and the C/S ratio in the C-S-H calculated by using Model 1 are listed in Table 3.4. Apparently, C-S-H is the most abundant product. Hydrotalcite exists in a significant amount as well. For all three slags, the C/S ratios corresponding to the formation of C_2ASH_8 (Case 2) accord well with the observations in hardened AAS pastes, whereas C/S ratios corresponding to the formation of C_4AH_{13} (Case 1) are generally lower than the measurements. The difference comes from the different calcium content in the two products: C_4AH_{13} contains comparably more C than C_2ASH_8, so less C is available for C-S-H.

Then, Model 2 is applied to the three slags. Quantities of the hydration products (in molar percentage) and the C/S and A/S ratios in C-S-H calculated using Model 2 are listed in Table 3.5. The C/S and A/S ratios calculated using Model 2 with all three slags agree better with the measurements than the results using Model 1. However, the quantity of the AFm phase for Slag 1 results in a negative value. The negative value indicates that it is unlikely this phase is formed in the mature paste, which is consistent with the experimental observation.

Comparing the oxide compositions of the three slags, one can see that Slag 2 and Slag 3 are relatively rich in A as compared with Slag 1. Thus, as discussed previously, the AFm phases can only be formed when there is enough A from the slag to achieve the maximum substitution degree for silicon in C-S-H. It is more likely formed from slags rich in A. Because A is also combined with M to form hydrotalcite, the hydration of slags poor in M probably also forms the

Table 3.5: Quantities of hydration products of AAS and composition of C-S-H predicted with Model 2 and the measured composition of C-S-H in different experiments.

Hydration	Slag 1 (mol %)		Slag 2 (mol %)		Slag 3 (mol %)	
product	Case 1	Case 2	Case 1	Case 2	Case 1	Case 2
$C_{\hat{a}}SA_{\hat{b}}H$	89.6	89.2	90.8	89.9	91.1	90.4
M_5AH_{13}	5.6	5.4	6.9	7.1	6.5	6.6
$C_6AFS_2H_8$	0.3	0.3	0.5	0.5	1	1
$C_6A\bar{S}_3H_{32}$	2.2	2.1	0	0	0.1	0.1
C_4AH_{13}	-2.2	0	1.8	0	1.3	0
C_2ASH_8	0	-3	0	2.5	0	1.9
Total	95.5	94	100	100	100	100
C/S ($\hat{a}$)	1.14	1.07	1.12	1.17	1.15	1.19
A/S ($\hat{b}$)	0.109	0.115	0.11	0.105	0.108	0.104
C/S Exp.	1.18[a]		1.2[b]		1.1[c]	
A/S Exp.	0.112[a]		0.12[b]		0.125[c]	

[a]: By Richardson and Groves (1992);
[b]: By Wang and Scrivener (1995);
[c]: By Brough and Atkinson (2002).

AFm phase.

To determine the formation of C_2ASH_8 or C_4AH_{13} theoretically in the mature AAS pastes is difficult. Thermodynamically C_2ASH_8 is stable with respect to C_4AH_{13} (Glasser et al., 1999). But, the existence of C_4AH_{13} is more commonly found in mature AAS pastes. The reason for the formation of C_4AH_{13} rather than C_2ASH_8 in mature AAS pastes is unclear. The high alkalinity of pore solution in the AAS paste probably favors the formation of C_4AH_{13}. Anion exchange may also take place and actually a solid solution of the AFm phases is formed. The AFm phases are generally closely mixed with C-S-H and are hard to characterize.

In general, Model 2 gives more satisfactory results than Model 1. The AFm phase (C_4AH_{13} or C_2ASH_8) is assumed in this model to be formed, which is not valid for slags low in A or high in M. For the slags for which Model 2 is not valid, Model 3 should be used for modeling.

Similarly, Model 3 is applied to the three slags selected. Neither C_4AH_{13} nor C_2ASH_8 is formed in the hydration products in this model. The C/S and A/S ratios in C-S-H are taken to be free. Quantities of the hydration products (in molar percentages) and the C/S and A/S ratios in C-S-H calculated using Model 3 are listed in Table 3.6. For all three slags, the predicted C/S and A/S ratios in C-S-H are consistent with the experimental observations. They vary slightly from the predictions of Model 2. The A/S ratios calculated with Slag 2 and 3 are slightly higher than the predictions of Model 2. Since in Model 2 the AFm phases are formed, containing some A in it, less A is available for the C-S-H and the A/S ratio is lower. As a whole, the C/S and A/S ratios calculated using Model 3 accord well with the experimental observations. Model 3 can be used if Model 2 is not valid for quantifying hydration products and determining the composition of C-S-H.

A schematic comparison between the measured and predicted C/S and A/S ratios in the hydration product C-S-H is shown in Figure 3.1a (C/S ratio) and 3.1b (A/S ratio). The C/S and A/S ratios (in moles) in the anhydrous slag are included in the figures as well. Values of C/S and A/S ratios as results of Model 1 and Model 2 are taken from the average values from Case 1 and Case 2.

On the one hand, the C/S and A/S ratios in C-S-H predicted using the proposed models are

Table 3.6: Quantities of hydration products of AAS and composition of C-S-H predicted with Model 3 and the measured composition of C-S-H in different experiments.

Hydration product	Slag 1 (mol %)	Slag 2 (mol %)	Slag 3 (mol %)
$C_{\hat{a}}SA_{\hat{b}}H$	91.63	92.44	92.26
M_5AH_{13}	5.73	7.06	6.61
$C_6AFS_2H_8$	0.36	0.5	1.01
$C_6A\bar{S}_3H_{32}$	2.28	0	0.12
C_4AH_{13}	0	0	0
C_2ASH_8	0	0	0
Total	100	100	100
C/S ($\hat{a}$)	1.04	1.2	1.2
A/S ($\hat{b}$)	0.084	0.13	0.122
C/S Exp.	1.18[a]	1.2[b]	1.1[c]
A/S Exp.	0.112[a]	0.12[b]	0.125[c]

[a]: By Richardson and Groves (1992);
[b]: By Wang and Scrivener (1995);
[c]: By Brough and Atkinson (2002).

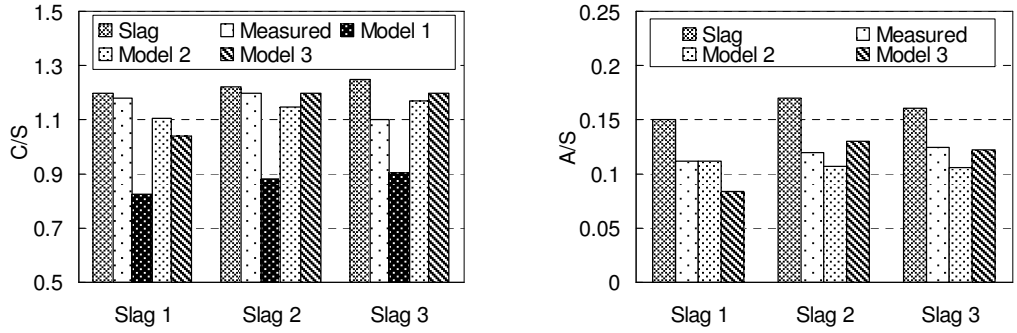

(a) (b)

Figure 3.1: The C/S and A/S ratio in slag and in the C-S-H: measured and predicted. The values for Model 1 and Model 2 are taken as the average value of the two cases. Measurements by Richardson and Groves (1992), Wang and Scrivener (1995) and Brough and Atkinson (2002).

generally in good agreement with the experimental observations. For Model 1, slightly lower values are predicted. On the other hand, these values differ considerably from the molar ratios of the respective oxides in the initial material. Therefore, for predicting the composition of C-S-H, the C/S and A/S ratios in the slags cannot be used directly, although C-S-H is obviously the most dominant product of slag hydration. Presence of the other hydration products, i.e. hydrotalcite, ettringite, hydrogarnet and AFm phases (if formed) obviously influences the composition of the main hydration product C-S-H, even though, as a total, they amount to approximately 10 percent

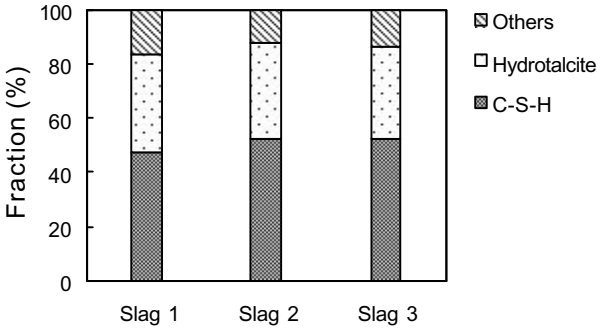

Figure 3.2: Distribution of aluminum from slag in C-S-H, hydrotalcite and all other products, following Model 2 (Slag 1 and 2) and Model 3 (Slag 3).

in moles. This influence is more prominent on the A/S ratio in C-S-H than that on the C/S ratio.

Since A is contained in all hydration products considered, its distribution can be used as an indicator for the relative amounts of the hydration products. The distribution of A from slags in the hydration products is analyzed and is shown in Figure 3.2. For Slag 1 the results from Model 3 and for Slag 2 and 3 the results from Model 2, Case 1 are used. The option of Case 1 or 2 in Model 2 does not make much difference because in both cases the AFm phase amounts less than 3% in moles and actually differs less than 1% from each other. A large part of A from the slag is shown in Figure 3.2 to enter the main hydration product C-S-H. Its quantity is comparable with that entering the other hydration products. Thus, the consideration of A substitution for S in C-S-H is of essential importance when modeling the hydration of AAS. The amount of A contained in the hydrotalcite is also remarkable, because of its relatively large amount (see Table 3.4, 3.5 and 3.6). Research has shown that the amount of aluminum in the slags might have a dominant influence on the reactivity of slags (Chapter 7). An clear relationship is observed between its distribution in the hydration products and the mechanical properties of slag cement mortars (Wassing, 2003). Using the models proposed in this thesis, the role of A from the slag in the hydration products can be clarified, providing opportunities for further revealing the influence of the oxide compositions on the reactivity of slags.

3.4 Model applications

3.4.1 Water retention

When the quantities of all hydration products are known by using the proposed model, the retained water in these products are concomitantly obtained, rendering the possibility of deriving the occurring reactions of AAS. The amount of retained water in the hydration products is calculated as:

$$n_H = \sum (H_i \cdot n_i) \tag{3.47}$$

in which n_H is the retained water in the hydration product; H_i is the water content in the hydration product, which is dependent on the hydration states and can be taken from Table 3.1; n_i is the quantity of the hydration product calculated using the proposed models.

The hydration reaction of AAS is thus written as:

$$C_{n_C^{sl}} S_{n_S^{sl}} A_{n_A^{sl}} M_{n_M^{sl}} \overline{S}_{n_{\overline{S}}^{sl}} F_{n_F^{sl}} + n_H H \rightarrow n_{C-S-H} C_{\hat{a}} S A_{\hat{b}} H_g + n_{HT} M_5 A H_{13} + n_{HG} C_6 A F S_2 H_8 + n_{AFt} C_6 A \overline{S}_3 H_{32} + n_{AH} C_4 A H_{13} + n_{ST} C_2 A S H_8 \tag{3.48}$$

Table 3.7: Retained water in the hydration products of AAS in different hydration states (g per g slag reacted).

Hydration state	Slag 1	Slag 2	Slag 3
105°C	0.21	0.20	0.20
80% RH	0.39	0.33	0.33
100% RH	0.51	0.47	0.47

Note that in the hydration equation above general formula of hydration products are used, although their water content might vary in different hydration states. The retained water in the hydration products in respective hydration states for the selected three slags is listed in Table 3.7. Again, for Slag 1 the results from Model 3 and for Slag 2 and 3 the results from Model 2, Case 1 are used. The retained water in the hydration products of AAS in the saturated state is prominently higher than that of typical Portland cement, about 0.44 g per g reacted cement at 100% RH (Taylor, 1997). This higher water content is consistent with the larger percentage of water in the hydration product hydrotalcite (about 53 m/m%) considering its relatively large amount. Collins and Sanjayan (2000) also observed this higher water retention capacity of AAS paste than Portland cement. Therefore, for achieving a high degree of AAS hydration, probably a larger initial water/binder (w/b) ratio than that of Portland cement can be preferential.

The non-evaporable water content of fully hydrated slags is around 0.20 gram per gram of reacted slag. This value is in good agreement with the measurements obtained by Song and Jennings (1999), i.e. 19.3% referred to the ignited mass, and with the measurement by Wolhuter et al. (1980), i.e. 0.19 gram per gram of reacted slag. In contrast to the saturated situation, the non-evaporable water of AAS (after being dried at 105°C) is apparently lower than that of Portland cement, which amounts to *ca.* 0.23 g per g of reacted cement (Taylor, 1997).

The procedure for deriving the hydration equation of the slag is summarized as:

1. Calculating or measuring the oxide composition in the glass part of slag; calculating the quantities of ettringite, hydrotalcite and hydrogarnet using Eqs. (3.8)–(3.10).
2. Calculating the remaining C, S and A available for the other hydration products using Eqs. (3.11)–(3.13).
3. Substituting the available quantity of C, S and A into Model 1, 2 or 3 in corresponding cases, yielding the C/S ratio (and A/S ratio in Model 2 and 3) in C-S-H and the quantities of C_4AH_{13} (or C_2ASH_8) and C-S-H.
4. Calculating the water retention by the hydration products of slag in respective hydration states using Eq. (3.47).
5. Writing the hydration equation of slag following Eq. (3.48).

3.4.2 Chemical shrinkage

Together with other hydration characteristics of the hardening cementitious system such as the non-evaporable water and heat evolution, chemical shrinkage is commonly used to follow the reaction process of slag. If the quantities of major hydration products are determined using the proposed models, their total volume can be obtained, enabling the calculation for the chemical shrinkage of AAS. Physical properties of the hydration products are listed in Table 3.8.

The physical properties of C-S-H, whose composition varies over a wide range, might vary with variable C/S ratios. In this thesis, the physical properties of C-S-H with different C/S ratios and in the saturated state are calculated using the model proposed by Brouwers (2004b). The

Table 3.8: Physical properties of hydration products of slag-blended cement in the saturated state[†].

Substance	M (g/mol)	ρ (g/cm^3)	ω (cm^3/mol)
$C_{\hat{a}}SA_{\hat{b}}H_{\hat{a}+1.5}$	Eq. (3.51)	Eq. (3.49)	Eq. (3.50)
M_5AH_{19}	645.5	2.0	322.8
C_4AH_{19}	668.4	1.8	371.3
$C_4A\bar{C}H_{12}$	564.5	1.98	284.54
$C_6A\bar{S}_3H_{36}$	1327.3	1.72	771.92
$C_6AFS_2H_8$	862.5	3.03	284.98
CH	74.1	2.24	33.05

[†] Molar mass calculated from the formula, the density of hydrotalcite after Xanthos (2005), the rest after Brouwers (2004a).

density of C-S-H is calculated as:

$$\rho_{C-S-H} = \frac{87.12 + 74.10\hat{a}}{38.42 + 33.05\hat{a}} \tag{3.49}$$

and the molar volume of C-S-H is calculated as (in cm^3/mol):

$$\omega_{C-S-H} = \frac{M_{C-S-H}}{\rho_{C-S-H}} \tag{3.50}$$

in which the molar mass of C-S-H (M_{C-S-H}) can readily be calculated from its composition as:

$$M_{C-S-H} = \hat{a} \cdot M_C + M_S + \hat{b} \cdot M_A + g \cdot M_H \tag{3.51}$$

Note that in Eq. (3.49) the A/S ratio is not included because at present the influence of A on the physical properties of C-S-H is not clear. Here, incorporating A into the C-S-H is assumed not to significantly change its density. Since incorporating A into the C-S-H will increase its molar weight, the molar volume of C-S-H increases as well. In severer hydration states, for example, oven drying at 105°C or 80% RH, the C-S-H dehydrates. Release of water from C-S-H in different hydration states will hardly change its volume (Brouwers, 2004a,b, 2005). Thus, in different hydration states, the molar volume of C-S-H stays constant.

The chemical shrinkage is defined as the volume reduction per mass of reacted slag as:

$$\Psi_s = \frac{V^{sl} + V_H - V_{hp}}{m^{sl}} = \frac{(m^{sl} \cdot \nu^{sl} + n_H \cdot \omega_H) - \sum(n_i \cdot \omega_i)}{m^{sl}} \tag{3.52}$$

in which i now stands for the hydration products; V^{sl} is the volume of initial slag in the paste; ν^{sl} is the specific volume of slag, taken to be 0.342 cm^3/g; ω is the molar volume of the substances. The amount of water in the products is taken from Table 3.7. Moles of hydration products are taken from Table 3.6 (Slag 1) and Table 3.5 (Slag 2 and 3) in different hydration states. The chemical shrinkages of the three selected slags are calculated using Eq. (3.52) (Table 3.9). The chemical shrinkage at 105°C and 80% RH can hardly be measured in experiments, but they are very relevant considering the subsequent drying after hydration and the preconditioning of the samples in experiments (D-drying or oven drying at 105°C).

As can be seen from the model predictions, the hydration of AAS results into much larger chemical shrinkage than Portland cement in the saturated state (approximately 6–9.9 mL per 100 g binder) (Czernin, 1956; Mills, 1986; Powers and Brownyard, 1948; Rößler and Odler, 1985; Tazawa et al., 1995). The trend that the chemical shrinkage increases with higher slag proportions is also observed in the experiments by Mills (1986). Extrapolation of these measurement to pure

slag (100% slag) yields the chemical shrinkage as 10.65 mL per 100 g slag, being in line with the predicted values with these methods (Table 3.9).

Larger shrinkage of AAS paste/mortar than Portland cement is observed in various studies (Collins and Sanjayan, 2000; Häkkinen, 1993). Since the chemical shrinkage normally increases the pore volume in the paste with hardly any external volume change, the shrinkage might have a dominant influence in the micro scale. Because of the self restraint (when aggregate presents), internal stress might develop due to the chemical shrinkage. Microcracks in the structure can take place, which is observed in various experiments (Andersson and Gram, 1987; Häkkinen, 1993).

3.4.3 Microstructure and porosity

Amongst other microstructural characteristics of AAS paste, such as composition, distribution and amount of hydration product, the presence of another phase in the paste, pore, is of essential importance while evaluating the performance of AAS. The porosity, pore size distribution and connectivity of pores can strongly influence the mechanical properties and durability of the paste. With the quantities of hydration product and composition of C-S-H computed using the proposed models, characterizing the microstructure development during the hydration procedure is possible if the physical properties of the products are known.

Brouwers (2004a,b, 2005) proposed two general models for the composition of C-S-H with different C/S ratios. Influence of C/S ratio on the water content in C-S-H is investigated. Two levels of gel water in C-S-H are proposed, namely constant "gel" water and variable "gel" water. Since until now the water content in C-S-H with variable C/S ratios is yet not well known, both models could be valid. Here, the model with the constant "gel" water is first used. While the procedures for calculation using the two different models are the same with each other, the option of these models yields significantly different results. Later, results using the other model are compared with those using the constant "gel" water model.

For the first model, where constant gel water in C-S-H is assumed, the gel porosity of C-S-H is calculated from its composition as (Brouwers, 2004a,b, 2005):

$$\Phi_{C-S-H} = \frac{32.44}{94.60 + 33.05(\hat{a} - 1.7)} \tag{3.53}$$

Again, incorporating A into C-S-H is assumed not to affect the gel porosity of C-S-H. Substituting a typical value for the C/S ratio of C-S-H from AAS, for example, 1.1, into Eq. (3.53) yields a porosity of 44.6%. The predicted gel porosity is much higher than the porosity of C-S-H from the hydration of calcium silicate in Portland cement (33%–38%), having a higher C/S ratio of about 1.7 (Brouwers, 2004a,b, 2005).

According to the classification of Mindess and Young (1981), the gel pores mainly comprise those with sizes smaller than 10 nm (see Table 2.3). Hence, it is reasonable to believe that a large part, probably most, of the gel pores in C-S-H have sizes smaller than 10 nm. Considering the large amount of C-S-H in the hardened AAS paste, it would be expected that in view of the AAS paste, a large part of pores are gel pores (size $\leqslant$ 10 nm). This conclusion is also in line with the observations in various researches (Collins and Sanjayan, 2000; Häkkinen, 1993; Shi, 1996).

Table 3.9: Chemical shrinkage of AAS in different hydration states (mL per 100 g slag reacted).

Hydration state	Slag 1	Slag 2	Slag 3
105°C	-5.9	-2.0	-2.0
80% RH	3.3	5.9	5.8
100% RH	11.5	13.9	13.7

Assuming all and only the pores in C-S-H are gel pores and they have the size 0–10 nm, the volume of gel pores in AAS paste is:

$$V_{gp} = V_{C-S-H} \cdot \Phi_{C-S-H} = n_{C-S-H} \cdot \omega_{C-S-H} \cdot \Phi_{C-S-H} \tag{3.54}$$

For simplification, among the models proposed in the preceding sections, Model 3 is selected here for the illustration purpose. Thus, practically the number of moles of C-S-H can be represented by:

$$n_{C-S-H} = n_S^{sl} - 2n_F^{sl} \tag{3.55}$$

Substituting Eq. (3.55) into Eq. (3.54) and considering the total volume of initial paste gives the gel porosity as:

$$\Phi_{gp} = \frac{V_{C-S-H} \cdot \Phi_{C-S-H}}{V^{sl} + V_{w0}} \tag{3.56}$$

The capillary pores are considered as those with the sizes ranging from 10 to 500 nm (Mindess and Young, 1981). If the sample is cured in the saturated state, water is always available for the hydration. Self-desiccation thus does not take place. All capillary pores are consequences of the chemical shrinkage and the remaining water in the system. Since the hydration proceeds under saturated conditions, extra water can always imbibe, enabling full hydration of the slag. In addition, as discussed previously, the chemical shrinkage of the reaction creates internal pores. Hence, the capillary porosity in case of full hydration of slag can thus be calculated as

$$\begin{aligned}\Phi_{cp} &= \frac{V^{sl} + V_{w0} - V_{hp}}{V^{sl} + V_{w0}} = \frac{m^{sl} \cdot \nu^{sl} + m_{w0} \cdot \nu_w - V_{hp}}{m^{sl} \cdot \nu^{sl} + m_{w0} \cdot \nu_w} \\ &= \frac{m^{sl} \cdot \nu^{sl} + w/b \cdot m^{sl} \cdot \nu_w - V_{hp}}{m^{sl} \cdot \nu^{sl} + w/b \cdot m^{sl} \cdot \nu_w} = 1 - \frac{1}{m^{sl} \cdot \nu_0} \sum (n_i \cdot \omega_i)\end{aligned} \tag{3.57}$$

in which $\nu_0 = \nu^{sl} + w/b \cdot \nu_w$, the specific volume of the initial paste; w/b is the water/binder ratio; V_w and m_{w0} are the volume and mass of water in the initial paste; ν_w is the specific volume of water, equal to 1 cm^3/g. The total porosity (sum of gel and capillary porosities) of the paste reads:

$$\Phi = \Phi_{gp} + \Phi_{cp} \tag{3.58}$$

A detailed calculation at the paste level using models proposed in this chapter yields the phase distribution in the hardened paste on a volume basis (Table 3.10). In the computation, the slag is assumed to react completely. Slag 1 is taken as example for computation. In the computation, air voids formed due to the initially entrapped air are not taken into account because they might migrate to the surface of the paste due to bleeding. Model 3 is used to model the hydration of slag. The w/b ratio of the paste is 0.5.

The model predictions are compared to the measurements in experiments by Collins and Sanjayan (2000) (Table 3.10). The slag used in the experiments has the similar composition as Slag 1. The w/b ratio of the paste is also 0.5. However, the samples in the experiments are exposed to 50% RH for up to 56 days. Obvious drying shrinkage is observed during experiments. Hence, the conditions that the paste is subject to in the experiments are not exactly the same as those used in the computation. Furthermore, considering the age of curing, complete reaction of slag can hardly be achieved. However, a comparison between the measurements and predictions shows fairly good agreements.

C-S-H is shown to be the most dominant product in the paste on a volume basis, followed by hydrotalcite and ettringite. The level of the Fe-containing hydrogarnet phase is minor. An important characteristic of the microstructure, the distribution of pores, is revealed using the

models. In both the predictions and the measurements, most pores in AAS paste are shown in the range of gel pores (67.5% and 79.2%, respectively). The predicted pore distribution is further compared to the experimental results by Häkkinen (1993) using mercury intrusion porosimetry (MIP). In the experiments, it is found that most of the pores in AAS mortar are in the range of gel pores and the volumetric ratio of gel pores to capillary pores is about 2.3, calculated by assuming the gel pore size is smaller than 10 nm. The calculation using the proposed model yields the ratio 2.2. In the studies by Collins and Sanjayan (2000) and by Häkkinen (1993), the pore size distribution of Portland cement paste is also measured. Both gave similar results: for Portland cement paste, most of the pores are in the range of capillary pores. Therefore, although the C-S-H from AAS hydration has larger gel porosity than the C-S-H from Portland cement hydration, from the viewpoint of the paste, most of the pores in AAS paste exist as gel pores. The capillary porosity of AAS paste is much lower than that of the Portland cement paste. As capillary pores are generally considered responsible for mass and water transfer in the paste, the hardened AAS paste is expected to have good resistance to release or ingress of substances. This can in turn explain the good performances of AAS concrete.

The predicted total porosity of the paste using the model is significantly higher than the measurement in the experiment. This would be expected because the drying shrinkage reduces the bulk volume of the paste; hence, the microstructure is compressed. The difference in capillary porosity is more prominent than that in the gel porosity. The computation of Collins and Sanjayan (2000) showed that at 50% RH, almost all the capillary pores are dry while parts of the gel pores are still filled with water. Hence, drying shrinkage can be more severe in capillary pores than in gel pores, which in turn reduces the capillary porosity.

In the other model for C-S-H, namely variable "gel" water model, proposed by Brouwers (2004a,b, 2005), the gel porosity of C-S-H in the saturated state is calculated as:

$$\Phi_{C-S-H} = \frac{32.44\hat{a} - 22.71}{65.49\hat{a} - 16.73} \tag{3.59}$$

A calculation using Eq. (3.59) and following the same procedure as in the first part of this section yields a comparable total porosity of 34.5%. However, the distribution of the pores is different. The calculated gel porosity amounts to 9.5% and the capillary porosity to 25%. In other words, 72% of the pores are in the range of capillary pores. This fraction of capillary pore is significantly higher than the measurement in experiments (Collins and Sanjayan, 2000; Häkkinen, 1993; Shi, 1996). Hence, the model with constant gel water for C-S-H seems in line the best with the

Table 3.10: Predicted phase distribution in hardened AAS paste and measured porosities by Collins and Sanjayan (2000).

Substance/property	Prediction	Measurement
Product proportion (vol %)		
C-S-H	57.7	-
M_5AH_{13}	16.3	-
$C_6AFS_2H_8$	1.3	-
$C_6A\overline{S}_3H_{32}$	12.8	-
C_4AH_{13}	0	-
C_2ASH_8	0	-
Gel porosity (%)	25.7	19.7
Capillary porosity (%)	11.9	4.5
Total porosity (%)	37.6	24.3

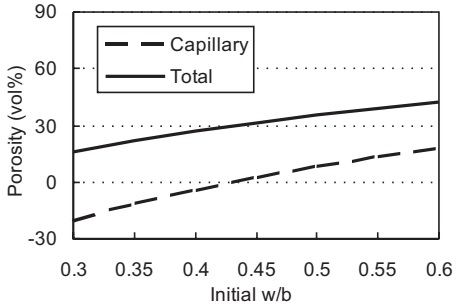

Figure 3.3: Predicted relationship between the total porosity, capillary porosity and the initial w/b ratio (Slag 1, Model 3).

experimental observations.

The initial w/b ratio has a dominant influence on the total porosity of the hardened paste because it determines the initial and capillary porosity in the system. As the hydration proceeds, these pores will be partially or completely occupied by the hydration products. The total porosity of AAS paste (Slag 1) at full hydration in the saturated state is plotted versus the initial w/b ratio in Figure 3.3. With higher initial w/b ratios, the total porosity of the hydrated structure is larger. As larger porosity is generally related to lower compressive strength of the hydrated paste, low w/b ratios would be preferred when designing the recipe, as is the case for Portland cement as well.

However, this is not necessarily true if the other factors influencing the hydration process of AAS pastes are considered. When a low initial w/b ratio is used, the starting microstructure is more compact, generating a denser barrier for water intrusion while hydration process proceeds. Therefore, the hydration process might progress at a lower rate than pastes with high initial w/b ratios. Furthermore, as shown in the relationship between the initial w/b ratio and the capillary porosity (Figure 3.3), if the w/b ratio is lower than a certain value (in the case of Slag 1, roughly 0.4), the capillary porosity is negative, indicating all the initial pores and pores generated by chemical shrinkage are occupied by the hydration products. When this full occupation takes place, further hydration of slag ceases or can only progress at a very low rate. Hence, combined with the conclusions on the water retention by AAS, larger initial w/b ratio (in case of Slag 1, $w/b > 0.4$) can be preferred with respect to full hydration of slag.

Summarizing, for achieving both complete reaction of slag in the paste and a dense microstructure (minimum capillary porosity), a w/b ratio of about 0.45–0.5 is recommended (see Table 3.7 and Figure 3.3). However, special attention should be paid to the potentially high chemical shrinkage.

3.5 Conclusions

Based on the investigations in this chapter, the following conclusions can be drawn:

1. The main hydration products in hardened AAS paste include C-S-H, a hydrotalcite phase, a hydrogarnet phase, tetracalcium aluminate hydrate, strätlingite and ettringite. C-S-H is the main hydration product. The quantities of the hydrotalcite, hydrogarnet and ettringite follow from the oxide content of M, F and $\overline{\text{S}}$ in the slag (Eqs. (3.8)–(3.10)), respectively.
2. The aluminum from the slag is first combined with the M, F and $\overline{\text{S}}$ to form the hydrotalcite, hydrogarnet and ettringite. The remaining A goes into the C-S-H for substituting the S.
3. The A substitution for S in C-S-H is limited to a certain degree structurally related to the

C/S ratio as given by Richardson (1999) and in Eq. (3.19). When there is sufficient A from the slag to achieve the maximum substitution degree in C-S-H, the remaining A reacts to the AFm phases (C_4AH_{13} or C_2ASH_8). The formation of the AFm phases more likely occurs with slag high in A and/or low in M.

4. The C/S and A/S ratios in the hydration product C-S-H are different from the C/S and A/S ratios in the initial material (slag). Although C-S-H is the most dominant hydration product, the presence of other products affects its composition significantly.
5. Three stoichiometric models are proposed, which can quantify the hydration products of AAS and determine the composition of C-S-H based on the mineral compositions of slags. Predictions of the models are consistent with the experimental observations.
6. With the proposed models, the retained water in the hydration products of AAS can be calculated in different hydration states. Accordingly, the hydration equation can be derived. The hydration of AAS exhibits a higher water demand than that of the Portland cement, but in the D-dried state (or being heated to 105°C), the AAS paste retains less water.
7. In the saturated state, the chemical shrinkage of AAS is significantly higher than that of Portland cement, which specially considered in its application.
8. The C-S-H from the AAS hydration has higher gel porosity than C-S-H from the Portland cement hydration. Most of pores in hardened AAS paste are in the range of gel pores. The AAS paste thus has a finer microstructure than the Portland cement paste.

Chapter 4

Reaction models for slag-blended cement[2]

4.1 Introduction

GGBFS is commonly blended with Portland cement or clinker to produce slag-blended cement after being ground to the fineness comparable to Portland cement used in construction practice. The two ingredients (Portland cement and slag) hydrate at different rates and their reactions interact with each other.

Efforts have been made to model the hydration of slags by using stoichiometry calculations. Taylor (1997) proposed a method for calculating the quantity of hydration product of slag. All the magnesium is assumed to enter the hydrotalcite and silicon to enter C-S-H. For facilitating this calculation, the C/S and A/C ratios in C-S-H are assumed beforehand to be 1.55 and 0.045, respectively. Richardson et al. (2002) investigated the stoichiometry of the reaction between slag and CH. Both the compositions of the hydration products and the consumption data of slag and CH are measured by using thermogravimetric analysis (TGA), SEM and XRD. Based on the compositions of the hydration products, the molar ratio between the reacted slag and CH are derived by using a molar balance calculation. The obtained molar ratios are compared to the measured data. An estimated hydration stoichiometry ratio (2.6 moles of CH consumed by each mole of slag reacted) is proposed. The C/S ratio in C-S-H is set beforehand to a value of 1.42.

However, the predetermination of C/S and A/C (or A/S) ratios in C-S-H, as used in aforesaid researches, is only applicable for particular slag proportions in the blended cement. Richardson and Groves (1992) found that the composition of C-S-H is clearly influenced by the slag proportions in the blended cement. They found that increasing slag proportions resulted in decreasing C/S ratios and increasing A/S ratios in C-S-H. Therefore, the stoichiometry proposed by Taylor (1997) and Richardson et al. (2002) is only applicable to some specific slag/clinker or slag/CH ratios.

Modeling the hydration of slag-blended cement is important for simulating the microstructure development and predicting some hydration-related properties like heat release, water-binding and chemical shrinkage. Outputs of the models can be used for further purpose, such as evaluating the durability of concrete, predicting strength and modeling the chemical composition of the liquid phase in concrete. Although there are some studies aiming to reveal the interaction between slag and pure CH, to the author's knowledge, studies on the overall hydration of slag-blended cement pertaining to their interactions are not sufficient, yet.

In this chapter, three general reaction models for slag-blended cement are proposed based on stoichiometry calculations. They correlate the compositions of the anhydrous slag-blended cement (the mineral compositions of the slag and Portland cement and the blending proportions) with the quantities and compositions of the hydration products. Mutual influence of the hydration of the two types of binders (slag and Portland cement) is investigated. The different hydration rates between the slag and Portland cement are accounted for.

The stoichiometric models are further used to predict some specific characteristics of hydrating slag cement pastes, including the fraction of products, water retention, chemical shrinkage

[2]Parts of this chapter were published elsewhere (Chen and Brouwers, 2007b).

and porosities of the pastes. These properties are either difficult to measure in practice, or available in experiments for validating the models. The models are validated with measurements in a series of experiments investigating slag-blended cements with various ingredients. The model predictions are compared to the measured data and good agreements are observed.

4.2 Stoichiometric models for slag cement hydration

Stoichiometric models for slag cement hydration are developed with the oxide compositions of the initial materials and their proportions in the mix. The hydration of the two constituents (slag and Portland cement) is first investigated separately, although they are homogeneously mixed in the cement and interact with each other. Then, models are established considering the interaction of their hydration products.

4.2.1 Reaction of pure slag

For the slag in the blended cement, the masses and moles of oxides in the glass are calculated in a similar way to Eq. (3.1) in Chapter 3 with additional consideration to the fraction of slag in the cement as:

$$n_i^{sl} = \frac{m_i^{sl}}{M_i} = \frac{m^{sl} \cdot [x_i^{sl} - \sum_j x_j^{cr} \cdot x_{i,j}^{cr}]}{M_i} = \frac{m \cdot \lambda \cdot [x_i^{sl} - \sum_j x_j^{cr} \cdot x_{i,j}^{cr}]}{M_i} \tag{4.1}$$

in which n_i^{sl} and m_i^{sl} are the mass and moles of oxide i (C, S, A, etc.) in the glass phase of slag in the cement, respectively; M_i is the molar mass of oxide i (see Appendix B); m^{sl} is the mass of slag in cement; x_i^{sl} is the mass fraction of oxide i in slag; x_j^{cr} is the mass fraction of crystalline mineral j in the slag; and $x_{i,j}^{cr}$ is the mass fraction of oxide i in mineral j. λ is the mass fraction of slag in the blended cement, which is defined as:

$$\lambda = \frac{m^{sl}}{m} = \frac{m^{sl}}{m^p + m^{sl}} \tag{4.2}$$

in which m^p is the mass of Portland cement. The masses of slag and clinker in the blended cement thus read:

$$m^{sl} = m \cdot \lambda \tag{4.3}$$

$$m^p = m \cdot (1 - \lambda) \tag{4.4}$$

If $\lambda = 0$, the cement is apparently neat Portland cement, and if $\lambda = 1$ the cement is pure slag and Eq. (4.1) turns into Eq. (3.1). The pure slag normally exhibits very weak hydraulic capability without alkali-activation.

Only the oxide in the glass phase of slag is considered because that contained in the crystalline minerals is not hydraulic and is thus deducted from the total.

For the same reasons in Section 3.2, the moles of products ettringite, hydrotalcite and hydrogarnet follow from Eqs. (3.8)–(3.10) in Chapter 3. The reaction equation accounting for the other hydration products of slag is written as:

$$C_{n'_C} S_{n_S^{sl}} A_{n'_A} + n_H H \rightarrow n_S C_{\hat{a}} S A_{\hat{b}} H_g + n_{AH}^{sl} C_4 A H_{13} \tag{4.5}$$

Methods for computing the parameters like n'_C, n_S^{sl}, n'_A, $\hat{a}$, $\hat{b}$ and n_{AH}^{sl} are given in Chapter 3. In Eq. (4.5) the product C_4AH_{13} is taken instead of the other possible product C_2ASH_8 because the latter is incompatible with CH, one of the main products from clinker hydration (Macphee et al., 1989). For some slags, neither products are formed (Richardson and Groves, 1992).

Substitution of S by A in the bridging tetrahedral of a dreierkette structure in C-S-H takes place in slag-blended cement as well (Richardson, 2000; Wang and Scrivener, 2003). The max-

imum degree of aluminum substitution follows the same equation as Eq. (3.19) in Chapter 3. If the maximum degree of substitution in C-S-H is achieved, the remaining A is combined with C to form C_4AH_{13} (see Section 3.2). The formation of C_4AH_{13} thus highly depends on the amount of the A in the slag. C_4AH_{13} is formed if the quantity of A in the slag is adequate for the formation of ettringite and hydrotalcite and for the maximum degree of substitution in C-S-H.

4.2.2 Reactions of calcium silicates in clinker

The exchange of CH formed by the hydration of calcium silicates with the slag hydration is important for modeling the slag cement hydration. Since the calcium silicates are the most abundant constituents in Portland cement, only the hydration of calcium silicates in Portland cement is coupled with the slag hydration. CH produced by their hydration is considered available for the slag hydration. Furthermore, since most reaction models available for Portland cement hydration are based on the hydration of individual clinker phase (Brouwers, 2004b, 2005; Taylor, 1997; Young and Hansen, 1987), the hydration of calcium silicates is assumed not to interact with the hydration of the other clinker phases (aluminate and ferrite) in Portland cement.

The phase composition of Portland cement is calculated quantitatively from its oxide composition by using the Bogue's equations (see Section 2.2.1) or measured experimentally by using techniques such as QXDA, microscopy and liquid extraction. The masses and moles of C_3S, C_2S, C_3A and C_4AF in Portland cement are calculated from the mass of Portland cement in the blended cement as:

$$m_i = m^p \cdot x_i = m \cdot (1-\lambda) \cdot x_i \tag{4.6}$$

$$n_i = \frac{m_i}{M_i} = \frac{m \cdot (1-\lambda) \cdot x_i}{M_i} \tag{4.7}$$

in which i is the clinker phase in Portland cement; m_i and n_i are the masses and moles of clinker phase i, respectively; x_i is the mass fraction of phase i in Portland cement; M_i is the molar mass of phase i (g/mol) (see Appendix B).

The hydration equations of C_3S and C_2S are summarized as:

$$C_3S + (1.2+g)H \rightarrow C_{1.8}SH_g + 1.2CH \tag{4.8}$$

$$C_2S + (0.2+g)H \rightarrow C_{1.8}SH_g + 0.2CH \tag{4.9}$$

In Eqs. (4.8) and (4.9), the C/S ratio in C-S-H equals 1.8, which is commonly observed in experiments (Richardson and Groves, 1992) and generally used in cement chemistry. Note that the C/S ratio used here (1.8) is considered to be the highest C/S ratio in C-S-H from the slag-blended cement hydration in the following discussions because replacing Portland cement with slag is found to lower the C/S ratio in the hydration product C-S-H (Richardson and Groves, 1992). The quantities of CH and C-S-H from the calcium silicate hydration are calculated from Eqs. (4.8) and (4.9) as:

$$n^p_{CH} = 1.2n_{C_3S} + 0.2n_{C_2S} \tag{4.10}$$

$$n^p_{C-S-H} = n_{C_3S} + n_{C_2S} \tag{4.11}$$

Reactions of the four clinker phases are treated independently. The calcium silicates react to form CH and C-S-H. The A substitution is not considered in C-S-H formed by the hydration of calcium silicate.

Modeling the interaction between the hydration of slag and calcium silicates is possible by using their hydration equations. In the following discussion, three reaction models are proposed for the hydration of slag-blended cement considering different degrees of interaction between the slag and clinker hydration.

4.2.3 Reaction models for the slag-blended cement

For modeling the hydration of slag-blended cement, the hydration degrees of slag and clinker at a certain age are important. As observed in experiments, the slag and clinker in the blended cement paste hydrate at different rates. Their hydration degrees depend on many factors such as the water/cement (w/c) ratio, temperature, reactivity of slag and the fineness of components, and thus are difficult to predict. However, for predicting the stoichiometry of the hydration reaction, the introduction of a relative hydration degree is necessary. It physically represents the ratio of the slag hydration degree to that of clinker. If the actual degree of clinker hydration is known, the slag hydration degree can be calculated by using the relative hydration degree. The actual degree of clinker hydration can be predicted by using empirical equations or numerical models.

In this chapter the clinker is assumed to hydrate completely, corresponding to a curing age of about one-year (Taylor, 1997). At this age, only part of the slag in the blended cement has hydrated, for example, about 50-70% (Battagin, 1992; Luke and Glasser, 1988; Lumley et al., 1996). Hence, with this assumption, the relative hydration degree equals the degree of slag hydration. The mass of hydrated slag is thus calculated as:

$$m^{sl,r} = \gamma \cdot m^{sl} \tag{4.12}$$

in which γ is the relative slag hydration degree, $m^{sl,r}$ and m^{sl} are the masses of the hydrated and initial slag, respectively. Hereafter, $m^{sl,r}$ is used instead of the mass of the initial slag content when calculating the moles of oxides from the hydrated slag.

Studies have shown that the amount of CH in the hardened blended cement pastes decreases with increasing slag proportions in blended cement (Macphee et al., 1989). It is even not detected if the slag proportion in the blended cement is high, indicating a complete consumption of CH by the slag hydration (Hill and Sharp, 2003; Macphee et al., 1989; Pietersen and Bijen, 1994; Regourd, 1980; Richardson and Groves, 1992). Therefore, to consider the consumption of CH by the slag hydration is important for modeling the hydration of slag-blended cement.

The moles of CH involved in the slag hydration, namely n^c_{CH}, can be the partial or total amount of CH produced by the clinker hydration. The hydration equation of the slag including this part of CH is thus written from Eq. (4.5) as:

$$C_{n'_C} S_{n^{sl}_S} A_{n'_A} + n^c_{CH} CH + n_H H \rightarrow n^{sl}_S C_{\hat{a}} S A_{\hat{b}} H_g + n^{sl}_{AH} C_4 A H_{13} \tag{4.13}$$

in which n'_C and n'_A are the quantities of C and A in the slag remaining for the C-S-H and C_4AH_{13}, which are computed with Eqs. (3.11) and (3.13).

In case that there is not adequate A from the slag to achieve the maximum substitution degree in C-S-H, C_4AH_{13} is not formed and the reaction equation reads:

$$C_{n'_C} S_{n^{sl}_S} A_{n'_A} + n^c_{CH} CH + n_H H \rightarrow n^{sl}_S C_{\hat{a}} S A_{\hat{b}} H_g \tag{4.14}$$

A molar balance calculation between the two sides of Eq. (4.14) yields the C/S and A/S ratios in C-S-H as:

$$\hat{a} = \frac{(n'_C + n^c_{CH})}{n^{sl}_S} \tag{4.15}$$

$$\hat{b} = \frac{n'_A}{n^{sl}_S} \tag{4.16}$$

If the blended cement is pure slag ($\lambda = 1$), no clinker exists in the cement and $n^c_{CH} = 0$. Eq. (4.13) is further coupled with the hydration equations of calcium silicates (Eqs. (4.8) and (4.9)) to yield

an equation as:

$$n_{C_3S}C_3S + n_{C_2S}C_2S + C_{n'_C}S_{n^{sl}_S}A_{n'_A} + n^T_H H \rightarrow (n_{C_3S} + n_{C_2S})C_{1.8}SH_g + (n^p_{CH} - n^c_{CH})CH + n^{sl}_S C_{\hat{a}}SA_{\hat{b}}H_g \quad (4.17)$$

in which n^T_H is the moles of retained water in the hydration product. This amount of water equals the amount of needed water for the hydration of blended cement.

The C/S ratios are averaged to an equilibrated value, namely $\bar{a}$, because of the compositional equilibrium in C-S-H from both Portland cement and slag hydration (Duchesne and Bérubé, 1995; Richardson and Groves, 1992). Hence, Eq. (4.17) is rewritten as:

$$n_{C_3S}C_3S + n_{C_2S}C_2S + C_{n'_C}S_{n^{sl}_S}A_{n'_A} + n^T_H H \rightarrow (n_{C_3S} + n_{C_2S})C_{\bar{a}}SH_g + (n^p_{CH} - n^c_{CH})CH + n^{sl}_S C_{\bar{a}}SA_{\hat{b}}H_g \quad (4.18)$$

Note that in the hydration equation (4.18), a distinction is made between the C-S-H from the clinker and slag hydration because A in slag is considered only available for substitution in C-S-H from the slag hydration. The C/S ratio of C-S-H ($\bar{a}$) is calculated from the molar balance as:

$$\bar{a} = \frac{3n_{C_3S} + 2n_{C_2S} + n'_C - n^p_{CH} + n^c_{CH}}{n_{C_3S} + n_{C_2S} + n^{sl}_S} = \frac{1.8(n_{C_3S} + n_{C_2S}) + n'_C + n^c_{CH}}{n_{C_3S} + n_{C_2S} + n^{sl}_S} \quad (4.19)$$

in which Eq. (4.10) is already substituted. The A/S ratio in C-S-H is calculated using Eq. (4.16).

Furthermore, for some slags and slag proportions, there is adequate A to enter the C-S-H and the maximum substitution degree for S is achieved and another equation for determining $\bar{a}$ needs to be derived. In this case, based on Eq. 3.19 in Chapter 3, the C/S and A/S ratios in C-S-H fit into:

$$\hat{b} = \frac{1 - 0.4277\bar{a}}{4.732} \quad (4.20)$$

The remaining A is combined with C to form C_4AH_{13}. The moles of C_4AH_{13} are equal to those of the available A ($n^{sl}_{AH} = n_{A,AH}$) based on its stoichiometry. Therefore, the quantity of remaining A reads:

$$n_{A,AH} = n^{sl}_{AH} = n'_A - n^{sl}_S \cdot (1 - 0.4277\bar{a})/4.732 \quad (4.21)$$

Now using the molar balance of C between the initial material and the hydration products, the C/S ratio in the C-S-H is calculated as:

$$\bar{a} = \frac{3n_{C_3S} + 2n_{C_2S} + n'_C - n^p_{CH} + n^c_{CH} - 4n^{sl}_{AH}}{n_{C_3S} + n_{C_2S} + n^{sl}_S} = \frac{1.8(n_{C_3S} + n_{C_2S}) + n'_C + n^c_{CH} - 4n^{sl}_{AH}}{n_{C_3S} + n_{C_2S} + n^{sl}_S} \quad (4.22)$$

in which Eq. (4.10) is already substituted. Substituting Eq. (4.21) into (4.22) and solving the equation gives:

$$\bar{a} = \frac{1.8(n_{C_3S} + n_{C_2S}) + n'_C + n^c_{CH} + 0.85n^{sl}_S - 4n'_A}{n_{C_3S} + n_{C_2S} + 1.36n^{sl}_S} \quad (4.23)$$

With the C/S ratio in Eq. (4.23), the A/S ratio and the quantity of C_4AH_{13} are calculated using Eqs. (4.20) and (4.21). The C/S ratio in C-S-H is lower than that in neat Portland cement because blending the slag (which has a lower C/S ratio) with Portland cement clearly lowers the C/S ratio

in C-S-H. Therefore, it holds that:

$$\bar{a} \leqslant 1.8 \tag{4.24}$$

In the case that there is not adequate A in the slag, C_4AH_{13} is not formed and C/S ratio follows from Eq. (4.19). Now substituting Eq. (4.19) into inequality (4.24) gives:

$$n^c_{CH} \leqslant 1.8 n^{sl}_S - n'_C \tag{4.25}$$

and in the other case that there is adequate A in the slag, C_4AH_{13} is formed and the C/S ratio follows from Eq. (4.23). Again substituting Eq. (4.23) into inequality (4.24) and rewriting it gives:

$$n^c_{CH} \leqslant 1.8 n^{sl}_S - n'_C - 4 n^{sl}_{AH} \tag{4.26}$$

In Eqs. (4.19) and (4.23), the C/S ratio in the hydration product C-S-H varies with the quantity of CH consumed by the slag hydration. Hence, three reaction models are put forward, depending on the amount of CH entering the slag hydration.

Model 1: No CH enters the C-S-H formed by the slag hydration

In this model, no CH produced by the hydration of the calcium silicates is available for the hydration of slag, indicating $n^c_{CH} = 0$. Only the C-S-H from the slag and the clinker hydration interacts with each other to obtain a compositional equilibrium.

Two cases are again distinguished, corresponding to the formation of C_4AH_{13} or not. In **Case 1**, in which there is not adequate A in the slag to reach the maximum substitution degree for S in C-S-H, C_4AH_{13} is not formed. According to Eq. (4.19) and because $n^c_{CH} = 0$, the C/S ratio in C-S-H reads:

$$\bar{a} = \frac{1.8(n_{C_3S} + n_{C_2S}) + n'_C}{n_{C_3S} + n_{C_2S} + n^{sl}_S} \tag{4.27}$$

Again, n_{C_3S} and n_{C_2S} etc. follow from Eq. (4.7). The A/S ratio is calculated using Eq. (4.16). Using the calculated C/S and A/S ratios, the formation of C_4AH_{13} is examined by substituting the C/S and A/S ratios in C-S-H into Eq. (4.20). If the A/S ratio exceeds the range defined by Eq. (4.20), C_4AH_{13} is formed and Case 2 is followed.

In this second case, **Case 2**, there is adequate A in the slag and C_4AH_{13} is formed. Thus, Eq. (4.23) is used with $n^c_{CH} = 0$, giving:

$$\bar{a} = \frac{1.8(n_{C_3S} + n_{C_2S}) + n'_C + 0.85 n^{sl}_S - 4 n'_A}{n_{C_3S} + n_{C_2S} + 1.36 n^{sl}_S} \tag{4.28}$$

in which n_{C_3S} and n_{C_2S} etc. follow from Eq. (4.7). The A/S ratio in the hydration product C-S-H follows from Eq. (4.20) and the quantity of the hydration product C_4AH_{13} follows from Eq. (4.21).

In this model, because no CH from the calcium silicate hydration is assumed to enter the slag hydration, the Portland cement and slag react independently and only their hydration products C-S-H are equilibrated. Therefore, this model corresponds to the lowest state of CH consumption in the system ($n^c_{CH} = 0$).

Model 2: CH enters C-S-H from the slag hydration to sustain a C/S ratio 1.8

In this model, CH from the calcium silicate hydration is assumed to enter the slag hydration to sustain C/S = 1.8 in the hydration product C-S-H. This C/S ratio is observed in the C-S-H from the Portland cement hydration (Richardson and Groves, 1992). It is also in line with the values used in other literature (Taylor, 1997). With increasing slag proportions in the blended cement, the quantity of CH for sustaining the constant C/S ratio in C-S-H also increases. At a

certain proportion all the CH is consumed. After the complete consumption of CH, the C/S ratio diminishes with increasing slag proportions. Therefore, the discussion is divided into two states, corresponding to the partial or complete CH consumption by the slag hydration, respectively.

In the first state, namely ***State 1***, part of CH from the clinker hydration is consumed by the slag hydration. In this state there is still some free CH present in the cement paste. Based on the model assumption, now the C/S ratio in the hydration product C-S-H is 1.8.

Two cases are distinguished depending on the formation of C_4AH_{13} from the slag hydration or not. In **Case 1**, the A content in the slag is not adequate to obtain the maximum degree of substitution in C-S-H. Hence, C_4AH_{13} is not formed. Now, $\bar{a} = 1.8$. Substituting $\bar{a}$ into Eq. (4.19) gives:

$$1.8 = \frac{1.8(n_{C_3S} + n_{C_2S}) + n'_C + n^c_{CH}}{n_{C_3S} + n_{C_2S} + n^{sl}_S} \tag{4.29}$$

Solving Eq. (4.29) gives n^c_{CH} as:

$$n^c_{CH} = -n'_C + n^{sl}_S \tag{4.30}$$

A transitional slag proportion, namely λ^0, is defined as the slag proportion at which all the CH is consumed ($n^c_{CH} = n^p_{CH}$). The transitional slag proportion is solved using Eqs. (4.10) and (4.30) as:

$$\lambda^0 = \frac{1.2z_{C_3S} + 0.2z_{C_2S}}{1.2z_{C_3S} + 0.2z_{C_2S} + \gamma \cdot (-z'_C + 1.8z^{sl}_S)} \tag{4.31}$$

in which z_{C_3S} etc. are the molar contents of clinker phases in Portland cement and oxides in glass of slag (in moles per mass). They are computed from the mass fractions of oxides or phases and their molar masses. For the molar content of clinker phase i in Portland cement:

$$z_i = \frac{x_i}{M_i} \tag{4.32}$$

and for the molar content of oxide i in the glass part of slag:

$$z_i = \frac{x^{sl}_i - \sum_j (x^{cr}_j \cdot x^{cr}_{i,j})}{M_i} \tag{4.33}$$

The value of z'_C is calculated with the same method as in Eq. (3.11) in Section 3.2. Therefore, the transitional slag proportion depends on the compositions of clinker and slag, and the slag hydration degree in the paste.

In **Case 2**, C_4AH_{13} is formed. According to the model assumption, $\bar{a} = 1.8$. From Eq. (4.23) it follows that:

$$1.8 = \frac{1.8(n_{C_3S} + n_{C_2S}) + n'_C + 0.85n^{sl}_S - 4n'_A}{n_{C_3S} + n_{C_2S} + 1.36n^{sl}_S} \tag{4.34}$$

and n^c_{CH} is solved as:

$$n^c_{CH} = -n'_C + 1.6n^{sl}_S + 4n'_A \tag{4.35}$$

If all the CH produced by the clinker hydration is consumed by the slag hydration, $n_{CH} = n^p_{CH}$. The transitional slag proportion for Case 2 is calculated from Eqs. (4.10) and (4.35) as:

$$\lambda^0 = \frac{1.2z_{C_3S} + 0.2z_{C_2S}}{1.2z_{C_3S} + 0.2z_{C_2S} + \gamma \cdot (-z'_C + 1.6z^{sl}_S + 4z'_A)} \tag{4.36}$$

At slag proportions higher than λ^0, the amount of CH produced by the hydration of clinker is

not sufficient to supply the constant C/S ratio of 1.8 in C-S-H. It is thus all consumed if $\lambda \geqslant \lambda^0$, resulting in the second state, State 2.

In ***state 2***, the slag proportion in the blended cement exceeds λ^0 ($\lambda \geqslant \lambda^0$). The slag hydration consumes all CH produced by the clinker hydration, indicating $n^c_{CH} = n^p_{CH}$. The C/S ratio in C-S-H is lower than 1.8 and is yet unknown. Depending on the formation of C_4AH_{13}, two cases prevail.

In **Case 1**, in which C_4AH_{13} is not formed, the C/S ratio is calculated from Eqs. (4.10 and (4.19) as:

$$\bar{a} = \frac{3n_{C_3S} + 2n_{C_2S} + n'_C}{n_{C_3S} + n_{C_2S} + n^{sl}_S} \tag{4.37}$$

Note that in Eq. (4.37), the C/S ratio in C-S-H is completely determined by the entire C contents (excluding those contained in the ettringite) and the entire S contents in the calcium silicates (from clinker) and in the slag. The A/S ratio in C-S-H from the slag hydration is calculated from Eq. (4.16).

In **Case 2**, the maximum degree of A substitution is achieved. Substituting Eq. (4.10 into Eq. (4.23), the C/S ratio in the hydration product C-S-H reads:

$$\bar{a} = \frac{(3n_{C_3S} + 2n_{C_2S}) + n'_C + 0.85n^{sl}_S - 4n'_A}{n_{C_3S} + n_{C_2S} + 1.36n^{sl}_S} \tag{4.38}$$

In the equation above, when $\lambda = 1$, $n_{C_3S} = n_{C_2S} = 0$ (see Eq. (4.4)), and it results in the equation in the reaction model for pure slags (Chapter 3). The A/S ratio in C-S-H from the slag hydration follows from Eq. (4.20) and the moles of C_4AH_{13} (n^{sl}_{AH}) follow from Eq. (4.21) with the C/S ratio from Eq. (4.38). In this model, because all the CH is available for maintaining a C/S ratio of 1.8 in C-S-H, it is in fact the model with the highest degree of CH consumption by the slag hydration.

Model 3: Part of the CH enters C-S-H from the slag hydration

In many experiments the C/S ratio in C-S-H is found already diminishing even when there is still some free CH prevailing (Duchesne and Bérubé, 1995; Richardson, 1997; Richardson and Groves, 1992; Taylor et al., 1985). Model 2 does not account for this limited degree of CH consumption. Hence, another model is proposed (Model 3), in which all CH produced by the calcium silicates is taken to be available for the slag hydration, but the quantity of CH entering the slag hydration is not sufficient to sustain a constant C/S ratio of 1.8 in the hydration product C-S-H.

First, define the proportion of the consumed CH to the total amount produced, namely p, as:

$$p = \frac{n^c_{CH}}{n^p_{CH}} \tag{4.39}$$

whereby $0 \leqslant p \leqslant 1$. Furthermore, the C/S ratio of C-S-H formed by the slag hydration cannot exceed the ratio in C-S-H from clinker hydration (1.8, as used in this chapter). Hence, inequality (4.25) or (4.26) applies, depending on the formation of C_4AH_{13}. Hence:

$$n^c_{CH} = p \cdot n^p_{CH} = 1.8n^{sl}_S - n'_C \leqslant 1.8n^{sl}_S - n'_C + 4n^{sl}_{AH} \tag{4.40}$$

The parts on the right side of inequality (4.40) ($1.8n^{sl}_S - n'_C$ or $1.8n^{sl}_S - n'_C + 4n^{sl}_{AH}$) are actually the surplus of CH needed for maintaining a C/S ratio of 1.8 in C-S-H formed by the slag hydration in the two cases.

A semi-empirical expression for p is proposed here as:

$$p = \frac{1.8n_S^{sl} - n'_C}{n_{CH}^p + 1.8n_S^{sl} - n'_C} = \frac{\gamma\lambda(1.8z_S^{sl} - z'_C)}{(1-\lambda)(1.2z_{C_3S} + 0.2z_{C_2S}) + \gamma\lambda(1.8z_S^{sl} - z'_C)} \tag{4.41}$$

The expression for p (Eq. (4.41)) states that the fraction of CH consumed by the slag hydration (p) is linearly proportional to the surplus of S (or equivalently, the shortage of C) in the slag for obtaining a C/S ratio of 1.8 in the C-S-H formed (from the slag hydration alone). In other words, a slag with a molar C/S ratio of 1.8 will not need/consume CH. Other (nonlinear) relations would also be conceivable, but in chemical engineering, it is a common approach to relate mass transfer linearly to a concentration gradient. Furthermore, by definition p obeys the requirement $0 \leqslant p \leqslant 1$. In what follows it will be seen that using this proposed semi-empirical expression for p results in good agreement with experimental observations.

Inequalities (4.25) and (4.26) automatically apply with the defined p. Note that in Eq. (4.41), if $\lambda = 0$, $p = 0$ (no CH consumption); if $\lambda = 1$, $p = 1$ (full CH consumption). The quantity of consumed CH by the slag hydration (per unit mass of slag) is calculated from Eq. (4.39) as:

$$n_{CH}^c = p \cdot n_{CH}^p = p \cdot (1.2n_{C_3S} + 0.2n_{C_2S}) \tag{4.42}$$

in which p follows from Eq. (4.41). It can be seen from Eq. (4.42) that the total amount of CH consumed by the slag hydration increases with increasing calcium silicates contents in the clinker, thus the C/S ratio in C-S-H is increased. But, the extent of the influence is minor. Even though more CH is produced by the clinker hydration, the proportion consumed by slag hydration is smaller (see Eq. (4.41)). Hence, the total amount of consumed CH remains approximately the same.

Similarly, two cases exist depending on the formation of C_4AH_{13} or not. In **Case 1**, C_4AH_{13} is not formed. The C/S ratio in C-S-H follows from Eq. (4.19) using n_{CH}^c from Eq. (4.42). The A/S ratio is calculated from Eq. (4.16). The results of Case 1 (C/S and A/S ratios) are always substituted into Eq. (4.20) to determine the formation of C_4AH_{13}. In **Case 2**, C_4AH_{13} is formed. The C/S ratio in C-S-H follows from Eq. (4.23) using n_{CH}^c from Eq. (4.42). The A/S ratio and quantity of C_4AH_{13} are calculated from Eqs. (4.20) and (4.21).

With the three reaction models proposed, quantities and compositions of the hydration products can be calculated from the oxide compositions of initial materials and the slag proportion in the blended cement. With this information, some characteristics of the microstructure of hydrating slag-blended cement paste can be predicted.

4.3 Microstructure of hydrating slag cement paste

4.3.1 Molar fractions of hydration products

Molar fractions of the hydration products (C-S-H, hydrotalcite, ettringite, etc.) in the hydrating slag cement paste are calculated by using the stoichiometry models proposed in the previous sections. In the hydrating cement paste, the other two clinker phases (aluminate and ferrite) also react and form some hydration products. The reactions of aluminate are represented by the following equations (Brouwers, 2005):

$$C_3A + CH + 12H \rightarrow C_4AH_{13} \tag{4.43}$$

$$2C_3A + C\overline{C} + CH + 23H \rightarrow 2C_4A\overline{C}_{0.5}H_{12} \tag{4.44}$$

$$C_3A + 3C\overline{S}H_2 + 26H \rightarrow C_6A\overline{S}_3H_{32} \tag{4.45}$$

Table 4.1: Water content in the hydration products of blended cement (mole per mole product, column headings indicate the hydration states).

Hydration product	105°C	80% RH	100% RH
$C_{\bar{a}}S_{\hat{b}}H_{\bar{a}+1.5}$	C/S	C/S + 0.8	C/S + 1.5
M_5AH_{19}	7	13	19
C_4AH_{19}	7	13	19
$C_4A\bar{C}H_{12}$	7	12	12
$C_6A\bar{S}_3H_{36}$	8	32	36
$C_6AFS_2H_8$	8	8	8
CH	1	1	1

in which full carbonation of monosulfate (an intermediate product from the reaction of C_3A with sulfate) takes place. In real hydrating cement pastes, ettringite is firstly formed from C_3A and gypsum. Then, it is converted into monosulfate. However, the monosulfate is not commonly observed in mature cement pastes. In a recent work of Brouwers (2005), the assumed absence of monosulfate in cement pastes is motivated by carbonation. The carbonation effect finally converts the monosulfate into ettringite and hemicarbonate or monocarbonate (Taylor, 1997). Therefore, in this chapter, the formation of ettringite from C_3A is considered. The remaining C_3A reacts with the CH to C_4AH_{13}. Quantities of ettringite, monocarbonate (n_{monoc}) and C_4AH_{13} from the hydration of Portland cement are appropriated by using the following equations, respectively (Brouwers, 2005).

$$n^p_{AFt} = 1/3 \cdot n_{gyp} \tag{4.46}$$

$$n^p_{AH} = n_{C_3A} - 2/3 \cdot n_{gyp} \tag{4.47}$$

$$n^p_{monoc} = 1/3 \cdot n_{gyp} \tag{4.48}$$

The hydration of ferrite is less well understood until now compared to other clinker phases. In this chapter, the reaction of ferrite follows from the work of Brouwers (2005) as:

$$C_4AF + 2C_2S + 10H \rightarrow C_6AFS_2H_8 + 2CH \tag{4.49}$$

in which the $C_6AFS_2H_8$ is a Fe-containing hydrogarnet phase with 8 OH^- replaced by 2 SiO_4^{4-}. Obviously, the quantity of $C_6AFS_2H_8$ (n_{HG}) equals the moles of C_4AF (n_{C_4AF}). It is noteworthy that in real clinker the composition of C_4AF can vary in a range, thus in Eq. (4.49) the stoichiometry of C_4AF is considered valid for all clinkers. The equation is used as an approximation to the actual reaction. According to Brouwers (2005), C_4AF can react with both C_3S and C_2S. Only the reaction of C_4AF with C_2S is here listed because the adoption of C_3S or C_2S does not significantly change the model. The quantity of hydrogarnet equals n_{C_4AF} according to the reaction equation (4.49). The quantities of all products present in the hydrating cement paste are calculated with Eqs. (4.46)-(4.49) and the stoichiometric models.

4.3.2 Water retention

If quantities of all hydration products from the slag and Portland cement hydration are known, water retention by these products can be calculated in different hydration states. The water content in the hydration products of slag-blended cement is listed in Table 4.1 (mole per mole product), part of which is taken from Table 4.1 in Chapter 3.

The total amount of water retained by the hydration products is calculated with Eq. (3.47) with the water content (H_i) in each hydration product taken from Table 4.1. The water retained at 105°C (or after being D-dried) is designated as the "non-evaporable water".

4.3.3 Chemical shrinkage

Similarly, chemical shrinkages of the slag-blended cements are predicted by using the physical properties of the hydration products (Table 3.8).

Chemical shrinkage is calculated as:

$$\Psi_s = \frac{(V^p + V^{sl,r} + V_H) - V_{hp}}{m} = \frac{(m^p/\rho^p + m^{sl} \cdot \gamma/\rho^{sl} + n_H \cdot \omega_H) - \sum(n_i \cdot \omega_i)}{m^{sl} + m^p} \tag{4.50}$$

in which V^p, $V^{sl,r}$, V_H, V_{hp} are the volumes of Portland cement, reacted slag, retained water and hydration products; i is the hydration product, respectively.

4.3.4 Porosity

As discussed in Section 2.4, Powers and Brownyard (1948) developed a general model for describing the structure of hardened Portland cement paste (hcp). In this model, the hcp is generalized to comprise three components, viz. the unreacted cement, hydration products and capillary pores. These concepts apply to the hydrating slag-blended cement as well. Quantities of these components are mathematically predicted considering the curing conditions and recipes of the pastes with the hydration models proposed in this chapter. Hence, the model proposed by Powers and Brownyard (1948) is further developed for hydrating slag-blended cement paste. The procedure is described below.

The total volume of the considered system (V_{hcp}) reads:

$$V_{hcp} = m \cdot [1/\rho^c + (w/c)/\rho_w] = m \cdot [\nu^c + (w/c) \cdot \nu_w] \tag{4.51}$$

in which ρ^c (g/cm^3) and ν^c (cm^3/g) are the density and specific volume of the binder (slag-blended cement), respectively; ρ_w and ν_w are the density of and specific volume of the pore water in the fresh paste, respectively. It is assumed that ρ_w = 1 g/cm^3; and w/c is the water/cement ratio in mass. ν^c is calculated from the specific volumes of Portland cement and slag as:

$$\nu^c = (1-\lambda) \cdot \nu^p + \lambda \cdot \nu^{sl} \tag{4.52}$$

in which ν^p is the specific volume of Portland cement, taken to be 0.313 cm^3/g and ν^{sl} is the specific volume of slag, taken to be 0.342 cm^3/g.

Complete hydration of Portland cement is assumed to occur always, rendering the hydration degree of slag in the paste as the uncertainty. As observed in experiments, all clinker in the blended cement has hydrated after about one year curing, while the hydration degree of slag can vary in a range.

The paste is assumed being cured in the saturated state, and all the capillary pores are thus permeable to external water. In other words, all the capillary pores are filled with water. Influences of autogenous shrinkage and drying shrinkage on the apparent volume of the paste are eliminated. The volume of capillary pores thus equals the difference between the volume of the initial slurry and that of the solids in the hydrating paste, comprising the volumes of the unreacted water and the chemical shrinkage (Figure 1.7). The volume of the capillary pores (V_{cp}) is calculated as:

$$V_{cp} = V_{hcp} - V_{hp} - V^{sl,ur} = m \cdot [\nu^c + (w/c) \cdot \nu_w] - \sum n_i \cdot \omega_i - m^{sl} \cdot (1-\lambda) \cdot \nu^{sl} \tag{4.53}$$

in which $V^{sl,ur}$ is the volume of unreacted slag and ω_i is the molar volume of hydration product i. The porosity of C-S-H is calculated as Brouwers (2004b):

$$\Phi_{C-S-H} = \frac{32.44}{94.60 + 33.05(\bar{a} - 1.7)} \tag{4.54}$$

If all and only the pores in the gel product C-S-H are considered as gel pores (as explained in

Chapter 3), the volume of gel pores (V_{gp}) reads:

$$V_{gp} = V_{C-S-H} \cdot \Phi_{C-S-H} = n_{C-S-H} \cdot \omega_{C-S-H} \cdot \Phi_{C-S-H} \tag{4.55}$$

The capillary and gel porosities of the paste are calculated, respectively, as:

$$\Phi_{cp} = V_{cp}/V_{hcp} \tag{4.56}$$

$$\Phi_{gp} = V_{gp}/V_{hcp} \tag{4.57}$$

The total porosity of the hardened cement paste reads

$$\Phi = \Phi_{gp} + \Phi_{cp} \tag{4.58}$$

The porosity of hydrating slag-blended cement paste depends on many factors, for example the hydration degree of ingredients, the slag proportion in cement, the initial w/c ratio and the hydration state of the samples. The influences of these factors are addressed in the following sections.

4.4 Validations

Six blended cements are selected from literature to validate the proposed models. The oxide compositions of the Portland cements in the blended cements are listed in Table 4.2. For the clinker of Cement 4, only the Bogue composition is given, from which the oxide composition is computed. The mass fractions of the four major clinker phases in the Portland cements are listed in Table 4.3 after being normalized to 100 percent. The mineralogical compositions of Cement 1–3, 5 and 6 are calculated from the oxide composition by using the Bogue's equations (Chapter 2). Free lime contents in Cement 1, 3, 5 and 6 are negligible and that in Cement 2 amounts to 0.5 m/m%. The oxide compositions of slags in the selected blended cements are listed in Table 4.4, also after being normalized to a total of 100 percent.

Cement 1 originates from the study of Richardson and Groves (1992). The microstructure and compositions of a group of hardened cement pastes with different slag proportions are analyzed using the TEM with microanalysis combined with EMPA. The slag proportions increased from 0 to 100 m/m% divided into nine different degrees. The w/c ratio of the blended cement pastes is 0.4. The pastes are cured up to three years in sealed plastic tubes at 20°C. Both the C/S and A/C ratios in the hydration product C-S-H are measured at 14 months (Table 4.5).

Cement 2 originates from the study of Taylor et al. (1985). Blended cement paste is made with 59 m/m% clinker, 39 m/m% slag and 2 m/m% gypsum. The blended cement is mixed with deionized water at a w/c ratio of 0.5 and is sealed into polyethylene vials. The samples are cured at 20°C for up to 540 days. The blended cement pastes are studied by using XRD, analytical electron microscopy (AEM) and TGA. Partial replacement of clinker by slag is found to decrease both the amount of CH existing in the cement paste and the mean C/S ratio of C-S-H.

Cement 3 originates from the study of Harrisson et al. (1987). Pastes of blended cement containing 40 m/m% slag are examined using SEM fitted with an EDX system. The pastes are prepared by hand mixing at a w/c ratio of 0.5 and cured at 25°C for 14 months. After the first two days, the sample is cured in sealed polyethylene containers in water. The observations are similar to those of Taylor et al. (1985): the CH content is reduced by the addition of slag into Portland cement and the C/S ratio of the C-S-H formed from the clinker hydration also decreases. None of the individual phases in the blended cement pastes show significant compositional variation over time in the period from 28 days to 14 months.

Cement 4 originates from the study of Richardson (1997). Water-activated white Portland cement/slag blend pastes with a w/c ratio of 0.4 are investigated using solid-state ^{29}Si NMR spectroscopy and analytical TEM. The blends have two slag proportions, 50 m/m% and 90 m/m%, respectively. The samples are cured at 25°C in sealed plastic tubes. C/S and A/S ratios in C-S-H are measured using both NMR and TEM. The test age is not given in the literature, but is assumed one year. Aluminum substitution for silicon is found in C-S-H in the experiments.

Table 4.2: Oxide compositions of Portland cement in blended cements[§].

Oxide	Cement 1[a]	Cement 2[b]	Cement 3[c]	Cement 4[d]	Cement 5[e]	Cement 6[f]
C	66.5	68.8	66	70.8	67.1	64.8
S	20.2	21.5	21.3	26.9	21.4	22.9
A	6.2	4.9	5.6	1.9	6.1	5.3
M	1.3	1.8	1.2	0	1.6	2.5
$\overline{S}$	2.7	1.2	2.7	0	0.9	1.8
F	3.1	1.8	3.2	0.4	2.9	2.7
Total	100	100	100	100	100	100

[a]: from Richardson and Groves (1992);
[b]: from Taylor et al. (1985);
[c]: from Harrisson et al. (1987);
[d]: from Richardson (1997);
[e]: from Schäfer (2004);
[f]: from Mills (1986);
[§]: Minor compositions are discarded and the mass percentages are normalized to a total of 100 percents. The compositions of Portland cement in Cement 4 are calculated from the mass fractions of clinker phases. Free lime content exists in negligible amount except in Cement 2 with a fraction of 0.5 m/m%.

Table 4.3: Mineral compositions of Portland cement clinkers in Portland cement in the blended cements. The compositions of Cement 1–3 and 5–6 are calculated by using the Bogue's equations.

Phase	Cement 1	Cement 2	Cement 3	Cement 4	Cement 5	Cement 6
C_3S	67.4	81.4	61.1	70.7	66.5	47.9
C_2S	10.6	2.5	18.7	23.9	12.9	33.7
C_3A	12.1	10.3	9.9	4.3	11.4	10.2
C_4AF	9.9	5.8	10.3	1.1	9.2	8.2
Total	100	100	100	100	100	100

Cement 5 originates from the study of Schäfer (2004). Cement paste samples are made with a w/c ratio of 0.5 and are cured up to one year with different slag proportions. The CH contents of the samples are determined by using TGA technique with the weight difference in the range between 450 and 600°C, in which the decomposition of the CH takes place. The measurements are further corrected for the weight loss of C-S-H. The amount of CH consumed by the slag hydration can thus be obtained by comparing the amount of CH in the slag cement pastes to that in neat Portland cement pastes. Together with the hydration degrees of slag in the samples, the extent of CH consumption by the slag hydration is calculated.

Cement 6 originates from the study of Mills (1986). Slag cement paste samples are made with a w/c ratio of 4, and containing different proportions of slag (from 0 to 90 m/m%) in the blended cements. The chemical shrinkage is determined by the mass increment of water needed to keep the pyknometer bottles filled to the mark. The amount of non-evaporable water is determined by first drying the slurry samples at 110°C and then igniting them at 1050°C. The measurements continue for about 3 years.

Table 4.4: Oxide compositions of slags in the blended cements. Only the oxides involved in the selected hydration products are listed (C, S, A, M and $\overline{S}$) and the mass percentages are normalized to a total of 100 percent. The total of all the other oxides is less than 3.5 m/m% for all cements.

Oxide	Cement 1[a]	Cement 2[b]	Cement 3[c]	Cement 4[d]	Cement 5[e]	Cement 6[f]
C	41.15	44.76	44.56	41.64	44	30.72
S	36.72	35.22	35.74	36.95	35.75	33.03
A	10.86	11.19	11.06	12.55	12.45	16.16
M	7.64	8.7	8.62	8.01	7.79	20.09
$\overline{S}$	3.63	0.13	0.02	0.85	0.01	0
Total	100	100	100	100	100	100

[a]: from Richardson and Groves (1992);
[b]: from Taylor et al. (1985);
[c]: from Harrisson et al. (1987);
[d]: from Richardson (1997);
[e]: from Schäfer (2004);
[f]: from Mills (1986).

4.4.1 Composition of C-S-H

First, the three models are employed to model the hydration of Cement 1. The hydration degrees of slag and Portland cement in the paste should be determined before the modeling process. The hydration degree is influenced by many factors, such as the curing conditions, test ages, water/binder ratios, slag proportions and probably the most important one, the slag reactivity. Therefore, to predict the hydration degree of slag in the blended cement paste is difficult. A tentative degree of 70% ($\gamma = 0.7$) for the slag hydration and complete hydration of Portland cement is assumed in this chapter. This hydration degree is further assumed valid for all slag proportions. The basic reasons for this assumption are the observations by Hinrichs and Odler (1989), Battagin (1992) and Lumley et al. (1996). The effect of the slag/clinker ratio on the slag reactivity is found to be quite limited. Only for high slag proportions (from 80 m/m% and higher) an obvious decline in the slag reactivity is observed. The influence of different slag hydration degrees on the model predictions will also be investigated in the later part of this chapter.

The measured A/C ratios in C-S-H are converted to A/S ratios by using the measured C/S ratios. The compositions of C-S-H predicted by the proposed models are compared to the ex-

Table 4.5: Measured C/S and A/C molar ratios of C-S-H in hardened slag-blended cement paste (Cement 1, w/c = 0.4, 20°C, 14 months, after Richardson and Groves (1992).

m/m% GGBFS	C/S	A/C
0	1.76	0.027
10	1.89	0.02
25	1.78	0.032
50	1.55	0.05
66.7	1.43	0.065
75	1.37	0.065
83.3	1.38	0.075
90	1.28	0.075
100	1.14	0.095

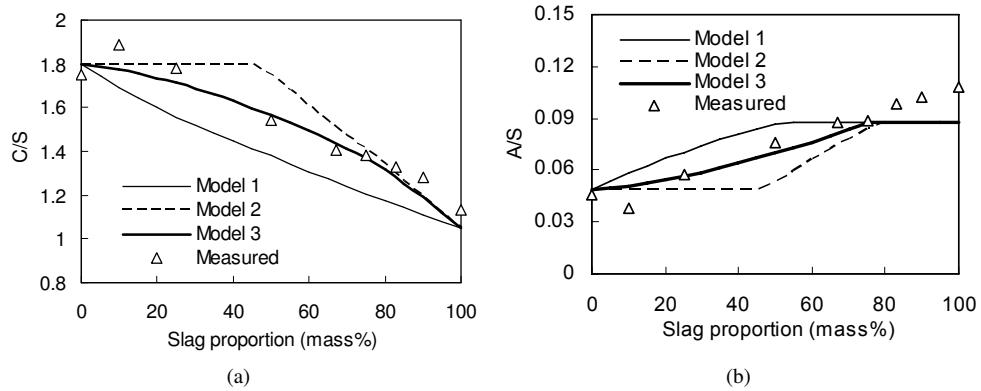

(a) (b)

Figure 4.1: C/S and A/S ratios in C-S-H versus slag proportions in cement: model prediction and comparison with measurements by Richardson and Groves (1992)

perimental observations (Figure 4.1(a), 4.1(b)). It can be seen that the C/S ratios predicted by Model 1 are slightly lower than the measurements in the experiments. The low C/S ratios indicate that the exclusion of CH from the slag hydration decreases the C/S ratios in C-S-H. Therefore, the underlying assumption is most likely not true. The A/S ratios predicted by Model 1 at low slag proportions are higher than the measurements. The discrepancy comes from the predicted low C/S ratio in C-S-H since C-S-H with a low C/S ratio can structurally incorporate more A, resulting in a higher A substitution degree in the C-S-H (higher A/S ratio).

The C/S ratios predicted with Model 2 accord better with the experimental observations as compared to those with Model 1. Therefore, most likely CH from the Portland cement hydration enters the C-S-H from the slag hydration and increases its C/S ratio. However, the C/S ratios predicted by Model 2 at some slag proportions are slightly higher than the measurements, especially at intermediate proportions, and the predicted A/S ratios are apparently lower than the measurements. The observations in the experiments show that blending Portland cement with slag even at low slag proportions (25 m/m% and 50 m/m% as used in the experiments) already lowers the C/S ratios in C-S-H and increases the A/S ratios. This trend is also evident in the experimental results for Cement 2–4. Therefore, the quantity of CH entering the slag hydration is not sufficient to sustain a constant C/S ratio (1.8).

The predictions by Model 3 accord best with the observations. Both the C/S and A/S ratios in C-S-H are well predicted. At slag proportions higher than 60 m/m%, the predicted A/S ratios do not increase any further due to the lack of aluminum available to achieve the maximum substitution degree. The A/S ratios are thus governed by the slag composition (see Eq. (4.16)). In the experiments, the A/S ratio in C-S-H kept increasing at high slag proportions ($\lambda > 60$ m/m%), which are slightly higher than the model predictions. A possible explanation for these higher A/S ratios is the probable intimate mixing of C-S-H and hydrotalcite in the hydration products. In the blended cement pastes with high slag proportions, a significant amount of hydrotalcite is formed and is closely mixed with C-S-H. To analyze the compositions of pure phase C-S-H in these pastes then becomes more difficult. Most likely higher A and M contents in it are measured. Hence, the measurement of C/S ratios is more reliable and more suitable for validation of the present models.

It is concluded from all experimental results and model predictions that CH produced by the Portland cement hydration is most likely to be available for the slag hydration. It enters the slag hydration to increase the C/S ratio in C-S-H compared to that of the anhydrous slag.

The three hydration models are also employed to model the hydration of Cement 2–4. The

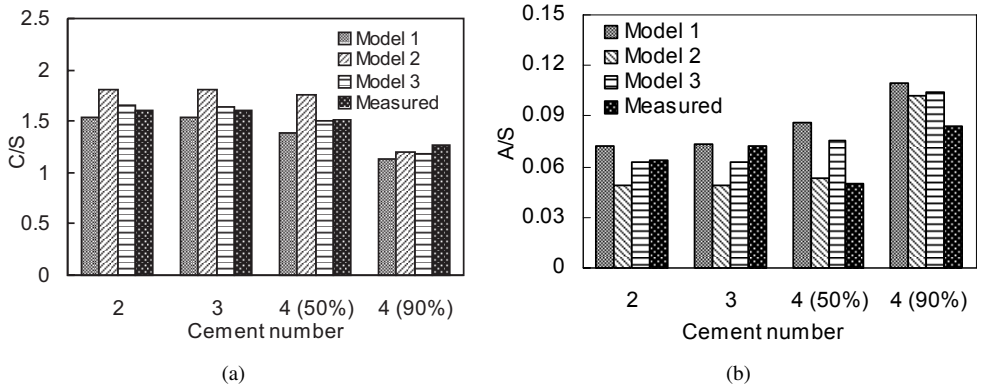

(a) (b)

Figure 4.2: Predicted and measured composition of C-S-H: predicted with Cement 2-4 and comparison with measurements by Taylor et al. (1985), Harrisson et al. (1987), Richardson (1997), (a) C/S ratio, (b) A/S ratio.

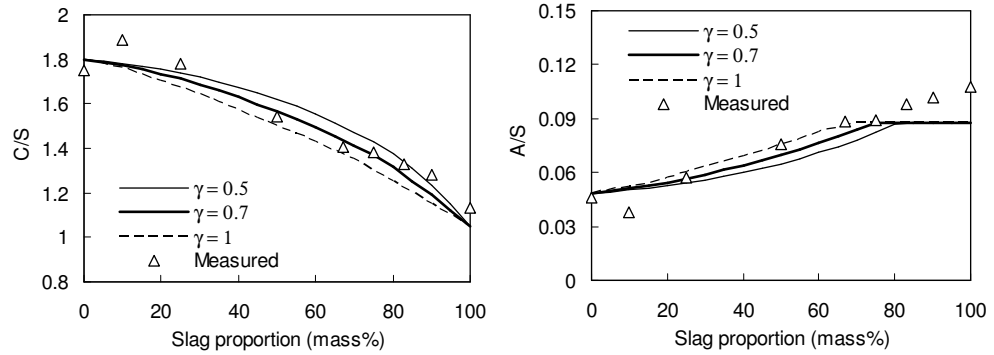

(a) (b)

Figure 4.3: Effect of slag hydration degree on the composition of C-S-H: computed with Model 3 and Cement 1, (a) C/S ratio; (b) A/S ratio. Measurements by Richardson and Groves (1992)

predicted compositions of C-S-H are compared to the measurements in experiments (Figure 4.2(a) and 4.2(b)). Similar conclusions are drawn. The compositions predicted by these models accord well with the experimental observations. Among these models, Model 3 generally gives the best predictions for the composition of the main hydration product, C-S-H, especially for its C/S ratio.

Model 3 is thus recommended for modeling the hydration of the slag-blended cement since it consistently gives the best predictions for all cements under investigation. It is also used in the following discussions.

Next, the influence of slag hydration degree (γ) on the prediction of the composition of C-S-H is investigated. To this end, Model 3 is again used and is applied to Cement 1. Although the hydration degrees of slag are assumed to vary over a wide range (0.5–1), this variation has only a very minor influence on the predicted composition of C-S-H (Figure 4.3(a) and 4.3(b)). This is especially true when considering the C/S ratio in C-S-H. The influence of slag hydration degree on the compositions of C-S-H is more prominent at intermediate slag proportions. But,

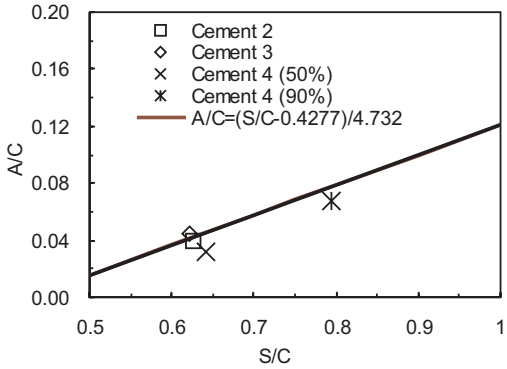

Figure 4.4: The S/C and A/C ratios in C-S-H of hydrated Cement 2–4, and comparison with the relation by Richardson (2000).

the variation of C/S ratios at 50 m/m% slag is within the range of 5.2% using the measured values in experiments as standard, which is probably less than the errors involved in the experimental data for C/S ratios. Therefore, Model 3 proposed in this chapter is not sensitive to the hydration degree of slag in the pastes. It is used for computing the composition of C-S-H, even though the hydration degree of slag is not completely clear.

In Figure 4.4, the relationship between the compositions of C-S-H (the S/C and A/C ratios) is examined by using the experimental measurements. The A/C and S/C ratios in C-S-H from Cement 2–4 are generally consistent with the relation proposed by Richardson (2000) (Eq. (7), included in the figure as well).

4.4.2 CH consumption

The proportion of CH consumed by the slag hydration is an important feature of the three hydration models proposed in this research. In this section, the proposed expressions for the amount and proportion of CH consumed by the slag hydration are validated with measurements in experiments using Cement 5. The validations are again based on Model 3 because this model provides the best agreements and is therefore recommended for modeling the hydration of blended cement.

The fraction and amount of CH consumed by slag hydration is calculated by using the semi-empirical equations (Eqs. (4.39–4.42)) in Model 3. It is further validated with the measurements by Schäfer (2004). They are calculated at different slag proportions and are plotted in Figure 4.5(b) and 4.5(a), together with the measured values in the experiments of Schäfer (2004). The influence of varying the degrees of slag hydration is also included.

It can be seen that the fraction of CH entering the slag hydration increases with increasing slag proportions in the blended cement. This is also the case while increasing the hydration degree of slag, since the net consequence is also to increase the quantity of hydrated slag. Both the predicted and measured amounts of CH consumed by the slag hydration are plotted in Figure 4.5(a). For 40 m/m% and 80 m/m% of slag in the blended cement, the measurements are within the range of the predictions. For the blends with 20 m/m% slag, the prediction is slightly higher than the measurement due to the higher prediction of proportion on CH consumption in the Model 3 (see Figure 4.5(b)).

As a total, the model predictions are in good agreement with the measurements, which proves that the use of Eq. (4.41) is appropriate for predicting the fraction of CH consumed by slag hydration.

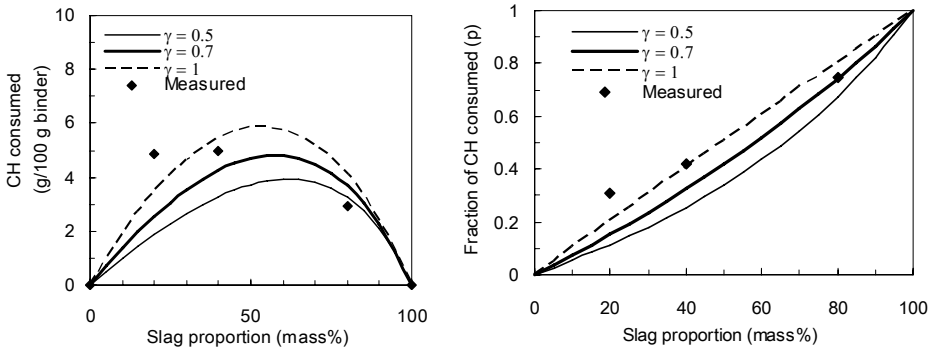

(a) Amount of CH consumed (b) Fraction of CH consumed

Figure 4.5: CH consumption by the slag hydration (γ = 0.5, 0.7, 1, predicted with Cement 5, Model 3). Measurements by Schäfer (2004). All the clinker has hydrated.

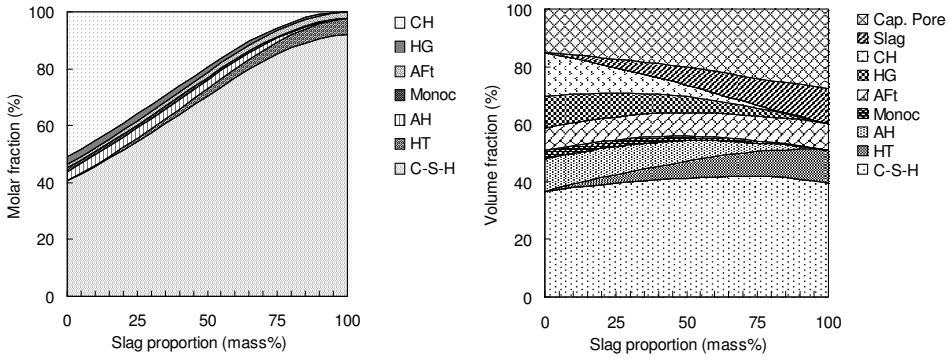

(a) Molar fraction (b) Volume fraction

Figure 4.6: Molar fractions of hydration products and volume fraction of phases in hydrating slag-blended cement paste using Model 3, Cement 1, w/c = 0.5, $\gamma = 0.7$ and Portland cement hydrated completely. Predictions are made assuming the paste is maintained in the saturated state (100% RH).

4.5 Model applications

In this section, several applications of the proposed models are demonstrated, including the molar and volume fraction of hydrating products, water retention, chemical shrinkage, and porosities. If experimental data are available, they are also used for validating the models.

4.5.1 Molar fractions of hydration products

The calculated molar fractions of hydration products versus the slag proportions are plotted in Figure 4.6(a), taking Cement 1 as example and again using Model 3. The relative hydration degree of slag is set to be 0.7. Clearly, C-S-H is the most abundant product at all slag proportions. With increasing slag proportions in the blended cement pastes, the amount of C-S-H also increases substantially. Meanwhile, the quantity of CH decreases, becoming very low when $\lambda = 0.8$. The quantities of hydrotalcite and ettringite increase with the slag proportions in the ce-

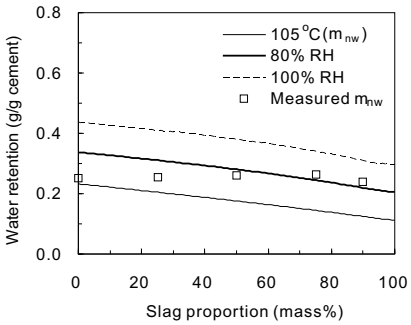

(a) $\gamma = 0.5$

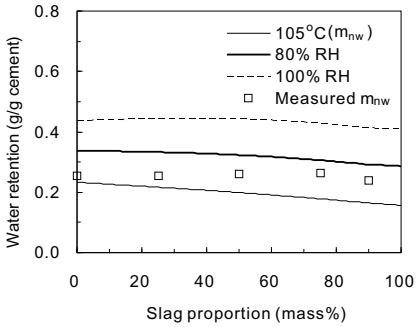

(b) $\gamma = 0.7$

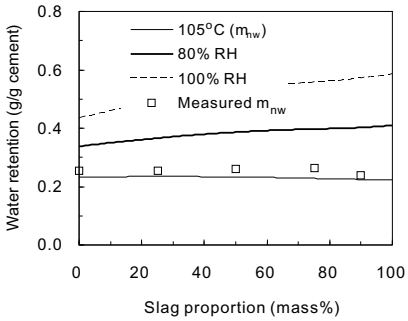

(c) $\gamma = 1$

Figure 4.7: Water retention in the hydration products in different hydration states versus the slag proportion in the blended cement (Cement 6, Model 3), measurements for non-evaporable water are taken from Mills (1986). All clinker has hydrated.

ment due to the quantity of slag from which they are formed. The proportion of C_4AH_{13} always remains very low. It is even entirely absent at some proportions .

The volume fractions of hydration products and other phases (capillary pores and unreacted slag) are predicted with the models and plotted in Figure 4.6(b). Cement 1 and Model 3 is again used and the relative hydration degree of slag is assumed to be 0.7. Portland cement has completely hydrated in the prediction and the paste is assumed being cured in the saturated state. It can be seen that C-S-H is again the dominant phase in the paste in volume for all slag proportions. However, its fraction is approximately constant, about 40 v/v% percent of the paste. The volume fraction of ettringite (AFt) is approximately constant as well, due to the comparable sulfate content in the Portland cement and in the slag. Remarkable reductions of the fractions of CH, C_4AH_{13} and hydrogarnet phases are noticed in the figure with increasing slag proportions. Since these phases are normally formed in crystals and their surfaces can act as channels for gas and liquid transfer in the matrix, it would be expected that pastes made with higher slag proportions will have denser microstructure and are less permeable. This effect is even enhanced by the increasing amount of hydrotalcite, which is normally formed as an inner product and is intimately mixed with C-S-H.

4.5.2 Water retention

The results of experiments carried out by Mills (1986) are used for validating the present model predictions on water retention. The retained water in the hydration products of Cement 6 in different hydration states (being heated to 105°C, equilibrated to 80% RH and 100% RH) is predicted (Figure 4.7).

Note that the water retention at 105°C corresponds to the non-evaporable water in the paste. Model 3 is used for modeling and different degrees of slag hydration in the blended cements ($\gamma =$

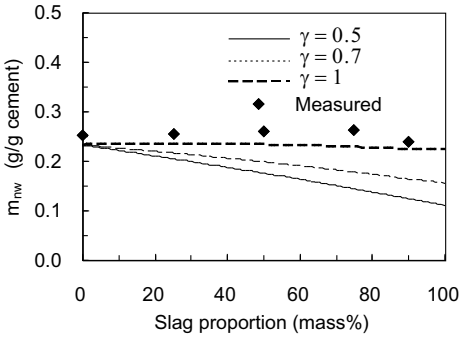

Figure 4.8: Measured and predicted m_{nw} of hydrated slag-blended cement paste (Cement 6, Model 3). Measurements by Mills (1986).

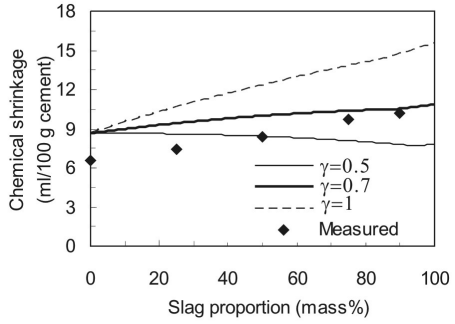

Figure 4.9: Measured and predicted chemical shrinkage of slag-blended cement hydration (Cement 6, Model 3). Measurements by Mills (1986).

0.5, 0.7 and 1.0) are considered. Increasing the slag proportions in the blended cement is shown in the predictions to have only a mild influence on the level of retained water in the hydration products.

The predicted amount of non-evaporable water (m_{nw}) with different slag hydration degrees is plotted in Figure 4.8 together with the experimental results. The predictions are in good agreement with the results. The measured values are slight higher than the predictions corresponding to full hydration of slag. The predicted values are also within the range measured by Cesareni and Frigione (1966) (0.1–0.22 g per g original cement), and the trend is also in good agreement with their measurements. A sharp decline in m_{nw} at high slag proportions (approximately >80 m/m%) is observed by Cesareni and Frigione (1966), while a plateau occurs in the model predictions. This discrepancy comes from the assumption that for all slag proportions and at the considered age, the slag hydration degrees are the same, which is shown to be invalid for high slag proportions (Hinrichs and Odler, 1989; Lumley et al., 1996). Therefore, at high slag proportions, the degree of slag hydration might decrease sharply, yielding a sharp decline in the retained water content. Considering this correction for the slag hydration degree at high slag proportions, a sharp decline is expected as a consequence.

4.5.3 Chemical shrinkage

Chemical shrinkage of the hydration of Cement 6 is predicted with the hydration models and is plotted in Figure 4.9 together with the measured values. Predictions by Model 3 are used with

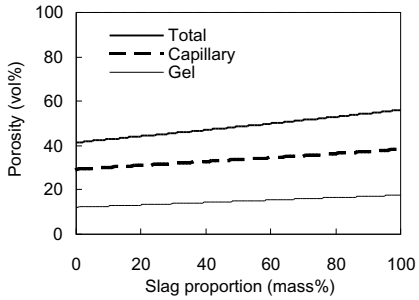

(a) versus slag proportion, w/c = 0.5, $\gamma = 0.7$

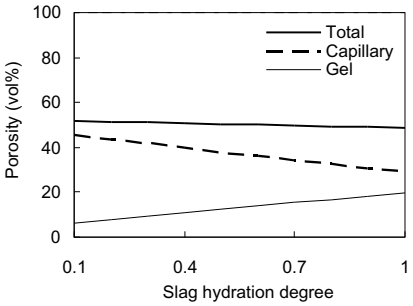

(b) versus slag hydration degree, w/c = 0.5, $\lambda = 0.6$

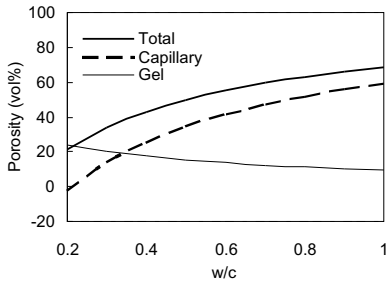

(c) versus w/c ratio, $\lambda = 0.6, \gamma = 0.7$

Figure 4.10: Effect of slag proportion, hydration degree and w/c ratio on the total, capillary and gel porosities of hydrating slag-blended cement paste (Cement 1, Model 3).

different slag proportions in the cement. It can be seen that the hydration degree of slag in the paste has a dominant influence on the chemical shrinkage of the blended cement, contrary to that on m_{nw}. At given ages, higher degrees of slag hydration are achieved for more reactive slags. Thus, larger chemical shrinkage is expected. For full hydration of reactants, the chemical shrinkage of slag-blended cement hydration (for 50 m/m% slag, about 12 mL per 100 g cement) is significantly higher than that of neat Portland cement (around 8.7 mL per 100 g cement reacted) (see Figure 4.9 for $\lambda = 0$). For slags with medium reactivity, the chemical shrinkage does not differ significantly from that of Portland cement and decreases slightly with increasing slag proportions. For low slag hydration degrees, which are typical for cements high in slag proportions or containing slag of low reactivity, lower chemical shrinkage is expected.

The measured values of chemical shrinkage for all slag proportions are slightly lower than the predictions corresponding to a full hydration slag because that not all the pores created by the chemical shrinkage of reactions are accessible to external water. However, the trend of the predictions is in good agreement with that shown in the measurements.

Based on both the model predictions and the data by Mills (1986), one can expect that the chemical shrinkage of blended cement increases with increasing slag proportions in the cement, and for the reaction of pure slag ($\lambda = 1$), the chemical shrinkage ranges between 11 and 15 mL per 100 g slag.

4.5.4 Porosity

Porosities of hydrating blended cement pastes are plotted in Figure 4.10, taking Cement 1 as example and using Model 3 for predictions. The predictions are made with the assumption that the pastes are cured in the saturated state (neither drying nor autogenous shrinkage) and dried at 105°C (or after being D-dried), a state in which the water remaining is regarded structurally bound in the product.

In Figure 4.10(a), the porosities are plotted versus the slag proportions in the cement. The

hydration degree of slag is assumed 0.7 for all proportions and the water cement ratio of the initial paste is 0.5. It can be seen in the figure that with increasing slag proportions in the paste, the total, capillary and gel porosities increase as well. The trends for all three porosities are similar, though the gel porosity increases less prominently. The influence of slag proportions on the porosities as predicted by the hydration model agrees with the observations by Uchikawa and Uchida (1986) and Cesareni and Frigione (1966), especially for gel porosities. A decline at high slag proportions, as observed in experiments, is associated with the low slag hydration degree in cement, which is not accounted for in the prediction. In general, pastes made with slag-blended cement show higher porosities than those made with Portland cement, but most of the pores are in the range of fine pores.

In Figure 4.10(b), the porosities are plotted versus the hydration degree of slag (γ) in the cement. The proportion of slag (λ) is assumed to be 60 m/m% and the water cement ratio of the initial paste (c) is 0.5. Contrary to the influence by slag proportions, the slag hydration degree influences more prominently the capillary and gel porosities. The capillary porosity increases with increasing slag hydration degrees, which is reasonable because of the continuous consumption of remaining water in the paste. The increasing gel porosity is associated with the increasing volume of gel products and its high porosity. If more slag has hydrated, more gel product (C-S-H as considered in this thesis) is produced, which has a lower C/S ratio (see Figure 4.3(a)). The porosity of C-S-H with lower C/S ratios is also higher. However, the total porosity remains almost constant.

The influence of initial w/c of the paste on the porosities is plotted Figure 4.10(c). Here, the slag proportion is 60 m/m% and the hydration degree (γ) is 0.7. Note that in all the calculations the clinker is assumed to hydrate completely. The total and capillary porosities increase dramatically with increasing initial w/c ratios, because of the presence of more free water in the paste. The gel porosity decreases with higher w/c ratios because of the increased volume of the initial pastes. This effect could be partially counteracted by the larger slag hydration degrees with higher w/c ratios. Therefore, the gel porosity would decrease very slightly, or keep almost constant. The trend for the influence of w/c ratios on the porosities is in good agreement with the observations by Cesareni and Frigione (1966). Negative values for low w/c ratios are predicted due to the hydration degrees assumed in the simulation, which cannot be achieved because of the limit of space for the growth of products (see Chapter 3).

The capillary pores are generally regarded responsible for the strength decay and permeability of the porous structure. Hence, its volume should normally be minimized. The use of slag in cement does not contribute to the strength and durability of concrete in this respect, because it increases both the total and capillary porosities. However, the capillary porosity is greatly influenced by the reactivity of slag. A high slag hydration degree in cement dramatically reduces the capillary porosity, and increases the gel porosity. Hence, the reactivity of slag deserves serious consideration in practice, and should be evaluated before applications. The w/c ratio of the recipe is essential concerning the porosities. Denser structures are obtained with lower w/c ratios and high slag reactivity.

4.6 Conclusions

Three stoichiometric models for the slag-blended cement hydration are established in this chapter by considering the interactions between the slag reaction and the hydration of calcium silicates in clinker. They are used to quantify the hydration products, determine the consumption of CH by slag reaction, and derive the composition of C-S-H. A compositional equilibrium of C-S-H is used in developing the models. Various blending proportions of slag are considered in the models. Three modes of CH consumption by the slag hydration is investigated, resulting in three reaction models. In the models, the degrees of slag and Portland cement hydration are accounted for using a relative slag hydration degree (γ), which is determined in practice according to the curing condition, age, slag reactivity, etc. Model 3 gives the best accordance with experimental

results. The variations in the relative degree of slag hydration show no significant influence on the predictions of models.

Based on the investigations in this research, the conclusions outlined below are drawn:

1. The main hydration products of slag-blended cement comprise C-S-H, CH, hydrotalcite, ettringite and C_4AH_{13}. C-S-H is the most abundant hydration product. CH is formed from the clinker hydration and interacts with the slag hydration to increase the C/S ratio in C-S-H. The amount of CH entering the slag hydration is related to the blend proportions of slag in the cement.
2. Increasing the slag proportions in the cement increases the proportions of C-S-H in the hydration products. Blending slag with Portland cement clearly lowers the C/S ratio in C-S-H and increases the A/S ratio.
3. The A content in slag is first combined with M to form the hydrotalcite and with $\overline{S}$ to form the ettringite. The remaining A enters C-S-H to substitute for S. If the maximum degree of A substitution is achieved, the remaining A reacts to the AFm phase (C_4AH_{13}).
4. The proposed models can successfully predict the compositions of the hydration products, such as the C/S and A/S ratios in C-S-H, and determine their quantities. Amongst the three models, Model 3 consistently yields the best predictions and its use is thus recommended for modeling the hydration of slag-blended cement. This model considers that the CH consumption by the slag is proportional to the shortage in C (surplus in S) to achieve a constant C/S ratio of 1.8 in C-S-H.
5. Change of the slag proportions at low or medium levels in the blended cement has only a minor influence on the level of water retained by the hydration products. But, the slag-blended cement might exhibit significantly higher chemical shrinkage than Portland cement. The difference in chemical shrinkage between the blended cement and Portland cement can be more prominent if the slag content in the cement is high and/or the slag has high reactivity.
6. Both the capillary and gel porosities increase slightly with slag proportions in the cement for a constant hydration degree of slag. The increase of slag hydration degree reduces the capillary porosity of the paste, but increases its gel porosity. The capillary porosity increases dramatically with increasing w/c ratios. Hence, the slag reactivity and w/c ratio deserve the most special attentions.

Chapter 5

Pore solution chemistry

5.1 Introduction

The cement hydration process can essentially be considered as the interactions between the solid compounds and the liquid phase in the paste. The liquid phase contains some ions and is therefore called "pore solution".

The pore solution is important in concrete applications because of at least five factors:

1. The liquid phase in the concrete is mainly responsible for substance transfer and provides channels for ingress of external substances.
2. The likelihood of ASR, a major deteriorative reaction observed in some concrete structures, is closely related to the hydroxyl concentration in the pore solution, although most time the term itself includes alkali ions (Diamond, 1975).
3. The hydration of cement mixture containing contaminants is influenced by the chemical composition of the pore solution by changing the solubility of compounds and the occurrence of precipitate (Van Eijk, 2001).
4. It is important to maintain a high alkalinity of the pore solution to stabilize the oxide film on the surface of steel bar, which inhibits further corrosion.
5. The reactivity of some supplementary materials (slag, fly ash, etc.) depends on the chemical composition of the pore solution (Brouwers and Van Eijk, 2002; Zhou et al., 1993).

Besides the chemical influences of pore solution on the properties of paste/concrete, it can have some physical effects on the overall properties of concrete as well. For example, as the hydration proceeds, the pore solution becomes more and more concentrated, which decreases the internal relative humidity in the pore space (in contact with the pore solution) and aggravates the self-desiccation.

Due to the reasons above, the number of researches on the pore solution composition of hardening cement paste and concrete has been rising rapidly in the past decades (Bérubé et al., 2004; Diamond, 1981; Larbi et al., 1990; Longuet, 1976; Longuet et al., 1973; Lothenbach and Winnefeld, 2006; Page and Vennesland, 1983; Rothstein et al., 2002; Schäfer, 2004; Van Eijk, 2001). Most of the researches are focused on the development of the pore solution composition in hydrating cement paste with the aids of experimental design. Effects of different factors on the pore solution composition are investigated, like the use of supplementary materials (Diamond, 1981; Longuet, 1976), addition of mineral salt (Page and Vennesland, 1983; Schäfer and Meng, 2001; Xu, 1997), alkalinity of cement (Dehwah et al., 2002), carbonation of concrete (Anstice et al., 2004) and leaching of substances (Sagüës et al., 1997). Most of the analyses are based on the pore solution compression method firstly introduced by Longuet et al. (1973).

Methods for predicting the ion concentrations in the pore solution of hydrating cement paste are useful, although the experimental setup is widely used to investigate the pore solution composition in hydrating cement paste. First, to measure the ion concentrations in mature concrete takes lots of efforts. Special care should be taken to minimize the environmental effect (Glasser, 2003). Second, the experiments cannot obtain quick results because no reliable methods are available to accelerate the hardening process of cement, the principal binder in concrete (Taylor,

1987b). Third, the different factors can hardly be considered in a single batch of experiments. A large set of experiments need to be carried out to clarify the effect of each factor. Therefore, models for the pore solution composition can on one hand help to design the experimental scheme, and on the other hand predict the effect of various factors without the need of carrying out the time-consuming and costly experiments.

In this chapter, new methods are proposed for modeling the pore solution composition of hydrating Portland cement and slag cement pastes. They are based on the methods developed by Taylor (1987b), Brouwers and Van Eijk (2003) and Van Eijk (2001). Special attention is paid to the determination of the type of hydration products that can bind alkali ions, and their alkali-binding capacities.

5.2 Development of pore solution composition

5.2.1 Portland cement paste

The dominant ions in the pore solution of normal hydrating Portland cement paste are K^+, Na^+, Ca^{2+}, SO_4^{2-}, OH^-, $Al(OH)_4^-$, $H_3SiO_4^-$, etc. (Bérubé et al., 2004; Diamond, 1981; Larbi et al., 1990; Longuet, 1976; Longuet et al., 1973; Lothenbach and Winnefeld, 2006; Page and Vennesland, 1983; Rothstein et al., 2002; Schäfer, 2004; Van Eijk, 2001).

Immediately after mixing with water, remarkable amounts of alkali ions are released into the water, together with sulfate ions (Figure 5.1(a)). After about 6 hours, the sulfate concentration starts to decline, accompanied by a rapid increase of the hydroxyl concentration. The drop of the sulfate ion is most likely caused by the formation of ettringite, which is proven by the rapid drop of aluminum in the pore solution. The sulfate concentration in the pore solution remains at a very low level in a long term (Figure 5.1(b)). The alkali concentrations increase very steadily during the first 24 hours, and they keep increasing to a maxima at about one week. Then, they start to decline and reach constant values. The calcium concentration remains always very low, although it is relatively higher in the first 20 hours than that in the later ages. The hydroxyl concentration in the pore solution is very low in the early ages, and it remains almost constant as long as sulfate presents in a large amount in the pore solution. Immediately after the sulfate ion becomes depleted, the hydroxyl concentration is increased greatly. The overall trend for the change of hydroxyl concentration is very similar to those of the alkali ions. The aluminum and silicon concentrations in the pore solution remain less than 0.5 mmol/L.

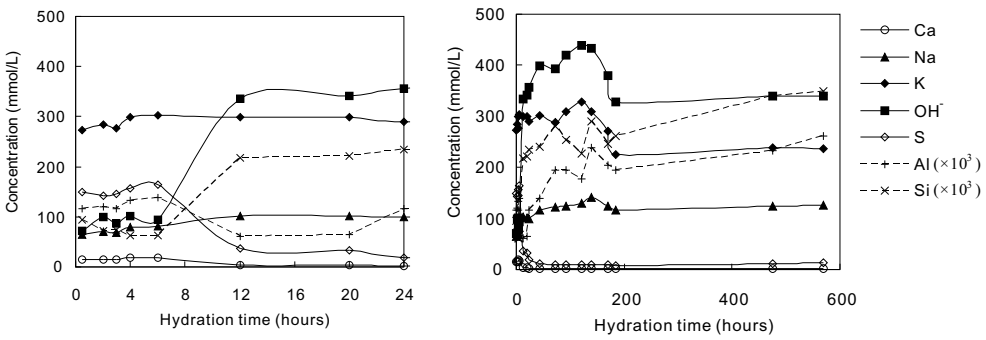

(a) up to 24 hours (b) up to 569 hours

Figure 5.1: Measured elemental concentrations in the pore solution of hydrating Portland cement paste (Data source: Rothstein et al. (2002), the OH^- concentration is calculated with the electroneutrality method; the Al and Si concentrations are multiplied by 10^3).

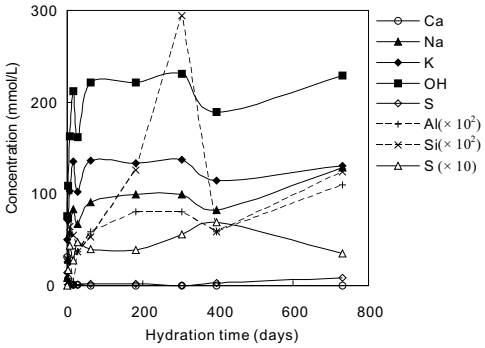

Figure 5.2: Measured elemental concentrations in the pore solution of hydrating slag cement paste (Data source: Longuet (1976), assuming the density of the pore solution is 1.01 g/mL based on the work of Taylor (1997)); the Al and Si concentrations are multiplied by 100 and that of S^{2-} by 10).

5.2.2 Slag cement paste

The ions observed in pore solution of hydrating slag cement paste are principally the same as those in Portland cement paste, with a remarkable amount of sulfide ion (S^{2-}) in the pore solution. The alkali concentrations in the pore solution increase sharply during the first week, and reach approximately constant values after that. The aluminum and silicon concentrations in the pore solution remain very low throughout the whole hydration process as well, but still remarkably higher than those in Portland cement paste (compare the scales in Figures 5.1 and 5.2).

5.3 Models for pore solution composition

The methods for modeling the ion concentrations generally comprise two parts: models for the alkali concentrations in the pore solution (Brouwers and Van Eijk, 2003; Taylor, 1987b) and models for the other ions which are in equilibrium with the solid compounds in the system (Van Eijk, 2001). The major reason for this categorization is as follows:

Alkali salts are normally very soluble, i.e. they have high solubilities in water; hence, considering the situation in the pore solution of hydrating cement paste, an equilibrium between the solid compounds of alkali salts and the pore solution can hardly be established. Thus, the alkali ions are always dissolved into the solution when they are available, and a non-equilibrium method should be used, which is discussed in more details in Section 5.3.1.

However, the other ions, mainly Ca^{2+}, SO_4^{2-}, $Al(OH)_4^-$, $H_3SiO_4^-$, etc., as discussed in Section 5.2, are much less soluble. The solid compounds containing these ions are in equilibrium with the solution and thus an equilibrium method should be used when predicting their concentrations. The hydroxyl ions are always generated from the ionization of water to maintain electro neutrality.

5.3.1 Non-equilibrium methods for alkali ions

For predicting the alkali concentrations, the methods proposed by Taylor (1987b) and further developed by Brouwers and Van Eijk (2003) are first introduced.

Taylor's method

Taylor (1987b) proposed a method for predicting alkali ion concentrations in the pore solution of hydrated cement paste from more than one day old. The method uses the total contents of Na_2O and K_2O in the components and the water available for the pore solution. The alkali ions are partitioned between the pore solution and the hydration products.

The amount of alkali ions taken up by the hydration products is assumed proportional to its concentration in the solution and the amount of products as adsorbent. The concentration of ions in the solution is calculated from the remaining amount of alkali ions and the volume of solution. An empirical constant, namely the binding factor, is defined and derived both for Na^+ and K^+. In the computations, the amounts of alkali ions released by the cement hydration and the hydration products are estimated using some empirical equations. The volume of pore solution is computed from the total water content in the paste and that combined in the products. The detailed procedure for predicting the alkali concentrations is as following.

Release The alkali oxides in cement can be divided into two groups according to their state, namely "soluble" and "insoluble" alkalis. Pollitt and Brown (1968) found part of alkali oxides in cement present as sulfate, which is instantly soluble after contact with water. The proportion of this part of alkali oxide depends on the sulfate content of cement. A detailed routine for computing this proportion is given by Taylor (1990). The rest of the alkali oxide is often found in solid solution in the alite, belite, aluminate and ferrite. It is released into the pore solution simultaneously as the hydration proceeds. Both of these two parts of alkali oxides are available for the pore solution.

The amount of alkali ions (Na^+ or K^+) in the cement can be computed as:

$$n_i^T = \frac{2x_i}{M_i} \cdot m^p \tag{5.1}$$

in which n_i^T is the moles of alkali ion i (K^+ or Na^+) in the cement; x_i is the mass fraction of alkali oxide i in cement; m^p is the mass of Portland cement.

The moles of alkali ions existing as sulfate can be calculated as:

$$n_i^{sul} = f_i^{sul} \cdot n_i^T \tag{5.2}$$

in which n_i^{sul} is the amount of alkali ion in the sulfate form (in moles); f_i^{sul} is the fraction of alkali ion in the sulfate form ($0 \leqslant f_i^{sul} \leqslant 1$).

The procedure for determining f_i^{sul} is given below as (Taylor, 1990):

1. Calculate the ratio $R_s = n_{\bar{S}}^T/(n_K^T + n_N^T)$ and $\chi = n_K^T/n_N^T$, in which $n_{\bar{S}}^T$ is the moles of sulfate in clinker, calculated as $n_{\bar{S}}^T = x_{\bar{S}}/M_{\bar{S}} \cdot m^p$;
2. If $R_s \leqslant 0.8$ and $\chi < 3.67$, $f_K^{sul} = 1.12R_s$ and $f_N^{sul} = 0.56R_s$;
3. If $R_s > 0.8$ and $\chi < 3.67$, $f_K^{sul} = 0.9$ and $f_N^{sul} = 0.56R_s$;
4. If $\chi > 3.67$, proceed as in (2) or (3) but multiply each result by $(n_K^T + n_N^T)/(1.12n_K^T + 0.56n_N^T)$.

Note that in the calculation above, the sulfate content in the clinker needs to be known, while sometimes that of the total amount including added gypsum in Portland cement is measured. In this case, estimated values for f_i^{sul} may be used, for example, 35% of Na_2O and 70% K_2O in the soluble sulfate form (Taylor, 1987b). The amount of the other alkali ions bound in the clinker phases is calculated as:

$$n_i^{clinker} = f_i^{clinker} \cdot n_i^T = (1 - f_i^{sul}) \cdot n_i^T \tag{5.3}$$

The exact amount of alkali ions in each clinker phase (C_3S, C_2S, C_3A, C_4AF, etc.) can be calculated by using $n_i^{clinker}$ and the distribution of alkali ion in clinker phases given in Table 5.1 (Taylor, 1987b). The amount of alkali ions which exist as non-sulfate and are released by the clinker hydration is calculated as:

$$n_i^{r,clinker} = n_i^T \cdot \sum_{j=1}^{4} (f_{i,j} \cdot f_i^{clinker} \cdot \alpha_j) = n_i^T \cdot \sum_{j=1}^{4} [f_{i,j} \cdot (1 - f_i^{sul}) \cdot \alpha_j] \tag{5.4}$$

in which j is the clinker phase (j = alite, belite, aluminate and ferrite); $f_{i,j}$ is the fraction of alkali ion (to the amount of non-sulfate ions in clinker) in phase j; α_j is the hydration degree of phase j. Hence, the total amount of alkali ion released by the cement hydration is:

$$n_i^r = n_i^{sul} + n_i^{r,clinker} = [f_i^{sul} + \sum_{j=1}^{4} f_{i,j}(1 - f_i^{sul})\alpha_j] \cdot n_i^T \tag{5.5}$$

Binding Obvious partition of alkali ions between the solid and aqueous phases takes place, deserving serious attention while evaluating the alkali level in the pore solution. The alkalis bound in the solid phases of cement are continuously released into the aqueous phase in the paste as the hydration proceeds. Parts of these alkali ions are adsorbed by the hydration products (Taylor, 1987b) and are immobilized, which are not available for the pore solution. The amount of alkali ions released by the cement hydration is accordingly divided into two parts: those in the solution and those bound in hydration products, yielding:

$$n_i^r = n_i^b + n_i^s \tag{5.6}$$

in which n_i^b is the amount of alkali ions bound in products; n_i^s is the moles in the solution. The amount in the solution reads:

$$n_i^s = C_i \cdot V_w \tag{5.7}$$

in which C_i is the concentration of alkali ion i (mol/L); V_w is the volume of pore solution (L).

Taylor (1987b) assumed that the amount of bound alkali ion is proportional to the concentration in the pore solution and the amount of hydration products, yielding:

$$n_i^b = b_{a,i} \cdot C_i \cdot F \tag{5.8}$$

in which $b_{a,i}$ is the binding factor (L) of alkali i; F is fraction between the quantity of hydration products (dimensionless), which are able to take up alkali cations in the paste and that after complete hydration of cement.

Substituting Eqs. (5.9) and (5.7) into (5.6), the alkali concentration in the pore solution is calculated as:

$$C_i = \frac{n_i^r}{V_w + b_{a,i} \cdot F} \tag{5.9}$$

Note that the computations of Taylor (1987b) are based on 100 g cement.

In Taylor's method, most of the parameters necessary for the computation are estimated us-

Table 5.1: Fraction of alkali ions in individual clinker phases to the amount of non-sulfate alkali ions in clinker (Taylor, 1987b).

Alkali	Alite	Belite	Aluminate	Ferrite	Total
Na_2O	0.44	0.17	0.36	0.03	1
K_2O	0.29	0.41	0.27	0.03	1

ing empirical equations. Thus, uncertainties are inevitable because those equations can hardly be valid for all cements under investigation. Furthermore, a constant value for $b_{a,i}$ is used, implying a constant binding capacity of the hydration products. As stated by Taylor (1987b), the assumption of this linear dependency had no theoretical basis. Experimental results by Hong and Glasser (2002), Stade (1989) and computations in this chapter prove that the relation is not necessarily linear, which will be discussed in Section 5.4 of this chapter.

Brouwers and Van Eijk's method

Brouwers and Van Eijk (2003) further developed the method proposed by Taylor (1987b). The concepts of alkali release and adsorption are taken over. Furthermore, the hydration degree of cement, the amount of alkali ions released by the cement hydration, the amount of C-S-H and volume of pore solution are computed from the output of one computer-based cement hydration model CEMHYD3D (*Van Eijk version*). Uncertainties in the theory of Taylor (1987b) induced by using some empirical equations are minimized by distinguishing the main hydration product C-S-H and all others. Hence, it is expected to give more accurate predictions over a wide range of cements. The authors take use of the results of the experiments by Hong and Glasser (1999) to compute the C-S-H binding factors of alkalis and compare them to those used by Taylor (1987b). Results from the experiments by Larbi et al. (1990) are used to validate the improved model. The model predictions agree fairly well with the experimental results.

Brouwers and Van Eijk (2003) proposed the amount of alkali ions bound in the products to be:

$$n_i^b = R_{d,i} \cdot C_i \cdot m_{C-S-H} \tag{5.10}$$

in which m_{C-S-H} is the mass of C-S-H in the solids and $R_{d,i}$ is the distribution ratio of alkali i (Na^+ or K^+), which is defined as:

$$R_d = \frac{\text{alkali in solid C} - \text{S} - \text{H (mmol/g)}}{\text{alkali concentration in solution (mmol/mL)}} \quad \text{(in mL/g)} \tag{5.11}$$

Assuming that 100 g cement hydrates into 80 g C-S-H, a relation can be established between the two expressions (5.8) and (5.10) (Brouwers and Van Eijk, 2003).

Again in this method, the alkali-binding capacity of C-S-H is assumed linearly proportional to the alkali concentrations in the solution because constant values for $R_{d,i}$ are used. Only C-S-H in the products is considered as adsorbent because it is the most abundant phase in the products and is concluded to be the main binder of alkali ions (Brouwers and Van Eijk, 2003).

Substituting Eqs. (5.7) and (5.10) into Eq. (5.6) yields:

$$n_i^r = C_i \cdot V_w + R_{d,i} \cdot C_i \cdot m_{C-S-H} \tag{5.12}$$

Hence, the concentration of alkali ion is solved from Eq. (5.12) as:

$$C_i = \frac{n_i^r}{V_w + R_{d,i} \cdot m_{C-S-H}} \tag{5.13}$$

in which n_i^r is computed from Eq. (5.5). The parameters in Eqs. (5.5) and (5.13) (α_j, m_{C-S-H} and V_w) can for instance be computed using the *Van Eijk's Model*.

5.3.2 Equilibrium methods for non-alkali ions

In this equilibrium model firstly introduced by Van Eijk (2001), a few considerations are taken for the non-alkali ions in the pore solution as:

1. H^+ can be neglected with respect to the OH^- due to the generally high pH of the solution.
2. Ca^{2+} is the only calcium containing ion in the solution.
3. Mg^{2+} is the only magnesium containing ion in the solution.

4. SO_4^{2-} is the only sulfate containing ion in the solution.
5. $Al(OH)_4^-$ is the only aluminum containing ion in the solution.
6. $H_3SiO_4^-$ is the only silicon containing ion in the solution.

These ions are taken because they constitute the solid phases (hydration product and reactant) in the water-solid binary system (see Table 1). Formation of other (complex) ions in the pore solution is neglected here. To find the concentrations of ions determined by equilibria in the pore solution, the following information is required:

1. The solubility properties of the solid compounds, i.e. what ions are formed when the solid dissolves, and their solubility products.
2. The activity coefficients of the ions at high concentrations.
3. The solids considered in equilibrium with pore solution during a specific hydration period.

When the solids in equilibrium are known and methods for computing the activity coefficients are available, for each solid an equation can be set up corresponding to its solubility product. Because electro neutrality always prevails, the charge balance also gives an additional equation. When the number of equations equals the number of unknown ion concentrations, the system of equations can be solved, giving the concentrations that satisfy all equilibria products and the charge balance.

In this method, because all the products/minerals are considered in equilibrium with the pore solution (although a definite equilibrium state of the actual cement system are never achieved), the concentrations of the ions in the pore solution as the result of their dissolution are only governed by their solubility properties. They are not dependent on the amount of the compounds dissolving, the degree of hydration, the volume of the pore solution and the dissolving history. In addition, the composition of cement, the kinetics of different clinker phases and the w/c ratio do not influence them.

Solubility of phases in hydrating paste

For each relevant hydration product, the composition in terms of constituent ions and its solubility is given in Appendix D. The solubility of ettringite, hydrogarnet, hydrotalcite and strätlingite are recalculated from Atkins et al. (1992, 1991); Bennett et al. (1992) using the ion interaction method (Pitzer's equations). The valued calculated are in line with those reported by other studies. For the hydration product C-S-H, the model by Reardon (1992) is taken to determine its solubility.

In this chapter, all the hydration products of cement are considered present as pure phases, although in the real cement paste, they may be chemically combined with each other to form solid solutions, e.g. the C_4AH_{13} may be in solid solution with monosulfate, yielding the commonly referred AFm phases. Generally, the solubility properties of solid solution compounds are not available and the theories on this are still subject of many researches.

Activity coefficients

Activity coefficients are important when the solution becomes concentrated, which is the case in pore solution of hydrating cement paste. Generally, two methods are used for computing the activity coefficients, namely the Davies equations and the Pitzer's method. The Pitzer's method is used in this thesis because using the Davies equation and other equations based on ion-specific parameters are not sufficient and will produce large errors in activity coefficients (Van Eijk, 2001).

Because Pitzer equations are used in this thesis, the activity products (K^0) values to be used should also be based on the Pitzer approach. Therefore, in all computations K^0 values determined

from solubility measurements in which the ion interaction approach is taken into account are used consequently, e.g. by Reardon (1992).

Set of equations

The set of equations and methods for reducing the number of equations follow those used by Van Eijk (2001) (Appendix D). Note that in the method by Van Eijk (2001), the solid C_3AH_6 is taken as one product from C_3A hydration, while in a recent research (Brouwers, 2005) it is found more likely to react with CH to form C_4AH_{13}. Therefore, the equilibrium between solid C_4AH_{13} and pore solution is given in Appendix D instead of the solid C_3AH_6.

Before solving the set of equations, the total alkali concentration $[Na^+]$ + $[K^+]$ and the activity coefficients are computed beforehand using the non-equilibrium approach discussed in Section 5.3.1. This value is used as an input parameter for the equilibrium model. Activity coefficients are determined at forehand using estimations. When these coefficients are known, concentration products can be derived from the solubility products and hence, concentrations can be used in the equations to be solved.

In the methods by Van Eijk (2001), two states of the cement-water system are distinguished, depending on the presence of gypsum or not. Transformation from the first state, **State 1**, in which gypsum exists, into the other one, namely **State 2**, will necessary result in a sharp drop in the sulfur concentration as the solubility of gypsum is about hundred times higher than that of the ettringite. Rapid changes in other ions, e.g. the OH^-, Ca^{2+} are also expected because of the equilibrium in the system. However, such a sudden shift of ion concentrations in the pore solution are not observed in experiments, because in the real cement paste the hydration of cement occurs incongruently due to some local factors such as different size of cement grains and local variations in hydration conditions. Therefore, the two states exist simultaneously in the hydrating cement paste, which is especially the case at early ages of hydration, and should be accounted for simultaneously.

Practically it is difficult to measure the chemical composition of localized pore solution and the measurements in experiments are always results of average compositions. Concerning the interests of numerous investigations, e.g. diffusion process, chemical attack and hydration behavior of cement, generalized compositions of the pore solution is more interesting than that in specific localized areas. Therefore, the concept of average is here taken when modeling the chemical compositions of the pore solution with respect to the two different states, with or without gypsum.

A distribution factor, namely δ_f, accounting for the inhomogeneity of the gypsum existence is proposed, with which the ion concentration in the pore solution is computed as:

$$[i] = \delta_f \cdot [i]_1 + (1 - \delta_f) \cdot [i]_2 \tag{5.14}$$

in which $[i]_1$ denotes the ion concentration computed in **State 1** (with the existence of gypsum) and $[i]_2$ denotes the concentration computed in **State 2** (without gypsum).

At early ages of hydration, relatively large amount of gypsum exists, indicating that **State 1** prevails and a large distribution factor is expected; while as the hydration proceeds, more gypsum is consumed and ettringite starts to govern the sulfur concentrations in the pore solution, resulting in a small distribution factor. The distribution factor is computed as

$$\delta_f = \frac{V_{gyp}}{V_{gyp} + V_{AFt}} \tag{5.15}$$

in which V_{gyp} and V_{AFt} are the volume of the substances gypsum and ettringite, respectively, which can be computed with the *Van Eijk's Model*. Here, the volumes of the two substances are taken for the pore solution distribution instead of the mass because the contact of the substances with the pore solution has more likely a volume basis than a mass basis.

Summarizing, the following steps are executed for simulating the evolution of chemical compositions in the pore solution during the hydration of Portland cement:

1. Computing microstructure parameters (degree of hydration, phase composition, porosity and calcium sulfate fraction) empirically, or using numerical models.
2. Computing alkali concentrations in the pore solution ($[Na^+] + [K^+]$) following the method presented in Section 5.3.1.
3. Computing the activity coefficients, or making estimations of their values at the start of the computation (see Van Eijk (2001) and Appendix D).
4. Computing solubility products from K^0 values and activity coefficients (Appendix D).
5. Solving $[OH^-]$ in both **State 1** and **State 2** (Appendix D).
6. Computing the distribution factor using Eq. (5.15).
7. Computing concentration of ions in the pore solution using the results and with Eq. (5.14).

5.4 New models for alkali concentrations in Portland cement pastes

The alkali-binding capacity of hydration products (or the main product C-S-H) is an essential factor in the methods proposed by Taylor (1987b) and Brouwers and Van Eijk (2003). In both methods, the alkali-binding factors are set to be constant based on the experimental results by using the synthetic C-S-H, or constant values largely based on assumptions. However, a constant alkali-binding capacity of C-S-H is not supported by the experimental results of Hong and Glasser (2002) and Stade (1989).

In this section, new non-linear methods for determining the binding factors of C-S-H to Na^+ and K^+ in hydrating Portland cement pastes are proposed, which are derived from a large set of experimental results reported in literature.

5.4.1 Alkali-binding capacity of C-S-H

Stade (1989) studied the incorporation of alkali hydroxides in synthetic C-S-H and C-A-S-H gels. It is found that the amount of alkali hydroxide incorporated in C-S-H gels increases with decreasing C/S ratio in it. The alkali-binding capacity of the Al-containing C-S-H gel is smaller than the Al-free gel at equal C/S ratios. No obvious differences between the binding capacities for Na^+ and K^+ are observed in the experiments.

Hong and Glasser (1999, 2002) studied the alkali-binding capabilities of synthetic C-S-H and C-A-S-H gels as well. For the alumina-free C-S-H, the alkali-binding capacity is found to increase linearly with increasing alkali concentrations in the solution. This linear relation is concluded from the approximately constant distribution ratios for C-S-H with fixed C/S ratios (see the columns for C/S = 1.8 in Table 5.2). However, if alumina is incorporated into C-S-H, which takes place in real hydrating cement paste (Richardson and Groves, 1992; Wang and Scrivener, 2003), the obtained C-A-S-H gels have obviously enhanced alkali-binding capacity, which is in contrast to the conclusion of Stade (1989). This enhancement is more obvious for C-A-S-H gels with low C/S ratios. On the one hand, for all C-S-H and C-A-S-H gels, with increasing alkali concentrations in the solution, more alkali ions are held in the gels. On the other hand, the distribution ratio decreases with increasing alkali concentrations in the pore solution, which indicates that a linear relationship between the binding capacity and the alkali concentrations is questionable. Similar to the conclusion of Stade (1989), there is no significant difference between the alkali-binding capacity of C-S-H for Na^+ and K^+.

A possible explanation for the different observations found in the experiments of Stade (1989) and Hong and Glasser (1999, 2002) is the way of preparing the C-S-H gel. Stade (1989) made the C-S-H gel at 150°C by the autoclave reaction with CaO and silica, and at 80°C by precipitation from sodium silicate solutions with calcium chloride. Hong and Glasser (1999, 2002) prepared the C-S-H gel by mixing $Ca(OH)_2$ and a very reactive, high surface area silica gel in double-

Table 5.2: Measured alkali distribution ratio (R_d) with synthetic C-S-H and C-A-S-H gel (after Hong and Glasser (1999, 2002)).

Na					K				
Concentration	C/S				Concentration	C/S			
(mmol/L)	0.85[♯]	1.2[♯]	1.5[♯]	1.8[♭]	(mmol/L)	0.85[♯]	1.2[♯]	1.5[♯]	1.8[♭]
15	62.1	6.39	2.56	0.42	15	54.1	5.69	1.8	0.30
50	44.8	4.85	1.98	0.44	50	47.4	4.88	1.44	0.40
100	33.9	4.77	1.35	0.34	100	38.1	3.28	2.44	0.40
300	12.9	3.21	1.3	0.39	300	10.8	3.16	1.76	0.38

[♯]: C/S ratio in C-A-S-H gel, after Hong and Glasser (2002);

[♭]: C/S ratio in alumina-free C-S-H gel, after Hong and Glasser (1999).

distilled, CO_2-free water, sealed for 12 months at 20±2 °C with regular agitation. The difference in the way of preparation and temperature may have a significant influence on the heterogeneity and structure of the C-S-H gel (Fujii and Kondo, 1984; Young, 1988). The influence of different preparation temperature is already observed in the experiments of Stade (1989) as well.

Furthermore, the alkali concentrations used by Hong and Glasser (1999, 2002) are between 0.015 to 0.3 mmol/L. The alkali concentrations in the hydrating cement pastes under investigation are frequently outside this range because normally they are evaluated due to their high alkali oxide contents, which can potentially induce ASR in concrete. Therefore, higher concentrations of alkali ions in the pore solution are more relevant. Furthermore, the distribution ratio in real hydrating cement pastes can be significantly different from that of synthetic ones, which is of primary importance in modeling the pore solution composition.

5.4.2 New methods for alkali-binding capacity of hydration products

In this section, new methods for determining the alkali distribution ratios in hydrating Portland cement pastes are proposed, which are based on the derivations with a large set of experimental data taken from literature. Thirteen recipes of cement pastes tested in experiments are taken as a basis. All the pastes are cured in a sealed environment at variable temperatures. Pore solutions are collected at the planned ages using the liquid compression method (Longuet et al., 1973). The oxide compositions of these cements are listed in Table 5.3 together with the recipe of the paste, the fineness of the cement and the curing temperatures.

The hydration of these cement pastes are first simulated by using the *Van Eijk's Model* described in Chapter 2. For cements whose fineness is unknown, a value of 380 m^2/kg is assumed, corresponding approximately to CEM I 32.5R produced in The Netherlands.

For facilitating the discussion, a similar concept as the "distribution ratio" is defined, called "Molality" (M_a) of alkalis in C-S-H. The molality physically represents the moles of alkali ions adsorbed by unit mass of the solid C-S-H gel.

According to its definition, the molality is calculated as:

$$M_a = \frac{n_i^b}{m_{C-S-H}} \quad (\text{mmol/g}) \tag{5.16}$$

By comparing Eqs. (5.10) and (5.16), one can see that actually:

$$M_a = R_d \cdot C_i \tag{5.17}$$

Table 5.3: Properties of the Portland cements and pastes used in experiments.

Num.	Bogue composition, magnesium, sulfates and alkalis (m/m%)								Blaine	w/c	Temp.
	C_3S	C_2S	C_3A	C_4AF	MgO	SO_3	Na_2O	K_2O	(m^2/kg)		(°C)
1[a]	56.8	19.7	6.9	11.3	3.72	3.25	0.43	1.23	380♯	0.42	23
2[a]	70	8.8	7.4	11.3	1.35	3	0.2	0.47	380♯	0.42	23
3[b]	54.5	21.3	10.9	9.2	1.5	3.1	0.21	0.82	321	0.4	22
4[b]	54.5	21.3	10.9	9.2	1.5	3.35	0.21	0.82	321	0.45	22
5[b]	54.5	21.3	10.9	9.2	1.5	2.7	0.21	0.82	321	0.56	22
6[c]	55	15	7.9	8.1	1.85	0.88	0.08	1.12	300	0.5	20
7[d]	58	16	7	12	4.15	0.91	0.16	0.51	312	0.35	22
8[e]	63.8	12.4	11	8.8	1.54	3.21	0.14	0.95	370	0.5	20
9[e]	69.8	6.8	9.6	9.7	1.47	2.59	0.19	1.22	369	0.5	20
10[e]	65.8	15.2	8.7	10.2	1.59	3.21	0.64	0.78	380♯	0.5	20
11[f]	64.3	17.3	8.5	9.9	1.22	3.1	0.32	0.6	310	0.4	23
12[g,†]	55.1	25	9.7	10.2	5.03	0.35	0.25	1.27	380♯	0.5	20
13[g,‡]	55.1	25	9.7	10.2	5.03	0.35	0.25	1.27	380♯	0.5	20

[a]: taken form Bérubé et al. (2004); [b]: taken from Larbi et al. (1990); [c]: taken from Lothenbach and Winnefeld (2006); [d]: taken from Rothstein et al. (2002); [e]: taken from Schäfer (2004); [f]: taken from Diamond (1981); [g]: taken from Longuet (1976);
†: 4.5 m/m% gypsum added;
‡: 8.6 m/m% gypsum added;
♯: assumed value.

Substituting Eqs. (5.16) and (5.7) into (5.6) gives:

$$M_{a,i} = \frac{n_i^r - C_i \cdot V_w}{m_{C-S-H}} \tag{5.18}$$

If the molality is known, the alkali concentration is calculated as:

$$C_i = \frac{n_i^r - M_a \cdot m_{C-S-H}}{V_w} \tag{5.19}$$

Similarly, the distribution ratio is calculated as:

$$R_{d,i} = \frac{n_i^r - C_i \cdot V_w}{C_i \cdot m_{C-S-H}} \tag{5.20}$$

The parameters n_i^r, V_w and m_{C-S-H} appearing in Eqs. (5.18) and (5.20) are obtained with *Van Eijk's Model*. The values for C_i are measured in the experiments. Therefore, the M_a and R_d for alkalis in C-S-H can now be computed. The calculated M_a for Na^+ and K^+ are plotted as a function of the alkali concentration in Figure 5.3 and the calculated R_d in Figure 5.4.

It can be seen in Figure 5.3(a) that there is a linear relationship between the molality of Na^+ in C-S-H and its concentration, implying a linear binding capacity of C-S-H for Na^+. This linear binding model is in agreement with the hypothesis by Taylor (1987b) and Brouwers and Van Eijk (2003).

However, for the molality of K^+ in C-S-H (Figure 5.3(b)), this linear relationship cannot be decerned. On the contrary, when observing the distribution ratio for K^+ (Figure 5.4(b)), it can be seen that it decreases with increasing K^+ concentrations, indicating a non-linear binding of C-S-H to K^+ ions. Most likely a non-linear binding model should be applied here.

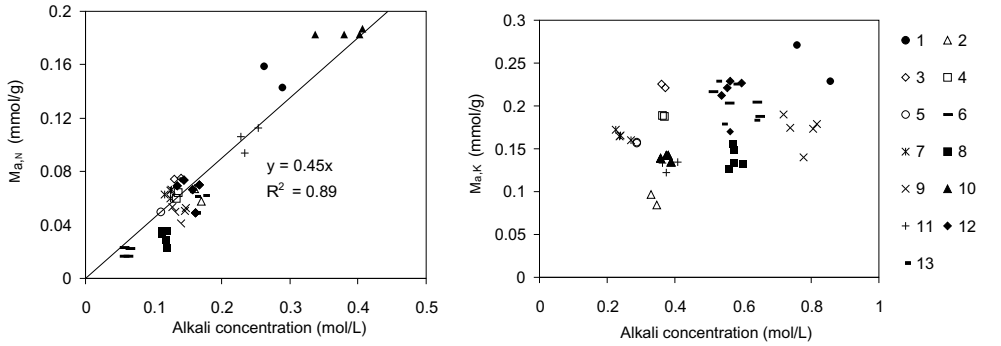

(a) Na^+ (b) K^+

Figure 5.3: Molality of alkalis versus alkali concentration in solution calculated with Eq. (5.18). Numbers in the legend correspond to the cement numbers in Table 5.3.

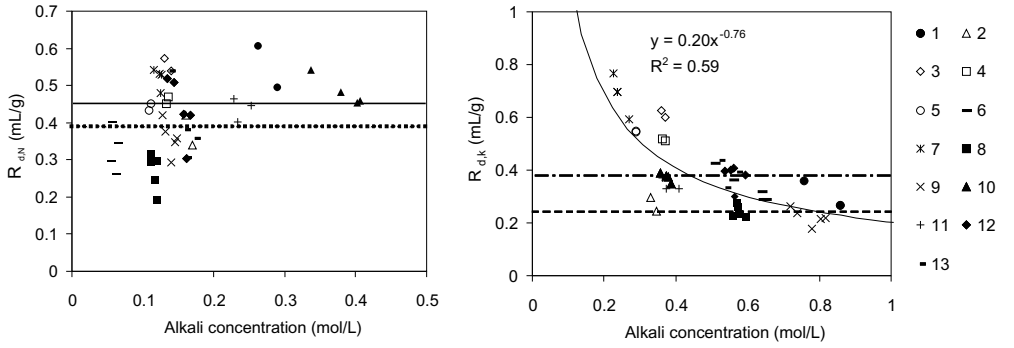

(a) Na^+ (b) K^+

Figure 5.4: Distribution ratio of alkalis versus alkali concentration in solution calculated with Eq. (5.20). Numbers in the legend correspond to the cement numbers in Table 5.3. "▪▪▪▪▪▪": values for Na^+ used by Taylor (1987b) and Brouwers and Van Eijk (2003); "–·–·–": values for K^+ used by Brouwers and Van Eijk (2003); "---": values for K^+ used by Taylor (1987b), "—": values suggested in the present work.

A linear regression analysis for the linear relation in Figure 5.3(a) gives:

$$M_{a,N} = 0.45 \cdot C_i \quad \text{mg/g}; \quad R_{d,N} = 0.45 \quad \text{mL/g} \tag{5.21}$$

The non-linear relation in Figure 5.4(b)) can be fitted with

$$R_{d,K} = 0.20 \cdot C_i^{-0.76} \quad (\text{in mL/g}) \tag{5.22}$$

The last expression complies with the Freundlich isotherm, which is widely used to describe the adsorption of solutes in solution by solid phases.

It can be seen in Figure 5.4 that for hydrating Portland cement paste, the distribution ratios of Na^+ and K^+ have similar values. A detailed comparison shows that for low alkali concentrations (about 0–400 mmol/L) the distribution ratio of K^+ is slightly higher than that of Na^+. With increasing alkali concentrations, the latter gradually surpasses the former.

The constant values of $R_{d,N}$ and $R_{d,K}$ used by Brouwers and Van Eijk (2003) and those

derived from the study of Taylor (1987b) are included in Figure 5.4 as well. It can be seen that the values of R_d in these two studies (Brouwers and Van Eijk, 2003; Taylor, 1987b) are in line with the calculations in this chapter. The used values of $R_{d,N}$ are the same in the two studies, because (a) the linear relation used is indeed valid for Na^+ and (b) the used values are very close to the predictions in this chapter. However, two remarkably different values are used for $R_{d,K}$, because of the differences in the concentrations of K^+ measured in the different experiments. The $R_{d,K}$ value used by Taylor (1987b)—0.25 mL/g—is valid for the high concentrations (e.g. 400–600 mmol/L in Figure 1 of Taylor (1987b), while the value used by Brouwers and Van Eijk (2003)—0.38 mL/g—is valid for relatively low concentrations (370 mmol/L). Therefore, for low K^+ concentrations, the predictions with Taylor's value are obviously higher than the measurements (see Figure 1c in Taylor (1987b)).

Furthermore, it is well illustrated in Figure 5.4 that C-S-H in hydrating cement paste can bind more K^+ than Na^+, due to the generally lower concentration of Na^+ than K^+. Therefore, it is essential to distinguish the alkali types in the cement while evaluating the alkali-binding capacity of C-S-H in hydrating cement paste. If the cement is low in both Na_2O and K_2O, relatively more K^+ is immobilized in the solid phases. If the levels increase for both alkalis, the binding capacity of Na^+ is much more enhanced than that of K^+, and surpasses the latter at a certain level.

Experimental data about the binding capacity of real hydrating cement paste in regard to different alkali concentrations in the pore solution is difficult to find. The reported data by Schäfer (2004) and Longuet (1976) are measured with different recipes. However, experimental data on the binding of chloride ion in the hydrating Portland cement paste have recently become available. Panesar and Chidiac (2006) measured the amount of bound Cl^- in the hydrating Portland cement paste that was equilibrated with solutions containing different amount of chloride ions. Paste samples were made and equilibrated with the solution at 23 °C. Five different concentrations of chloride were used, ranging between 0 and 3.0 mol/L. The distribution ratio ($R_{d,Cl}$) is calculated from the data reported by Panesar and Chidiac (2006) with Eq. (5.17) and is plotted in Figure 5.5. The calculated values of R_d are also fitted with Eq. (5.22), yielding:

$$R_{d,Cl} = 0.25 \cdot {C_{Cl}}^{-0.62} \quad (\text{in mL/g}) \tag{5.23}$$

in which C_{Cl} is in mol/L.

It can be seen that the binding characteristic of hydrating Portland cement paste on chloride ions are very similar to that on the potassium (see Figure 5.4(b)). Both the trend and the fitted values are in good quantitative agreement, though they concern the binding of the anion (Cl^-)

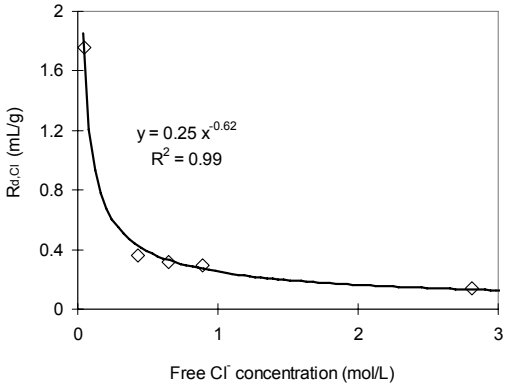

Figure 5.5: Distribution ratio of chloride ions in hydrating Portland cement paste at 23 °C, calculated from the work of Panesar and Chidiac (2006).

instead of the cations (Na^+ and K^+). Hence, from this results, one might conclude that the Freundlich isotherm could be appropriate for the binding of other ions as well. Eq. (5.23) can be used in the modeling of chloride transport in concrete and relevant durability studies.

5.5 New models for alkali concentrations in slag cement paste

The use of supplementary cementitious materials (SCM), for example, fly ash, slag and silica fume, in concrete is proven beneficial for depressing the alkali levels in its pore solution, and hence mitigating the risk of ASR, supposing the materials do not supply too much alkali ions themselves (Duchesne and Bérubé, 1994; Kollek et al., 1986; Schäfer, 2004; Taylor, 1987b). Slag, as one of these materials, is an industrial byproduct and is already widely used in constructions as explained in Chapter 1. Its usage has many other advantages such as energy saving, high ultimate strength, and a dense microstructure in addition to its depressive effect on the alkali levels of pore solution.

The depressive effect of slag on the alkali levels is commonly regarded as due to three factors:

1. The C-S-H in the slag cement pastes formed by the cement hydration has a remarkably lower C/S ratio than that in Portland cement paste (see Chapter 4 and (Richardson and Groves, 1992)), which can bind more alkali ions (Hong and Glasser, 1999, 2002; Stade, 1989);
2. The C-S-H with a lower C/S ratio can structurally incorporate more aluminum in its structure (Richardson and Groves, 1992), enhancing its binding capabilities for alkali ions (Hong and Glasser, 2002);
3. The hydration degree of slag in the cement is remarkable lower than that of Portland cement, releasing considerably less alkali ions and hence diluting the source of alkali ions (Schäfer, 2004).

In the previous section, a method for determining the alkali-binding capacity of C-S-H in hydrating Portland cement pastes is proposed, which is shown to vary in a range and depend on the alkali concentrations in the solution.

In this section, efforts are made to predict the alkali concentrations in the pore solution of hydrating slag cement paste in a long term. The partition theory of Taylor (1987b) and Brouwers and Van Eijk (2003) is again taken over as the starting point.

The method for predicting the alkali concentrations in the pore solution of Portland cement paste in the preceding section cannot be applied directly to hydrating slag cement paste, due to at least four difficulties. First, the mass of the principle binder (C-S-H) and the volume of pore solution are different from those of the hydrating Portland cement paste. They cannot be predicted without appropriate theories on the reaction of slag in blended cement. Second, the two principle components in slag-blended cement—Portland cement and slag—hydrate at different rates. Therefore, at a given age the two components have different hydration degrees, and these differences will in turn change the amount and composition of hydration products, and the amount of alkali ions released. Third, the binding capacity of C-S-H from slag cement hydration, which has different composition with that formed by the Portland cement hydration, is also different. Therefore, the distribution ratio is different as well. The last, some other hydration products than those in the hydrating Portland cement paste exist in slag cement paste, which may possess alkali-binding capacity as well.

Similar to the theory for hydrating Portland cement paste, the alkali release from the hydrated cement and the binding in the solids are first discussed.

5.5.1 Alkali release

The amounts of alkali ion (Na^+ or K^+) in the Portland cement can be computed again with Eq. (5.24), with consideration to the slag proportion in the cement, as:

$$n_i^{T,p} = \frac{2x_i^p}{M_i} \cdot m^p = \frac{2x_i^p}{M_i} \cdot m \cdot (1-\lambda) \tag{5.24}$$

and those in the slag are computed as:

$$n_i^{T,sl} = \frac{2x_i^{sl}}{M_i} \cdot m^{sl} = \frac{2x_i^{sl}}{M_i} \cdot m \cdot \lambda \tag{5.25}$$

in which $n_i^{T,p}$ and $n_i^{T,sl}$ are the total amounts of alkali ions i in the Portland cement and slag, respectively; x_i^p and x_i^{sl} are the mass fraction of alkali oxides in Portland cement and slag, respectively; m is the mass of cement; λ is the slag proportion in the cement (Eq. (4.2)).

The alkali ions released by the hydration of Portland cement is calculated again with Eq. (5.5) with n^T replaced now by $n^{T,p}$ (i.e. by multiplying with $1-\lambda$). In slags, the parts of alkali ions present in the readily soluble form are negligible (Barlow and Jackson, 1988). Normally, most of the alkali oxides in slag exist in the glass form and the crystalline minerals do not contain alkalis (Smolczyk, 1980). Furthermore, all oxides in the glass phase of slag react congruently, as also used in Chapter 4 for modeling the slag hydration.

Similarly, the amount of alkali ions released by the slag hydration is calculated as:

$$n_i^{r,sl} = \alpha^{sl} \cdot n_i^{T,sl} \tag{5.26}$$

in which α^{sl} is the hydration degree of slag. The total amount of alkali ions released by the slag cement hydration reads:

$$n_i^r = n_i^{r,sl} + n_i^{r,p} = [f_i^{sul} + \sum_{j=1}^{4} f_{i,j}(1-f_i^{sul})\alpha_j] \cdot n_i^{T,p} + \alpha^{sl} \cdot n_i^{T,sl} \tag{5.27}$$

5.5.2 Alkali-binding

Partition of alkali ions between the solution and the solid phase is known to occur. Therefore, the alkali ions released by the cement hydration are accordingly divided into two parts: those in the solution and those bound in hydration products, as given in Eq. (5.6). The amount in the solution can be computed with Eq. (5.7).

If the solid product C-S-H is assumed the only alkali binder in the hydration products, the amount of bound alkalis is computed with Eq. (5.10) again. Substituting Eqs. (5.7) and (5.10) into Eq. (5.6) again gives Eq. (5.12). Rewriting Eq. (5.12) gives the same expression as Eq. (5.19) for computing the concentration of alkali i (C_i).

5.5.3 Modeling the slag cement hydration

When modeling the alkali concentrations in the pore solution of hydrating slag cement paste, the following parameters are needed: the hydration degree of clinker phases and slag (α_j and α^{sl} in Eq. (5.27), the volume of pore solution (V_w) and the mass of the binder C-S-H (m_{C-S-H}). Note that in the discussion above it is assumed that C-S-H is the only alkali binder. If the alkali-binding capacity of some other products is investigated, their amounts are required as well.

The 3-D computer model *Van Eijk's Model* introduced in Chapter 2 is used to predict the hydration degree of clinker in blended cement. It is already proven a useful tool for modeling the hydration of Portland cement (Bentz, 2000; Brouwers and Van Eijk, 2003; Van Eijk, 2001). The model accounts for the clinker composition, its PSD, the temperature and the w/c ratio of

Table 5.4: Parameters for predicting the hydration degree of slag in blended cement according to Eq. (5.29). Values of k_1, k_2, and k_3 are taken from Taylor (1987b), values of a^{sl} and b^{sl} are fitted from the measurements by Schäfer (2004).

k_1	k_2	k_3	a^{sl}	b^{sl}
0.46	0.12	0	-0.0036	0.86

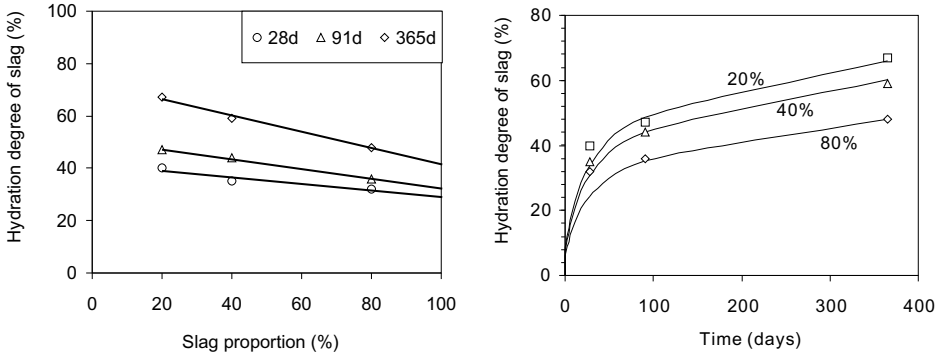

(a) Versus slag proportion (b) Measurement and prediction

Figure 5.6: Hydration degree of slag in blended cement. Symbols: measurements by Schäfer (2004); solid lines: trend line (a) and predictions with Eq. (5.29) (b).

the paste.

The determination of the slag hydration degree in the blended cement is more complex than that of the clinker hydration. The reactivity of slag, the slag proportion, the pore solution composition, temperature, w/c ratio and its PSD are important, and no general methods for predicting its reaction degree are available. A more detailed discussion about the reaction rate of slag in cement is presented in Chapter 7.

In this chapter, a simplified expression is used to predict the hydration degree of slag in the blended cement. It is based on the methods used by Taylor (1987b) for predicting the hydration degree of clinker phases in Portland cement, as:

$$\alpha^{sl} = 1 - \exp[-k_2(t/24 - k_3)^{k_1}] \tag{5.28}$$

in which k_1, k_2, and k_3 are three characteristic parameters (dimensionless), t is the hydration time (in hour), The values of k_1, k_2 and k_3 for predicting the hydration degree of belite in Portland cement by Taylor (1987b) is taken over, listed in Table 5.4.

Furthermore, the hydration degree of slag in cement is obviously influenced by the slag proportions in the cement. The higher proportions result in lower hydration degrees of slag. Schäfer (2004) measured the hydration degrees of slag in blended cement with different slag proportions (see Figure 2.7). It appears that at given age there is a linear relation between the hydration degree of slag and the slag proportions in cement (Figure 5.6(a)). Therefore, Eq. (5.28) is further corrected for the slag proportions in cement as:

$$\alpha^{sl} = \{1 - \exp[-k_2(t/24 - k_3)^{k_1}]\} \cdot (a^{sl} \cdot \lambda + b^{sl}) \tag{5.29}$$

in which a^{sl} and b^{sl} are the two characteristic parameters for the linear relationship. A linear regression analysis with the experimental data by Schäfer (2004) yields the values for a^{sl} and b^{sl} as given in Table 5.4. The predicted hydration degree of slag with Eq. (5.29) is plotted in

Table 5.5: Oxide composition of clinker and slag used in the experiments of Longuet (1976) and Schäfer (2004) (m/m%).

Oxide	Clinker			Slag						
	C1†	C2‡	C3‡	S1†	S2†	S3†	S4†	S5‡	S6‡	S7‡
SiO_2	21.36	21.05	20.69	35.16	31.64	36.06	33.43	34.6	30.37	38.52
Al_2O_3	5.36	5.99	5.64	11.86	17.39	12.16	14.8	12.05	16.1	9.49
TiO_2	0.32	0.3	0.23	0.41	0.59	0.58	0.74	0.62	1.14	0.97
P_2O_5	0.12	0.12	0.08	0.15	0.16	0.1	0.08	0.01	0.02	0.02
Fe_2O_3	3.26	2.88	3.17	1.2	1.4	0.71	1.13	0.58	1.25	1.6
MnO	0.06	0.07	0.04	0.82	0.37	0.68	1.18	0.28	0.4	1.24
CaO	62.58	65.83	66.15	44.68	44.17	39.72	38.48	42.58	38.02	36.79
MgO	5.03	1.54	1.47	4.31	4.53	7.8	8.2	7.54	10.25	8.49
SO_3	0.35	0.88	0.91	0	0	0	0	0.01	0.53	0.01
K_2O	1.27	0.95	1.22	0.22	0.76	1.13	1.08	0.38	0.39	1.25
Na_2O	0.25	0.14	0.19	0.2	0.31	0.6	0.73	0.29	0.41	0.41

†: taken from Longuet (1976);
‡: taken from Schäfer (2004).

Figure 5.6(b). It can be seen that the hydration degree of slag in cement is well predicted with the proposed equations.

Eq. (5.29) and parameters in Table 5.4 are taken valid for all slag cements used in this chapter. Actually, the slag reactivity depends on many factors and may differ from one slag to the other. However, it is shown in Section 5.7.2 that the slag hydration degree (varying with different slag reactivities) does not influence the predicted alkali concentrations significantly. Therefore, most likely this method can be employed directly when predicting the alkali concentrations in pore solution of hydrating slag-blended cement. In Chapter 7 of this thesis, the slag hydration degree can be predicted with the *Van Eijk's Model*, which considers explicitly the various factors on the slag reactivity.

When the hydration degrees of clinker and slag in blended cement are known, the amount of hydration products, their composition, and the volume of pore solution can be predicted with the models for the hydration of blended cement presented in Chapter 4.

5.5.4 Alkali-binding capacity of C-S-H

For hydrating slag-blended cement paste, the determination of alkali-binding capacity of C-S-H is more complicated with its varying composition and the presence of other products. The composition of C-S-H is influenced by the mineral compositions of clinker and slag, the slag proportion in the cement and the slag hydration degree. Furthermore, as concluded in the previous section, the slag hydration degree is affected by the alkali ions released by the cement hydration as well.

A series of experiments are selected from the studies of Longuet (1976) and Schäfer (2004), who measured the chemical compositions of pore solutions in hydrating slag cement paste with different slags and clinkers. The compositions of clinkers and slags used in the experiments are listed in Table 5.5.

The eighteen recipes of slag cements made with the clinkers and slags in Table 5.5 are listed in Table 5.6. Note that in the experiments of Longuet (1976) (recipe number 1–8), different proportions of gypsum are added into the mix, being 4.5 m/m% and 8.6 m/m%. It can be seen that the slag proportions in the paste vary in a wide range from 20 percent to 80 percent. The

Table 5.6: Recipes of slag cement pastes used in the experiments by Longuet (1976) and Schäfer (2004). The w/c ratio is 0.5 and all pastes are cured in a sealed environment at 20°C. Numbers in the recipe indicate the slag proportions in the cement.

Num.	Recipe	Num.	Recipe
1	C1-S1-75†	10	C2-S5-40
2	C1-S1-75‡	11	C2-S5-80
3	C1-S2-75†	12	C2-S6-40
4	C1-S2-75‡	13	C2-S6-80
5	C1-S3-75†	14	C2-S7-40
6	C1-S3-75‡	15	C2-S7-80
7	C1-S4-75†	16	C3-S5-40
8	C1-S4-75‡	17	C3-S6-40
9	C2-S5-20	18	C3-S7-40

†: 4.5 m/m% gypsum added;
‡: 8.6 m/m% gypsum added.

pastes are made with a w/c ratio of 0.5 and cured at 20°C up to 2 years. The pore solutions are squeezed out of the paste at different ages and the ion concentrations are analyzed. For the detailed results of the measurements, the reader is referred to Longuet (1976) and Schäfer (2004) are referred.

Simulations are carried out for the hydration of clinker in these 18 recipes with the *Van Eijk's Model*. The hydration degree of slag in cement is predicted with Eq. (5.29). The amounts of alkalis released by the hydration (n_i^r), available in the pore solution (n_i^s) and bound in the hydration products (n_i^b) and the masses of the hydration products are computed from the simulation results and the measurements in the experiments.

The computed molarities of alkalis in C-S-H with Eq. (5.18) are plotted in Figure 5.7. It appears that there are no obvious relations between the molarities in C-S-H and the alkali concentrations in the pore solution. Two factors most likely contribute to the big scatter in the

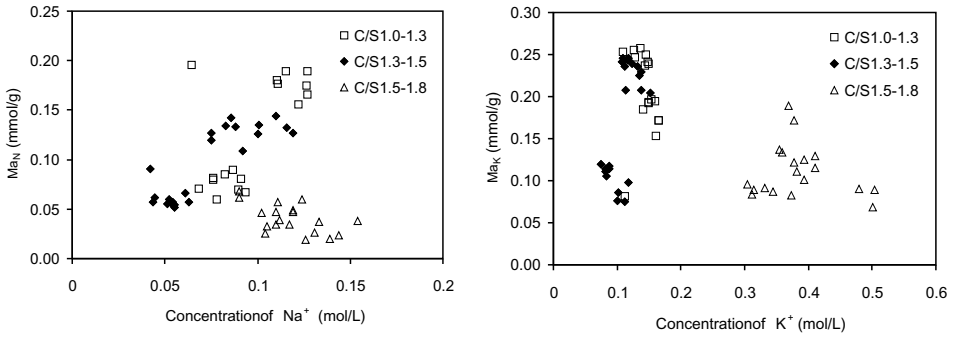

(a) Na^+ (b) K^+

Figure 5.7: Calculated molarities of alkalis in C-S-H according to Eq. (5.18) and measurements from the experiments of Longuet (1976) and Schäfer (2004). The predicted range of C/S ratios in C-S-H is indicated in the legend.

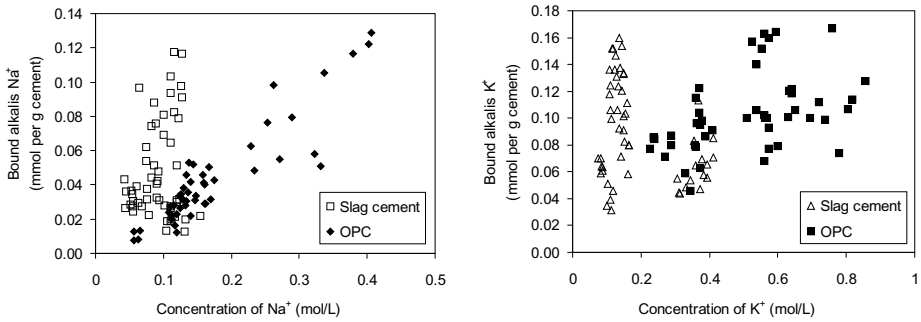

(a) Na^+ (b) K^+

Figure 5.8: Amount of bound alkalis in hydration products versus alkali concentrations in pore solution, calculated from Eq. (5.30) and including the results for the 13 Portland cement pastes in Table 5.3.

figures. The first factor is that the C-S-H has various compositions, which possesses different alkali-binding capacities. The second one is that in the computations it is assumed that C-S-H is the only binder of alkalis, which actually still needs to be verified.

According to Stade (1989) and Hong and Glasser (2002), C-S-H with lower C/S ratios has stronger alkali-binding capacities (see also Table 5.2). However, when observing the molality in C-S-H with different C/S ratios (indicated in the figures), it can be seen that there are no clear trends of effects of C/S ratio on the alkali-binding capacity of C-S-H, i.e. higher C/S ratios do not consistently lead to higher binding capacities. Therefore, it appears that the cause of the scatter by the ranges in C/S values can be ruled out. In the following section, the effect of the second factor—alkali-binding by other products—is discussed.

5.5.5 Hydrotalcite as alkali binder

The second factor—the contribution of other products—is investigated in this section. For every recipe tested in the experiments and at the given age, the amount of alkalis bound in the hydration products is computed with the following equation:

$$n_i^b = n_i^r - n_i^s = n_i^r - C_i \cdot V_w \tag{5.30}$$

The parameter C_i is measured in the experiments; n_i^r and V_w are predicted with the computer model. The calculated values of n_i^b for both Na^+ and K^+ are plotted in Figure 5.8 together with the values for the 13 Portland cement recipes given in Table 5.3 as well.

It can be seen in Figure 5.8 that there are obvious differences among the trends of the alkali binding between the slag cement pastes and the Portland cement pastes. The amount of bound alkalis in Portland cement pastes is obviously influenced by the alkali concentrations, while that in slag cement pastes is not strongly influenced. It appears that the presence of some other solids changes the alkali-binding capacity in the solids dramatically.

A careful observation on the effects of slag on the amounts and types of hydration products in hydrating slag cement pastes compared to the hydrating Portland cement paste reveals that adding slag into the pastes remarkably increases the amount of hydrotalcite, a distinct product from slag reaction.

Normally, both the Portland cement and slag contain some MgO. However, the MgO in Portland cement normally hydrates into brucite (MH) (Ali and Mullick, 1995; Taylor, 1997), whereas the MgO from slag hydrates into hydrotalcite (see Chapter 3 and 4). The brucite exists in the crystalline form, commonly used as the sources for compensating shrinkage (see also

Chapter 8). Quite contrary to the brucite, the hydrotalcite formed in hydrating slag cement paste is highly amorphous, and is closely mixed with the product C-S-H (Gollop and Taylor, 1996a; Harrisson et al., 1987; Richardson and Groves, 1992; Wang and Scrivener, 1995).

The hydrotalcite belongs to a family of inorganic materials known as layer double hydroxides (LDH). It has a layered crystal structure composed of hydroxide layers and interlayers containing anions and water molecules (Figure 5.9). The hydrotalcite-like compounds are known for their large specific area, and high anion-exchange capacities. Researches have shown that it is able to adsorb and remove large amount of cations as well (Duan and Evans, 2006). This cation binding capacity of hydrotalcite-like compounds is probably due to their strong adsorption capacity for anions, which is accompanied by an adsorption of cations as well due to the charge balance (Li, 2006).

Based on the discussion above, it is interesting to include the hydrotalcite as a potential binder for alkali ions in the system besides the C-S-H and to study its effects on the experimental results. Now, the amount of bound alkalis in the solids is plotted as a function of hydrotalcite in the pastes in Figure 5.10. The amount of hydrotalcite formed from slag reaction is predicted with the computer model based on the theories in Chapter 3 and 4.

It can be clearly seen that there is a relationship between the amount of bound alkalis in the solid and that of the hydrotalcite formed from the slag hydration. The inclusion of hydrotalcite is obviously important when predicting the alkali concentrations in the pore solution.

5.5.6 New methods for binding capacities of C-S-H and hydrotalcite

Similar to Eq. (5.16), the amount of bound alkalis now considering also the hydrotalcite reads:

$$n_i^b = M_{a,i}^1 \cdot m_{C-S-H} + M_{a,i}^2 \cdot m_{HT} \tag{5.31}$$

in which $M_{a,i}^1$ and $M_{a,i}^2$ stands for the molarities of alkali i in C-S-H and hydrotalcite, respectively.

According to Eq. (5.17), Eq. (5.31) is written as:

$$n_i^b = R_{d,i}^1 \cdot C_i \cdot m_{C-S-H} + R_{d,i}^2 \cdot C_i \cdot m_{HT} \tag{5.32}$$

Based on the discussion for alkali-binding capacity of C-S-H in hydrating Portland cement paste (Section 5.4), it is assumed that C-S-H in hydrating slag cement pastes has a linear binding of alkalis as well, with respect to the alkali concentrations, i.e. the values of $R_{d,i}^1$ do not change with different alkali concentrations. However, the C/S ratio in C-S-H is varying in this case, which should be taken into account.

The experimental results on the alkali-binding capacity of C-S-H with various C/S ratios by Hong and Glasser (2002) are used here. A log-log plot of the measured R_d values (Table 5.2) versus the C/S ratios in the synthetic C-A-S-H gel gives Figure 5.11(a) and 5.11(b). A linear relation is observed again between the logarithm of R_d and that of the C/S ratios. A comparison between the effects of Na^+ and K^+ shows that the alkali-binding of C-S-H to these two ions are similar. The mean values for the slope coefficients in Figure 5.11 are -6.12 and -6.21 for Na^+

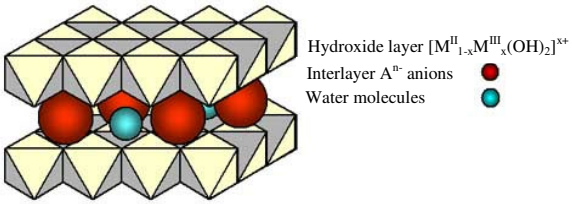

Figure 5.9: Layered structure of hydrotalcite-like compounds (Courtesy of Kovanda, F.).

Table 5.7: Fitted values of Y and R_d^2 for Na^+ and K^+ according to Eq. (5.34) using the calculated amounts of bound alkalis and the multiple linear regression analysis, together with the used values of r.

	Y (mL/g)	r	R_d^1 (mL/g)		R_d^2 (mL/g)	R^2
			(C/S = 1.1)	(C/S = 1.8)		
Na^+	0.10	-6.12	0.056	0.0027	9.6	0.62
K^+	0.23	-6.21	0.13	0.0059	10.2	0.56

and K^+, respectively.

Based on the relation shown in Figure 5.11, it is proposed that the values of $R_{d,i}^1$ are related to the C/S ratio of C-S-H as:

$$R_{d,i}^1 = Y \cdot \hat{a}^r \tag{5.33}$$

in which $\hat{a}$ is the C/S ratio in C-S-H, Y is a constant (mL/g) and the values of r are -6.12 and -6.21 for Na^+ and K^+, respectively.

Constant values of $R_{d,i}^2$ are used for the hydrotalcite as well. Therefore, substituting Eq. (5.33) into Eq. (5.32) gives:

$$n_i^b = Y \cdot \hat{a}^r \cdot C_i \cdot m_{C-S-H} + R_{d,i}^2 \cdot C_i \cdot m_{HT} \tag{5.34}$$

A multiple linear regression analysis with the data points presented in Figure 5.10 gives the values of Y and $R_{d,i}^2$ in Table 5.7 together the used values of r.

It can be seen that in hydrating slag cement paste, the hydrotalcite has a much stronger alkali-binding capacity then the C-S-H. The R_d value for the hydrotalcite is much bigger than that of C-S-H in hydrating Portland cement pastes as well (indicated in Figure 5.4). On the contrary, the C-S-H in hydrating slag cement pastes shows relatively weak alkali-binding capacity as compared to that in hydrating Portland cement pastes. By substituting typical values for the C/S ratio of C-S-H in hydrating slag cement, for example, 1.1 and 1.8, into Eq. (5.33) and the values in Table 5.7 yields the values for $R_{d,N}^1$ and $R_{d,K}^1$ as listed in Table 5.7. These values are much lower than

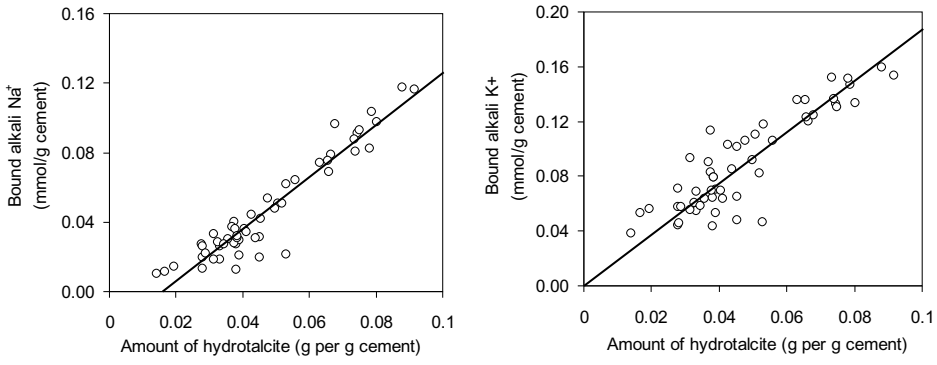

(a) Na^+ (b) K^+

Figure 5.10: Amount of bound alkalis in hydration products versus amount of hydrotalcite in the paste, calculated from Eq. (5.30) for the 13 Portland cement pastes in Table 5.3 at ages later than 68 days. The amount of hydrotalcite is predicted with the theoretical model in Chapter 4.

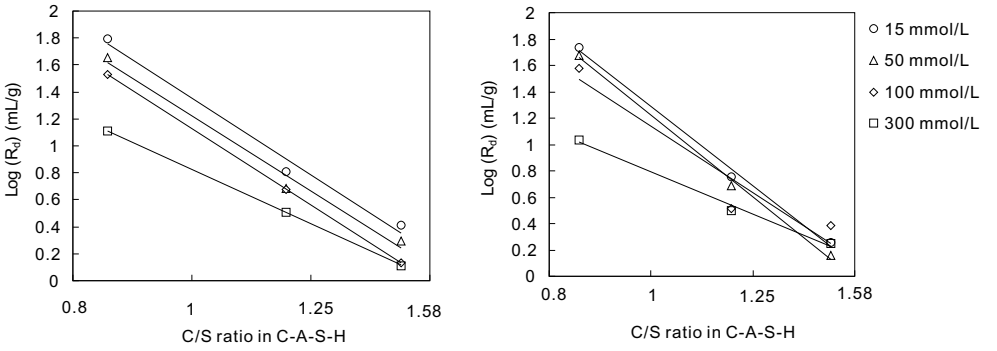

(a) Na^+ (b) K^+

Figure 5.11: Distribution ratio of alkalis in synthetic C-A-S-H gel versus its C/S ratio, after Hong and Glasser (2002).

those for C-S-H in hydrating Portland cement (see Figure 5.4).

The alkali-binding capacity of C-S-H in hydrating slag cement paste is not directly measured in experiments before. The replacement of clinker with slag is known to lower the C/S ratio in C-S-H, as discussed in Chapter 4. According to Hong and Glasser (2002), C-S-H with lower C/S ratios has higher alkali-binding capacities. Therefore, it is expected that C-S-H in hydrating slag cement paste has higher alkali-binding capacity than that in hydrating Portland cement paste. However, in the experiments by Stade (1989), the a higher alkali-binding capacity of C-S-H with a lower C/S ratio is not obvious for synthetic C-S-H prepared at ambient temperature. Furthermore, in the experiments of Stade (1989), it is found that the Al-containing C-S-H has even weaker alkali-binding capacities than the Al-free one, which is contrary to the conclusions of Hong and Glasser (2002) as well. The contrary conclusions about the role of alumina substitution in C-S-H on its alkali-binding capacity could be partially due to the alumina substitution level. The A/S ratio used by Hong and Glasser (2002) is about 0.031–0.038, while that used by Stade (1989) is 0.07, the latter being more close to the actual values measured in the hydrating slag cement pastes (Richardson and Groves, 1992).

The weak alkali-binding capacity of C-S-H in hydrating slag cement is partially confirmed by the experiments of Schäfer (2004) as well. The author measured the alkali concentrations in hydrating slag cement pastes with different proportions of slag. When 20 m/m% of the Portland cement is replaced by GGBFS, the Na^+ concentration in the pore solution is even *higher* than that in the neat Portland cement paste. Replacing the Portland cement with slag does not change the C/S ratios in C-S-H very much (Chapter 4 of this thesis and Richardson and Groves (1992)), while it dilutes the amount of alkalis in cement, being beneficial for lowering the alkali concentrations in the pore solution. However, the measured alkali concentrations are raised. Therefore, it can be concluded that the C-S-H in hydrating slag cement paste has actually weaker alkali-binding capacities than that in hydrating Portland cement paste. Similar trends are observed in the experiments of Kollek et al. (1986), too. 20 m/m% replacement of Portland cement by slag is found unable to significantly reduce the hydroxyl concentration and in three out of nine cases, the hydroxyl concentration raises.

As discussed above, the weak binding capacity of C-S-H in slag cement paste is probably due to the high aluminum content in it. On the one hand, the alumina in slag normally exists in the glass network, which is released into the pore solution and becomes available for the hydration products spontaneously as the hydration of slag goes on. Furthermore, it is shown in Chapter 3 that *ca.* half of the aluminum in slag enters the C-S-H and substitutes for silicon

in it. Therefore, if Portland cement is partially replaced by slag, there is sufficient aluminum to enter the C-S-H, even though the slag proportion is low. The C-S-H with high contents of aluminum has a remarkably low alkali-binding capacity. On the other hand, in the neat Portland cement paste, most of aluminum exists in the aluminate or ferrite phases. In some clinkers, part of the aluminum may exist in the glass form as well, but the proportion is very small (Taylor, 1997). The aluminum in the aluminate or ferrite phases reacts into stable hydration products like ettringite, C_4AH_{13} and monosulfate. Normally, aluminate reacts much faster than the alite and belite, while the latter two form C-S-H in the hydration products. Therefore, it is expected that the amount of aluminum available for the substitution of silicon in C-S-H is very limited, and the substitution takes place more likely in a heterogeneous way. Thus, C-S-H in hydrating Portland cement paste may have a higher alkali-binding capacity than that in hydrating slag cement paste.

This part of hypothesis about the influence of aluminum substitution on the alkali-binding capacity of C-S-H is based on the observations in the experiments of Stade (1989), the calculations in this thesis, and the reasoning considering the situations in both the Portland and slag cement pastes. Further detailed experiments with low slag substitution proportions in Portland cement paste (e.g. 0–20 m/m%) may further reveal the role of aluminum in C-S-H on its alkali-binding capacity. Experiments on the alkali-binding capacity of synthetic hydrotalcite are also necessary. The measured concentrations of Na^+ and K^+ are distributed in small ranges (0.05–0.15 mmol/L for Na^+ and 0.1–0.4 mmol/L for K^+), as compared to those measured in hydrating Portland cement pastes (see Figure 5.8). Thus, it is difficult to investigate the influence of the alkali concentrations as well. In this thesis, it is taken that the alkali-binding capacities of C-S-H and hydrotalcite in hydrating slag-blended cement are not significantly influenced by the alkali concentrations in the pore solution.

5.5.7 Predicting the alkali concentrations

Substituting Eqs. (5.31) and (5.7) into Eq. (5.6) and rewriting it gives a formula for computing the alkali concentration in hydrating slag cement pastes as:

$$\begin{aligned} C_i &= \frac{n_i^r}{V_w + R_{d,i}^1 \cdot m_{C-S-H} + R_{d,i}^2 \cdot m_{HT}} \\ &= \frac{n_i^r}{V_w + Y \cdot \hat{a}^r \cdot m_{C-S-H} + R_{d,i}^2 \cdot m_{HT}} \end{aligned} \tag{5.35}$$

The parameters n_i^r, m_{C-S-H} and m_{HT} are given by the simulation results with the *Van Eijk version* of CEMHYD3D, and Y, r and $R_{d,i}^2$ are taken from Table 5.7.

5.6 Validations of the new models

5.6.1 Models for hydrating Portland cement

Taylor (1987b) determined the value of the binding factor from measurements in nine laboratories and validate it with four batches of samples in these laboratories. A similar idea is used here as well, by validating the new method with 6 of these 13 cements in Table 5.3. The proposed method for determining R_d of Na^+ and K^+ in hydrating cement paste (Eqs. (5.21) and (5.22) is used to predict the alkali concentrations in the pore solution.

The hydration of these six cements is simulated with the *Van Eijk's Model*. The results are included in Figure 5.12, together with the experimental measurements with Cement 4-9. It can be seen that concentrations are correctly predicted for both Na^+ and K^+, to a better extent for Na^+.

Therefore, it can be concluded that the proposed method can predict the alkali concentrations in a wide range. The method takes different factors into account, for example, the mineral

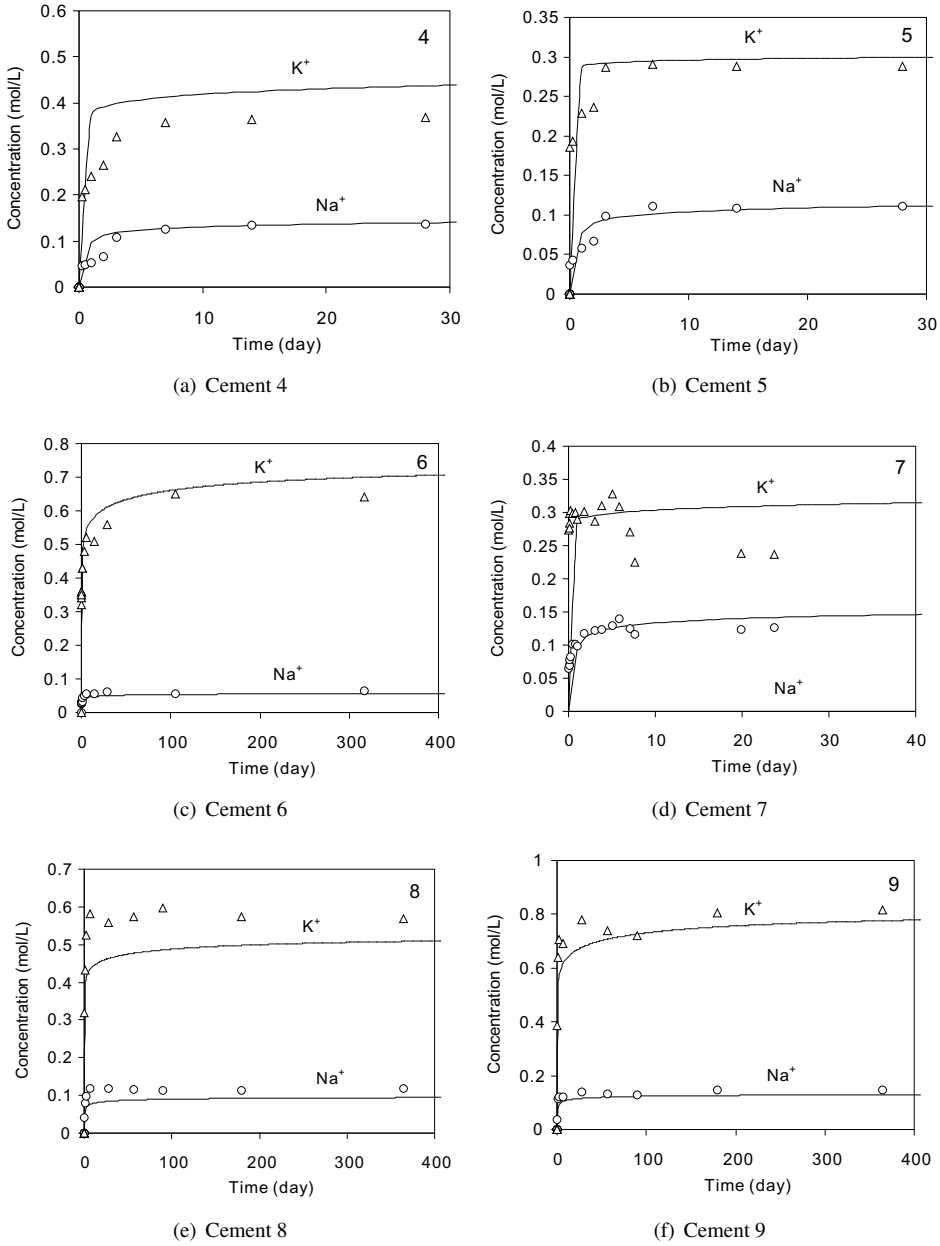

(a) Cement 4 (b) Cement 5

(c) Cement 6 (d) Cement 7

(e) Cement 8 (f) Cement 9

Figure 5.12: Predicted and measured concentration of alkali ion in the pore solution for Cements 4–9 from Table 5.3.

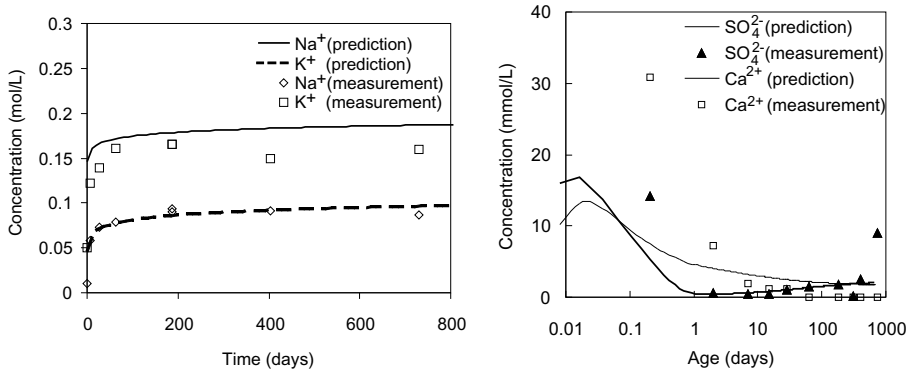

(a) Alkalis (b) $[Ca^{2+}]$ and $[SO_4^{2-}]$

Figure 5.13: Predicted and measured pore solution composition of the hydrating slag cement paste with *Recipe 4* in Table 5.6 (experimental data: Longuet (1976)).

composition of cement, its fineness, the w/c ratio, the alkali contents in cement, and the curing temperature. For modeling the Na^+ concentration, the linear model by Taylor (1987b) and Brouwers and Van Eijk (2003) is indeed valid, and for modeling the K^+ concentration, the nonlinear method given in Eq. (5.22) should be followed.

5.6.2 Models for hydrating slag cement

The formula for computing the alkali concentrations in hydrating slag cement pastes (Eq. (5.35) is also used for predicting the alkali concentrations in the pore solution of hydrating slag cement pastes.

The experimental data from Longuet (1976) are used to validate the models proposed for the hydrating slag cement paste. The oxide compositions of clinker and slag are listed in Table 5.5. The w/c ratio is 0.5 and the paste samples are cured at 20°C in a sealed environment. The paste contains 19.1 m/m% of C1, 4.5 m/m% gypsum and 76.4 m/m% S2 (*Recipe 4* in Table 5.6). The pore solution is collected by the compression method at different ages. The measurements in the experiments are presented in Figure 5.13.

The hydration of clinker in the blended cement is simulated with the *Van Eijk's Model*. The hydration degrees of slag are predicted with Eq. (5.29). The predicted hydration degrees of clinker and slag are used as model inputs for modeling the hydration of slag-blended cement. The predicted amounts of hydration products and their compositions, the volume of pore solutions are used as inputs for the parameters in Eq. (5.35). The alkali concentrations predicted with the methods proposed in this chapter are plotted in Figure 5.13(a). It can be seen that the predicted alkali concentrations in the pore solution agree well with the measured values by using the proposed method.

The predicted and measured Ca^{2+} and SO_4^{2+} concentrations are plotted in Figure 5.13(b). These two ions are chosen because they are the abundant ones in the pore solution (Longuet, 1976; Rothstein et al., 2002), and they are relevant to a lot of durability considerations (Taylor, 1997). Again, the predictions are in good agreement with the measurements. At early ages, the predictions are lower than the measurements, because the saturation condition is used in the model, while in real paste and at early ages, obvious supersaturation takes place, especially for CH and ettringite (Rothstein et al., 2002). In a long term, the pore solution composition is well predicted.

5.7 Model applications

As mentioned before, numerous researches have been done to investigate the pore solution development in hydrating Portland cement and slag cement pastes and efforts are made for clarifying the effect of different factors on the pore solution compositions. The alkali concentrations are especially interesting for the scientist due to the factors presented in Section 5.1. In this section, the effect of these factors is investigated with the pore solution models developed in this chapter. The discussion is divided into two parts, one for the hydrating Portland cement paste, and the other for the hydrating slag cement paste.

5.7.1 Pore solution of Portland cement paste

Many factors influence the alkali concentrations in pore solution of Portland cement pastes, including the alkali ion binding capacity of C-S-H, the w/c ratio of the paste, the mineral composition of cement, the form of alkali oxides and the alkali contents. The binding capacity of C-S-H (R_d) is an important factor and can hardly be measured directly in experiments. In this chapter, a method for determining its value is presented. In this section, the proposed methods are employed to investigate the influences of some other factors, and their significance for engineering practice is presented. **Cement Z1** from the work of Schäfer (2004) (*Cement 8* in Table 5.3) is used as example in the following discussion, and the complete hydration of cement is assumed to occur. The fractions of alkali ions in pore solution and in solids are further discussed.

w/c ratio of paste

With the model for predicting the alkali concentrations in pore solution, investigation of the alkali concentrations in pastes with different w/c ratios is possible. Low w/c ratios are more and more commonly used in concrete to achieve high-strength and low porosity. While the advantage of low w/c ratios on the strength development has been widely investigated, its influence on the alkali concentrations in the pore solution has not yet been completely clarified.

For simplification purpose, the complete hydration of Portland cement is assumed to occur, and all parameters (for example, clinker composition and temperature) except the w/c ratio of the paste are kept the same, so that the investigation is focused on the effect of w/c ratio. The complete hydration of cement might be doubtful for paste with low w/c ratios, but it is found even for pastes made with a w/c ratio of 0.22 (Odler and Rößler, 1985).

The predicted alkali concentrations are plotted in Figure 5.14(a).

It can be seen that while the w/c ratio has only a very mild influence on the Na^+ concentration, the influence on the K^+ concentration is obvious. The latter increases dramatically with decreasing w/c ratios, especially with low w/c ratios. The increase of alkali concentrations with decreasing w/c ratios are expected because they both increase the amount of alkali ions in the paste, and reduce the volume of water available for these alkali ions.

The different trends for Na^+ and K^+ are caused by the different binding capacities of C-S-H to these two cations. On the one hand, it can be seen in Figure 5.3 that the binding capacity increases approximately linearly with increasing concentrations of Na^+. Hence, a large part of the additional Na^+ induced by the increased amount of cement is bound in C-S-H. On the other hand, the binding capacity of C-S-H to K^+ changes only very slightly with K^+ concentrations. The flat changes of Na^+ concentration are also partially due to its low level in the pore solution.

Mineral composition of clinker

The influence of mineral composition on the alkali concentrations is investigated with the methods developed in this chapter. The w/c ratio is 0.5. The C_3S content in the clinker ranges from 30 m/m% to 70 m/m%, while the C_2S content ranges from 46 m/m% to 6 m/m%, accordingly. They total to 76 m/m% of the clinker. The C_3A and C_4AF contents in clinker are kept constant. It can be seen that concentrations of both Na^+ and K^+ increase with increasing C_3S content in

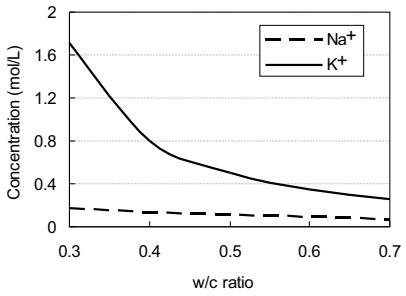

(a) w/c ratio

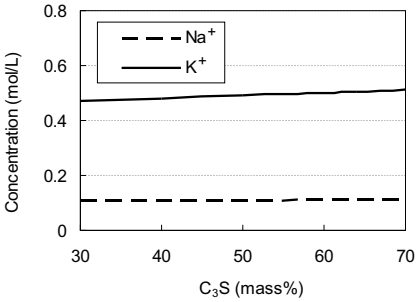

(b) C_3S in Portland cement

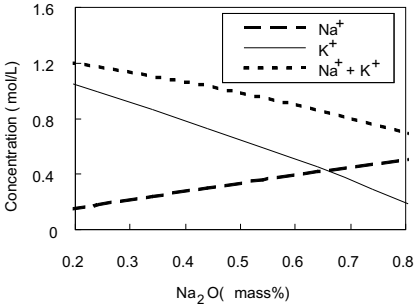

(c) alkali form in clinker

Figure 5.14: Effect of different factors on the alkali concentrations in pore solution of hydrating Portland cement paste. (a) w/c ratio; (b) C_3S content in clinker; (c) alkali form. Predicted with *Cement 8*.

clinker, due to the reduced amount of C-S-H formed in the paste (Figure 5.14(b)). The hydration of C_3S per unit mass can produce less C-S-H and more CH than that of C_2S. Hence, less alkali ions are bound in C-S-H and more is available for the pore solution. However, the influence of a shift from C_3S to C_2S on the alkali concentrations is very limited, because the hydration of C_3S consumes less water than that of C_2S (see Eqs. (2.23) and (2.24)), remaining more water available for the pore solution, which in turn dilutes the alkali ions in the solution.

The alkali concentrations decline naturally with increasing calcium silicates in clinker because more C-S-H is formed and thus more alkali ions are bound. Furthermore, more water with increasing calcium silicates would be available for pore solution because the hydrations of C_3S and C_2S consume less water than those of C_3A and C_4AF.

Alkali form

The influence of alkali forms on the alkali concentration and total alkalinity is discussed in this section. Different forms of alkalis are sometimes added to cement in experiments to achieve a higher level of alkalis to evaluate the potential risk of ASR. Both Na^+ and K^+ are used, mostly in the form of NaOH and KOH. Little attention is paid to the different forms of alkalis, though the resulting alkalinity of the pore solution can be quite different.

The alkali level of *Cement 8* is intentionally raised to 1.2 m/m% (Na_2O_{eq}) by using either NaOH or KOH solutions. The w/c ratio is 0.5. The predicted concentrations are plotted in Figure 5.14(c) with changing Na_2O in clinker. It can be seen that for the constant alkali level in clinker, the Na^+ concentration increases steadily with Na_2O, and the K^+ concentration decreases sharply. Special attention should be paid to the total alkali concentration, which clearly decreases when K_2O is replaced by Na_2O. The drop is explained by the higher binding capacity of C-S-H to K^+ than that to Na^+ in the range of low concentrations (0–0.5 M) (Figure 5.3). For higher concentrations, they are identical. Hence, if K^+ is gradually replaced by Na^+, more Na^+ is

bound in C-S-H.

The different behaviors of C-S-H concerning the Na^+ and K^+ binding are also observed in the experiments by Bérubé et al. (2004). They raised the alkali levels in cement pastes by adding NaOH and KOH solutions separately. While the same levels are used in the pastes (1.25 m/m% Na_2Oeq), after hydration for 91 days, significantly different pH values of the pore solutions are measured. The OH^- level by using KOH is about 30 percent higher than that by using NaOH, indicating that C-S-H can bind more Na^+ than K^+ at high concentrations of ions.

Hence, special care should be taken when additional alkali oxides are added into the paste to raise the alkali levels because the form of alkalis in cement can influence their actual concentrations in the pore solution. K^+ is preferred since the resulting alkali concentration is higher than Na^+, eliminating the risk of underestimating the alkali level in the pore solution.

Furthermore, this part of additional alkali oxide normally dissolves immediately after mixing. From a long point of view, these alkalis have the same effect on the pore solution composition as those inherently bound in clinker phases. However, at early ages, the alkali concentration of pore solution in the former case is remarkable higher than that in the latter one.

5.7.2 Pore solution of slag cement paste

In this section, factors influencing the alkali concentration in pore solution of hydrating slag-blended cement pastes are discussed and their significance for engineering practice is presented. These factors include the slag proportion, reactivity, the magnesium content of slag, and the alkali levels of clinker and slag. Combinations of clinker **C2** and slag **S5** taken from the study of Schäfer (2004) are used as examples. The compositions of the clinker and slag are listed in Table 5.5. Cement pastes with different recipes are investigated and their hydrations are simulated with the *Van Eijk's Model*. The hydration age is taken to be one year since this will give an adequate base for evaluating the properties, for example, the likelihood of ASR.

Slag proportion

The effect of slag proportion on the alkali concentrations is plotted in Figure 5.15, the w/c ratio being 0.5.The paste is cured in a sealed environment at 20°C. It is shown clearly that the alkali concentration decreases with increasing slag proportions in the paste. The predicted trend and values agree well with the measurement in the experiments. The diminishing effect of increasing slag proportion is due to at least three factors. First, higher slag proportions result in more unreacted slag in the paste, reducing the amount of alkali ions available for the pore solution (the dilution effect). Second, the volume of water available for the pore solution is even bigger

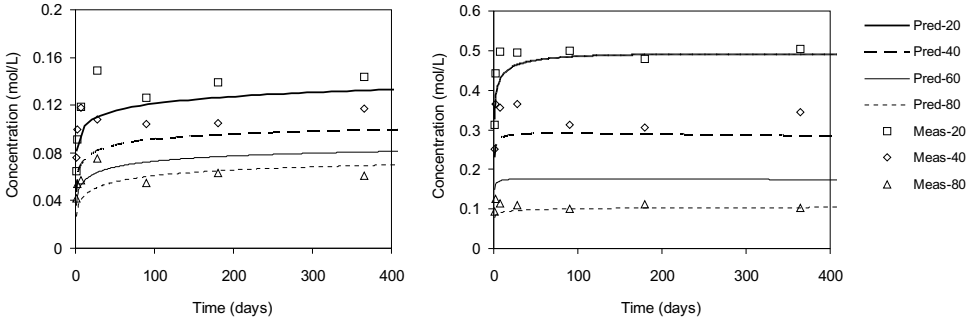

(a) Na^+ concentration (b) K^+ concentration

Figure 5.15: Effect of slag proportion on the alkali concentrations in pore solution of slag cement with C2 and S5, w/c = 0.5, numbers in the legend indicate the slag proportion in the cement.

for higher slag proportions due to the smaller amount of hydration products. Third, more of the hydration product hydrotalcite has been formed, which is able to bind more alkalis. Hence, high slag proportions in the blended cement are clearly preferential when aiming at lowering the alkali ion levels in the pore solution.

Reactivity of slag

The slag reactivity in the cement paste is influenced by many factors and normally high reactivities are preferred in practice with respect to the strength development and the durability of the concrete. Hence, in the various norms the reactivity of slag is regulated by some index or strength test. The influence of slag reactivity is investigated in this chapter by using the proposed methods as well.

Cement pastes with 40 m/m% slag replacement are used, with the w/c ratio of 0.5. The different slag reactivities are simulated by changing the parameter k_1 in Table 5.4. Beside the value 0.46 recommended by Taylor (1987b), three other values are used as well (0.26, 0.36, 0.56), The simulated hydration degree of slags with different slag reactivities are presented in Figure 5.16. After one year hydration, the simulated hydration degrees of slag are 56.8%, 63.3%, 69.8% and 76.1%, respectively. The simulation results are used for predicting the alkali levels.

The model predictions are plotted in Figure 5.17 together with the measurements in experiments. It can be seen that the alkali concentrations in the pore solution are not significantly influenced by the slag reactivity in cement. For slags with higher reactivity, the alkali concentrations are lowered slightly.

The influence of the slag reactivity on the alkali concentrations is much more limited compared to the influence of slag proportions. Hence, the slag hydration degree does not seem to be essential with respect to the alkali concentrations in the pore solution. On the other hand, as will be illustrated in Chapter 7 of this thesis, the pore solution composition highly affects the slag reaction rate.

Alkali distribution in clinker and in slag

There are primarily two sources of alkali ions in hydrating slag cement, the clinker and slag, and normally alkali ions from them are not distinguished in regulations. For example, according to the German standard (DIN 1164-1) the total alkali ions in the cement should not exceed a certain limit, which is adjusted by the slag cement type and proportions. However, alkali ions from the clinker and the slag are released at different rates and change the hydration rate of slag, which in

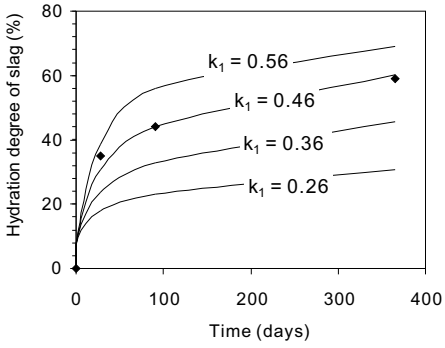

Figure 5.16: Predicted hydration degree of slag in cement paste with different slag reactivities. w/c = 0.5, C2 and S5 are used. k_1 is the parameter used for determining the hydration degree of slag (see Eq. (5.29)). Symbols represent the measured data by Schäfer (2004).

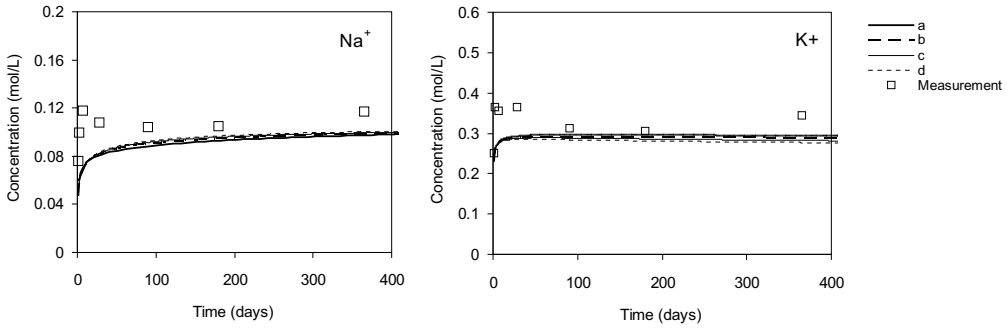

(a) Na^+ (b) K^+

Figure 5.17: Effect of slag reactivity on the alkali concentrations in pore solution of hydrating slag cement (*Recipe 10* in Table 5.5). a, b, c, and d correspond to the different values of k_1 used in predicting the slag reactivities, i.e. 0.26, 0.36, 0.46, 0.56, respectively. The measurements are taken from Schäfer (2004).

turn influences the alkali concentration in the pore solution.

Hence, the influence of different distributions of alkali ions in slag-blended cement between the clinker and slag on the alkali concentration are investigated with the proposed model in this section. Again the *Recipe 10* listed in Table 5.6 is used. The w/c ratio is 0.5. The alkali level of the slag cement is raised in two ways, by increasing the Na_2O or K_2O in slag or in cement, respectively. Four alkali levels are used, which are listed in Table 5.8. The added alkalis to the original recipe are always 0.3 m/m% (in Na_2O_{eq}). The simulated alkali concentrations in the pore solution are plotted in Figure 5.18.

It can be seen that for both Na^+ and K^+, an increase in the alkali content in the clinker results in much higher concentrations than an increase in that of the slag. An increase of alkalis in slag yields only a slight increase of alkali concentrations in the pore solution, to a less extent for K^+ than for Na^+. The main reason for this difference is the relatively low hydration degree of slag in the paste, which reduces the total amount of available alkali ions. In other words, a part of the alkali ions in the slag remains encapsulated in the unreacted slag. Hence, for a certain blending proportion in the slag cement, the alkali level of Portland cement clinker deserve special attention because it is more important than that of slag.

There is no significant difference between the Na_2O and K_2O when the additional amount of alkali is in the clinker.

Table 5.8: Slag cement recipes with different alkali levels in slag and clinker, modified from the compositions used by Schäfer (2004) (m/m%).

Material	Oxide	Recipe				
		Orig.†	1	2	3	4
Clinker	Na_2O	0.14	0.44	-‡	-	-
	K_2O	0.95	-	1.40	-	-
Slag	Na_2O	0.29	-	-	0.59	-
	K_2O	0.38	-	-	-	0.835

†: Original values used by Schäfer (2004).

‡: The same as the original recipe.

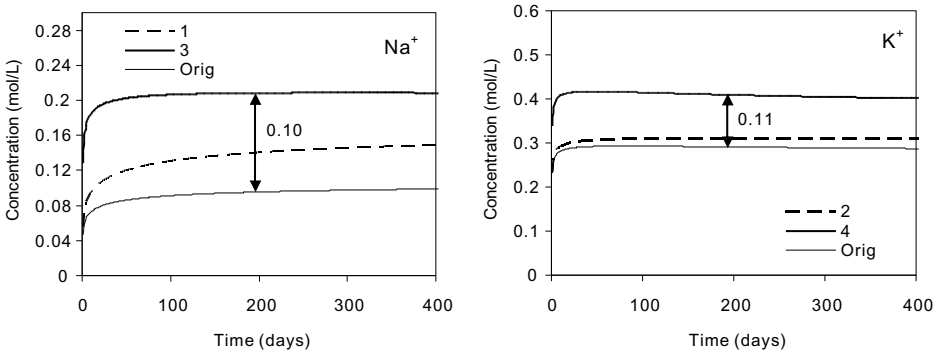

(a) Na^+ (b) K^+

Figure 5.18: Effect of the alkali distribution in cement on the alkali concentrations, predicted with *Recipe 10* in Table 5.6, w/c = 0.5, T = 20°C. "1", "2", etc. correspond to the recipes in Table 5.8.

Partition of alkali ions in solid and in solution

The fractions of bound alkalis (Na^+ and K^+) in the hydration products to the amount released by the slag cement hydration in the selected cement pastes are plotted in Figure 5.19, together with those of the four Portland cement pastes 8, 9, 12 and 13 in Table 5.3. This fraction is computed with:

$$f_i^b = \frac{n_i^b}{n_i^r} = \frac{n_i^r - n_i^s}{n_i^r} = 1 - \frac{C_i \cdot V_w}{n_i^r} \tag{5.36}$$

It can be seen that the fractions of alkali ions bound in hydration products of hydrating slag cement pastes are slightly higher than those of Portland cement pastes. The enhancement in the alkali-binding capacity of the hydration products of slag cement is mainly due to the large amounts of hydrotalcite in the pastes.

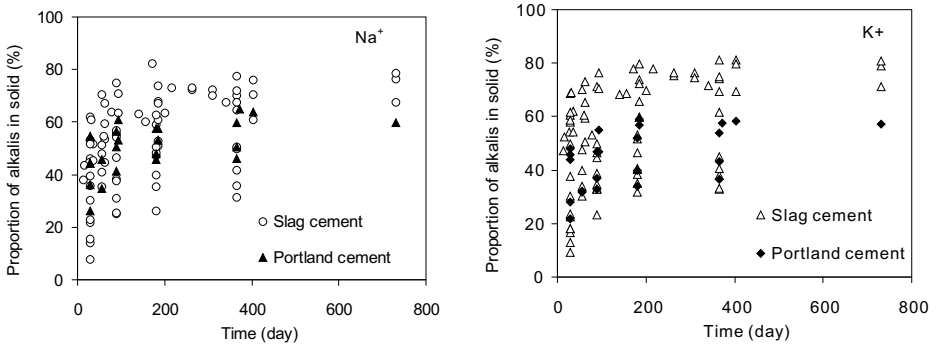

(a) Na^+ (b) K^+

Figure 5.19: Fraction of alkali ions in the solids to the total amounts released by the cement hydration, calculated with the slag cement recipes in Table 5.6 and Cement 8, 9, 12 and 13 in Table 5.3.

5.8 Conclusions

Based on the model and discussions presented in the previous sections, several conclusions can be drawn:

1. The original (Taylor, 1987b) and later (Brouwers and Van Eijk, 2003) theories about the linear partition of alkali ions in the solid and aqueous phases in hydrating cement paste are useful for predicting the alkali concentrations.
2. The method proposed in this chapter can determine the distribution ratio of alkalis in both hydrating Portland cement and slag cement pastes. It is derived from experimental results taking use of a large number of cement pastes selected from literature. The predictions agree well with the measurements in the experiments.
3. The adsorption of alkali ions by the solid product C-S-H in hydrating Portland cement pastes complies with the Freundlich isotherm. The higher alkali concentrations, the more alkali ions are bound in the solid products. The linear binding model used by Taylor (1987b) and Brouwers and Van Eijk (2003) is indeed valid for Na^+, but a non-linear method should be followed for K^+.
4. Both the C-S-H and the hydrotalcite can bind alkalis in the hydrating slag cement pastes. Their alkali-binding capacities can be calculated with the methods proposed in this thesis. The hydrotalcite shows a stronger alkali binding capacity than the C-S-H.
5. The equilibrium method for non-alkalis in Portland cement paste proposed by Van Eijk (2001) is valid for slag cement paste as well.
6. The models can predict the pore solution composition development of hydrating slag cement paste. Both the alkali and non-alkali ion concentrations can be well predicted.
7. The models can be used to investigate the effects of some factors on the pore solution development of Portland cement and slag cement paste.

The model proposed and developed in this chapter will be further used in developing a 3-D computer-based computer model based on the *Van Eijk's Model* for predicting the pH value of the pore solution, which affects the slag reaction rate.

Chapter 6

Computer modeling of Portland cement hydration

6.1 Introduction

New theories about cement hydration and the microstructure development of hydrating cement paste are proposed continuously based on the developments in cement chemistry (Brouwers, 2004b, 2005). It is important to update the computer models by using these new theories that can give computer models a more solid theoretical background and can extend the model applications.

In this research, the *Van Eijk's Model* is chosen for extension because of its advantages discussed in Section 2.5. First, the properties of hydration products are updated because that the reactions stoichiometries used in this model have a volumetric basis. Second, new knowledge available in cement chemistry about the reaction of clinker phases is incorporated into the computer model. Third, a new concept considering the reaction mechanism is introduced into the computer model.

The predictions from both the *Van Eijk's Model* and the modified model (named *New Model*) are compared with each other, and are further validated with experimental measurements. It is shown that the *New Model* can simulate the hydration process and the microstructure development in a more efficient way and minimizes the influence of system resolution on the model predictions. The computing efficiency of the *New Model* seems to be also much higher than the *Van Eijk's Model*.

6.2 Extension of the *Van Eijk's Model*

As the *Van Eijk's Model* is quite advanced and flexible for changes, it is used in this thesis as a basis. Firstly, enhancements are made according to the actual reaction conditions and taking use of the recent development in cement chemistry. In the later part of this thesis, it is subject to extension for modeling the hydration of slag cement.

One prominent advantage of the *Van Eijk's Model* is that it uses the fundamental knowledge about cement hydration during modeling. In the procedure of generating the microstructure, modeling the diffusion and executing the reaction, new knowledge can readily be incorporated, which can in turn enhance the performance of the model. As a matter of fact, the model is subject to continuous modifications and enhancements (Van Eijk, 2001). In this section, extensions made in this thesis are presented.

6.2.1 Properties of the hydration products

Physical properties of substances used in the computer model are important since the model is operated on a volume basis. In the *Van Eijk's Model*, fixed values of the properties of hydration products are used. As commonly known, water content in the hydration products depends on the hydration state (the assembly of temperature, relative humidity (RH), drying history and so on). So changes in the hydration state will change the water content and the properties of products, which consequently changes the overall properties of the microstructure.

In this chapter, the *Van Eijk's Model* is modified by uniforming the physical and chemical properties of hydration products in the saturated sate. In the *Van Eijk's Model*, the water content

Table 6.1: Properties of phases used in the *New Model* in the saturated state.

Name	Density (ρ, g/cm^3)	Molar volume (ω, cm^3/mol)	Molar mass (M, g/mol)	Heat of formation (kJ/mol)	P^0
C_3S	3.12	73.18	228.33	-2,928	0.027
C_2S	3.33	51.79	172.25	-2,312	0.005
C_3A	3.06	88.3	270.2	-3,588	0.027
C_4AF	3.73	130.3	485.97	-5,090	0.003
$C\bar{S}H_2$	2.31	74.54	172.18	-2,023	0.0017
$C\bar{S}H_{0.5}$	2.73	53.22	145.15	-1,575	0.005
$C\bar{S}$	2.56	53.22	136.14	-1,425	0.001
C-S-H	Eq. (3.49)	Eq. (3.50)	Eq. (3.51)		
CH	2.24	33.05	74.1	-986	
$C_6AF\bar{S}_3H_{36}$	1.72	771.9	1,327.3	-17,539	
$C_4A\bar{S}H_{12}$	2.01	309.1	622.6		
FH_3	3.0	69.8	209	-824	
S	2.2	27	59	-908	
M_5AH_{13}	2.0	322.8	645.5	-286	
C_4AH_{19}	1.8	371.3	668.4		
$C_6AFS_2H_8$	3.03	285.0	862.5		
H	1.0	18	18	-286	

P_j^0: Base dissolution probability of phase j

in the hydration products other than C-S-H is determined in the dry state (for example, at 25°C and 80% RH). The properties of C-S-H, however, originate from the work of Young and Hansen (1987). While Young and Hansen derived the water content in C-S-H in the saturated state, in the *Van Eijk's Model*, the saturated state for C-S-H is tentatively used. Clearly, the consideration on the hydration states of the products is discrepant.

As the hydration of cement particles starts with suspension in water, the hydration products have the water content in the saturated state. As the hydration proceeds, water is combined in the products. If the samples are cured under water or in the saturated state, external water can be imbibed, and the saturated state always applies. If the samples are cured in the sealed state, free water is consumed by the cement hydration, which may ultimately lead to a drop of relative humidity in the pores (self-desiccation). However, the drop of the internal relative humidity is limited. It is found that the internal relative humidity in pores of concrete that is made with w/c ratios of 0.25 and 0.57 dropped to about 70% RH after curing for about 450 days in open air (Persson, 2002). The drop of internal relative humidity is less in samples made with higher water-cement ratios. Mejlhede Jensen et al. (1999) found that the hydration of C_3S and C_2S hardly proceeds when the RH is below 95%. Therefore, it can be concluded that most likely the hydration products in the hydrating cement paste exist in the saturated state.

The properties of hydration products involved in the *New Model* in the saturated state are listed in Table 6.1. Some properties are calculated assuming water released or adsorbed has the molar volume of 16.22 cm^3/mol. This "gel" part of bound water is regarded as "compressed" water (Brouwers, 2004b). Some other products than those used in the *Van Eijk's Model* are included since they are used in the following modifications.

6.2.2 Reaction of calcium silicates

The reaction of calcium silicates is of major importance in the computer model because they are normally the most abundant clinker phases. The volumetric stoichiometry is largely dependent on the physical properties of the hydration product C-S-H. Hence, updating the properties of C-S-H based on the most recent developments in cement chemistry is necessary (Brouwers, 2004b, 2005).

The properties of C-S-H are variable and they are dependent on its composition, i.e. the C/S, A/S and H/S ratios. The water content in C-S-H is complex because it is influenced not only by the hydration state, but by the composition itself, which is variable. In the original model, two types of C-S-H are distinguished, one from the hydration of calcium silicates with a C/S ratio of 1.7 and the other from the reaction of pozzolans (silica fume and fly ash) with CH (Bentz, 2000), namely pozzolanic C-S-H. This pozzolanic C-S-H has a C/S ratio of 1.1. Physical properties of these two types of C-S-H are derived from their chemical formula, which is to a large extent an approximation because the C-S-H is normally highly amorphous and has variable composition.

In the work by Brouwers (2004b), new models for C-S-H with different compositions in the hydrating cement paste are proposed. For C-S-H in the saturated Portland cement paste, it has the formula $C_{1.7}SH_{3.2}$. The new model for C-S-H from the Portland cement hydration is derived from the work by Powers and Brownyard (1948) and some others. This new model is further modified to C-S-H with varying C/S ratios. These types of C-S-H exist in the hydrating paste containing some supplementary materials such as fly ash, silica fume and slag. Two models for the C-S-H in the saturated state are proposed, referred to as constant and variable "gel" water model, respectively. As demonstrated in Chapter 3, the constant gel water model produces good agreements with experimental results and is thus used in this thesis. Then, C-S-H with various C/S ratios in the saturated state has the general formula $C_{\bar{a}}SH_{\bar{a}+1.5}$, in which $\bar{a}$ is the C/S ratio. The value of $\bar{a}$ is fixed to be 1.7 for C-S-H in Portland cement paste and is varying for pastes containing slag or fly ash. General expressions for calculating the density and porosity of C-S-H are given in Eqs. (3.49) and (3.53) in Section 3.4.3.

6.2.3 Reactions of aluminate and ferrite

The reactions of the two interstitial phases in clinker, namely aluminate and ferrite, are quite complex and are still subjects of much research (see discussions in Chapter 2). In this section, the reactions of aluminate and ferrite in the clinker are used in the computer model are updated with the theories proposed by Brouwers (2005), and are thus different from those adopted in the *Van Eijk's Model* (Eq. (2.25)-(2.30)). The state transition diagram for the *New Model* is shown in Figure 6.1.

As discussed in Chapter 2, with the presence of CH, C_3 reacts more likely to form C_4AH_{13}. C_3A changes into diffusing C_3A when a C_3A pixel dissolves. Then, the pixel moves randomly in the system until it collides with other species or the maximum number of diffusion steps is reached. If it collides with diffusing gypsum, solid or diffusing ettringite, or diffusing CH, it turns into solid ettringite, monosulfate and C_4AH_{13}, respectively, following the reaction equations (2.26), (2.27) and (2.13).

C_4AF changes into diffusing C_4AF when a C_4AF pixel dissolves. Similarly, random walk of the pixel is executed and possibilities for its nucleation are first checked with the "nucleation probability". In the *Van Eijk's Model* there is chance of nucleation of the diffusing C_4AF into solid C_3AH_6, CH and FH_3. The *New Model* keeps the nucleation possibility of diffusing C_4AF, but the hydration products are now C_4AH_{13} and FH_3 following the reaction equation:

$$C_4AF + (3+g)H \rightarrow C_4AH_g + FH_3 \tag{6.1}$$

The user can turn off this nucleation function by giving zero values to the nucleation possibility since the FH_3 is rarely found in real mature cement paste.

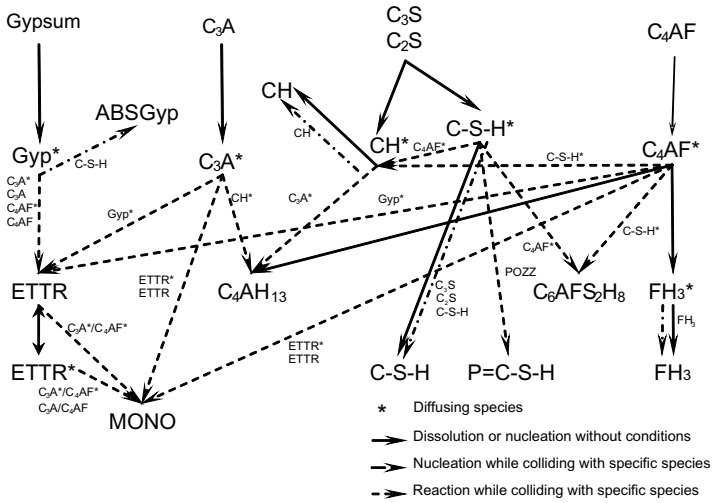

Figure 6.1: State transition diagram for cement hydration used in the *New Model*.

In the *New Model*, the reactions of C_4AF with the calcium silicates follow from Eq. (2.16) and (2.17). It is further written in the form of reaction between diffusing C_4AF and diffusing C-S-H (the hydration product of calcium silicates) as:

$$C_4AF + 2C_{\bar{a}}SH_{\bar{a}+1.5} + (g-5)H \rightarrow C_6AFS_2H_g + (2\bar{a}-2)CH \tag{6.2}$$

The reason for this change is that neither C_3S nor C_2S diffuses in the system; the calcium silicates turn into diffusing C-S-H and CH immediately after the dissolution. Therefore, it is more reasonable that the diffusing C_4AF reacts with their hydration product, diffusing C-S-H. The reactions of diffusing C_4AF with sulfates and solid or diffusing ettringite are the same as those used in the *Van Eijk's Model* (see Eqs. (2.29 and (2.30)).

Summarizing, the reactions of Portland cement hydration accounted for in the new model in the saturated state are listed below as:

$$\begin{array}{rcl} C_3S + 4.5H & \rightarrow & C_{1.7}SH_{3.2} + 1.3CH \\ 1 \quad 1.11 & & 1.29 \quad 0.59 \end{array} \tag{6.3}$$

$$\begin{array}{rcl} C_2S + 3.5H & \rightarrow & C_{1.7}SH_{3.2} + 0.3CH \\ 1 \quad 1.22 & & 1.82 \quad 0.19 \end{array} \tag{6.4}$$

$$\begin{array}{rcl} C_3A + CH + 18H & \rightarrow & C_4AH_{19} \\ 1 \quad 0.37 \quad 3.67 & & 4.20 \end{array} \tag{6.5}$$

$$\begin{array}{rcl} C_3A + 3C\bar{S}H_2 + 30H & \rightarrow & C_6A\bar{S}H_{36} \\ 1 \quad 2.53 \quad 6.12 & & 8.74 \end{array} \tag{6.6}$$

$$\begin{array}{rcl} 2C_3A + C_6\bar{S}_3H_{36} & \rightarrow & 3C_4A\bar{S}H_{12} \\ 1 \quad 4.37 & & 5.25 \end{array} \tag{6.7}$$

$$\begin{array}{rcl} C_4AF + 22H & \rightarrow & C_4AH_{19} + FH_3 \\ 1 \quad 3.04 \quad 2.85 & & 0.54 \end{array} \tag{6.8}$$

$$\begin{array}{rcl} C_4AF + 3C\bar{S}H_2 + 34H & \rightarrow & C_6A\bar{S}_3H_{36} + CH + FH_3 \\ 1 \quad 1.72 \quad 4.70 \quad 5.92 & & 0.25 \quad 0.54 \end{array} \tag{6.9}$$

$$2C_4AF + C_6A\bar{S}_3H_{36} + 8H \rightarrow 3C_4A\bar{S}H_{12} + 2CH + 2FH_3 \quad (6.10)$$
$$1 \qquad 2.96 \qquad 0.55 \qquad 3.56 \qquad 0.25 \qquad 0.54$$

$$C_4AF + 2C_{1.7}SH_{3.2} + 3H \rightarrow C_6AFS_2H_8 + 1.4CH \quad (6.11)$$
$$1 \qquad 1.45 \qquad 0.41 \qquad 2.19 \qquad 0.36$$

6.2.4 New methods for dissolution

Three different mechanisms are used to explain the kinetics of hydration of cement particles (Bezjak and Jelenic, 1980): nucleation and growth, phase-boundary reaction and diffusion. The first mechanism considers the formation of solid products from the solution and its nucleation or precipitation. The second mechanism considers the process of dissolution of solid at the surface, its diffusion in the close neighboring locations and precipitation on the grain. The difference of these two mechanisms is that the former can take place throughout the available pore space filled with solutions, while the latter occurs close to the dissolution source. The phase-boundary reaction, as indicated from its designation, occurs only at the boundary of different phases. The third mechanism corresponds to diffusing through the C-S-H and other colloidal products covering the core. The reaction rate is controlled by the capability of species to diffuse through the layer formed by the hydration products.

The *Van Eijk's Model* simulates the phase-boundary reactions by setting the possibilities of dissolution for pixels on the surface of the digitized particles. The dissolution of a solid pixel takes place when three conditions are met, as pointed out in Section 2.5. After the dissolution, the pixel diffuses in the neighboring locations and nucleates in the pores, or reacts with other species to form solid products, or precipitates on the surface of solids.

The *Van Eijk's Model* also simulates the nucleation and growth mechanism by putting some diffusing species randomly throughout the microstructure and by enabling possibilities for nucleation or growth on some solids.

However, the other mechanism, namely the diffusion-controlled reaction, is not considered in the *Van Eijk's Model*. At early hydration ages, the first and second mechanisms dominate, while at later ages the diffusion process controlled the reaction progress (Pignat et al., 2005), which means that the third mechanism is important and should be considered.

Effect of system resolution on the model prediction

One direct consequence induced by the absence of the third reaction mechanism (diffusion-controlled reaction) in the *Van Eijk's Model* is the effect of system resolution on the model predictions. Changing the system resolutions will change the model predictions significantly (Garboczi and Bentz, 2001), which should be avoided in a robust system. The reason for the effect of system resolution on the model performance is explained below.

The physical size of one real cement particle is irrelevant to the resolution of the system representing it. However, the relative amount of pixels on the surface layer to the total volume of the particle is lower for a system with a larger value of system resolution (Figure 6.2). Furthermore, only the pixels on the surface of a particle are able to dissolve. Therefore, for the same dissolution probability, the fraction of dissolved pixels to the total in a system with higher values of system resolutions is larger to that with low values. This effect of system resolution on the dissolution chances of pixels in a cement particle is illustrated in two dimensions in Figure 6.2.

A cement particle of physical size 7 μm is chosen as example, which is regenerated in two systems. The resolution of system (a) is 1 μm, and that of system (b) is 7 μm. The particle has the same area in the two different systems (49 μm^2), representing particles with the same physical sizes. The pixels on the edge of the particle are marked in the figure as well. The fraction of pixels on the surface layer that are susceptible to dissolve is one in system (b) and is 0.41 in system (a). Hence, for the same dissolution probabilities (for example one), the hydration degree

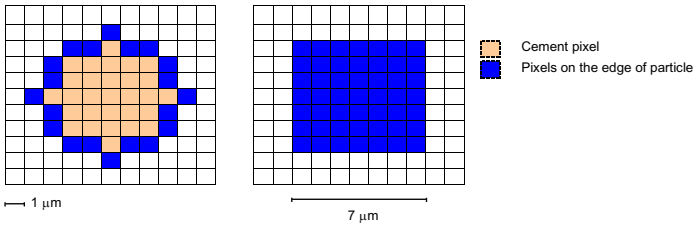

Figure 6.2: 2-D illustration of effects of system resolution on the dissolution chances of one 7 μm particle. (a) system resolution 1 μm, and (b) system resolution 7 μm. Pixels on the edge of a particle is susceptible to dissolve. The two particles have the same area (49 μm^2) indicating the same physical sizes.

of particle in system (b) is higher than that in system (a). Therefore, increasing the size of the system resolution of the model increases the amount of hydrated cement per cycle (Garboczi and Bentz, 2001), and result in higher hydration degrees.

In the following section a method is presented, which simulates the third mechanism—diffusion-controlled reaction—in the cement hydration process besides the other two mechanisms discussed in Section 6.2.4 and renders the system scale invariant.

New method for dissolution

In this section, a new method for dissolution of cement pixels is presented, which simulates both the phase-boundary and diffusion-controlled reactions. During the dissolution process of one hydration cycle, the system executes a scan on all the pixels of unreacted cement. However, the method for determining the chances of the pixels to dissolve is modified.

In the *Van Eijk's Model*, only pixels in direct contact with water are able to dissolve, and the chances for dissolution is governed by a dissolution probability, which is defined beforehand. More details for this dissolution process in the *Van Eijk's Model* are given in Section 2.5. As said, only the mechanism of phase-boundary reaction is simulated in this process and the diffusion-controlled mechanism is missing.

In the *New Model*, a new method in the dissolution process is introduced, which can simulate both mechanisms. The dissolution process starts with a scan of all cement pixels, the same as in the *Van Eijk's Model*. However, the occurrence of dissolution of the cement pixel under evaluation does not depend on whether it is in direct contact with water. If the cement pixel is covered with hydration products, it can still dissolve, although the chances are smaller and depends on the diffusion of substances through the layer of hydration products.

Dissolution In the dissolution process, each cement pixel is evaluated for dissolution in one hydration cycle. The cement pixel under evaluation is called *source pixel*. In addition, the dissolution of the *source pixel* depends on the occupation of another pixel, namely *target pixel*. Theoretically, the dissolution of a *source pixel* is accompanied by a volume increase (Taylor, 1997), hence, more than one pixel are occupied by the hydration products when one *source pixel* dissolves. The phase of a *target pixel* is water in this computer model.

The procedure for the dissolution of one *source pixel* is described as follows. First, the system starts with the *target pixel* being the adjacent pixels to the *source pixel* and evaluates what phases the adjacent pixel is. A random number is generated, possessing the value 1, 2 or 3, and representing the direction the evaluation continues, for example, 1 for the x direction, 2 for the y direction and 3 for the z direction. In this way, the preferential dissolution in one directly is avoided. If the *target pixel* is water, dissolution of the pixel is possible, and the chances for

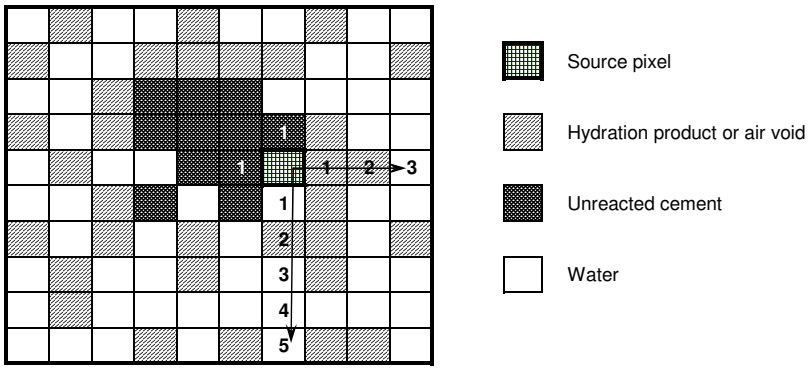

Figure 6.3: Schematic illustration of hydration layer concept. Numbers indicate the layer thickness of the *target pixel*, The arrows indicate the directions that the diffusion takes place.

the dissolution is again governed by a randomly generated number whose value is smaller than the predefined dissolution probability (see Table 6.1). If the *target pixel* is hydration product, cement, air void or aggregate (if present), dissolution of the *source pixel* cannot take place.

Then, after evaluating all the adjacent pixels around the *source pixel* and if it does not dissolve, the dissolution continues for other pixels surrounding the cement pixel. This is not possible in the *Van Eijk's Model*. A concept, namely "hydration layer", is defined, which physically represents the distance of the *target pixel* to the *source pixel* subject to dissolve. A number is assigned to the *target pixel*, named "layer thickness" and equal to the distance of the *target pixel* to the *source pixel*. Therefore, the pixels adjacent to the cement pixel have all a layer thickness of one (see Figure 6.3).

Similar to the adjacent pixels, the pixels with layer thickness greater than one are then evaluated for the dissolution of the *source pixel*. The procedure is as following:

1. A random number is again generated with value 1, 2 or 3 for choosing one random direction. Then, the *target pixel* in the randomly chosen direction and with a layer thickness two is evaluated.
2. Check if the adjacent pixel to the *source pixel* in this direction is cement. If it is, stop evaluation in this direction and choose another direction. The major reason for this condition is that the cement pixel is regarded as being impermeable and diffusion of substances in this direction is not possible. Hence, reaction in this direction is prohibited;
3. Calculate the value of dissolution probability for the *source pixel* on layer two. The methods for calculating this value is given in the following section.
4. Get the phase of the *target pixel*. If it is water, generate a random number and compare it to the dissolution probability calculated in step 3. If the randomly generated number is smaller, the dissolution of the *source pixel* takes place, and then evaluate the next *source pixel*.
5. If the *source pixel* does not dissolve in step 4, choose another random direction, till all three directions are tried.
6. Increase the layer thickness and continue steps 1–5 until the *source pixel* dissolves or the layer thickness exceeds half of the system size (50 if it is a $100 \cdot 100 \cdot 100$ ℓ^3 system). The latter condition corresponds to a complete evaluation of the *target pixel* throughout the whole microstructure.

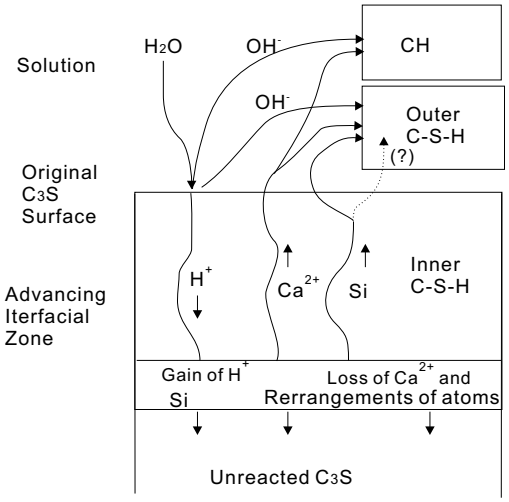

Figure 6.4: Suggested mechanism for reaction of C_3S with water in cement paste by Taylor (1985).

This dissolution procedure continues for all the cement pixels in the microstructure.

Dissolution probability of cement pixels

In this section, the dissolution probability for cement pixels in the *New Model* is addressed. The dissolution probabilities for pixels in direct contact with pore space in the *New Model* are taken the same as those used in the *Van Eijk's Model*, which are empirically determined and calibrated using some experimental results. The discussion in this section is thus focused on the method for determining the dissolution probability when the layer thickness of the *target pixel* is bigger than one.

The relative hydration rate of a cement pixel is governed by two factors: the transport rate of the reaction-controlling substances through the coating layer, and the reaction speed of the cement pixel. The former is considered as the flux through the coating layer (Eq. (6.12)), and the latter corresponds to the dissolution probability, as used in the computer model.

Diffusion of substances through the products layer During the hydration process, some substances can diffuse through the product layer. The substance that controls the reaction rate could be water, moving toward the anhydrous cement core, or ions (Ca^{2+}, $H_3SiO_4^-$, SO_4^{2-}, etc.) moving outward (Taylor, 1985). Considering a hydrating C_3S particle and at the surface, the Ca^{2+} and $H_3SiO_4^-$ enter the solution, and ultimately precipitate, along with the OH^- ions released from the H_2O molecules, as CH and outer product C-S-H (Figure 6.4). Migration of silicon is suggested as the probable rate-determining step by Taylor (1985).

According to the Fick's law:

$$J = -D\frac{\partial C \times 10^3}{\partial x_p} \tag{6.12}$$

in which J is the diffusion flux of substances through the product layer (mol/(s·m^2)), C is the concentration of the limiting substance (mol/L), D is the diffusion coefficient of the substance through the coated layer (m^2/s), and x_p is the particle size (m). In Eq. (6.12) it is assumed that the diffusion of controlling substance through the coating layer is a steady state process.

The flux of water through the coating layer is used as example here for facilitating the discussion. This does not imply that the diffusion of water is the rate controlling mechanism in this stage. Diffusion of other substances is also possible, as shown in Figure 6.4. However, the fluxes of the rate-controlling substances can be analyzed in a similar way as used in this section.

Assuming the concentration gradient of water in the coating layer is constant, the rate of water diffusion to the reaction front is calculated as:

$$J_0 = \frac{D(C_\infty - C_0) \times 10^3}{\delta} \tag{6.13}$$

in which C_0 (mol/L) is the concentration of water at the reaction front (surface of the anhydrous cement core); C_∞ (mol/L) is the concentration of water in the pore solution surrounding the hydrating cement particle, set to be a constant value assuming that the pore solution in the paste is a homogenous mixture of substances, and is independent on the coating layer thickness. C_0 equals to zero if an instant reaction of cement with water is assumed; and δ (in m) is the thickness of the coating layer (Figure 6.5). It is taken in Eq. (6.13) that the flux of diffusion at the reaction front is proportional to the concentration difference across the coating layer ($C_\infty - C_0$) and is inversely proportional to the thickness of the coating layer (δ).

The dissolution probability for the surface layer (pixels in direct contact with porosity, $\delta = 1$) follows the same procedure as that used in *Van Eijk's Model* (see Chapter 2). The dissolution probability of the *source pixel* in hydration layer further than layer one is calculated as:

$$P_i = P^0 \cdot \frac{J_0}{J_0^{max}} = P^0 \cdot \frac{D(C_\infty - C_0) \times 10^3}{J_0^{max} \cdot \delta} \tag{6.14}$$

in which J_0^{max} is the maximum flux of water diffusion, corresponding to the case when $\delta = 1$ and is a constant; P_i (dimensionless) is the dissolution probability of the *source pixel* when the layer thickness is i, P^0 (dimensionless) is the base dissolution probability (i.e. when the *source pixel* is in contact with water, $i = 1$). Separating the constants in Eq. (6.14) and rewriting it gives:

$$P_i = P^0 \cdot \frac{D(C_\infty - C_0) \times 10^3}{J_0^{max}} \cdot \frac{1}{\delta} = \frac{P^0 \cdot \Omega}{\delta} \tag{6.15}$$

in which:

$$\Omega = \frac{D(C_\infty - C_0) \times 10^3}{J_0^{max}} \tag{6.16}$$

Ω (in m) is a model parameter independent of the layer thickness.

Comparing Eq. (6.15) to the Eq. (6.45b) by (Van Breugel, 1997), one can see that the method for computing the dissolution probability as Eq. (6.15) is similar to that used in HYMOSTRUC for computing the penetration depth with the factors $\lambda = 1$ and $\beta_1 = 1$ in Eq. (2.21). The param-

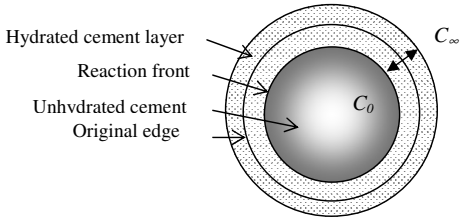

Figure 6.5: Schematic illustration of a hydrating cement particle.

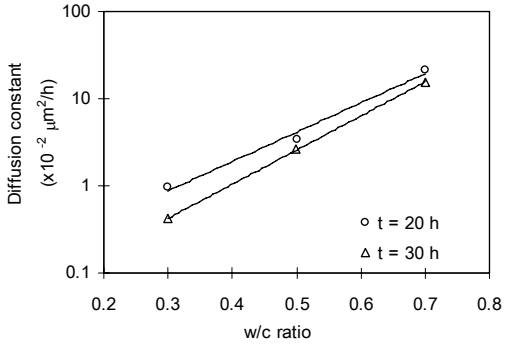

Figure 6.6: Diffusion constant of C-S-H produced from C_3S hydration as a function of initial w/c ratio (Berliner et al., 1998).

eter P^0 is similar to K_i in HYMOSTRUC, which represents the reaction rate, and Ω represents the effects of water shortage in the system, to be discussed in the later parts of this section.

Effect of water consumption During the hydration process, the capillary pores in the paste, initially filled with water, gradually become empty due to the continuous consumption of water by the cement hydration, a phenomenon called "self-desiccation". The self-desiccation takes place if the paste is cured in a sealed environment, and in the saturated state due to the depercolation of pores (Geiker and Knudsen, 1982), although to a less extent. It causes a drop of the internal relative humidity, which further impedes the hydration process.

A further effect of the initial water in the paste on the cement hydration rate is the gel/space ratio. The higher water/cement ratios result in larger gel/space ratios. Some researches have shown that the relative hydration rate of cement is clearly affected by the gel/space ratio of the paste (Copeland et al., 1960).

Berliner et al. (1998) found that the w/c ratio of the C_3S paste influences the diffusion constant of the hydration product C-S-H. The larger w/c ratios correspond to higher diffusion constants. A log-linear relationship was found between the diffusion constants and the initial w/c ratios (Figure 6.6). This effect of w/c ratio on the diffusion constant could be explained by its influence on both the morphology and the composition of hydration products. For a C_3S paste, the C/S ratio of the product C-S-H increased with decreasing water/solid ratio (Van Breugel, 1997). According to Brouwers (2004b), C-S-H with higher C/S ratios has lower porosities. Surface area measurements with the BET method by Mikhail and Selim (1966) confirmed that the w/c ratio has a dominant effect on the internal structure of the hydration products (Table 6.2). Higher surface area corresponds to more porous internal microstructure, via which substances illustrated in Figure 6.4 can diffuse through. Therefore, for pastes with higher w/c ratios, the substances can diffuse more easily through the coating layer.

Determining Ω The parameter Ω in Eq. (6.16) is an inherent property of the paste, depending on the diffusion coefficient of substances in the hydration layer and its determination is arbitrary. A major conclusion drawn from the discussion above is that it depends on the w/c ratio of the starting paste. If the w/c ratio is zero, indicating a complete dry cement bulk, there is no diffusion. Therefore, Ω then equals to zero. If the w/c ratio is high, the diffusion process is not space limited. In this latter case, Ω is close to unity. In addition, at the beginning of the hydration, the diffusion coefficient is large because of the small amount of hydration product in the paste.

The computer model HYMOSTRUC accounts for the most fundamental knowledge in cement chemistry, and is believed to represent the particle hydrations in an accurate way. Hence,

Table 6.2: Surface area of hydrated cement paste at 28 days as a function of the initial w/c ratio (Mikhail and Selim, 1966).

w/c ratio	N_2 BET (m^2/g)
0.35	56.7
0.4	79.4
0.5	97.3
0.57	132.2
0.7	139.6

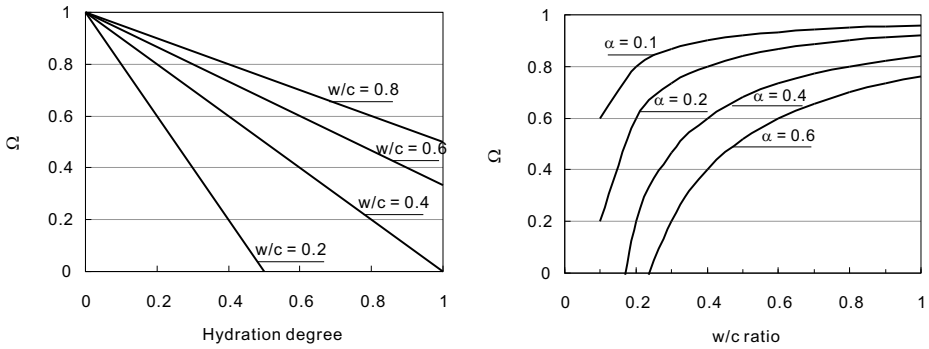

(a) Versus hydration degree α

(b) Versus w/c ratio

Figure 6.7: Value of Ω as a function of the hydration degree of cement and w/c ratios, according to Eq. (6.17).

the chemical principles about the diffusion of substances via the coating layer as used in HYMOSTRUC are taken over in this thesis. It provides the inclusion of the third mechanism with a solid chemical background. Van Breugel (1997) proposed in HYMOSTRUC the following factor to account for the water shortage as a function of the w/c ratio as:

$$\Omega = \frac{w/c - 0.4\alpha}{w/c} = 1 - \frac{0.4\alpha}{w/c} \tag{6.17}$$

in which α is the overall hydration degree of cement in the paste. A schematic representation of the parameter Ω as a function of the hydration degree and for different w/c ratios is shown in Figure 6.7(a). It can be seen that the value of Ω decreases with increasing hydration degree, and decreasing w/c ratios.

It is important to note that the coefficient 0.4 used in Eq. (6.17) is actually very close to the amount of retained water in the saturated and completely hydrated Portland cement paste (0.42–0.44 g water per g original cement, according to Taylor (1997). Hence, the expression $w/c - 0.4\alpha$ corresponds actually to the amount of water left in the paste (per unit mass of cement) in the saturate state. And, Eq. (6.17) is actually the ratio between the amount of water left and the initial amount of water in the paste. However, in Eq. (6.17), the coefficient 0.4 is largely an approximation and the hydration degree (α) for all clinker phases is an average one. Since the *New Model* represents the hydrating microstructure in a digitized way and all phases are

distinguished, it is expected that the ratio between the amount of water left and the initial amount of water can be computed in a more accurate way. Taking use of the model outputs and the water contents of products in the saturated state (Table 3.1), a new expression for determining Ω is proposed as:

$$\Omega = \frac{m_w/m - \frac{M_w}{m} \cdot \sum_i n_i \cdot H_i}{m_w/m} \tag{6.18}$$

in which i is the hydration product, n_i is the moles of hydration product i, and H_i is the water content in the hydration product (in moles per mol, see Table 3.1).

Note that according to the new method for determining the dissolution probability of pixels as Eq. (6.15), systems with higher resolutions have larger values of dissolution probabilities as well for the same layer thickness due to the smaller value of δ. One of the advantages of this extension is that the dissolution probabilities take into account the system resolution. If the resolution is 2 μm, the physical size of one hydration layer is larger than that of the system with the resolution of 1 μm. Therefore, a smaller value of P_i is calculated, half of that for system resolution of 1 μm. In this way, the influence of the system resolution on the model output (as pointed out by Garboczi and Bentz (2001)) can be effectively eliminated, which is discussed in details in Section 6.4.

6.3 Validation of the *New Model* with experiments

Two series of simulations are carried out using the *New Model*. The simulation results are compared to the experimental results in two independent studies (Copeland et al., 1960; Mounanga et al., 2004), which are well documented. The properties of the two cements used in the two studies, Cement A and Cement B from Mounanga et al. (2004) and Copeland et al. (1960), respectively, are listed in Table 6.3. The clinker composition of Cement A is computed from its oxide composition by using the Bogue's equations and that of Cement B is given in the literature.

Mounanga et al. (2004) measured the hydration degree of cement pastes with various w/c ratios. The cement pastes are cured at different temperatures (10, 20, 30 and 40°C). The hydration degree is derived from the non-evaporable water measurement using TGA technique. The amount of non-evaporable water for complete cement hydration is estimated by Mounanga et al. (2004) from its Bogue composition to be 0.23 g per g cement. The PSD of the cement is presented in Figure 6.8. The oxide composition and the Bogue composition are included in Table 6.3.

Simulations are carried out using the relevant w/c ratios investigated at T = 30°C. The influence of the w/c ratio on the hydration degree of the cement in the first 24 hours is shown in Figure 6.9(a). The time conversion factor B used for relating the cycles to the real time is fitted as 3.8×10^{-3} hour/cycle^2(see Eq. (2.34)).

It can be seen that the w/c ratio has very limited influence on the hydration degree of cement at early hours. As the hydration proceeds, the hydration degrees differ from each other due to the different w/c ratio. This conclusion of the influence of w/c ratio on the hydration degree is in line with the observation by Taplin (1959). At early hydration ages, the hydration degree is mainly controlled by the surface of cement particles in contact with water. As hydration proceeds, the water is combined in the hydration product and thus less water is available for the hydration. Hence, for pastes with lower w/c ratios, the hydration process is slower.

The simulated hydration degrees of the cement pastes with w/c ratio of 0.4 and cured at 30°C using both the *Van Eijk's Model* and the *New Model* are shown in Figure 6.9(b). The time conversion factors for both models are 3.8×10^{-3} hour/cycles^2. It can be seen that the *New Model* can predict the hydration degree of Cement A in a more efficient way (less hydration cycles).

The mineral composition of Cement B is shown in Table 6.3. The cement pastes are made with a w/c ratio of 0.4 and are cured for intervals of time ranging from 2 hours to 6 months. The hydration degree of each phase is measured by Copeland et al. (1960) at the planned ages.

Table 6.3: Chemical composition of employed cements.

Name	m/m%	
	A[a]	B[b]
CaO	66.39	
SiO_2	21.17	
Al_2O_3	2.69	
MgO	0.65	
SO_3	2.43	
Fe_2O_3	1.96	
Na_2O	0.3	
K_2O	0.22	
Loss on ignition	2.26	
Insoluble residue	0.96	
Free lime	0.84	
Bogue composition		
phase	m/m%	
C_3S	70.15	53.1
C_2S	7.77	25.9
C_3A	3.81	6.9
C_4AF	5.95	9.7
Gypsum	5.22	3.0[§]
Total	92.9	98.6
Fineness (Blaine, m^2/kg)	332	380[§]

[a]: Mounanga et al. (2004);
[b]: Copeland et al. (1960);
[§]: estimated value.

Simulations are carried out for the hydration of Cement B. The particle size distribution of Cement B is unknown and is assumed to follow the data tested in this thesis with a CEM I 32.5R cement (Figure 8.5). No data about the gypsum content are available and 3 m/m% of gypsum is assumed to be present in the cement. The hydration degree of cement is calculated from mass fraction of each phase and its hydration degree at various ages. The simulation is carried out in the same curing condition and the paste has the same phase compositions. The cycle-time conversion factor for this cement is 3.8×10^{-3} hour/cycle^2 as well. The simulated and measured hydration degrees of the model cement are shown in Figure 6.10. It can be seen again that the hydration degree of cement is well predicted.

It should be noted that the time conversion factor for both Cement A and B are actually the same, 3.8×10^{-3} hour/cycle^2, although the experimental conditions differ greatly. The compositions and fineness of the two cements are different; the w/c ratio of the pastes and the curing temperatures are different as well. Therefore, it appears that most of the essential factors that affect the hydration rate of the cement, like clinker composition, fineness, w/c ratio, temperature, are appropriately accounted for by the model. It is proven in the later parts of this thesis that this time conversion factor is applicable for several other Portland cement and slag cement pastes as well. Therefore, it appears that this factor is appropriate for simulating the hydration of cement in the case that there are no experimental data available for calibrating the simulations.

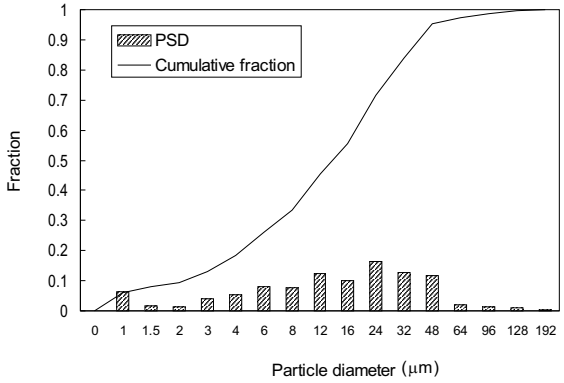

Figure 6.8: Differential and cumulative particle size distribution of Cement A used in the experiments of Mounanga et al. (2004).

6.4 Discussions

6.4.1 Effect of system resolution in the *New Model*

Simulations by using *New Model* with three system resolutions, namely 0.5 μm, 1 μm and 2 μm, and with cement A (Table 6.3) are carried out in the saturated state. The simulated hydration degrees of the cement with the two different system resolutions with the *Van Eijk's Model* ("hydration layer" disabled) are plotted in Figure 6.11(a). It can be clearly seen that the system resolution plays a significant role in the *Van Eijk's Model*, as discussed earlier.

Simulation using the *New Model* with three different resolutions are carried out again and the results are plotted in Figure 6.11(b). Now, the predicted hydration degrees of models with the three resolutions are almost identical. Hence, it appears that the influence of the system resolution on the model performance is successfully eliminated.

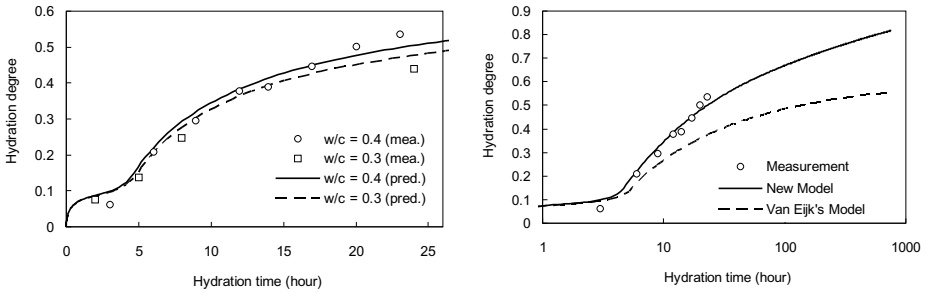

(a) Effect of w/c ratio

(b) Prediction with w/c = 0.4

Figure 6.9: Predicted and measured hydration degree of Cement A. Experimental data from Mounanga et al. (2004), T = 30°C, time conversion factor is 3.8×10^{-3} hour/cycle^2.

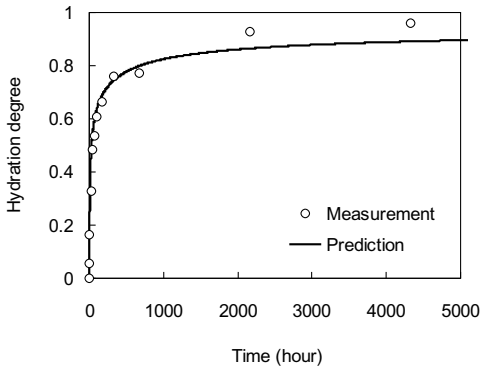

Figure 6.10: Measured and predicted hydration degree of Cement B; w/c = 0.4, T = 21°C, B = 3.8×10^{-3} hour/cycle^2, experimental data from Copeland et al. (1960).

6.4.2 Reaction mechanism

The mechanisms controlling the cement hydration are topics of numerous researches (Bezjak and Jelenic, 1980; Pignat et al., 2005; Tomosawa, 1997). It is also investigated in this section by using the new computer model developed in this chapter.

A concept, namely relative hydration rate, is defined to measure the rate of cement hydration and is calculated in each hydration cycle. First, in every hydration cycle, the number of pixels dissolved in the cycle is counted. Then, when all the hydration simulation cycles are executed, the maximum number of pixels dissolved in one cycle is recorded, normally taking place during the early ages. Third, the relative hydration rate is subsequently calculated as:

$$HR_i = \frac{[I]^i_{dis}}{[I]^{max}_{dis}} \tag{6.19}$$

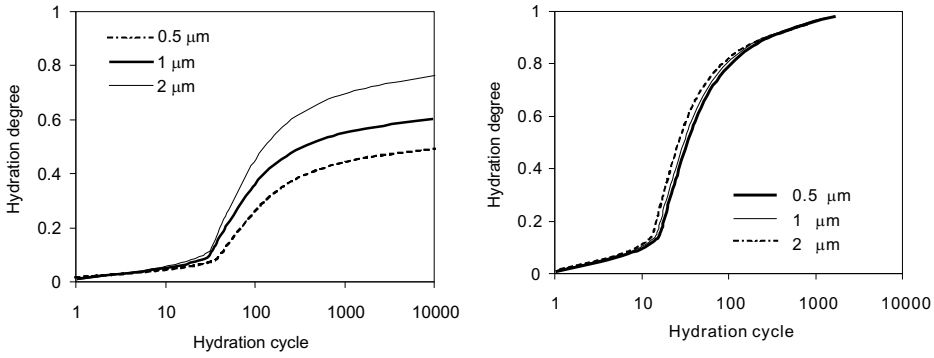

(a) *Van Eijk's Model* (b) *New Model*

Figure 6.11: Simulated hydration degrees of Cement A using the *Van Eijk's Model* and the *New Model* with three different system resolutions, T = 21°C, w/c = 0.4.

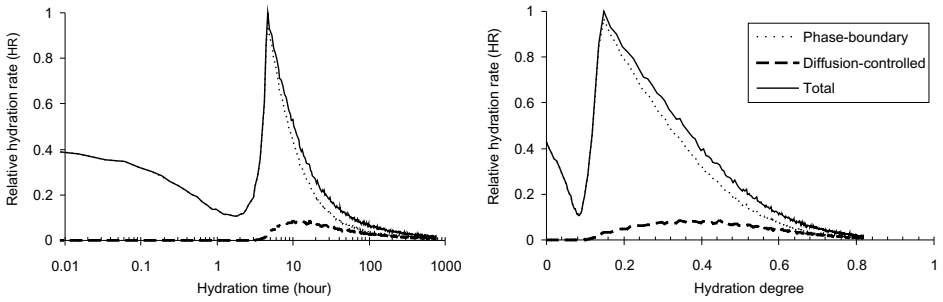

(a) Versus hydration time (b) Versus hydration degree

Figure 6.12: Simulated relative hydration rate of cement versus (a) hydration time and (b) hydration degree, with Cement A (Mounanga et al., 2004), w/c = 0.4, T = 21°C, in sealed condition, time conversion factor is 3.8×10^{-3} hour/cycle[2].

in which $[I]^i_{dis}$ is the number of pixels dissolved in cycle i and $[I]^{max}_{dis}$ is the maximum $[I]^i_{dis}$ in all the cycles executed. The value of $[I]^{max}_{dis}$ is obtained *a posteriori* when the predetermined number of hydration cycles are executed.

Three categories of relative hydration rate are distinguished, namely the phase-boundary controlled rate, the diffusion-controlled rate and the total rate. The total rate is the sum of the former two. Dissolutions of pixels located on the surface layer are considered to be phase-boundary controlled and all others are considered as diffusion-controlled.

The simulated relative hydration rates of the two different reaction mechanisms (phase-boundary reaction controlled and diffusion-controlled) as a function of hydration time are shown in Figure 6.12(a), which are simulated with the *New Model*. As can be seen, at early hydration age, the hydration is clearly phase-boundary controlled, which means the reaction rate is controlled by the contact surface between the cement particles and water. The reaction as a result of the diffusion process is low at this age because of the dormant characteristic of cement hydration. The hydration proceeds slowly as the result of the surface reaction. After approximately 3 hours the hydration accelerates, showing a sharp increase in the total relative hydration rate. Both the phase-boundary controlled rate and the diffusion-controlled rate show a sharp increase, too. However, up to about 100 hours, the total rate is still dominated by the phase-boundary controlled rate. After about 5 hours, all rates show a drop, while drop of the phase-boundary-controlled rate is much sharper than the other. After about 200 hours, the diffusion-controlled rate starts to dominate, indicating that at this moment almost all the cement particles are coated by the hydration products. After 1000 hydration hours, the total relative hydration rate is quite low, and the diffusion-controlled mechanism contributes the most.

The mechanisms controlling the hydration process as predicted by the model are in good agreement with the studies by Tomosawa (1997) and Bezjak and Jelenic (1980). The sequence of the mechanisms controlling the reaction is successfully predicted with the *New Model*. The variation age, at which different mechanisms start to dominate, is also in general agreement with the conclusions of Tomosawa (1997) and Bezjak and Jelenic (1980). Small discrepancies exist because the presence of alkalis and variation in phase composition influence the different mechanisms (Bezjak and Jelenic, 1980). The first mechanism among those proposed by Bezjak and Jelenic (1980) is inherently included in the model by nucleation and precipitation of hydration products. Therefore, the conclusion can be drawn that the major mechanisms controlling the cement hydration are all considered in the model.

The relative hydration rates are also plotted as a function of the hydration degree in Figure 6.12(b). The trends are similar to those shown in Figure 6.12(a). At the end of the dormant period the hydration degree of cement is about 0.1. When the rates start to decline, the overall degree is about 0.2. About 60 percent of cement has already hydrated when diffusion-controlled mechanism proposed by Bezjak and Jelenic (1980) overtakes the phase-boundary mechanism.

6.5 Conclusions

Several conclusions can be drawn based on the model results, discussions and validations in this chapter, which are summarized as:

- The new model uses the properties of products in the saturated state, which are more realistic than those used in the *Van Eijk's Model*. The properties of C-S-H with various compositions are calculated based on newest developments in cement chemistry by Brouwers (2004b). This modification enables the possibility for incorporating the reactions of some mineral admixtures in the model, such as fly ash, silica fume and slag, since C-S-H with varying composition is produced by the reactions of such admixtures.
- The new model is updated with respect to the reactions of the clinker phases calcium silicates, aluminate and ferrite. New reactions are introduced into the model, for example, C_3A reacts with CH to form C_4AH_{13} and C_4AF reacts with C_3S and C_2S.
- A new concept, namely hydration layer, is introduced into the new model. It accounts for different reaction mechanisms during the hydration process and clarifies the dominant mechanism. The influence of system resolution on the model predictions can be successfully mitigated taking use of the new concept—hydration layer—in the *New Model*.
- The time conversion factor 3.8×10^{-3} hour/cycle^2 appears to be an appropriate value for simulating the hydration of a wide range of cements, and is thus recommended if there is not sufficient experimental data available.

The introduced changes make the model theoretical more solid and practically more useful. The *New Model* can simulate the hydration process and the microstructure development in a more accurate way and mitigates the influence of system resolution on the model predictions. It will be further extended in Chapter 7 of this thesis for simulating the hydration and microstructure developed of slag cement paste.

Chapter 7

Computer modeling of slag cement hydration

7.1 Introduction

Many researches have been carried out on the hydration and performance of slag cement since its first application. As an outcome, long-established knowledge is obtained, according to which various national standards are established for guiding practice purpose. However, until now most of the knowledge is empirically established. In many national standards, the criteria for the acceptance and processing of slag are performance-related (EN 197-1, ASTM C989-05, GB/T203-1994). In other words, a series of time-consuming and costly tests need to be conducted before one type of slag cement is accepted for application in engineering practice.

Benefiting from the rapid development in cement chemistry knowledge and computer science, computer modeling of the cement hydration process is possible. Several computer models have been developed in various groups, which can simulate the chemical reactions going on during the hardening process of cement paste, and the microstructure development (Bentz, 1997; Van Breugel, 2004; Van Eijk, 2001). Most of these models deal with Portland cement hydration, with or without some mineral additives like fly ash and silica fume. Typical model outputs of the computer models are the hydration degrees of constituents, heat evolvement, microstructural characteristics, etc. (see also Chapter 6).

Bentz (2005) did an attempt to simulate the reaction of slag with CEMHYD3D (NIST version). The model treats the hydration products of slag as a homogenous mix, namely "slag gel", whose properties are postulated from the slag composition and are independent on other factors. However, the individual hydration products identified in experiments (Narang and Chopra, 1983; Richardson and Groves, 1992; Shi and Day, 1995; Wang and Scrivener, 1995) are not distinguished. As the hydration products in hydrating slag cement paste are principally similar to those existing in the Portland cement system and their compositions vary with the recipes of the paste and compositions of the initial materials (Chapter 3 and 4), it would be expected that this "slag gel" does not actually exist in the paste, and the assembly of the products can have various physical and chemical properties. Therefore, treating the products individually and representing the changing microstructure with precise descriptions of their properties is expected to give accurate predictions of the real hydrating paste.

The new development of the theories about the reaction of slag in cement addressed in Chapter 3 and 4 enables modeling this process of individual reactions with a 3-D computer-based model. The types of reaction products, their quantities and properties can be predicted with the new theories, with considerations to the interactions between the reactions of slag and clinker in cement.

In this chapter, the *New Model* is extended for modeling the slag reaction in hydrating cement paste. First, the reactivity of slag is discussed, considering various factors. Second, the *New Model* is extended for simulating the slag cement hydration. Methods for predicting the reactivity of slag with different compositions and in various alkaline environments are proposed based on experimental observations. The extended model is able to predict a wide range of properties of hydrating slag cement paste. Third, some properties of the hydrating paste, including the water retention, CH content and the composition of the main hydration product (C-S-H), are predicted with the extended computer model.

7.2 Reactivity of slag

The hydration rate of slag is an indispensable parameter when simulating the reaction of slag in cement (see Chapter 3 and 4). It depends among others on the intrinsic reactivity of slag. The latent hydraulic property of slag is well known, i.e. the slag reacts at a remarkable rate when the environment is suitable, an alkaline environment in case of concrete. The reactivity of slag is the objective of numerous researches, and is still not adequately understood, yet. Several factors are known to contribute to the reactivity of slag, for example, the presence of crystalline minerals, chemical composition, geometrical characteristics, temperature, glass structure, and the alkaline environment.

7.2.1 Methods to characterize the reactivity

The reactivity of slag can be characterized in several different ways, including the strength development, hydration degree of slag, corrosion rate, the amount of retained water in hydrating slag cement paste, etc. Each of these methods has its advantages and disadvantages, which are briefly reviewed below.

Strength development

Strength development of mortar or concrete samples made from slag cement is probably the most commonly used method in the past. Mortar or concrete samples are made with binders containing slag mixed with a certain proportion of activators or clinker. The samples are cured and their strength is tested at planned ages. The differences of the strength are used to evaluate the reactivity of slag. The strength development is used as the grading requirement on the slag reactivity index in ASTM C989-05 (Appendix C).

The advantages of this method include:

1. It tests the most relevant property of cement and concrete to engineering practice, the strength. Hence, the results can be connected to construction demand directly.
2. The facilities and knowledge involved in this test are widely available, and the procedure is well documented.

However, the disadvantage of this method is also obvious: the strength development of the samples is not necessarily proportional to the slag reaction degree in the paste, mortar or concrete. It is influenced by the slag composition as well. Some slags produce more C-S-H—the principle binder in cement paste—than the others (Chapter 4). In other words, the more reactive slag does not always lead to higher strength of the samples.

Reaction degree

The reaction degree of slag at given age is the most direct result accounting for the different slag reactivities. It is defined as the proportion of slag that reacts at a certain age to the total amount present at the beginning. The more reactive slags have higher hydration degrees if the other test conditions are kept the same. The reaction degree of slag in cement can be determined by measuring the quantity of unreacted slag in the paste via selective dissolution (Luke and Glasser, 1987), thermal decomposition (Fernández-Jimenéz and Puertas, 2001), or point counting (Feng et al., 2004).

The advantage of using this factor to evaluate the reactivity of slag is that it gives directly the quantity of slag that has reacted. Therefore, the results can closely represent the different slag reactivities. However, the disadvantages deserve special attention as well. First, measuring the reaction degree of slag demands complex experimental setups, and specific knowledge about the chemical reactions going on during the treatment. Careless operation and inadequate experience can lead to significant errors in the results. Second, uncertainties in the methods in the measurements add to the disadvantages. For example, in the selective dissolution method,

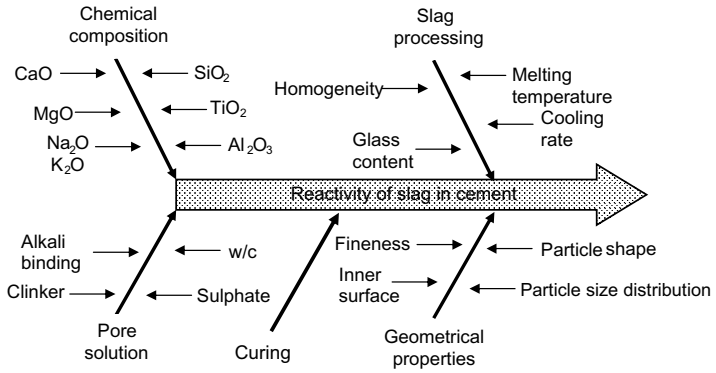

Figure 7.1: Factors on the reactivity of slag, modified from Wolter et al. (2003).

some hydration products of slag are not dissolvable in the liquid, leading to a higher amount of unreacted slag and hence to an underestimation of the reaction degree of the slag. Third, the measured hydration degrees of slag by using different techniques do not always agree with each other (Fernández-Jimenéz and Puertas, 2001). Hence, the validity of the techniques is frequently questioned.

Corrosion rate

The corrosion rate of slag in an alkaline solution can also be used to evaluate the reactivity of slag in an alkaline environment (Olbrich and Frischat, 2001). It is originally proposed to determine the resistance of glass to external corrosion (German standard DIN 12111). The slag is boiled in alkaline water for some time, and the weight loss, or the amount of alkali released from the glass, is measured. While this method is relatively easy to realize, and gives direct results about the slag reaction rate, it is an accelerated method, which can hardly represent the real reaction process of slag in practice.

Water retention

The amount of water retained in hydrating slag cement pastes is also used to evaluate the slag reactivity in blended cement, besides its common use for Portland cement paste (Daimon et al., 1977). It uses the amount of water retained in the paste after standard drying procedures, for example, D-Dried, P-Dried, or heated at 105°C. Like the strength development, this index is also indirectly related to the slag hydration degree and contributions from other reactants should be taken into account, which is normally difficult.

Besides the methods mentioned above, there are also some other ones used, such as the quantification of the -74 ppm signal in ^{29}Si MAS-NMR spectra and heat evolvement (Fernández-Jimánez, 1997; Fernández-Jimenéz and Puertas, 2001). Results from these measurements give indications about the reactivity of slag as well.

7.2.2 Factors on the reactivity

The reactivity of slag is influenced by several factors, some being the inherent properties of the slag itself, and the other being environmental factors. A schematic illustration of factors on the reactivity of slag is included in Figure 7.1. Some of these factors are discussed in the following sections.

Structure of slag

The structure of slag is an inherent property of slag itself. It involves how the structure of slag is built up. Among the various structural theories of glasses, the random network theory proposed by Zachariasen (1932) for the structure of oxide glasses may be the most suitable one to describe the structure of vitreous slag. This structure is based on a distorted 3-D network formed by oxides. The network forming elements are characterized by small ionic radii and by high possible ionic valences. They are surrounded by four oxygen atoms (co-ordination number 4) in the form of a tetrahedron. The network is formed in such a way that distinct oxygen atoms belong to two tetrahedra at the same time, called bridging oxygens (BO) (Figure 7.2). One typical network former is silica. With the vitreous blastfurnace slag it forms SiO_4^{4-}-tetrahedra, $Si_2O_7^{6-}$ groups, chains and other polymerization products. The negative valences of these anionic groups are neutralized by the positive valences of cations, called network modifiers. The inclusion of network modifiers break the bonded oxygens and form non-bridging oxygen (NBO), O^-, and free oxygen O^{2-}. The most typical network modifier within the vitreous blastfurnace slag is the Ca^{2+} ion. The polymerization grade of the network forming SiO_4^{4-}-tetrahedra is reduced with increasing content of network modifiers, indicating that the glass has a smaller stability and a higher chemical reactivity.

Aluminum and magnesium are two amphoteric metals that could exist both in four-fold and in six-fold co-ordinations. The ratio of the four-fold and six-fold co-ordinations depends on the chemical composition and the thermal treatment (granulation of the glass). Forms of these elements in the network influence the glass structure significantly. If they are present in six-fold co-ordination and thus in form of network modifiers, they reduce the degree of polymerization of the SiO_4^{4-}-tetrahedra, increasing the reactivity of the glass (Smolczyk, 1980). Since magnesium is bound in the network as a constituent, no periclase could exist in slag and hence no expansion is expected due to the formation of MH, which is discussed in Chapter 8.

The minor components of the blastfurnace slag, such as manganese, titanium and sulphur, are also constituents of the glass structure in the granulated slag. Sulphur is probably incorporated homogeneously as S^{2-} to substitute oxygen in the network. The precipitation of sulphate starts at contents of >3.3 m/m%. Manganese is found in six-fold co-ordination in synthetic vitreous slags with MnO-contents up to 7.5 m/m%. TiO_2 in slag can exist both in the four-fold and six-fold

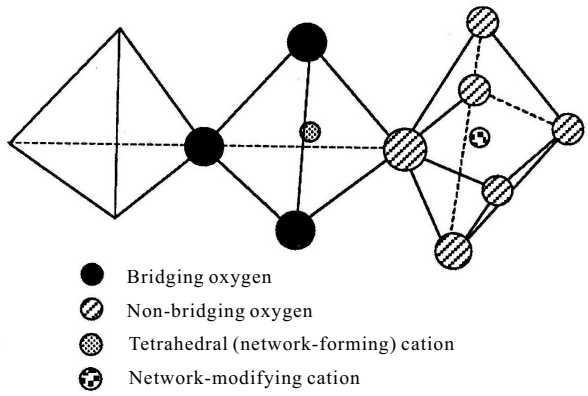

Figure 7.2: Definition of non-bridging oxygen per tetrahedrally coordinated cations (NBO/T), after Mysen (1988).

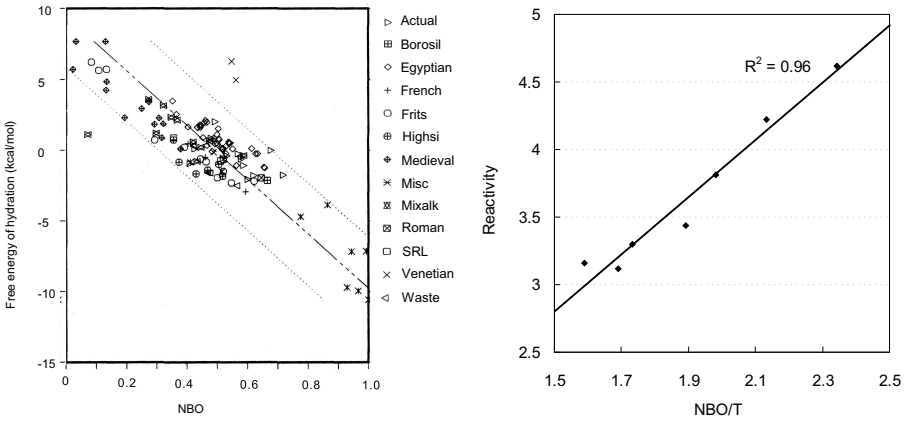

(a) Free energy of glass hydration (b) Hydraulic reactivity

Figure 7.3: Correlation between NBO (or NBO/T) value and reactivity of glasses and slag. (a) Free energy of glass hydration, from Clark and Zoitos (1992); (b) Hydrolytic reactivity of GGBFS, from Wolter et al. (2003).

forms.

To determine the structure of slag involves complex techniques and equipments which are not widely available. Furthermore, the states of bond and coordination numbers of constituents do not always lead to the same conclusions on the reactivities of the blastfurnace slag. The most significant conclusion for this research so far is that the more strongly the structure is distorted, the more reactive the slag is (Smolczyk, 1980).

An important property with respect to how severe the network is distorted is the degree of depolymerisation of a silicate melt. This can be expressed by the ratio of non-bridging oxygen atoms to the number of tetrahedrally co-ordinated atoms (e.g. Si), usually denoted as NBO/T ratio (Figure 7.2). The NBO/T ratio is suitable for this purpose because (Stebbins et al., 1997):

1. The number of NBO is proportional to the number of moles of oxide addition;
2. Addition of alkali or alkaline-metal oxides to silica increases the overall O/Si ratio of the silicate;
3. Increasing the number of NBO results in the progressive breakdown of the silicate structure into smaller units.

It is known in the silicate chemistry that both the physical properties of slag melt and chemical resistance of glasses in it depend on the NBO/T ratio (Jantzen and Plodinec, 1984; Mills, 1995). The NBO/T ratio of glass in normal granulated blastfurnace slag can be directly calculated from its oxide compositions (see Appendix E).

Clark and Zoitos (1992) correlated the calculated free energy of glass hydration for over 150 glasses with the number of non-bridging oxygen (calculated in a similar way as in Appendix E with the T replaced by the total moles of oxides $\sum y_i$). The results are shown in Figure 7.3(a). It appeared that there is a linear relationship between the calculated free energy and the NBO of glasses. Since generally lower free energy of hydration corresponds to also lower stability of glass in the alkaline environment, glasses with higher NBO values are more reactive than those with lower NBO values.

Wolter et al. (2003) measured the hydrolytic reactivity of ground slag grains by boiling 0.03

g of slag with various compositions for 1 hour in 50 mL distilled water and titrating the leached alkalis with 0.01 mol/L HCl. The amount of HCl needed is taken as a indicator for the hydrolytic reactivity. The authors also investigated the glass structure of the slags. A good correlation between the hydrolytic reactivity and the NBO/T ratio of the glass in slag is observed (Figure 7.3(b)), indicating that the structure of slag has an important influence on the reactivity of slag. An approximately linear relationship between the reactivity of slag in the distilled water and its NBO/T value is observed.

Activators

The blastfurnace slag is known to be a latent hydraulic material, i.e. certain kinds of activators need to be present to trigger the reaction. However, this effect is dependent on the nature of the activator itself, besides its dosage in the mix. Gypsum, lime and alkali hydroxides are the most typical activators, closely related to the slag-blended cement and super-sulphated slag cement. Water-glass (i.e. sodium silicate solution) is sometimes used as well.

When the slag is activated with Portland cement, it is actually a combined effect by the solutions of alkali hydroxide (NaOH, KOH), gypsum (early ages) and CH. If they are considered separately, the alkali hydroxide shows the most efficient activation effect compared to the others. CH shows a good effect during the early ages, but the effect is surpassed by gypsum after about two weeks. However, if the alkali hydroxides are used as activator, the reaction at later ages is obviously impeded, of which the mechanism is unknown, yet.

Compared to the activation effect of alkali hydroxide, water-glass shows better performance (Fernández-Jiménez, 1997). Even if the pH value of the water-glass solution is lower than the NaOH solution, the reaction rate of slag is higher when the former is used as activator. Na_2CO_3 has an inferior activation effect compared to both NaOH and water-glass solution. When water-glass is used as activator, there seems to be an optimum dosage, corresponding to 4 m/m% (as Na_2O) (Fernández-Jiménez, 1997).

According to the discussions in Chapter 3 and 4, the CH and gypsum cannot be taken as simple activators only. They also enter the slag reaction and are bound in the hydration products. Hence, they might change the reaction behavior as well. The role of NaOH and KOH is simply that of activators.

Presence of crystalline minerals

It is known that a certain fraction of crystalline minerals could form during the cooling process of slag. On the one hand, the effect of crystalline mineral is obvious if a big part of the ground slag is present in the form of totally crystallized grains; the strength will accordingly be much lower than that without any crystalline minerals. If, on the other hand, crystals of smaller size are tightly intergrown with the vitreous slag, they will most likely be of minor influence on the strength. A higher strength could be expected if the crystals are homogeneously distributed in the vitreous slag as submicroscopic crystal nuclei. Furthermore, it has to be considered that tiny crystalline grains improve the grindability of slag. It is observed that crystalline content up to about 5 m/m% could be beneficial for the strength development (Frigione, 1986; Maekawa et al., 1996).

Oxide composition of slag

The oxide composition of slag can be analyzed in a simple and quick way, and it represents the inherent nature of the slag to some extent as well. Therefore, a lot of efforts are made to characterize the reactivity of blastfurnace slags by chemical composition analysis.

Some hydraulic moduli are proposed for evaluating the slag reactivity, the most well-known ones summarized in Table 7.1 (Smolczyk, 1980). It can be seen that the roles of oxides do not always accord with each other in the moduli. For example, the presence of A is regarded beneficial in most moduli except in HI_1, HI_{11} and HI_{12}.

Table 7.1: Hydraulic moduli for granulated blastfurnace slag (Smolczyk, 1980). C, S and A ect. represent the mass percentages of corresponding oxide in the slag.

Hydraulic index	Calculation
HI_1	$100 - S$
HI_2	$\frac{100-S}{S}$
HI_3	$\frac{C+M+A}{S}$
HI_4	$\frac{C+M+A-10}{S+10}$
HI_5	$\frac{C+1.4M+0.6A}{S}$
HI_6	$C + 0.5M + A - 2.0S$
HI_7	$\frac{6C+3A}{7S+4M}$
HI_8	$\frac{C+0.5M+A+CaS}{S+MnO}$
HI_9	$\frac{C+0.5M+A}{S+FeO+(MnO)^2}$
HI_{10}	$\frac{C+M+A+BaO}{S+MnO}$
HI_{11}	$\frac{C+M+0.3A}{S+0.7A}$
HI_{12}	$\frac{C+M}{S+0.5A}$

Smolczyk (1980) drew the following conclusions based on the large set of experiments involving 24 slags and 192 slag cements made from them:

1. An increase of the A content above 13 m/m% increases the early strengths only. The 91-day strengths are even lower at higher A contents.
2. Partly the effect of the minor components is so strong that after 7 days some blastfurnace slags with 11 m/m% A show already higher strengths than those with 15 m/m% A.
3. M in the range up to 11 m/m% has quantitatively the same effectiveness as C has.
4. In every case MnO has a negative effect.
5. The influences of P and alkalis depend on the kind of clinker used and on the testing age. After 28 days P always proves positive.
6. The statistical examination of T (up to 1 m/m%), F (up to 2 m/m%), and sulphur (up to 2 m/m%) does not prove any significant influence.
7. Besides the clinker content and the fineness, the strength developments of the blastfurnace slag cements also considerably depend on the kind of clinker.

As mentioned before, on the one hand, the reactivity of slag is strongly influenced by the structure of the slag, which is difficult to determine in practice. On the other hand, the oxide composition is relatively easy to measure. The NBO/T ratio builds the bridge between the structure of glass in normal granulated blastfurnace slag and its oxide compositions. It can be calculated from the oxide composition of glass in slag and be used to evaluate the reactivity of slag. In this research, the NBO/T ratio is used to evaluate the effect of oxide composition of glass in slag on its reactivity.

Geometrical characteristics

Particle shape and particle size play an important role on the reactivity of the slag. Sato et al. (1986) did a series of experiments on the hydration of blastfurnace slag particles. The hydration of ground commercial slag, with various particle sizes and various activators is investigated. Samples with five different particle sizes (3.27, 4.05, 5.86, 8.66 and 13.36 μm mean diameter by volume) are prepared. The samples hydrate with a solution-slag ratio of 10 in NaOH solutions, saturated CH solutions or previously stirred Portland cement suspension as alkaline activators. The amount of hydrated slag is measured by determining the soluble part of the hydration products using salicylic-acid-acetone-methanol solution. The thickness of hydrated layer with time is calculated using the slag hydration rate and the PSD of slag, assuming the slag particles to be spherical. The authors concluded that the thickness of hydrated layer of particle does not depend on the particle size. The rate of hydration is actually proportional to the total surface area. Therefore, it is expected that fine slag particles hydrate much faster than the coarser ones.

pH value of pore solution

The reaction rate of glass is known to be highly dependent on the chemical environment it is subject to (Paul, 1977). It is regarded as a concern to the "durability" of glass if the structural glasses are the interests in investigation. A typical example is the archaeological glass. The composition of pore solution is thus important concerning the reactivity of glass in slag cement.

Considering the stability of two major network-forming elements in glass, the silica and alumina, the solutions can be characterized roughly into three regions: the acid (pH value below 5), the natural (pH value between 5–9) and the basic (pH values above 9) (Doremus, 1979). Normal glass is quite stable in the natural environment, as proven by its wide use in the construction industry. The most relevant region in cementitious material system is the basic environment. When the pH value of the solution increases above 9, the breakdown of the silicate lattice is enhanced.

Reaction of silicate glass with aqueous solution The corrosion of silicate glasses by aqueous solutions can be described in terms of three chemical reactions (Paul, 1977):

1. The penetration of a proton from water into the glassy network, replacing an alkali ion;
$$\equiv Si{-}OR + H_2O \leftrightharpoons \equiv Si{-}OH + R^+ + OH^- \tag{7.1}$$
in which R is the alkali ion.
2. The hydroxyl ion in solution disrupts siloxane bond in glass:
$$\equiv Si{-}O{-}Si\equiv + OH^- \leftrightharpoons \equiv Si{-}OH + \equiv Si{-}O^- \tag{7.2}$$
3. The non-bridging oxygen formed in Eq. (7.2) interacts further with a molecule of water producing a hydroxyl ion, which is free to repeat reaction 2 over again:
$$\equiv Si{-}O^- + H_2O \leftrightharpoons \equiv Si{-}OH + OH^- \tag{7.3}$$

Penetration of a bare proton, as suggested in reaction (7.1), is energetically improbable as the hydration energy of H^+ to H_3O^+ is very high and negative (about -367 kcal per mole). Therefore, reaction (7.2) and (7.3) dominate the dissolution of silicate glass. The hydroxyl ion serves as the source of hydroxyl for further breaking of siloxane bond on the glass surface in reaction (7.2). Therefore, an increase in the activity of hydroxyl ion in the solution will favor increased removal of silica.

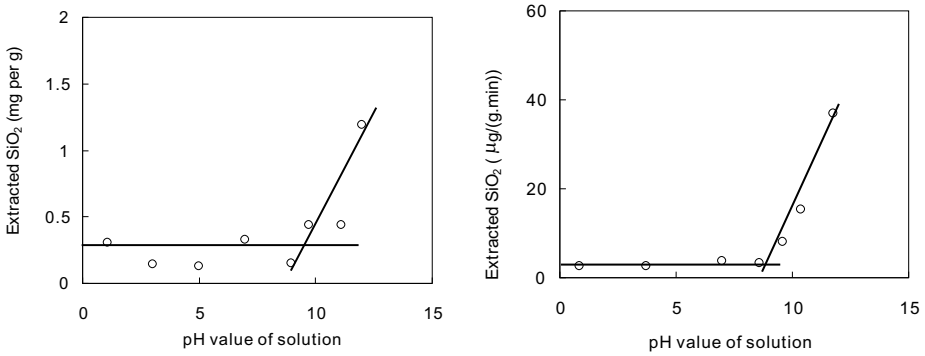

(a) (b)

Figure 7.4: Effect of pH value of solution on the rate of extraction of SiO_2 from (a) a fused silica powder at 90°C; (b) 25 Na_2O, 75 SiO_2 glass grains at 35°C, after El-Shamy et al. (1972).

Dependence on the pH value After mixing the water with cement, the liquid phase contains substantial amount of ions, giving it the name "pore solution". The pore solution is normally basic, due to the instantaneous dissolution of alkalis in clinker (Chapter 5). The pH of the pore solution depends on many factors, like the w/c ratio, alkali level and type of cement and cement compositions.

The high pH value of the pore solution obviously promotes the dissolution process of glass in slag (Song and Jennings, 1999). The study of El-Shamy et al. (1972) showed that all the silicate glasses become particularly susceptible to decomposition for pH 9 to 10 (Figure 7.4).

Paul (1977) calculated the solubility of SiO_2 using a thermodynamic approach and considering the effect of pH of the solution. The results are shown in Figure 7.5. Again, it is confirmed that the solubility of SiO_2 is greatly enhanced when the pH goes above 9.

Zhou et al. (1993) measured the hydration degree of slag in AAS pastes at different ages. The fineness of the slag is 600 m^2/kg. Paste sample are prepared with a w/c ratio of 0.45. Activators are prepared by adding NaOH to the water glass to achieve different alkalinities. Their pH values range from 12.5 to 14.7 (estimated from the composition of the activator, see Zhou et al. (1993)). The degree of slag reaction is measured by a solvent extraction method. The measured hydration degrees at given age are plotted in Figure 7.6 versus the pH value of the activators. It can be seen that an approximately linear relation exists between the hydration degree and the pH values of

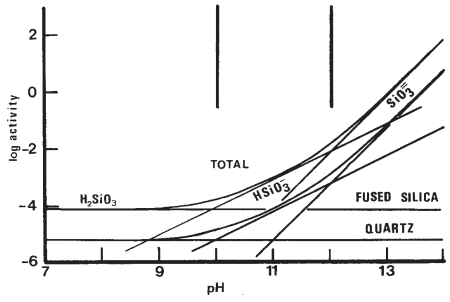

Figure 7.5: Stability of SiO_2 in aqueous solutions at different pH (25°C, after Paul (1977)).

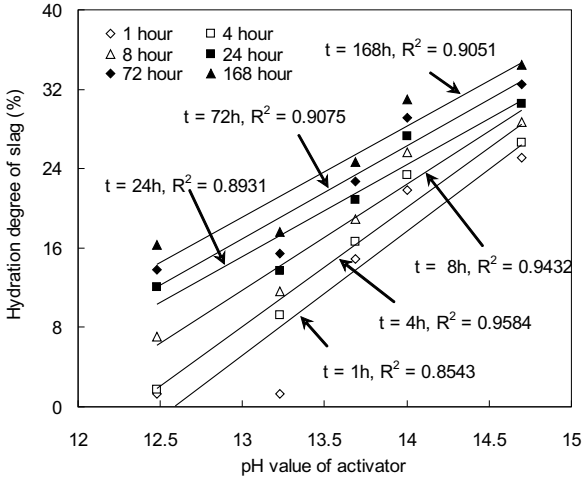

Figure 7.6: Hydration degree of AAS at various ages as a function of the pH value of activators (after Zhou et al. (1993), pH values above 13.69 are calculated from the composition of the activators).

the activators at the ages investigated. Therefore:

$$\alpha = a \cdot \mathrm{pH} + b \tag{7.4}$$

in which a is the slope coefficient of the line and b is the intercept. The mean value of a is fitted using the experimental data of Zhou et al. (1993) is 0.105. The value of b depends on the age of the tests.

Effect of temperature

The influence of temperature on the slag reaction rate is very obvious. The slag reaction rate is even more sensitive than that of Portland cement systems. Several investigators have determined the temperature dependence of the heat evolution by calorimetry and applied the Arrhenius equation, or some variant of it, to the data thus obtained in order to calculate an activation energy, E_a for hydration (Fernández-Jimenéz and Puertas, 1997; Krishnan, 2002; Wu et al., 1983). The Arrhenius equation can be written in the form:

$$k_T = A \cdot \exp\left(\frac{-E_a}{\mathrm{R}T}\right) \tag{7.5}$$

in which k_T is the rate constant, R is the gas constant ($(8.314\times10^{-3}$ kJ/(mol·K)) and A is a constant. Typical values for the activation energy of slag are between 50–59 kJ/mol (Fernández-Jimenéz and Puertas, 1997). This value is apparently higher than the values measured for Portland cement hydration, about 38.44 – 40.20 kJ/mol for normal Portland cement (Zhang et al., 1999).

Concluding remarks

The conclusions on the effect of different factors on the hydraulic reactivity can divert due to the characterization methods. Several methods are available, including direct and indirect ones. While their significance to different applications can vary, the conclusions might be merely drawn

from the tests designed for the specific objectives. The hydration rates and degrees measured with different methods could differ from each other greatly (Fernández-Jimenéz and Puertas, 2001).

As said, the strength test is probably the most widely used and easiest method employed generally. The principle strength-bearing agent in hydrating slag paste is calcium silicate hydrate (C-S-H), similar to that of the Portland cement system. Therefore, reaction of glasses containing only calcium and silicon is expected to yield the highest strength. However, the reaction can only proceed very slowly. The presence of other constituents is thus important for distorting the network structure. Therefore, the glass is on a higher energy level, therefore less stable and possessing a higher reactivity.

7.3 Computer modeling of slag cement hydration

With the knowledge about the chemistry and reactivity of slag reaction in cement, computer modeling of the hydration of slag cement paste and its microstructure development is possible. The *New Model* is chosen as the basis and extensions are made for modeling the slag cement hydration.

The computer modeling process for the slag cement hydration is essentially similar to that for the hydration of Portland cement (Chapter 6). An initial microstructure is firstly generated, representing the starting system. Then, a number of hydration cycles are executed to simulate the continuous disappearance of cement and formation of products. A series of reaction rules are obeyed in each hydration cycle, established with the chemical knowledge on slag cement reaction. One specialty of the slag reaction is its reactivity, which is influenced by some factors and is addressed in the previous section.

7.3.1 Regenerating the initial microstructure

The initial microstructure of slag cement paste is reconstructed using the water/binder ratio and the PSD of clinker, slag and gypsum (if present in the system). The way of distributing clinker phase follows from those used by Bentz (1997) and Van Eijk (2001), using totally random distribution or phase correlation files. The glass and crystalline minerals in the slag are distributed using random partition based on their volume fractions in the slag, which is calculated beforehand from their mass fractions in the slag. The density of the crystalline mineral is assumed to be 3.15 g/cm^3 (density of merwinite) if the crystalline mineral is not identified. The user can also opt to assign all the slag particles as glass phase since in some slags the crystalline mineral exists in such a small extent that it is not detected. In the *New Model* modified for slag cement hydration, PSD of slag is accounted for in two ways. The user can calculate the numbers of particles for each particle size using the PSD of slag; or, if the PSD of slag is unknown, the user can opt to use the cement PSD for slag. If the slag and cement is ground together, they have identical PSD. The same options for gypsum are also provided.

7.3.2 Dissolution of slag pixel

In each hydration cycle, the pixels marked as glass are enabled to dissolve. The occurrence of dissolution is determined by the "dissolution probability" of slag pixel and its position in the hydrating particle.

Consideration to the OH^- concentration

Since the dissolution rate of glass is dependent on the ion concentration of pore solution in the real paste (El-Shamy et al., 1972; Paul, 1977; Song and Jennings, 1999; Zhou et al., 1993), the dissolution probability is related to the pH value of the activation solution. For solutions other than the Portland cement suspension, the pH value can be determined from the ion concentrations. If Portland cement is used as activator, the methods described in Chapter 5 for modeling the pore solution composition of hydrating slag cement pastes are used. Then, the pH value is

calculated from the concentration of OH^-. The calculated value of pH in each cycle is used for the dissolution of a glass pixel in the next cycle.

In the methods for predicting the alkali concentrations in the pore solution of hydrating cement paste presented in Chapter 5, two different binding capacities for C-S-H in hydrating cement paste are found, either for the neat Portland cement or for the blended cement. They are significantly different from each other. However, it is less likely that the replacement of Portland cement clinker with a small proportion of slag can change the binding capacity of C-S-H dramatically. All the data calculated for blended cement are obtained with slag proportions higher than 20 m/m% slag. For very low slag proportions (for example, 5 m/m%), the alkali binding behavior of C-S-H may be close to that of C-S-H in neat Portland cement paste. The hydrotalcite content in the paste is also very low. In this case, most of the alkalis are still bound in the C-S-H, which is not accounted for in the methods presented in Chapter 5.

In the computer model, distinction is therefore made between C-S-H formed by the Portland cement hydration and that by the slag reaction. In each hydration cycle, the numbers of C-S-H pixels formed by the Portland cement hydration and by the slag reaction are counted. The C-S-H pixels originated from the Portland cement hydration is taken to possess the alkali-binding capacity of C-S-H in neat Portland cement paste (C/S = 1.8, see Section 5.4); and the C-S-H from slag reaction has the alkali-binding capacity presented in Section 5.5. Again, the partition theory presented in Chapter 5 is applied. Three types of hydration products in the blended cement paste can actually bind alkalis: the C-S-H from the Portland cement hydration, that from the slag reaction and the hydrotalcite (from the slag reaction as well). The alkali-binding capacity of C-S-H from the Portland cement hydration follows from Eqs. (5.21) and (5.22). The alkali-binding capacity of C-S-H and hydrotalcite from the slag reaction follows from Eq. 5.33 and Table 5.7 (R_d^2). Again, a non-linear equation similar to Eq. (5.34) is established with the alkali concentration as the only unknown. Solving the equations gives the alkali concentrations in the pore solution (C_{Na} and C_K).

According to Figure 7.6, the reactivity of slag is linearly proportional to the pH value of the activation solution. Hence, a coefficient accounting for the pH of the activator is proposed as:

$$\beta_1 = \begin{cases} 0 & (\text{pH} \leqslant 9) \\ a_1 \cdot (\text{pH} - 9) & (\text{pH} > 9) \end{cases} \tag{7.6}$$

in which pH is the pH value of the pore solution; a_1 is a slope coefficient of the linear correlation, equal to 0.105 in the experiments of Zhou et al. (1993). The pH value of 9 is set according to the relations presented in Figure 7.4.

Note that in Eq. (7.6), if the pH value of the pore solution is lower than 9, $\beta_1 = 0$, indicating that the glass in slag does not react. This case corresponds to the very slow reaction rate of slag if there is no activator in the system, known as the latent hydraulic property. For the pore solution of hydrating cement paste and concrete, normally pH > 9 (see Chapter 5).

Consideration to the chemical composition

The effect of the chemical composition of glass in slag on its reactivity is accounted for with its NBO/T value. It is shown in Section 7.2.2 that there is a linear relationship between the reactivity of glass in slag and its NBO/T value. Therefore, a coefficient regarding the oxide composition of slag is proposed as:

$$\beta_2 = a_2 \cdot (NBO/T) \tag{7.7}$$

in which a_2 is the slope correlation of the linear relation between the NBO/T ratio of glass in slag and the reactivity, equal to 2.116 if calculated from the data of Wolter et al. (2003) (see Figure 7.3(b)). Note that the data by Wolter et al. (2003) cannot be applied directly because of the employed accelerated methods.

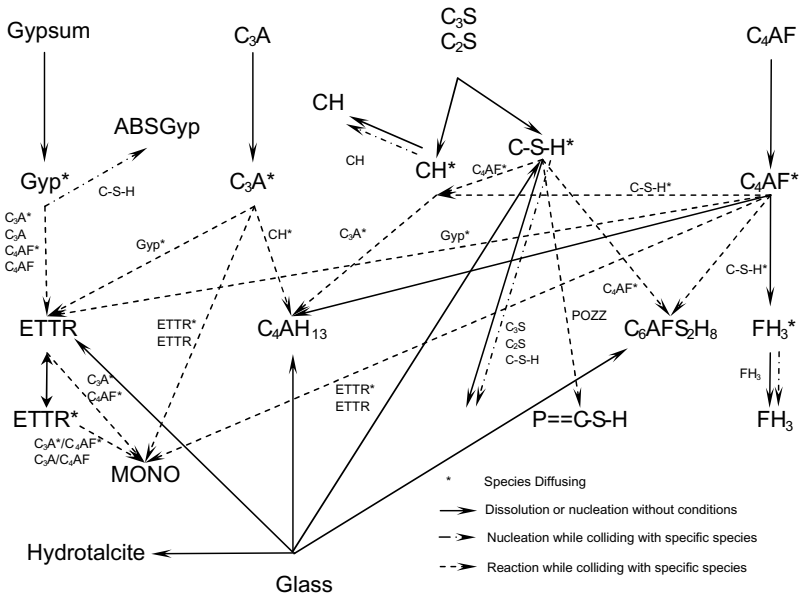

Figure 7.7: State transition diagram for the new computer model with slag hydration, modified from Figure 6.1.

Dissolution probability of glass pixel

Considering the effects of oxide composition and alkalinity of pore solution on the slag reactivity, the dissolution probability of a glass pixel in the *New Model* is thus calculated as:

$$P_{glass} = P^0_{glass} \cdot \beta_1 \cdot \beta_2 = \begin{cases} 0 & (\text{pH} \leqslant 9) \\ P^0_{glass} \cdot \beta' \cdot (NBO/T) \cdot (\text{pH} - 9) & (\text{pH} > 9) \end{cases} \tag{7.8}$$

in which P^0_{glass} is the dissolution probability of glass pixels, empirically set beforehand. In this thesis, the value of P^0_{glass} is set to be 0.0013, which should not be varied by the user of the computer model. $\beta' = a_1 \cdot a_2$ and is a parameter depending on some other factors that influence the slag reactivity, for example, structural defects, micro-crystalline grains. The value of β' is set empirically by the user and can be calibrated from experimental results.

Note that in Eq. (7.8) the effect of temperature is not included since in the *New Model* this effect is considered by changing the time conversion factor B in Eq. (2.34).

7.3.3 Reaction of slag pixel

Immediately after the glass pixel dissolves, it converts into several phases, including diffusing ettringite, hydrotalcite, diffusing C-S-H and C_4AH_{13} (if formed) preserving the right volume stoichiometry (Figure 7.7). The volume stoichiometry is calculated from the reaction theory presented in Chapter 4 with the properties of the products. Note that in the volume stoichiometry, the volume of C-S-H furthermore depends on its composition, namely C/S and A/S ratios.

When simulating the hydration of slag cement, models proposed in Chapter 4 are slightly modified taking use of the model output. In Chapter 4, the C/S and A/S ratios of C-S-H are determined by the compositions of slag and clinker and the slag proportions in the cement. The

degree of slag hydration is based on the conditions in which the pastes are cured and the curing age. The complete hydration of the clinker is assumed. In the real pastes of slag-blended cement, the clinker phases and slag are reacting simultaneously. These simultaneous reactions are represented in the computer model by the congruent dissolution of slag and clinker pixels. At each hydration cycle, the number of reacted clinker phases and slag can be counted. Therefore, to chemically represent the reactions going on in the paste, they are calculated in each cycle using the number of dissolved calcium silicates and glass pixels in the modified model. While the number of dissolved species can differ in each cycle, local variation in the compositions of C-S-H exists in the resultant microstructure. This local variation of compositions of C-S-H is observed in the experiments of Richardson and Groves (1992) as well.

The hydrotalcite forms in the exact situation of glass pixels because the magnesia content of slag is the least mobile and it is used to demarcate the original location of slag grains in practice (Glasser, 1991). In this way, the microstructure of the slag cement paste can be represented accurately. The diffusing C-S-H is located again in the neighbor site of the reactant in a 17·17·17 ℓ^3 box to simulate the growth of C-S-H around the grains. Diffusing ettringite and solid C_4AH_{13} pixels are located randomly inside the microstructure.

The reaction stoichiometry of clinker hydration is also changed because the composition of C-S-H in the modified model is influenced by the presence of slag. In each hydration cycle, a scan over all the reactants is performed; hence, a batch of pixels is dissolved. Due to the dissolution of C_3S, C_2S and glass pixels, additional diffusing C-S-H, diffusing ettringite, diffusing CH, solid C_4AH_{13} and hydrotalcite pixels are to be added after the dissolution. Hence, after the scan, the amount of dissolved C_3S, C_2S and glass pixels are counted. The composition of C-S-H at the respective cycles is calculated accordingly. Then, the properties of C-S-H are also calculated. With the properties of C-S-H, the number of pixels to be added is determined according to the reaction stoichiometry.

The consumption of CH by the slag hydration is simulated by reducing the number of diffusing CH pixels to be added. The number of pixels to be reduced is calculated from Eq. (4.42) using the numbers of diffusing CH pixels generated by the clinker hydration and dissolved glass pixels. The remaining diffusing CH pixels are added randomly, as described previously.

7.3.4 Relating the cycles to real time

Bentz (1997) proposed a method to relate the number of cycles executed in the simulation to the real time as Eq. (2.34) in Section 2.5. Since the empirical relation is proven successful for Portland cement hydration (Bentz, 1997), it is postulated and is verified valid for slag cement hydration as well.

7.3.5 Simulation results

For simulating the hydration of slag cement, the following information is needed: (a) the composition and PSD of clinker and gypsum (if present); (b) the composition of slag, including the oxide composition and fractions of glass and crystalline part; (c) PSD of slag; (d) fraction of slag in the paste; (e) water/binder ratio and (f) curing condition, including the temperature and sealed/saturated state. The hydration is carried out on a cycle basis and then converted into time.

After each hydration cycle, properties evolving during the hydration process such as chemical shrinkage, heat release, non-evaporable water and porosity, are calculated using the inherent properties of the reaction and physical or chemical properties of the products. They can be used for calibrating and validating the model, and for further use, for example, predicting properties of the paste. In the following discussion, model outputs are compared to the experimental results. They are further used to investigate several factors on the hydration of slag cement.

The microstructure development of slag cement pastes is first simulated using the slag cement from the research of Richardson and Groves (1992). The compositions of slag and Portland

Table 7.2: Composition of Portland cement and slag used in experiments.

Oxide	PC I[a]	PC II[c]	Slag I[a]	Slag II[b]	Slag III[c]
C	65.9	64.09	41.7	41.8	43.39
S	20	19.46	37.2	35.4	35.46
A	6.19	4.87	11	12.9	12.16
M	1.33	0.48	7.74	6.3	6.32
$\overline{S}$	2.65	3.52	3.68	0	0
F	3.03	0.281	0.38	0.3	0.63
T	0.3	0	0.68	1.65	0
P	0	0	0	0	0
N	0.19	0.02	0.64	0.26	0.15
K	0.86	0.6	0.55	0.38	0.5
NBO/T	-	-	2.026	1.864	1.980
Bogue composition					
C_3S	65.52	75.54			
C_2S	10.61	3.77			
C_3A	11.98	13.46			
C_4AF	9.16	0.92			
$C\overline{S}H_2$	4.68	6.46			

[a]: from Richardson and Groves (1992);
[b]: AAS, from Sato et al. (1986);
[c]: from Battagin (1992).

cement (Slag I and PC I) are listed in Table 7.2. The same w/c ratio of 0.4 as in the experiment is used in the simulation, as well as curing in a sealed condition at 20°C. The slag proportion in the solid is 50 m/m%. More details of the experiments are presented in Chapter 4. The value of β' used in the simulation is 0.25 (dimensionless), and the time conversion factor is 3.5×10^{-3} hour/cycle[2].

The phase development of hydration products and the disappearance of slag and clinker are plotted in Figure 7.8 in volume fractions. Minor products are excluded from the plot because of the scale. It can be seen from the results that the clinker phases react much faster than the slag. After one year, almost all the clinker phases have reacted, while about 50 % of the slag is still unreacted. C-S-H is the most abundant product in the paste. One remarkable characteristic of the phase composition is the low content of CH. Instead of increasing continuously as the case in hydrating Portland cement paste, the level of CH is almost constant after 4 weeks of hydration. The distribution of phases can partially explain the low permeability of the resultant microstructure. As C-S-H is a highly amorphous product, the pores in it are normally so small that it can be regarded impermeable for gas and liquid. Therefore, with increasing volume fraction of C-S-H, the paste becomes less permeable as well.

7.4 Discussion

7.4.1 Influence of particle size on the slag hydration

The effect of particle size on the slag hydration is investigated using the *New Model* and compared to the measurements by Sato et al. (1986). They measured the hydration degrees of alkali-activated slag particles with narrow-ranged sizes. The microstructure is generated in such a way that all the particles have the same size as the mean diameter (on volume basis) used in the ex-

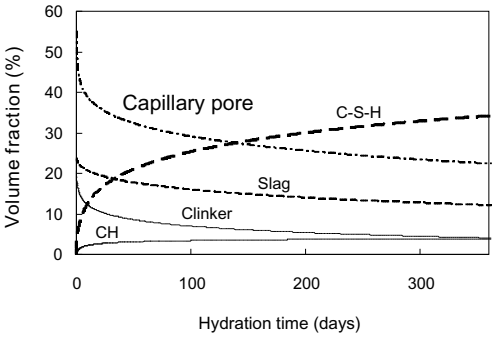

Figure 7.8: Simulated volume fraction of hydration products and reactants in hydrating slag cement paste, with the slag cement from Richardson and Groves (1992), slag proportion 50 m/m%, w/c = 0.4, T = 20°C, $B = 3.5\times10^{-3}$ hour/cycle^2, $\beta' = 0.25$.

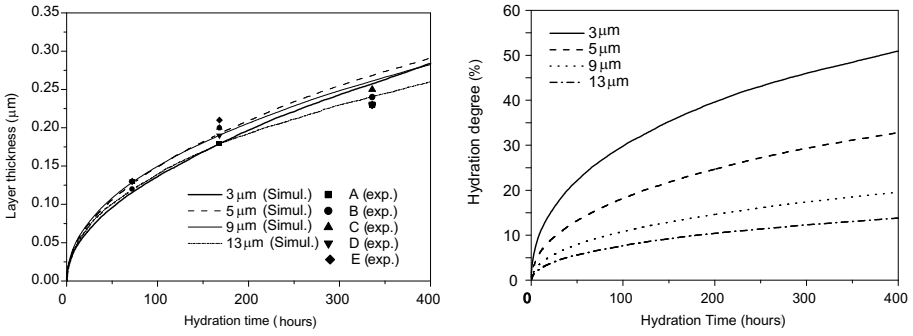

(a) Hydrated layer thickness (b) Hydration degree

Figure 7.9: Hydrated layer thickness and hydration degree of slag particles, (a) predicted hydrated layer thickness and measurements by Sato et al. (1986), (b) predicted hydration degree. T = 20°C, $B = 4.2\times10^{-3}$ hour/cycle^2, $\beta' = 0.25$.

periments. Particles with the closest size to the mean diameter are used because particles used in the simulation are not exactly spherical and the particle size distribution is discrete. For example, for the sample with a mean diameter of 3.27 μm, the digital particles with the size of 3 μm are used. The microstructure has the same water/binder ratio as that used in the experiments. The slag has also the same composition as in the experiment, which is listed in Table 7.2 (Slag II).

A simulation is carried out with the same condition as also used in the experiments. The water/slag ratio is 10. The activator used is NaOH solution with the concentration 0.1 mol/L. The slurry is cured at 20°C. The parameter β' is again set to be 0.25 and the time conversion factor is 4.2×10^{-3} hour/cycle^2. The average size of remaining slag particles is calculated using the amount of unreacted slag pixel, the number of particles and the PSD of slag given in the literature preserving the total volume. The hydrated thickness is calculated according to the difference between the initial size and the size of the hydrated slag particle. The simulation results are shown in Figure 7.9(a).

It can be seen from the results that the thickness of the hydrated layer is not significantly influ-

enced by the particle sizes of slags. The layer thickness increases with time due to the continuous dissolution of glass from slags. But, it does not change significantly with different particle sizes. The predictions also show a good agreement with the measurement in the experiment, in which the activator NaOH solution is used. The presence of activators in AAS paste is simulated by introducing the corresponding ions (for example, Na^+ and OH^- ions for NaOH solution) with the planned concentrations in the initial pore solution. Part of these ions are incorporated into the solid products. The change of the pore solution composition is predicted with the methods presented in Chapter 5.

For the particles with different sizes, although they have the same hydrated layer thickness, the amount of hydrated slag is different due to the different size. The hydration degree of slag particles as a function of curing time is shown in Figure 7.9(b). One can see that slag particles with different sizes have significantly different hydration degree at the same curing age. The hydration degree for finer particles (from fine to coarse ones, A, B, C, D, E) is larger. The finest particle (A) has a hydration degree approximately three times higher than the coarsest particle (E). A simple calculation using the same hydrated layer thickness yields the same value. The difference in the hydration degree illustrates how the finer particles achieve higher hydration degrees.

7.4.2 Hydration degree of slag in cement

Since the computer can predict the layer thickness and the hydration degree of single particle quite well, it can be used to predict the overall hydration degree of slag in the hydrating cement. The influences of slag proportion in the cement and w/c ratio on the slag hydration degree are investigated in this section.

The slag cements used by Battagin (1992) are used for the simulation. Battagin (1992) used a selective dissolution method with EDTA solution to determine the hydration degree of slag in the laboratory-made cements. Slag cements with 35, 50 and 70 m/m% slag proportions are selected for comparison. The compressive strength of mortar samples and degree of slag hydration are measured. The compositions of cement (namely PC II) and slag (namely Slag III) are listed in Table 7.2, respectively. The PSD of the slag and Portland cement is not given in the literature, and is taken to be the same as those of the slag and Portland cement used in Chapter 8 (see Figure 8.5). The simulations are carried out with a w/c ratio of 0.48 at 23°C, as also used in the experiment. The value of β' is set again to be 0.25. The fitted value of B is 4.5×10^{-3} hour/cycle^2. The degrees of slag hydration are shown together with the degrees measured in the experiments in Figure 7.10(a). One can see that the hydration degrees of slag in the hydrating slag cement are well predicted. For the slag proportions tested in the experiment, their influence on the hydration degree is shown to be minor, which is again in good accordance with the experimental observations. The minor influence of slag proportions in cement on its hydration degree is also observed in other studies (Hinrichs and Odler, 1989; Lumley et al., 1996).

Simulations on the hydration of slag cement pastes with different w/c ratios are carried out as well. The slag cement in the study of Battagin (1992) with 50 m/m% slag is used. The simulation results are shown in Figure 7.10(b). One can see that the hydration degrees with relatively larger w/c ratio (0.48 and 0.60) are obviously higher than the degree with a smaller w/c ratio (0.30). Therefore, larger w/c ratios are favorable for achieving higher slag hydration degrees. This is reasonable because for pastes with larger w/c ratios, there is more water and space available for the reaction and growth of products. At a paste level, there is also more water available for the hydration of cement. In the sealed state, as the hydration is largely dependent on the amount of water available, the larger w/c ratios enhance the glass hydration. With regard to the model, there is a larger chance for the dissolution of glass pixels because more of them are in contact with pores. However, this "expedition effect" diminishes with increasing w/c ratios, according well with the experimental observations by Battagin (1992). The difference between the hydration degrees with a w/c ratio of 0.48 and 0.60 is already quite small.

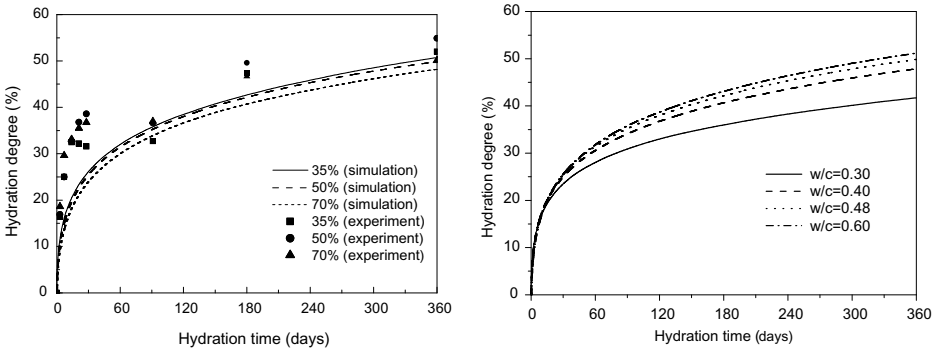

(a) Effect of slag proportion, w/c = 0.48

(b) Effect of w/c ratio, 50 m/m% slag

Figure 7.10: Hydration degree of slag in slag cement: Effect of slag proportion and w/c ratio. T = 23°C, $B = 4.5\times10^{-3}$ hour/cycle^2, $\beta' = 0.25$. Measurements in (a) are taken from Battagin (1992).

The attenuation of the expedition effect is explained as following: If the w/c ratio is low, the pastes will gradually be densified; hence, all the capillary pores are filled with products. Then, the hydration is impeded due to the limit of space for the growth of products. As pointed out in Chapter 3, for the AAS paste, if the water/slag ratio is lower than approximately 0.40, achieving a complete hydration of slag is difficult because of the limit of space. This limiting effect also applies to the slag cement. However, if the w/c ratio keeps increasing, the hydration of slag particles becomes more dissolution-controlled, which means the possibility of dissolution governs the hydration degree. As the possibility of dissolution depends on the reactivity of slag, the chemical composition of pore solution and the chances of being attacked (in contact with water), the limit of space for product growth no longer determines the slag hydration degree. Therefore, for pastes with large w/c ratios, the hydration degree of slag does not vary significantly.

7.4.3 CH content in the paste

DTA combined with TGA can be used to quantify the various phases in cement paste. It is shown to be an accurate and reliable technique to determine the amount of CH in slag cement paste (Pane and Hansen, 2004). The interaction between the CH produced by the clinker hydration and the slag hydration is of primary interest for investigating slag cement hydration, and is also predicted with the computer model. Again the slag cement from the study of Battagin (1992) is used (PC II and Slag III in Table 7.2). The simulation is carried out with the same conditions as used in Section 7.4.2. Different slag proportions as 0, 35 m/m%, 50 m/m%, 65 m/m% and 90 m/m% are used. The amount of CH in the paste is plotted in Figure 7.11(b) versus the curing time in g per 100 g original cement.

One can see from Figure 7.11(a) that the CH content in the slag cement paste is clearly lower than the level in Portland cement paste. It decreases with increasing slag proportions in the cement and increases rapidly at early ages due to the fast hydration of clinker phases, followed by approximately constant values at later ages. The trend of the increase and the values are in good agreement with the measurements by Kondo and Ohsawa (1968) and Hinrichs and Odler (1989). They found that the level of CH is obviously lower in slag cement paste than in Portland cement paste, and is lowered with increasing slag proportions. While the contents in Portland cement pastes keep increasing during the curing ages, the contents in the slag cement pastes remains almost constant after 7 days of curing. For some slag cement pastes, it decreases slightly with

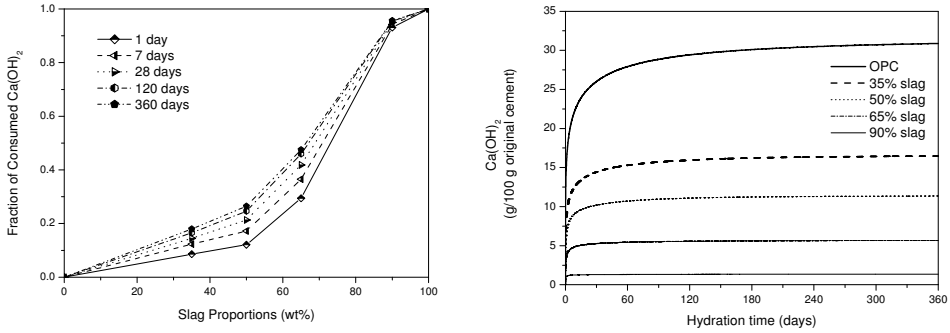

(a) Fraction of CH consumed by slag reaction

(b) Amount of CH formed in the paste

Figure 7.11: Simulated CH consumption by the slag reaction, predicted with the recipe from Battagin (1992) (PC II and Slag III in Table 7.2). T = 20°C, $B = 4.5\times10^{-3}$ hour/cycle^2, $\beta' = 0.25$.

increasing time. It is clear that replacing Portland cement with slag reduces the CH level in the paste, and with increasing proportions the level is reduced.

7.4.4 Composition of the hydration product C-S-H

The composition of C-S-H is important in the studies on cementitious material because C-S-H is the principle binder providing most of the desirable properties. The composition of C-S-H governs its various properties, including both physical and chemical properties. It is the subject of numerous researches, and one general conclusion is that replacing Portland cement with slag clearly decreases the C/S ratio in C-S-H (Harrisson et al., 1987; Richardson, 1997; Richardson and Groves, 1992; Taylor et al., 1985). Increasing the slag proportions in the slag cement decreases the C/S ratio in C-S-H, as also seen in Chapter 4.

The composition of C-S-H is predicted with the computer model and is compared with the experimental results by Richardson and Groves (1992). Both the C/S and A/S ratios are measured in the experiments at different ages. The predicted and measured average C/S ratios are plotted in Figure 7.12(a), and the average A/S ratios in Figure 7.12(b). During the simulation, the C/S and A/S ratios in each hydration cycle are calculated according to the numbers of dissolved clinker and glass pixels. Since at each cycle the numbers are different from numbers in the other cycles, the C/S and A/S ratios actually fluctuate in a certain range. This gives some local variations in the composition of C-S-H, which is observed in the experiments. The model outputs are the average compositions of C-S-H calculated at each cycle and in time.

One can see that both the trend and values of the compositions are well predicted with the model considering the scatter in the measurement. At early hydration stages, the C/S ratios are slightly lower than at the later ages because more clinker phases dissolve at this moment. As a consequence, more CH is available for the hydration of slag. As a whole, the composition of C-S-H changes only slightly with curing time.

7.5 Conclusions

In this chapter, the *New Model* developed in Chapter 6 is further extended for simulating the hydration and microstructure development of slag cement paste. The theoretical models developed in Chapter 3 and 4 are used and incorporated into the computer model, with special considerations on the reactivity of slag. A few factors on the slag reactivity are discussed, and methods are proposed to account for these factors in the simulation process. The model predictions are validated with measurements in experiments, and it is further used to investigate a few properties

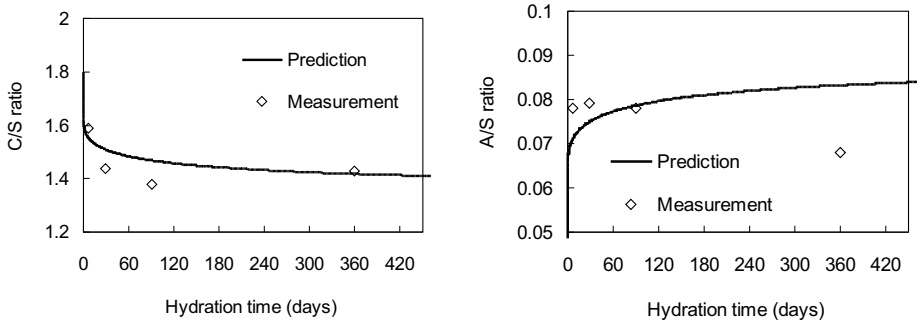

(a) C/S ratio (b) A/S ratio

Figure 7.12: Predicted and measured composition of C-S-H as a function of hydration time, experimental data taken from Richardson and Groves (1992). T = 20°C, $B = 3.4\times10^{-3}$ hour/cycle^2, $\beta' = 0.25$.

of hydrating slag cement paste, for example, the CH content in the paste, effect of particle size on the slag hydration, hydration degree of slag, and composition of the C-S-H. The results show that the extended model is able to simulate the hydration process of slag cement paste and can be used to predict various properties of the hydrating paste.

Chapter 8

Shrinkage-compensating cement for concrete

8.1 Introduction

In this chapter, the historical development of shrinkage-compensating cements (SCC) is firstly discussed based on the formation of metal hydroxide (portlandite and brucite) or ettringite. The reactions and mechanisms inducing the expansion are investigated. Computer models are established for simulating the hydration reactions of SCC based on the research in the previous chapters. Subsequently, a new mineral shrinkage-compensating admixture (MSA) for concrete is developed containing some mineral additives. Experimental tests are carried out, which prove that the new MSA can successfully compensate the autogenous shrinkage. Computer simulations are executed to predict some other properties of cement paste involving certain dosages of this MSA. Practical suggestions are proposed for improving the performance of SCC based on the experimental results and simulations.

8.2 Development of SCC

As discussed in Section 1.6, shrinkage is one of the most obvious disadvantages of concrete, which deserves special attention when designing a concrete structure. It causes cracking in the structure due to internal restrains (for example, by steel bar) or external ones (for example, other structural elements). The shrinkage can also cause loss of initial stress in the tendons in prestressed concrete.

The use of SCC in concrete appears to be an effective method to mitigate the shrinkage of concrete. The idea is to counteract the negative volume change (shrinkage) with some reactions that exhibit expansive potentials. The shrinkage is thus compensated. Sometimes slight expansion of plain concrete is also observed due to the excessive expansion. This will not be a problem supposing the expansion is not too large because normally the concrete elements are restrained internally or externally. The slightly excessive expansion generates tension in the restrains and compression (0.2–0.7 MPa, according to Taylor (1997)) in the concrete, which normally is advantageous for concrete.

SCC is widely used in situations where cracking of elements must be strictly prohibited, for example, bridge decks, pavement slabs, and liquid storage tanks. It is also useful in massive concrete construction, like dams and foundations, and in high-strength and high-performance concrete in which normally the paste content is high (see Section 1.6).

The start of research about SCC dates back to about 60 years ago when Lossier (1946) used a mixture of Portland cement, an expanding agent, and a stabilizer to make a concrete with controlled expansion. The expanding agent is made by burning a mixture of gypsum, bauxite and chalk to form calcium sulfate and calcium aluminate (mainly C_5A_3). These compounds react with water to form ettringite (Neville, 2000). The work on SCC is continued by Lafuma (1952) and Klein and Troxell (1958), the latter being the foundation of the modern SCC widely used in engineering.

Nowadays, SCC is widely used in construction industry already. It can be produced directly in a cement plant, or by mixing cement with some shrinkage-compensating admixtures. The latter are specially designed admixtures which are expected to replace a certain proportion of

Table 8.1: Types of SCC and their expanding compounds according to ASTM C845-04

Type	Expanding compounds
Type K	$C_4A_3\overline{S}$, calcium sulfate and quick lime
Type M	Calcium aluminate cement[♮] and calcium sulfate
Type S	Excessive C_3A and calcium sulfate

[♮]: Cement consisting essentially of hydraulic calcium aluminate.

cement in concrete and show expanding potential. The advantage of using this admixture is that its amount in concrete can be flexibly adjusted on construction site according to different requirements.

Three types of SCC are distinguished in the ASTM C845-04 standard, in which the compounds showing expansive capacity are listed in Table 8.1. All the SCC in Table 8.1 take use of the ettringite formation and the Type K cement uses the formation of portlandite as well. The source of sulfate necessary for the formation of ettringite comes from calcium sulfate and the specially made clinker (for Type K). The sources of alumina are diverse, being the specially made clinker for Type K, the calcium aluminate cement for Type M, and C_3A for Type S. Other sources for alumina are frequently used, like slag and impure alunite ($KA_3\overline{S}_4H_6$) (Taylor, 1997).

Another type of SCC takes use of the formation of some metal hydroxides. The reactions of quick lime and periclase fit into this group and are treated together in this chapter due to the similarity in the nature of their reactions and in the properties of the hydration products—portlandite and brucite.

The use of quick lime as expanding agent is mostly applied in Japan (Nagataki and Gomi, 1998), and the application of periclase has been employed in dam constructions as expanding agent in China for decades (Du, 2006).

Henceforth, cements with ettringite as the expanding agent are called “ettringite-based” SCC, and those with portlandite and brucite as the expanding agent are called “hydroxide-based” SCC. In the next section, the hydroxide-based SCC is discussed and in Section 8.4 the ettringite-based SCC is discussed.

8.3 Hydroxide-based SCC

Portland cement clinker may contain small amounts of free lime and periclase (crystalline MgO). The free lime comes from the excessive lime that is not bound in clinker phases. The periclase is formed from the excessive magnesium besides the solid solution in the clinker. It exists normally in the dead-burnt status. The free lime and periclase produced during clinker production normally show a delayed hydration compared to the other clinker phases. Their hydration takes considerably longer time to achieve a remarkable degree in normal curing conditions. Since the hydration of free lime and periclase is normally accompanied by a volume increase of the cement paste, this will lead to a disruption of the hardened paste, called unsoundness. The unsoundness of cement can be tested in accordance with the standards EN 196-3, ASTM C151-05 and GB/T1346-2001.

However, the expanding potential of the quick lime and periclase reactions can also be used in a beneficial way. If the expansion time and magnitude is properly regulated, it can be used to compensate the shrinkage of concrete as well.

8.3.1 Reaction of quick lime

The free lime in clinker is harmful for the volume stability of cement paste, because it is not completely exposed to water during the hydration and its reaction is highly localized. However, quick lime is frequently added intentionally into cement to compensate the shrinkage, supposing it is homogenously mixed with cement particles. The quick lime react with water in the form:

$$\begin{array}{c} C + H \rightarrow CH \\ 1 \quad 1.08 \quad 1.96 \end{array} \tag{8.1}$$

Numbers below the formula indicate corresponding volumes of substances. The hydration product, portlandite, is a natural mineral normally existing in the crystalline form.

It is important to note that in Eq. (8.1), the formation of CH is actually accompanied by some chemical shrinkage, i.e. the volume of the reaction product (1.96 in Eq. (8.1)) is smaller than the total volume of the reactants ($= 1 + 1.08$). Therefore, the formation of CH in cement pastes is not able to eliminate the chemical shrinkage. However, by comparing the volume of solid (C or CH) between the two sides of Eq. (8.1), one can see that it has been approximately doubled (from 1 to 1.96) during the hydration of C. This volume increase of solid can cause expansion in cement pastes in two ways: (1) if the water is supplied externally, the reaction product CH occupies much more space than the initial solid C, generating expansion; (2) the formation of CH crystals change the morphology and distribution of solid in the pastes. They are formed between solid particles and grow in a preferential way, pushing the solid particles away and generating the expansion.

Yamazaki and Sakakibara (1986) studied the hydration of lime paste with a very low water/solid ratio 0.28. The pressure generated by the lime hydration is monitored, and the hydrated microstructure is studied with various techniques including XRD, TG-DTA, photomicroscope, SEM and EPMA. The amount of reacted lime is calculated from weight loss of samples caused by dehydration of CH and decomposition of $CaCO_3$. It is found that the size of the CH crystals hardly increases after about 8 hours although the lime keeps hydrating (Figure 8.1). The size remains about several hundred Å. The increase of expansion pressure is accompanied by also a pore volume increase. The authors concluded that the expansive pressure is a result of the continuous enlargement of the thickness of the rim surrounding the lime grains. The crystals of CH are massive and irregular in the paste.

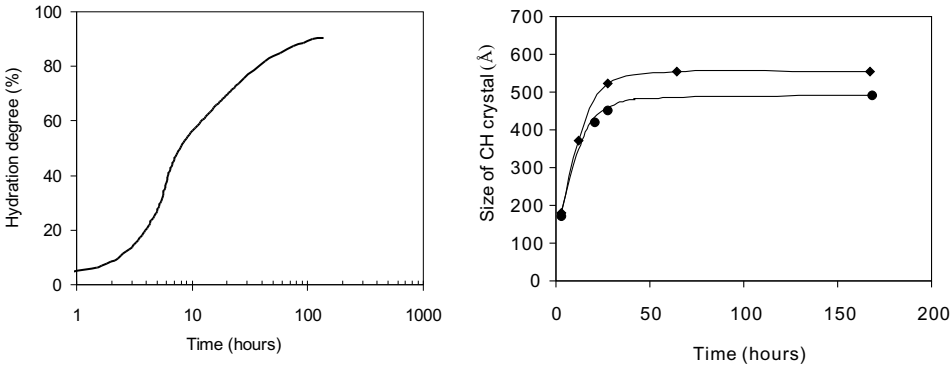

(a) Hydration degree of lime

(b) CH crystal size

Figure 8.1: Hydration degree of lime (a) and CH crystal size (b) in hydrated lime paste, water/solid ratio = 0.28, T = 25°C, after Yamazaki and Sakakibara (1986).

It should be noted that the reaction of quick lime with water releases a lot of heat, which can raise the element temperature and in turn aggravates its thermo-shrinkage.

8.3.2 Reaction of periclase

The reaction of periclase in cement is:

$$\begin{array}{cccc} M + H & \rightarrow & MH \\ 1 \;\; 1.70 & & 2.30 \end{array} \tag{8.2}$$

Similar to the reaction of quick lime (Eq. (8.1), on the one hand, the reaction of periclase is accompanied by some chemical shrinkage. On the other hand, the volume of solid increases 130% after the reaction.

Kasselouris et al. (1985) tested synthesized clinkers containing 10 m/m% MgO using XRD and DTA. Industrial raw materials are used for synthesizing the clinker. The pastes of high magnesia cements are cured in water at 18°C up to eight years. MH is detected in the paste, although its level is low at early ages (earlier than three years). Then, the hydration proceeds steadily up to six years. After this age, a very small or a nil hydration of the contained MgO took place. At eight-year age, for Portland cement paste about 75% of the periclase has hydrated. With the presence of some highly reactive pozzolanic additives (fly ash and santorin earth), the hydration of MgO is much depressed.

Ali and Mullick (1995) studied the hydration of high MgO cement paste under autoclave conditions. Rapid formation and crystallization of magnesium hydroxide is found, leading to the creation of larger pore sizes. The formation of MH crystals results in the loss of mechanical strength and higher expansion values. Under ambient water curing, precipitation and distribution of gelatinous C-S-H into the finer network causes a homogeneous morphology and the development of smaller pores. The resultant higher mechanical strength associated with partial hydration of MgO yields reduced expansion. High MgO cement paste containing fly ash also showed considerable pore refinement and improved hydrate morphology, favoring volume stability under both autoclave and ambient water curing.

Lou et al. (1998) studied the hydration and expansion property of periclase in clinker using XRD and differential scanning calorimetry (DSC) under isothermal conditions in water. The amount of periclase in clinker and the curing temperature are shown to have dominant influences on the expansion capacity. In all cases of tests, the periclase reacts in a low rate, especially if cured at room temperature.

Ye et al. (2004) studied the hydration of periclase in clinker considering the influence of the curing temperature. Elevated curing temperature clearly accelerates the hydration rate of periclase. If cured at 90°C, periclase hydrates completely after 120 days. However, if cured at 20°C and in water, it starts to hydrate at 60 days and the hydration completes at 2000 days. As a product of the periclase hydration, brucite is formed.

It should be noted that the hydration rate of periclase highly depends on the burning temperature (Du, 2006). The dead-burnt (above 1200°C) periclase reacts slow with water and thus causes unsoundness. The lightly-burnt periclase (850–1200 °C) hydrates at a high rate, suitable for expanding agent in concrete.

In the following section, a literature on the hydration of periclase in clinker is presented on the volume changes of pure cement paste. The *New Model*, which is already proven useful in modeling the hydration of Portland cement and slag cement (Chapter 6 and 7), is extended for simulating the microstructure development of cement pastes containing periclase.

Table 8.2: Effects of burning temperature on the hydration rate of MgO powder (%), after Du (2006).

Hydration time	Burning temperature (°C)		
(days)	800	1200	1400
1	75.40	6.50	4.70
3	100	23.40	9.30
30	ł	94.80	32.80
360	ł	97.60	

Table 8.3: MgO and periclase contents and periclase distributions in the cements used in the experiments by Lou et al. (1998).

Sample	MgO (m/m%)	Periclase (m/m%)	Distribution of periclase
A	5	3.89	Pocket-like
B	5	3.85	Uniform
C	7.87	6.79	Pocket like

8.3.3 Experiments on SCC made from periclase

Lou et al. (1998) carried out a series of experiments to investigate the hydration of periclase in cement and its influence on the volume change of cement paste. Clinkers containing preplanned amounts of periclase are made by incinerating raw feeds added with dolomite. 1.8 m/m% of dihydrate calcium sulfate ($H_2\bar{S}O_4$) is added into the clinker, and ground together. Three recipes are tested, viz. A, B, and C, listed in Table 8.3. Samples are made with each cement paste. For testing the compressive strength, cubes with rib size 200 mm are used, and for the length change tests, prisms sized 200·200·2500 mm^3 are used). The samples are cured in water at 20, 50, 70, and 90°C. The periclase contents and distribution form are different in each group (Table 8.3). The fraction of MgO in the solid solution form is about 1.1 m/m%.

Hydration degree of periclase

The hydration degree of periclase in cement is calculated from the differential scanning calorimetry (DSC) test results and plotted in Figure 8.2. It can be clearly seen that temperature has a

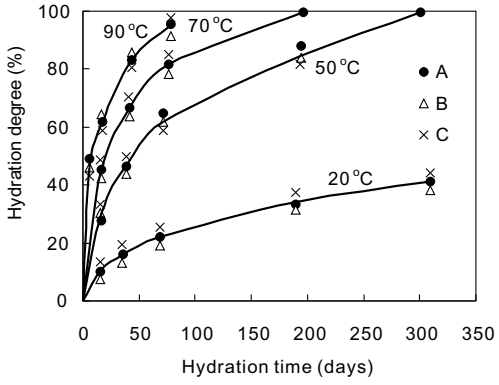

Figure 8.2: Hydration degree of periclase at various temperatures, after Lou et al. (1998).

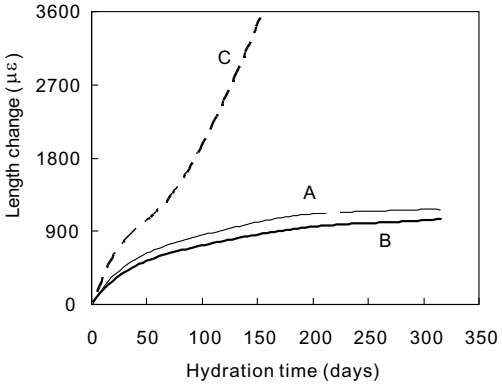

Figure 8.3: Length change of samples containing various amounts of periclase at 50°C, after Lou et al. (1998). A, B and C denote the corresponding recipe in Table 8.3.

dominant influence on the hydration degree of periclase in cement. If cured at room temperature, periclase hydrates at a low rate, achieving a hydration degree of about 40% after one year. However, raised temperature significantly accelerates the periclase reaction.

Length change

The length change of paste samples made with different periclase contents and cured at 50°C is plotted in Figure 8.3. The dramatic increase for recipe C after 100 days could be due to the cracking of the samples. It can also be seen in Figure 8.4 that the expansion force generated by the hydration of periclase is very stable. It starts typically after 20 days and increases steadily. The trends for recipe A and B are quite similar, due to the similar amounts of periclase. It appears that the distribution of MgO in the cement does not influence the expansion potential significantly.

Compressive strength

The compressive strength of cement pastes containing various amounts of periclase is plotted in Figure 8.4. The curing temperature is 50°C. For low contents of periclase (recipe A and B), the compressive strength is slightly lower than that of Portland cement. However, if a larger amount of periclase is used, the compressive strength is remarkably reduced. When comparing Figure 8.3 and Figure 8.4, one can see that the decrease of the compressive strength is accompanied by a sharp increase in the linear expansion, indicating that possible cracking might occur.

8.3.4 Kinetics of periclase hydration

Lou et al. (1998) found that the reaction degree of periclase (α) can be related to the curing age (t, in hours) as:

$$1-\frac{2}{3}\alpha-(1-\alpha)^{2/3}=k_T\cdot t \tag{8.3}$$

in which k_T is a rate constant (in hour^{-1}) and is related to the curing temperature (T, in K) as:

$$k_T=A\cdot\exp\left(-\frac{E_a}{\mathrm{R}T}\right)=0.2404\cdot\exp\left(-5623[K]/T\right)\quad \text{hour}^{-1} \tag{8.4}$$

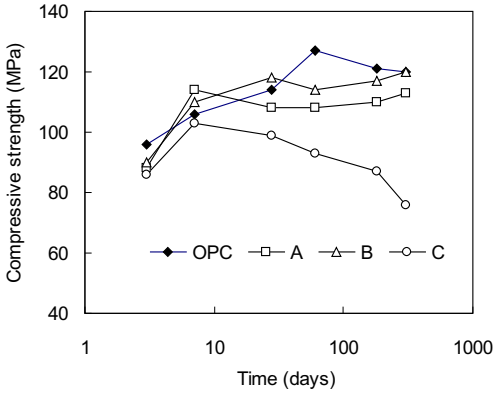

Figure 8.4: Compressive strength of hardened cement paste samples containing various amounts of periclase at 50°C, after Lou et al. (1998).

in which R is the gas constant (8.314×10^{-3} kJ/(mol·K)). The activation energy (E_a) is calculated from the parameters as:

$$E_a = 5623 \cdot \mathrm{R} = 46.75 \quad \mathrm{kJ/mol} \tag{8.5}$$

The relation in Eq. (8.3) indicates that a diffusion-controlled mechanism dominates during he hydration process of the periclase particles according to Levenspiel (1999). This value is apparently higher than the values measured for Portland cement hydration, about 38.44–40.20 kJ/mol (Zhang et al., 1999).

8.3.5 Computer modeling of quick lime and periclase hydration

Incorporating the reactions

The reactions of quick lime and periclase in cement are incorporated into the *New Model*, which is discussed in Chapter 6 and 7. The detailed procedure for simulation of their reactions are presented below.

Regenerating the initial microstructure First, an initial microstructure is regenerated, now including the reactants quick lime and periclase amongst the others. The same PSDs for both quick lime, periclase and cement particles are used if no specific information about their PSDs is available.

Hydration Then, hydration cycles are executed following the dissolution, diffusion, reaction and participation procedure. When a periclase pixel dissolves, it turns into diffusing MH immediately, following the reaction equation (8.3). The same happens to a quick lime pixel, now into diffusing CH.

Note that since the volume of hydration product MH is 1.3 times bigger than the periclase (see Eq. (8.3), additional solid pixels are needed for the dissolution. When one solid periclase pixel turns into diffusing MH at the exact place, another 1.3 diffusing MH pixels are added randomly in the structure. The additional pixels are added on a statistical basis. For example, instead of adding 1.3 pixels when one pixel of periclase turns into diffusing MH, 13 pixels of diffusing MH are added when 10 pixels of periclase react. The corresponding value for the quick lime reaction is 0.96, i.e. when 100 pixels of quick lime react, they turn into 100 diffusing CH pixels, and in addition, 96 pixels of diffusing CH is added randomly into the microstructure.

The diffusing MH or CH pixels perform a random walk in the structure. They may nucleate into pixels solid MH or CH at the exact place. The probability of the nucleation process is

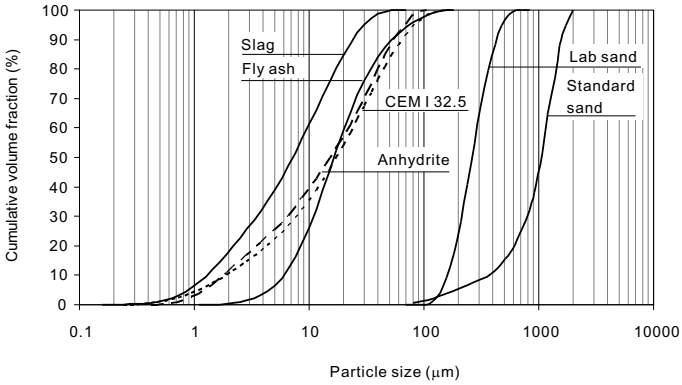

Figure 8.5: Particle size distribution of materials used in the experiments.

controlled by a nucleation capability given by the user before the run. The diffusing MH turns into solid MH if it collides with other solid MH, and diffusing CH turns into solid CH, or reacts with C_3A with or without gypsum to form C_4AH_{13} or ettringite, as described in Chapter 6. Because the relatively low mobility of Mg^{2+} ions in the structure, the nucleation capability is set to be a higher value than that for diffusing CH, which means that diffusing MH is less mobile and is more likely to nucleate on the spot. Nucleation or precipitation of diffusing MH on the surface of other species is prohibited to promote the growth of large MH crystals in the structure, which is observed in experiments and used in the mechanism (Chatterji, 1995; Lou et al., 1998). When the solid MH is formed, it is indissoluble and is thus stable, while solid CH is still soluble.

Numerical simulation and validation

Numerical simulations are performed using cements containing different levels of quick lime and periclase. The simulation results for periclase are compared to the experimental results by Lou et al. (1998).

The mineral compositions of clinker in the experiments are not given by Lou et al. (1998) directly. The composition of one clinker used by the authors and reported in another parallel work (Ye et al., 2004) is used, which is listed in Table 8.4. No information about the PSD of the materials are given, and the Blaine fineness ranges between 300–350 m^2/kg. Hence, the PSD of one CEM I 32.5R is used, which is shown in Figure 8.5, due to their similar Blaine fineness. The water/binder ratio is 0.28. The same levels of periclase (in the form of periclase) as used in the experiments (3.89 and 6.79) are added into the cement.

The simulation is carried out in the saturated and isothermal condition. The temperature is set to 20°C. The experimental results on the hydration degree of periclase in cement are shown in Figure 8.6(a), together with the results of the simulations. The time conversion factor is set to be

Table 8.4: Mineral composition of clinker used by Lou et al. (1998), taken from Ye et al. (2004).

Mineral	Fraction (m/m%)
C_3S	49.7
C_2S	20.8
C_3A	4.3
C_4AF	17.8

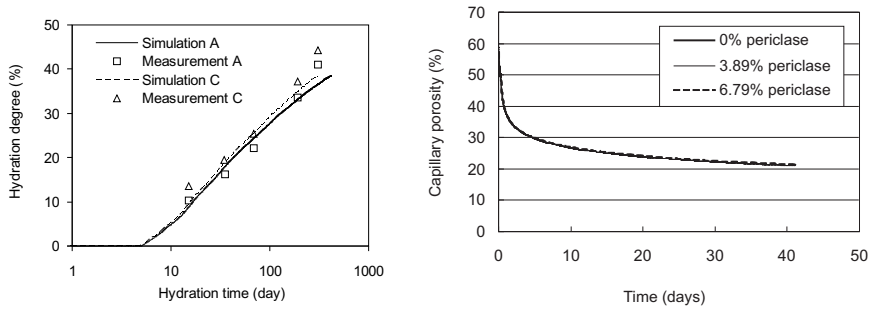

(a) Hydration degree (b) Capillary porosities

Figure 8.6: Hydration degree of periclase and capillary porosity of hydrating cement pastes containing different amounts of periclase, (a) simulated and measured degrees; (b) simulated capillary porosities.

4.2×10^{-3} hour/cycle^2. The dissolution probability of periclase pixel is set empirically as 0.001, which is one fifth of the probability of C_2S (0.005, see Table 6.1). This value is determined by fitting the simulation results for cement with 3.89 m/m% periclase (sample A in Table 8.3) to the measurements. It is further used for simulating the hydration of cements with other fractions of periclase as well, which are presented in Figure 8.6. Note that an induction period of 10 days for the periclase hydration is artificially introduced according to Ye et al. (2004) and Lou et al. (1998).

It can be seen that for the period simulated, the predicted hydration degrees of periclase are quite close to the measurements. The influence of different levels of periclase in the cement on its hydration degree is also well predicted; they do not significantly affect the hydration degree of periclase. This effect is expected because the hydration degree of periclase depends mainly on its PSD, the reactivity, the water/cement ratio and temperature.

The influence of periclase hydration on the microstructure of cement paste is also investigated. The capillary porosity of cement paste containing different levels of periclase is plotted in Figure 8.6(b). It can be seen that for dosages up to 6.79 m/m% in cement, the capillary porosity does not change significantly. This minor influence again confirms the mechanism of expansion induced by periclase hydration. Instead of reducing the porosity of the cement paste, the growth of periclase crystals exerts pressure on the surrounding particles. They will grow in a preferential way so that the obstacles to there growth are pushed apart. Therefore, it can be concluded that the morphology of products, instead of the shrinkage of the reaction itself, is important when considering or selecting the expansive reactant to counteract the shrinkage of cement paste.

8.3.6 Relation between amount of brucite and expansion

The relation between the amount of brucite formed by periclase hydration and the length changes of prisms are investigated with the data from the experiments of Lou et al. (1998) and the simulation results (Figure 8.7). The amount of brucite is calculated as its mass fraction in the paste in the saturated state. The hydration degrees of clinker phases at the considered age are simulated. The mass of brucite is computed from the hydration degree of periclase (Figure 8.6(a)) and its initial mass fraction in cement. It appears that an approximately linear relationship between the amount of brucite in the paste and the length change of the samples can be observed.

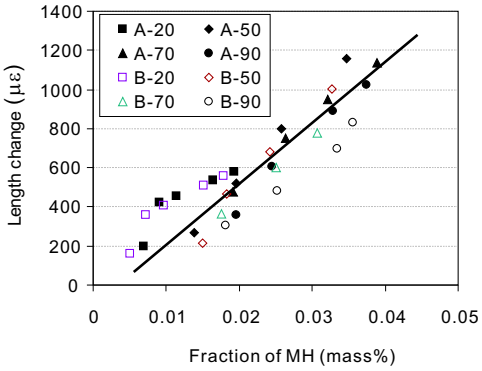

Figure 8.7: Relation between the mass fraction of MH in the pastes and the length change of prisms containing various amounts of periclase. The number in the legend indicates the temperature at which the samples are cured, A and B stand for the two groups of samples listed in Table 8.3. The mass fraction of MH is predicted with the computer model, and the length change is taken from the experimental data of Lou et al. (1998).

8.4 Ettringite based SCC

In cements, the sulfate occurs partially in the clinker and partially in the added calcium sulfate. The added calcium sulfate is generally called gypsum, but it can include anhydrite and hemihydrate. During grinding, gypsum can be partially dehydrated to form hemihydrate or even ɣ-calcium sulfate ("soluble anhydrite"). Anhydrite is sometimes added deliberately to combine good setting behavior with good early strength. Hemihydrate and ɣ-calcium sulfate react faster than gypsum; anhydrite reacts more slowly.

The ettringite-based SCC has been developed for several decades, as discussed in Section 8.2, and has been intensively investigated (Höglund, 1992; Mehta, 1976; Mehta and Wang, 1982; Nagataki and Gomi, 1998; Yan et al., 2002). However, difficulties have been encountered frequently in its applications due to the complexity in regulating its hydration. The expansion is highly dependent on the reactivity of the components and their spatial distribution within the cement powder (Bentz and Jensen, 2004). Therefore, these two factors are very essential in designing the concrete recipe. First, though the chemical and autogenous shrinkage is generally uniform throughout the concrete, expansion due to the ettringite formation can be a localized phenomenon due to the discrete nature of the growing crystals and an inhomogeneous mixture of ingredients. Second, the expansion should occur neither too early nor too late. During the early ages, the hydrating concrete is plastic, and cracking is very unlikely to occur during this time. Hence, the expansion potential of ettringite does not compensate the shrinkage at all. Furthermore, since the ettringite formation consumes much water, its formation during early ages is more likely to increase the cracking later. If the ettringite formation takes place in a later stage when concrete has probably developed most of its strength, it damages the compact structure and causes unsoundness.

Furthermore, normal SCC like Type K, M and S is much more expensive than Portland cement. Special equipments and techniques are required to produce SCC, which increases the costs. Due to its high price, quality control and broad application is difficult in production.

In this section, a new type of ettringite-based mineral shrinkage-compensating admixture (MSA) is developed, taking use of industrial by-products. It is intended to compensate the autogenous shrinkage, which is essential in massive, high-strength and high-performance concrete.

(a) Natural mineral (b) Crystals in cement paste

Figure 8.8: Natural ettringite crystals and needle-like crystals formed in hydrating cement paste.

8.4.1 Formation of ettringite

Ettringite is one type of AFt ($A1_2O_3$-Fe_2O_3-tri) phases with the formula $C_6A\overline{S}_3H_g$, in which the water content (g) can vary in different hydration states (see Chapter 2). It is named after the place where for the first time the natural mineral ettringite is discovered, Ettringen in Germany (Figure 8.8). Structurally, the aluminum can be replaced by iron, manganese or silicon. The SO_4^{2-} can also be replaced by CO_3^{2-} or $2OH^-$. Ettringite, or a phase with similar composition, is formed during the early hydration of most Portland cements. In the early literatures, it is also called high-sulfate calcium sulfoaluminate (Taylor, 1997).

The existence of ettringite in hardened cement paste can be detected by using XRD, DTA, or differential scanning calorimetry (DSC). Determining the amount of ettringite is difficult because of the ease with which water is lost and crystallinity decreased during isolation or grinding (Taylor, 1997).

The formation of ettringite during the hardening process of cement paste is mainly due to the reaction of C_3A with gypsum and water in the form:

$$C_3A + 3C\overline{S}H_2 + 26H \rightarrow C_6A\overline{S}_3H_{32} \tag{8.6}$$

This process normally takes place during the early age and continuously consumes sulfate provided by gypsum. If the sulphate concentration in the concrete pore solution drops, which is the case when all the gypsum is consumed, ettringite may be transformed to the metastable mineral monosulphate. Thermodynamic calculations show that the formation of ettringite is favored by high sulphate concentrations in the pore solution and it is stable at sulphate concentrations above 3×10^{-6} mol/L (Höglund, 1992).

After being in contact with water, the sulfate ions are released rapidly from the clinker sulfates and calcium sulfate, whereas alumina is released mainly from the aluminate phase more slowly, and the resulting high ratio of available SO_4^{2-} to available $Al(OH)_4^-$ favors the formation of ettringite. After about 24 h, substantially all the SO_4^{2-} has been released, and the continuing supply of $Al(OH)_4^-$ leads to the dissolution of ettringite and precipitation of monosulfate.

However, the sulphate deficiency can be moderated by the sulfate desorbed from C-S-H. It is found in experiments that up to 1/6 mole of SO_4^{2-} could be adsorbed in the hydrated paste of 1 mole C_3S (Odler, 1980). After a certain age, subsequent desorption of sulphate from the calcium silicates occurs, renewing the ettringite formation (Taylor, 1997). Some data indicate that reaction with carbonate may actually promote the formation of ettringite (Höglund, 1992). The CO_3^{2-} reacts with monosulfate to form hemicarbonate and ettringite (Taylor, 1997).

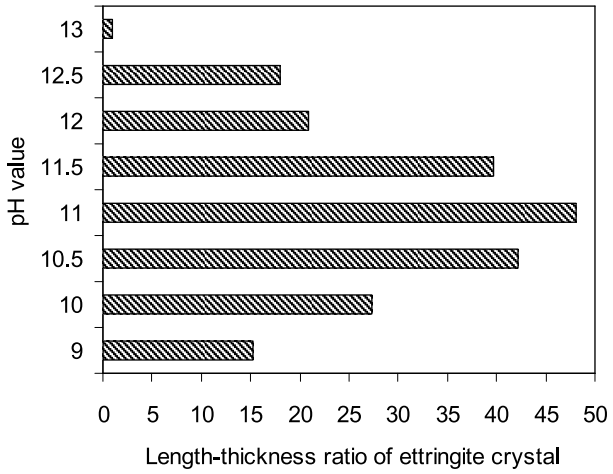

Figure 8.9: Effect of pH value of the solution on the length-thickness ratio of ettringite crystals, after Chartschenko and Stark (1995).

8.4.2 Expansion mechanism

The expansion mechanism of ettringite formation is complex and is not completely understood yet. A preferential crystal growth theory similar to that about brucite formation is proposed, but frequently accompanied by another theory associated with adsorption of water by ettringite and the induced swelling pressure. Mehta and Wang (1982) looked into the mechanisms of expansion induced by ettringite formation via two types of ettringite prepared in two different ways and showing different morphology. They concluded that the expansion associated with ettringite appears to be mainly due to water adsorption by ettringite, and is not influenced by the source of ettringite, i.e. whether ettringite is formed by precipitation/nucleation from solution, or by paste hydration of C_3A-gypsum mixture.

Odler and Gasser (1988) drew some contrary conclusions based on the experiments on different origins of sulfate expansion using a series of cements of different compositions and on mixes of pure compounds. The observed data supported the theory that the expansion is related to a top-chemical formation and/or preferential growth of ettringite. An uptake of water from the environment is not essential for the expansion to occur even though it enhances the extent of expansion.

Deng and Tang (1994) investigated the formation and expansion of ettringite crystals based on the principles of physico-chemistry. They suggested that ettringite forms by a through-solution mechanism and that the expansive forces are results of the crystallization pressure as well as swelling pressure generated by the selective absorption of ions combined with a large amount of water on tiny ettringite crystals. Both mechanisms act simultaneously, but the former has a much higher magnitude than the latter. The hydroxyl concentration of the pore solution plays an important role by regulating the distribution and morphology of ettringite crystals in the cement pastes (Figure 8.9). Hence, the chemical environment should always be accounted for when efforts are made to explain the mechanisms.

It is difficult to draw any clear conclusion about the mechanism of expansion generated by the formation of ettringite. The morphology of ettringite clearly plays an important role in finding out the corresponding mechanisms.

8.4.3 Effect of mineral additives

It is generally found that the use of super fine GGBFS and silica fume aggravates the autogenous shrinkage of concrete (Li, 2002). The finer the GGBFS is, the more obvious this aggravating effect is. The explanation is that the finer GGBFS particles hydrate faster than the coarser ones, thus more water is combined in the products, and the self-desiccation is more severe. In addition, GGBFS particles adsorb much water on their surface due to the angular shape, which aggravates the autogenous shrinkage.

The addition of fly ash might reduce the autogenous shrinkage. The reduction effect of fly ash is influenced by the replacement level in the cement. This reduction effect could partially attribute to its smooth particle surface, which consequently adsorbs less water than the angular nature of clinker and slag particles. Therefore, more water is left free in the microstructure. Furthermore, fly ash is normally rich in alumina, which could potentially react as a source for ettringite formation, especially when sulfates are abundant.

8.5 Development of a new MSA

8.5.1 Introduction

In this section, a mineral shrinkage-compensating admixture is developed, which takes use of some industrial by-products, and is made from mineral materials. Its composition is designed with special considerations to the stoichiometry of ettringite formation, i.e. it should provide stable sources of sulfate and alumina which are necessary for the ettringite formation (see Section 8.4.1). This admixture is made completely with mineral materials and the durability, which normally should be considered when using some organic admixtures, is expected to be as good as normal concrete.

Compensating the autogenous-shrinkage is chosen as the objective because it is important in high-performance concrete, massive concrete and high-strength concrete. Furthermore, the autogenous-shrinkage is more difficult to handle while the drying shrinkage can be mitigated by appropriate curing. Compensating the drying-shrinkage is feasible with the admixture designed in this thesis, given appropriate curing at early ages.

The admixture is tested for its influence on the length change and compressive strength of mortar samples. Different dosages, calcium sulfate form, and varying compositions of this MSA are investigated, combined with aggregate and w/c ratio of the concrete. The main expanding component—ettringite—is analyzed with XRD. It is confirmed that this MSA can successfully compensate the autogenous shrinkage, and practical suggestions for industrial applications are presented.

8.5.2 Materials

The materials used for making the MSA is listed in Table 8.5. One slag from Orcem, one fly ash from Euroment, pure anhydrite and one type of premixed anhydrite from Rethmann are used. Five different MSA are made from the these ingredients, in which the mass fractions of ingredients are listed in Table 8.6. One Portland cement CEM I 32.5R from Knauff is used in making the samples. Two types of sands are used in making mortar samples, one with the particle size 0–1 mm, named “lab sand”, and one norm sand with the particle size between 0–2 mm, named “standard sand” from Normensand GmbH. Tap water is used, except when measuring the chemical shrinkage, in which double distilled and deionized water is used. Superplasticizer is used only for samples with w/c ratio of 0.4.

The PSD of the materials used in the experiments is shown in Figure 8.5. It can be seen that the slag is the finest material, and the CEM I 32.5R and anhydrite have comparable fineness. The PSD of the two sands are quite different from each other.

The recipes of the mortar samples tested with different dosages of the mineral expansive

Table 8.5: Oxide composition and properties of Portland cement and materials used in MSA (m/m%).

Oxide	CEM I 32.5R[♯]	Ingredients of MSA			
		Fly ash[♯]	Slag	Anhydrite	Pre. Anh.[♯,§]
CaO	63.8	3.17	40.2	41.2	46.1
SiO_2	19.9	53	34.57	0	1.41
Al_2O_3	4.54	24.3	13.86	0	0.40
MgO	0.98	2.39	8.04	0	0.20
SO_3	3.27	0.38	0.1	58.8	49.4
Fe_2O_3	3.19	7.43	0.77	0	1.3
TiO_2	0.18	0	0	0	0
P_2O_5	0	0.43	0	0	0
Na_2O	0.39	1.02	0.38	0	0
K_2O	0.614	3.76	0.56	0	0.49
L. O. I.	2.8	2.86	1.33	0	1.85
Total	99.67	98.74	99.81	100.0	101.14
Fineness (Blaine, m^2/kg)	365.4	310.6	460	825	802
Bogue composition					
Mineral	(m/m%)				
C_3S	71.96				
C_2S	9.98				
C_3A	7.71				
C_4AF	10.35				

[♯]: From Pöllmann (2006);
[§]: One premixed anhydrite.

agent (MSA) are listed in Table 8.7. The water/binder ratio is 0.5 for all samples except those for the chemical shrinkage tests and those with which the effect of water/binder ratio is investigated. For the chemical shrinkage measurements, a w/b ratio of 0.4 is used to minimize the bleeding of the paste. A w/b ratio of 0.4 is also used to investigate its effect on the performance of this admixture. The sand/binder ratio is 3 for mortar samples. Here, both the cement and the MSA are taken as binders. The same recipe is used for paste samples, without sand.

Table 8.6: Composition of five different MSA tested in the experiments (m/m%).

Material	MSA1	MSA2	MSA3	MSA4	MSA5
Anhydrite	36.6[†]	36.6[‡]	36.6[‡]	20.0[‡]	31.6[§]
Fly ash	13.9	13.9	33.4	60.0	0
Slag	49.5	49.5	30.0	20.0	0
CEM I 32.5R	0	0	0	0	68.4
Total	100.0	100.0	100.0	100.0	100.0

[†]: Premixed anhydrite.
[‡]: Pure anhydrite.
[§]: Pure anhydrite, all the rest is CEM I 32.5R.

Table 8.7: Recipe of mortar samples[♮].

Recipe	m/m%	
	CEM I	MSA1[†]
Portland cement	100	0
MSA-5	95	5
MSA-10	90	10
MSA-15	85	15
MSA-20	80	20

[♮]: Water : binder : sand = 0.5 : 1 : 3, in mass.
[†]: Mineral shrinkage-compensating admixture.

8.5.3 Sample preparation

Mortar samples are made for the length change, compressive strength tests and paste samples are made for the chemical shrinkage measurement and XRD analysis. The mortar is made with a force mixer following the European standard EN 196-1. Two groups of mortar samples are made for each recipe, one for the length change test and the other for the compressive strength test. All the samples are prepared by pouring the mixed mortar into the moulds in two steps with manual tapping in between.

For the length change test, steel tips are inserted into the moulds before pouring the mortar. The size of the mould is $40\times40\times160$ mm^3. The redundant mortar above the top surface of the moulds is removed carefully by scraping with a palette knife. Immediately after this, the moulds are moved into the humid cabinet, in which the temperature is kept at 23 ± 1 °C and relative humidity $> 95\%$. After being cured in the humid cabinet for 24 hours, the samples are demoulded and immediately wrapped to minimize the moisture loss. Polyethylene film and aluminum type are used to wrap and seal the samples. After being sealed, the samples are moved into a environmental cabinet, in which the temperature is kept at 23 ± 1 °C and the RH kept between 60% and 90%.

For the compressive strength tests, mortar is poured into a cubic mould with the rib size 50 mm. The samples are first cured in the humid cabinet for 24 hours and are then demoulded followed by curing in water till the planned ages.

Paste samples are made following the same procedure as used by Williams et al. (1999). First, half of the pre-calculated quantity of cement powder and MSA is added to the mix water in a small cup. The mixture is then briefly stirred to break up large heterogeneities. The remaining cement powder is then added and stirred in a manner as gentle as possible to produce consistent pastes. The total mixing time is about 15 seconds.

The chemical shrinkage measurement follows the methods by Van Eijk (2001), with the

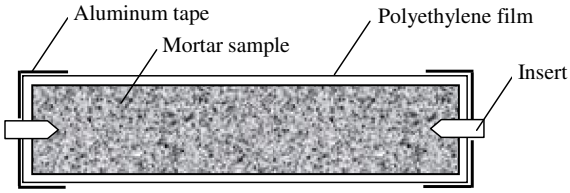

Figure 8.10: Schematic illustration of sample wrapped with polyethylene film and aluminum tape.

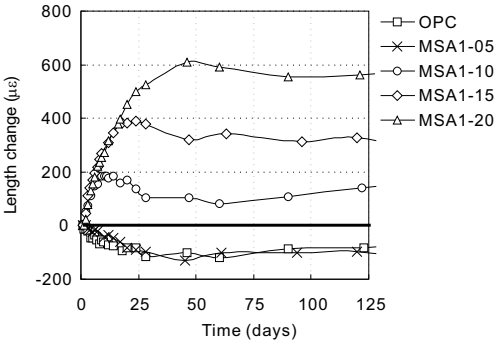

Figure 8.11: Autogenous length change of mortar samples containing various amounts of MSA1, cured at 23±1 °C (w/c = 0.5). numbers in the legend correspond to the mass percentages of MSA in the binder.

temperature at 23±1 °C. About 10 g of cement paste is fed into a glass bottle. The bottle is sealed with a silicate stop, through which is a graded glass pipette. The rest of the glass bottle is filled with de-ionized water. Extra water is added into the pipette at the start of the test. A thin layer of mineral oil is added onto the surface of the water in the pipette to prevent the evaporation of water. The level of the oil in the pipette is recorded at the planned ages, from which the chemical shrinkage is calculated.

Paste samples for XRD analysis are cured in saturated lime water at 23±1 °C till the test ages. Sample preparation follows Chatterji (2001). The hydrated paste is submerged into isopropyl alcohol to stop the hydration for 30 min, and is wet ground in ethanol to a fineness passing through the 150 μm sieve. The slurry is filtered and washed with ethanol and further with diethyl ether. Then, the dry sample is loaded into a metallic sample holder, avoiding preferred orientation of crystals and assuring that there is a smooth surface. The scan starts from 7.5 degree at a step size of 0.03 degree and step time 20 seconds (all angles for 2θ).

8.5.4 Results

Length change The first reading for the length change test is made 30 minutes after the samples are wrapped and cured in an environmental cabinet to allow a temperature equilibrium. This reading is taken as the initial length of the prism. Then, the length of the prisms is measured at planned ages. The length changes of the five recipes in Table 8.7 with MSA1 are presented in Figure 8.11.

It can be seen that 10 m/m% of MSA1 (by mass) in cement can already efficiently compensate the autogenous shrinkage. The expansion increases steadily during the first 8 days and reaches a stable value after that. Similar trends are also observed for samples containing 15 and 20 m/m% MSA. The expansion develops even more rapidly than that of samples containing 10 m/m% of MSA.

However, the trend for samples containing 5 m/m% of MSA is quite different. The autogenous shrinkage of this group of samples is comparable to that of samples made from neat Portland cement. No expansion is observed during the whole process. It appears that 5 m/m% of MSA is not sufficient to compensate the shrinkage.

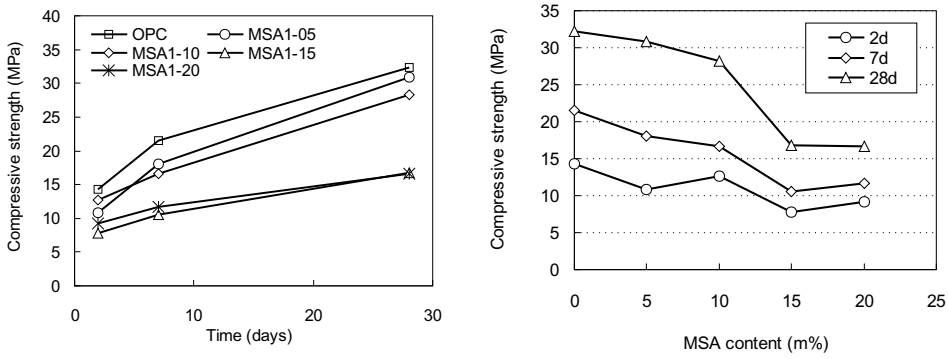

(a) Versus curing time (b) Versus MSA content

Figure 8.12: Compressive strength of mortar samples containing various amounts of MSA1, cured at 23±1 °C, (a) versus time; (b) versus MSA content.

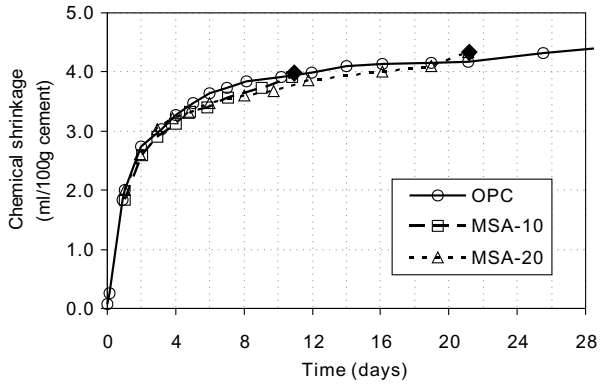

Figure 8.13: Chemical shrinkage of paste samples containing various amounts of MSA1, ♦ indicates the time when the bottles broke.

Compressive strength The compressive strength is tested for all recipes in Table 8.7 at 2, 7 and 28 days, with MSA1 given in Table 8.6. The results are presented in Figure 8.12. At two days, all the samples have a comparable compressive strength, with samples made as neat Portland cement being the highest (Figure 8.12) They all show a strength gain with increasing ages. The samples made with 5 m/m% and 10 m/m% MSA1 have similar trends in strength development, while those with 15 m/m% and 20 m/m% show a much less extent of strength gain.

It appears that dosages of MSA1 above 15 m/m% result in an obvious strength reduction, while those with 5 m/m% and 10 m/m% have comparable strength as neat Portland cement. The trend about the reducing effect of MSA on the compressive strength of samples is also observed in the experiments of Li (2002) and Hori and Morioka (1998).

Chemical shrinkage The results of the chemical shrinkage measurements are presented in Figure 8.13. Three recipes are tested, including neat Portland cement, 10 m/m% and 20 m/m% MSA1. The measurements for the latter two groups stopped at 11 and 21 days, respectively, due to the break of the bottles caused by the paste expansion. The water/binder is 0.4 instead of 0.5

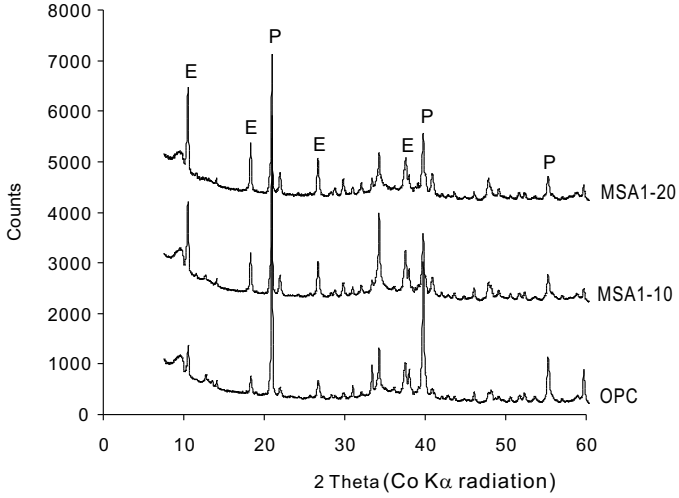

Figure 8.14: X-Ray diffraction pattern of paste samples containing various amounts of MSA1 and hydrated for 120 days, numbers in the legend indicate the mass percentage of MSA1 in the sample. E stands for ettringite and P for portlandite.

to prevent the bleeding of samples.

For all three recipes tested, the chemical shrinkage increases rapidly during the first 7 days, and slows down after that. All three recipes show comparable chemical shrinkage, which is expected. On the one hand, the addition of MSA into cement will reduce the chemical shrinkage because the fly ash and slag in MSA hydrate remarkably slower than the clinker (Li, 2002). On the other hand, the MSA contains anhydrite calcium sulfate, which will react into ettringite. The formation of ettringite involves more water than the hydration of clinker (Chapter 4), which results in larger chemical shrinkage because more water is compressed. Hence, at the outcome of these two factors, the hydration of the three recipes shows comparable chemical shrinkage.

Since chemical shrinkage normally aggravates the autogenous shrinkage (see Section 1.6), it is important that the cements containing MSA show comparable chemical shrinkage. The inclusion of fly ash and slag can reduce the chemical shrinkage, which is advantageous compared to the use of anhydrite only.

The results of the chemical shrinkage measurements are also used to determine the time conversion factor during the computer modeling of cement paste with and without MSA in Section 8.5.6.

XRD analysis of hardened paste XRD analysis of the hydrated cement pastes with various amounts of MSA1 is carried out. The pastes are cured in saturated lime water for 120 days at 23$\pm$2 °C. The X-Ray powder diffraction patterns of the samples are shown in Figure 8.14. It can be seen that with increasing amount of MSA1 in the sample, the amount of ettringite (E) in the samples is increasing and that of portlandite (P) is decreasing. Since the formation of ettringite is the major cause of the expansion potential, the trend about the amount of ettringite is in agreement with the trend about the length change of the samples.

The increasing amount of ettringite is mainly due to the increasing dosages of MSA in the paste. The decrease of portlandite can be affiliated with two factors: (1) the dilution effect of MSA in cement, i.e. less calcium silicates in cement with more MSA, and (2) the pozzolanic reaction of fly ash and latent reaction of slag, which consume portlandite as well.

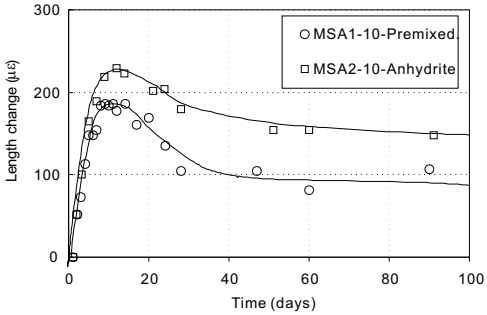

Figure 8.15: Effect of calcium sulfate type on the autogenous length change of mortar samples with 10 m/m% MSA1 and MSA2.

8.5.5 Investigation on various factors

In this section, effects of various factors on the shrinkage-compensating capability of the MSA are investigated, including the calcium sulfate type, the fraction of ingredients in the MSA, the aggregate and the water/binder ratio.

Effect of calcium sulfate type First, the effect of calcium sulfate type is investigated. In all the measurements in Section 8.5.4, the MSA1 is used, which contains a premixed anhydrite. The premixed anhydrite is a mixture of anhydrite and other compounds, which are believed to change the slow reaction rate of the anhydrite.

Another MSA is made, namely MSA2, with the same mass proportion of calcium sulfate, but now with pure anhydrite. Length change of mortar samples containing 10 m/m% replacement of binder by MSA1 and MSA2 are tested (Figure 8.15). The trends of the length changes are quite similar for the two MSA, but the magnitude for MSA2 is obviously higher than that for MSA1, for both the peak and the steady state values.

A possible explanation could be that the premixed anhydrite hydrates much faster than the pure anhydrite, thus most of the expansion potentials occur during the first 24 hours, which is typically observed for dihydrate gypsum in cement (Taylor, 1997). However, as discussed in Section 8.4, during this stage the mortar is relatively plastic, for which expansion can hardly be generated. The measurement starts from 24 hours after the mixing, hence, the volume change of the first 24 hours is not monitored.

A conclusion can be drawn that pure anhydrite is more suitable for MSA than the premixed anhydrite. It results in higher and more stable expansion compared to those made with premixed anhydrite. Pure anhydrite is thus always used in the following recipes for MSA, designated as MSA2, MSA3, MSA4 and MSA5.

Effect of MSA composition The effect of MSA composition is investigated by changing the mass fractions of different ingredients in the MSA. Three more MSA are made beside MSA1 and MSA2, namely MSA3, MSA4 and MSA5. Their compositions can be found in Table 8.6. Note that in all these three MSA, the pure anhydrite is used, instead of the premixed anhydrite based on the discussion in the previous sections.

In MSA3, the mass fraction ratio of fly ash to slag is changed, from 0.28 to 1.11, while the fraction of anhydrite is kept constant. In MSA4, the fraction of anhydrite is lowered to 20 m/m% and the ratio of fly ash to slag is raised to 3.0. In MSA5, the same fraction of anhydrite as that in MSA2 is used, but the fly ash and slag is replaced by CEM I 32.5R. All the mortar samples contain 10 m/m% of these MSA.

The length change of samples containing the different MSA is plotted in Figure 8.16(a).It can

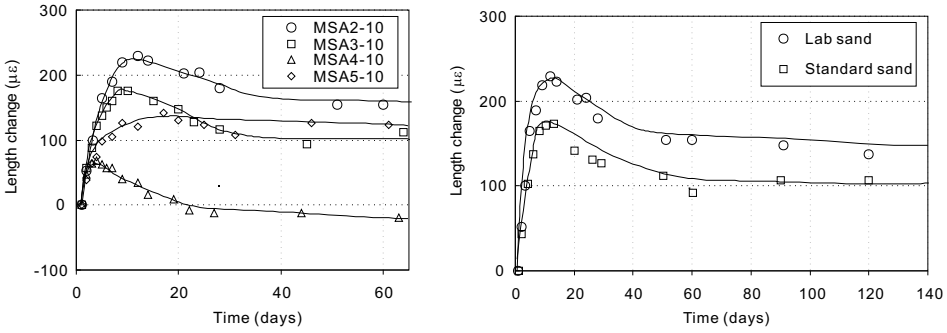

(a) MSA composition (b) Aggregate

Figure 8.16: Effect of MSA composition and aggregate on the autogenous length change of mortar samples with 10 m/m% MSA.

be seen all the samples show similar trends of length change except those with only anhydrite, which show no clear maximum. The use of MSA2 has the highest efficiency for shrinkage compensation. Increasing the ratio of fly ash to slag is not favorable for compensating the autogenous shrinkage (see the lines MSA2 and MSA3). Lowering the fraction of anhydrite in the MSA is also detrimental for the shrinkage-compensating capacity (see line MSA4). Using simply pure anhydrite in concrete appears to be able to compensate the autogenous already, although the magnitude of expansion is lower than the MSA2 with fly ash and slag.

Effect of aggregate Next, the effect of aggregate on the efficiency of the MSA is investigated. Two types of sands are used in the mortar, together with 10 m/m% of MSA2. PSD of the sands are included in Figure 8.5 as well. The autogenous length change of the samples are shown in Figure 8.16(b). The use of lab sand, which is finer than the standard sand, yields higher expansion of the samples.

The different shrinkage-compensating capability of MSA with the two different sands is most likely associated with the strength of the samples. The samples made with the standard sand probably have higher strength than those made with the lab sand due to the better grading.

Effect of water/binder ratios The effect of water/binder ratio on the autogenous length change is investigated. Mortar samples with water/binder ratio of 0.4 and 0.5 are made, with neat Portland cement, or 10 m/m% of the Portland cement replaced by MSA2. When a w/b ratio of 0.4 is used, 1.33 m/m% of superplasticizer is used. The measured length change is presented in Figure 8.17.

The w/b ratio shows an obvious influence on the shrinkage-compensating capacity of the MSA. For samples made with w/b ratio 0.4 and MSA2, the magnitude of expansion is greatly reduced, compared to those with w/b ratio of 0.5. For samples made with neat Portland cement, the autogenous length change with w/b ratio of 0.4 is slightly smaller than that with a w/b ratio of 0.5, probably due to the starting time of the measurement. After 24 hours, the average strength of mortar samples with a lower w/b ratio is higher than that of samples with a higher w/b ratio. Hence, the expansion is smaller because it appears that a higher strength is associated with lower autogenous shrinkage (Hori and Morioka, 1998; Li, 2002).

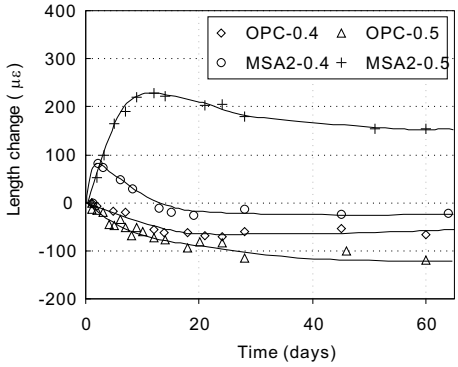

Figure 8.17: Effect of water/binder ratio on the autogenous length change of mortar samples, with 10 m/m% MSA2 and cured at 23±1 °C.

Table 8.8: Average compressive strength and length change of mortar samples with 10 m/m% and without MSA after 7 days

Sample	Portland cement	MSA1	MSA3	MSA4	MSA5
Compressive strength (MPa)	21.5	16.6	17.2	24.2	17.76
Length change (με)	-52.1	154.2	159.4	56.3	104.7

Compressive strength The compressive strength of mortar samples made with the lab sand and the various MSA at 7 days is shown in Table 8.8. Again, it appears that the higher expansion leads to the lower compressive strength. While all the compressive strength is measured as free strength, i.e. without any restraints, the compressive strength of samples with higher expansion is expected to be higher when they are restrained because of the denser microstructure of the samples.

8.5.6 Numerical testing of SCC

In this section, the hydration of cements with various amounts of MSA is simulated by using the new CEMHYD3D developed in Chapters 6 and 7. The model is used to simulate the hydration degrees of phases (clinker, MSA) and the microstructure of the hardened paste.

Determination of time conversion factor

First, the results of the chemical shrinkage tests are used to determine the time conversion factor "B" in Eq. (2.34) which relates hydration cycles to real time. It is proven in experiments that there is a linear relationship between the hydration degree of cement and the chemical shrinkage of its hydration (Geiker and Knudsen, 1982; Knudsen and Geiker, 1985; Parrott et al., 1990). The chemical shrinkage is measured in experiments as a function of hydrating time, and the hydration degree is simulated as a function of the hydration cycles. Hence, a linear regression analysis can be used to determine "B" which gives the best linear relation between the measurements and the hydration degree. The results of the analysis for neat Portland cement is shown in Figure 8.18. The fitted value of the time conversion factor ($B = 4.0\times10^{-3}$ hour/cycles^2) is in line with the values found in Chapter 6 ($B = 3.8\times10^{-3}$ hour/cycles^2).

The extrapolated chemical shrinkage for the complete hydration of Portland cement is 6.3 mL per 100 g cement, which is in good agreement with the measurements by Czernin (1956), and the prediction by Geiker and Knudsen (1982). The fitted time conversion factor ($B = 4.0\times10^{-3}$

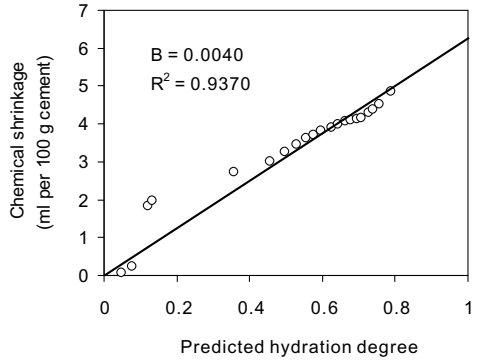

Figure 8.18: The linear relationship between the chemical shrinkage measurement and the simulated hydration degree of neat Portland cement together with the fitted time conversion factor.

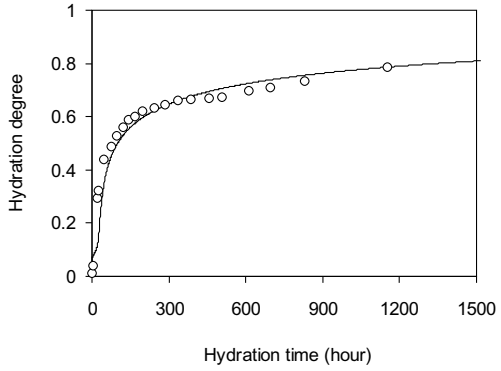

Figure 8.19: Predicted and measured hydration degree of cement paste with 10 m/m% MSA1, w/b = 0.40, T = 23±1 °C, $B = 4.0\times10^{-3}$ hour/cycles^2.

hour/cycle^2) is very close to the values for different cements presented in Chapters 6 and 7. It is further used in the following simulations for other cements containing different amounts of MSA.

The simulated hydration degree of Portland cement without MSA is plotted in Figure 8.19, together with the calculated degree from the measurements. In the calculation, the chemical shrinkage of Portland cement hydration is taken to be 6.3 mL per 100 g cement based on the discussion above. It can be seen that the hydration degree of Portland cement in the paste is well predicted.

Simulating the hydration of cements with various amounts of MSA

The hydration of cements with various amounts of MSA is simulated with the computer model. MSA1 is taken as an example. It is shown in the results that MSA shows similar reaction degree in all the recipes (Figure 8.20(a)).

However, the major components in MSA, viz. anhydrite, fly ash, and slag, react in significantly different rates. Anhydrite reacts much faster than the other two components. A detailed comparison about the reaction degree of anhydrite shows that in all the recipes anhydrite reacts

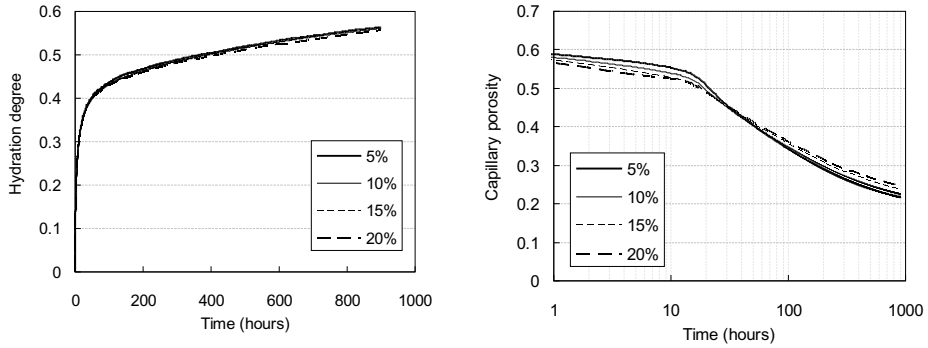

(a) Hydration degree (b) Capillary porosity

Figure 8.20: Simulated hydration degree of MSA1 in the paste (a) and its capillary porosity (b) with various amounts of MSA, w/c = 0.5, T = 23°C, $B = 4.0\times10^{-3}$ hour/cycles^2.

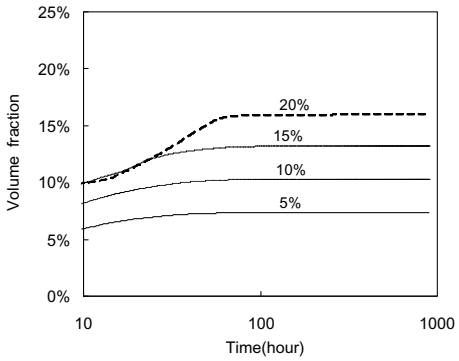

Figure 8.21: Simulated volume fraction of ettringite in pastes with various amounts of MSA1.

in an almost identical rate (not included in figures). After 24 hours, about 90 m/m% of anhydrite has reacted, and after 80 hours all the anhydrite has reacted. The reaction degrees of fly ash and slag are low. After 28 days, their reaction degrees are between 0.3 and 0.35, varying with different dosages of MSA.

The volume fraction of ettringite in the paste is plotted in Figure 8.21 in pastes with different dosages of MSA1. In the simulation it is assumed that no external volume change of the paste occurs.

It can be seen that with increasing dosages of MSA in the paste, the volume fraction of ettringite increases as well, in line with the results of the XRD analysis (Figure 8.14). If 5 m/m% MSA1 replacement is used, most of the ettringite is formed during the first 10 hours already, while for 20 m/m% MSA, the amount of ettringite keeps increasing to about 100 hours, and reaches an approximately constant fraction after that.

8.5.7 Discussions

Relation between length change and dosage of MSA

If the length change of mortar samples containing various amounts of MSA is plotted as a function of the MSA dosage in cement (Figure 8.22), it can be seen that there is a threshold value for

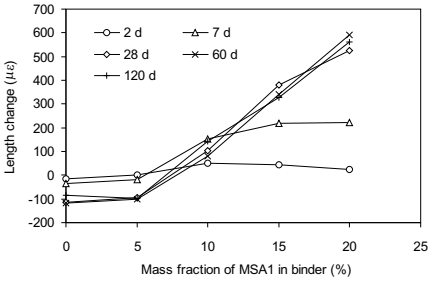

Figure 8.22: Length change of mortar samples at various ages as a function of MSA fraction in binder.

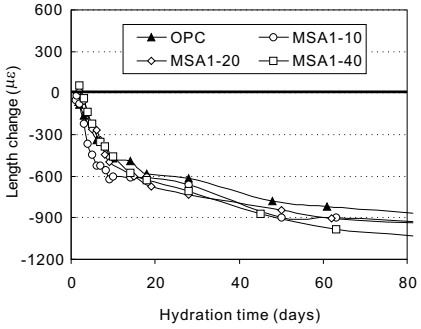

Figure 8.23: Length change of mortar samples containing various amounts of MSA1 and cured at 60% RH without sealing, T = 23±2 °C.

the dosage of MSA to compensate the autogenous shrinkage, between 5 and 10 m/m%, below which no shrinkage-compensating effect is generated at all.

For samples containing more than 10 m/m% MSA and at later ages (60d and 120d), there is an approximately linear relation between the dosage and length change. Hence, the magnitude of the expansion can be easily controlled by adjusting the dosage. This is very important in practice because in construction industry different requirements are frequently encountered. Hence, a robust method to predict the expansion is useful.

Effect of curing conditions

The length changes of prisms cured in a dry environment (23±1 °C, 60±5% RH) with different dosages of MSA added into the cement are plotted in Figure 8.23. It seems that the addition of MSA into the cement does not significantly influence the length change of the samples being cured in the dry environment, and even increases the drying shrinkage very slightly. Thus, special care should be taken when curing concrete made with MSA. Moist or at least sealed curing should be implemented, especially during the early ages.

The larger shrinkage of the prisms containing MSA than that of Portland cement when cured in a dry environment is probably due to two factors. First, the ettringite formation has a high water demand. For every mole of ettringite formed, 32 moles of water is needed. Hence, if the cement contains more aluminum and sulfate, more ettringite is formed, which in turn aggravates the self-desiccation effect. Second, the formation of ettringite shows a larger chemical shrinkage than normal Portland cement, which increases the porosity of the paste and results in numerous

meniscuses.

If the prisms are cured in a sealed environment, no water loss from the mortar occurs. Hence, the hydration of cement can proceed to a relatively high degree, considering the water/binder used in the experiments (0.5). The expansion effect given by the ettringite formation can thus counteract the effect of the self-desiccation. As a net result, expansion of prisms is observed and the autogenous shrinkage is counteracted.

Regulation

In various national and multinational standards, the maximum contents of sulfate (SO_3) in cement is regulated, as listed in Table 8.9. Cements with 15 m/m% replacement of clinker by the MSA developed in this thesis are included in the table as well, taking MSA2 as example. It can be seen that a cement with 15 m/m% replaced by MSA2 still fits into the regulations, which is most likely the maximum replacement in practice, and cements containing this MSA2 can be marketed.

For mixing MSA2 with Portland cement instead of clinker, the maximum proportion that can be used and still complies with the standards depends on the sulfate content in the Portland cement. The maximum replacement level of Portland cement by MSA is computed as:

$$\lambda_{MSA} = \frac{x_{\overline{S}}^{standard} - x_{\overline{S}}^{p}}{x_{\overline{S}}^{MSA} - x_{\overline{S}}^{p}} \times 100 \tag{8.7}$$

in which λ_{MSA} is the maximum mass percentage of MSA that can be used to replace Portland cement; $x_{\overline{S}}^{standard}$, $x_{\overline{S}}^{p}$ and $x_{\overline{S}}^{MSA}$ are the mass percentages of SO_3 prescribed in the standard, in Portland cement and in MSA, respectively. For example, if MSA2 is used to replace the Portland cement CEM I 32.5R in Table 8.5) to meet the requirement for CEM I 32.5R in the standard EN 197-1, values of $x_{\overline{S}}^{standard}$, $x_{\overline{S}}^{p}$ and $x_{\overline{S}}^{MSA}$ are 3.5, 3.27 and 21.6, respectively. The computed value of λ_{MSA} is 1.3 m/m% in this case. The dosages used in the experiments are much higher than the maximum dosage in this case. Therefore, for marketing Portland cement partially replaced with the MSA, the sulfate content in the Portland cement itself is very important in regard to the maximum replacement level.

However, the MSA can also be used in another way, i.e. directly mixing on the construction sites according to the specific demand. This applicability is highly flexible and is already widely used in different projects in China and Japan (Ma et al., 2005). But, due to the differences in

Table 8.9: Maximum sulfate (SO_3) content in cement according to various standards

Standard	Cement type	Class	Maxima (m/m%)
EN 197-1	CEM I CEM II CEM IV CEM V	32.5 N	3.5
		32.5 R	
		42.5 N	
		42.5 R	4.0
		52.5 N	
		52.5 R	
	CEM III	all	
ASTM C595-05	I (SM), I (SM)-A, IS, IS-A	all	3.0
	S, SA, I (PM), I (PM-A), P, PA, IP, IP-A	all	4.0
GB175-1999	all	all	3.5
15 m/m% MSA2[§]			3.23

[§]: 15 m/m% replacement of clinker by MSA2.

dosages, recipes and construction conditions, a series of experiments are necessary before using the MSA, which test the strength and volume stability of the concrete with the MSA.

8.6 Conclusions

Based on the discussions in this chapter, the following conclusions can be drawn:

1. The hydration of quick lime and periclase mixed with cement shows good shrinkage-compensating capability. The expansion caused by the formation of brucite is very stable. The hydration of periclase is marked by a long induction period.
2. A computer model is developed, which can simulate the hydration of quick lime and periclase in cement. It is shown that the expansion generated by the formation of portlandite and brucite is more due to the morphology change and distribution of crystals instead of the reduction of pore spaces.
3. Ettringite-based MSAs are developed, which take use of industrial by-products. It is shown in experimental tests that 10 m/m% of this MSA can already successfully compensate the autogenous shrinkage of mortar samples.
4. For dosages above 5 m/m% of MSA in cement, there is a linear relationship between the free expansion of mortar samples and the dosage of MSA in cement. Hence, the dosage used in practice can be flexibly adjusted according to different expansion requirements.
5. Various factors on the expansion performance of the MSA are investigated. The use of anhydrite is recommended instead of a pre-mixed anhydrite. The expansion is slightly influenced by the aggregate, the proportioning of its ingredients, but strongly influenced by the w/b ratio in concrete and the curing conditions. The drying shrinkage of concrete containing this MSA is comparable to normal concrete. Therefore, appropriate sealing should be used to prevent the lost of moisture from the concrete in practice.
6. The increasing dosage of MSA in cement is accompanied by a reduction in the compressive strength of the samples. For 5 and 10 m/m% replacement levels by this MSA, the compressive strength is comparable to that with Portland cement, but for 15 and 20 m/m% of replacement levels, the compressive strength is obviously reduced. Therefore, dosages between 5 and 10 m/m% MSA are preferred, which can compensate the autogenous shrinkage and avoid loss of strength.
7. The hydration of cement pastes containing various amounts of MSA is simulated with the 3-D cement hydration model developed in Chapter 6 and 7. Cement pastes containing higher dosages of MSA have a bigger fraction of ettringite crystals, which is confirmed by XRD analysis.
8. The sulfate content in binder with the replacement level of 15 m/m% clinker by this MSA is complying with the standards in Europe, United States and China. There seems to be a great possibility that this admixture can be marketed and applied in construction.
9. For marketing Portland cement that is partially replaced with the MSA, the sulfate content in the Portland cement itself is very important in regard to the maximum replacement level.

Chapter 9

Conclusions and recommendations

In this thesis, the hydration of slag cement and its microstructure development is investigated. The principle motivation is that the understanding of slag cement hydration is less sufficient than that of Portland cement hydration, although in the Netherlands and in some other countries the slag cement is one of the major types of cements shipped on market. The use of slag in cement attracted many interests at the beginning of its application because slag was normally much cheaper than clinker several decades ago. Nowadays, the price of GGBFS is already comparable to that of Portland cement clinker due to the continuously increasing demand. However, the application of slag cement in concrete is still growing due to the environmental benefits and the better engineering performance as compared to the Portland cement concrete, for example, the low heat release.

However, questions are frequently encountered on using slag cement in a certain condition or the applicability of one specific slag in concrete. One example of the former case is that some researches have shown the salt scaling of slag cement concrete is severer than that of Portland cement concrete (Deja, 2003; Stark and Ludwig, 1997). The microstructure of the paste and ITZ is important in understanding the mechanism and providing possible mitigation solutions. Another example for the latter case is the request from companies when they want to import GGBFS from another country. It is normally difficult to test the slag before the shipment in accordance with the corresponding national standards. In most cases, the information like the glass content, oxide composition, PSD, etc. of the slag is provided. Therefore, it is important to predict the performance of slag cement made from these slags before the actual order.

Researches in this thesis are carried out to answer the questions raised in the practice. They are based on fundamental chemical knowledge about the reaction of slag and Portland cement (*Chapters 2, 3 and 4*). Special attention is paid to the liquid phase in the hydrating slag cement paste (*Chapter 5*), whereas most of the existing researches focus on the solid phases. The liquid phase is closely related to the reactivity of slag, the durability of concrete and stability of a concrete structure. CEMHYD3D is chosen for modeling the hydration of slag cement, which has been developed and used in the author's group for over 10 years (*Chapter 2*). The model is further developed with respect to the newest developments in cement chemistry about Portland cement hydration (*Chapter 6*). One of the important developments is the introduction of the "hydration layer" concept into the model, which accounts for the diffusion-controlled reaction stage in cement hydration. This development can successfully eliminate the effects of system resolution on the model predictions and increase the model efficiency. Furthermore, the new theories developed in this thesis about slag reaction are incorporated into the *New Model* (*Chapter 7*). The new model is validated with experimental data taken from literature and obtained in this thesis. The theories and computer models developed in this thesis is used to design shrinkage-compensating admixtures, which are made from slag, fly ash and anhydrite (*Chapter 8*). These admixtures are tested both in the lab and with the computer models developed in this thesis.

9.1 Conclusions

The main conclusions of the researches in this thesis are summarized below, with implications to other researches and potential applications.

9.1.1 Theoretical models for the reaction of slag in cement

A few theoretical models are available for the hydration of Portland cement and its microstructure development (Jennings and Tennis, 1994; Powers and Brownyard, 1948). The most well-known one is probably the Powers and Brownyard model (Powers and Brownyard, 1948), which enables the calculation on the volume fractions of phases in a hydrating Portland cement paste and other related properties such as the water-binding and the chemical shrinkage. These theoretical models have been proven valuable for understanding the microstructure of hydrating Portland cement paste.

However, so far no such models for the reaction of slag cement are available. Numerous experiments are carried out to characterize the microstructural characteristics of both hydrating AAS and blended cement pastes. The hydration products, hydration degree of slag and clinker, water content in the pastes, heat release and other properties are well documented.

In this thesis, stoichiometric models are established based on the observations in experiments and balances between the initial materials and the hydration products. The reaction of AAS is taken to be that of pure slag. For blended cement, the interactions between clinker hydration and slag reaction are important.

The hydration products for pure slag include C-S-H, hydrotalcite, an Fe-containing hydrogarnet, ettringite, tetracalcium aluminum hydrate, and strätlingite. The C-S-H in AAS paste has a low C/S ratio (typically between 0.8–1.3) and a high aluminum substitution for silicon in the structure. The amounts of hydrotalcite, hydrogarnet and ettringite depend on the M, F, and $\overline{S}$ contents in the slag. The rest of C, S, and A forms C-S-H and C_4AH_{13} (or C_2ASH_8). The formation of C_4AH_{13} (or C_2ASH_8) depends on the composition of slag. If the slag contains sufficient A and the maximum aluminum substitution degree in C-S-H is reached, the rest of A goes into C_4AH_{13} or C_2ASH_8. Otherwise, the C_4AH_{13} or C_2ASH_8 is not formed. The maximum aluminum substitution degree for silicon in C-S-H complies with the equation proposed by Richardson (1999) (see Eq. (3.19)).

In hydrating slag-blended cement paste, the hydration of both clinker and slag has to be considered. The hydration product C-S-H formed by both the clinker hydration and by the slag hydration has the same composition due to the product equilibrium. The consumption of CH by the slag reaction is critical. In these models, different extents of CH consumption are discussed. Validations with experimental results show that *Model 3* is the most suitable for modeling the hydration of slag-blended cement. In this model, the amount of CH consumed by the slag reaction is proportional to the difference between the C/S ratio of the slag (the glass part) and 1.8.

These models are further used as illustrations for predicting some properties of hydrating AAS or slag-blended cement pastes, like water-binding, chemical shrinkage and porosities. The comparison with experimental results is used to validate the model predictions. It is demonstrated that the theoretical models are useful when predicting the microstructural development of hydrating AAS or slag-blended cement paste.

9.1.2 Pore solution composition of hydrating cement paste

Theoretical models are proposed to investigate the pore solution composition of hydrating slag cement paste. The discussion starts from the pore solution composition of Portland cement pastes. The methods by Taylor (1987b) and Brouwers and Van Eijk (2003) for alkali concentrations are taken over, which is combined with the outputs of the computer model developed by Van Eijk (2001). A large number of experimental results are used to compute the alkali binding capacity of real hydrating Portland cement pastes. The computation with real pastes shows that,

on the one hand, the linear binding capacity of C-S-H used by (Taylor, 1987b) and (Brouwers and Van Eijk, 2003) are indeed valid for Na^+. However, on the other hand, for K^+, a non-linear binding relation is found. Methods for determining the alkali-binding capacity of C-S-H are proposed, which are concluded from computations with real hydrating Portland cement pastes.

The same methods are applied for hydrating slag cement, i.e. the concept of alkali release and binding is taken over. To predict the amounts of hydration products, their compositions and the volume of pore solution, theories proposed in the preceding chapters are employed. Measurements presented in literature are used for computing the alkali-binding capacity of hydration product. It is found that the alkali binding in hydrating slag cement paste is different from that in Portland cement pastes. The hydration product hydrotalcite is found to be a major alkali-binding product, and C-S-H shows some alkali-binding capacity as well, be not as strong as the C-S-H in Portland cement pastes. The weak alkali-binding capacity of C-S-H in slag cement pastes has not been found before, yet. However, hydrotalcite is known to have a high specific surface area and is used in industry for binding media frequently.

The methods used by Van Eijk (2001) for non-alkali ions are used as well, with modifications for the transition from gypsum-containing paste to that without gypsum. The dissolution equations of various substances (CH, ettringite, gypsum, C_4AH_{13}, etc.) constitute a system of equations with the concentration of OH^- as the only unknown. Therefore, the system can be solved, yielding the concentrations of other ions (see Appendix D). The Pitzer's method is used to compute the activity coefficient. It is shown by comparing the model predictions with experimental results that this method is valid for hydrating slag cement pastes as well.

The method proposed in this section is used in this thesis for determining the reactivity of slag in slag cement paste. It may also be used to investigate the effects of various factors on the pore solution composition, and the long-term durability of concrete, which are topics of numerous researches. Parts of these feasibilities are shown in this section.

9.1.3 3-D computer modeling of Portland cement hydration

Several computer models for Portland cement hydration are available, three of which are introduced in *Chapter 2*. The *Van Eijk's Model* is chosen in this thesis for simulating the hydration of Portland cement paste and is taken as the basis for simulating the hydration of slag cement. The main reason for choosing this model is that the CA rules it uses are very flexible. New phases and reactions can be incorporated by establishing new modules, while the other modules of the model keep relatively intact. The computer model CEMHYD3D used in this thesis is mainly based on the version developed by Van Eijk (2001) in the Netherlands.

A few modifications are made to consolidate the chemical background of the model. First, all the properties of phases in the model are renewed in the saturated state, instead of the dry state used in the *Van Eijk's Model*. Second, chemical reactions of clinker phases are renewed according to the new developments in cement chemistry. Third, an important concept, "hydration layer" is established in the model, which accounts for the diffusion-controlled reactions in the pastes. This mechanism is very important at the later ages of the hydration.

It is demonstrated with the latter modifications that the *New Model* can successfully eliminate the effect of system resolution on the model predictions, especially the hydration degree of cement. The model can be used to investigate the various stages of cement hydration as well. Calibrations with a few experimental sets of data show that the time conversion factors in the *New Model* are quite close to each other. Therefore, it may be concluded that most of the important factors on the hydration of Portland cement are considered in the *New Model*, like the PSD, composition of cement, w/c ratio, temperature, sealing condition, reaction mechanisms etc. A time conversion factor 3.8×10^{-3} hour/cycles^2 follows from a number of Portland cements investigated in experiments.

9.1.4 3-D computer modeling of slag cement hydration

Although there are a few computer models for the hydration of Portland cement, researches on the computer modeling of slag cement hydration is relatively scarce. In this thesis, the *Van Eijk version* of CEMHYD3D is further extended for simulating the hydration of slag cement. The theories for slag cement reaction and pore solution composition are used to determine the reaction and reactivity of slag. The model predictions are validated with measurements in experiments, and it is further used to investigate a few properties of hydrating slag cement paste, for example, the CH content in the paste, effect of particle size and w/c ratio on the slag hydration, hydration degree of slag, and composition of the C-S-H. The results show that the extended model is able to simulate the hydration process of slag cement paste in a precise way and can be used to predict various properties of the hydrating paste.

The simulated microstructure can be used further to evaluate some durability-related properties of slag cement concrete. Because the recipe and curing conditions can be easily adjusted in the model, it can be used to investigate various factors on the long-term properties of concrete.

9.1.5 Development of MSA with the aid of the *New Model*

The shrinkage of concrete is a common phenomenon and causes lots of problems in practice. Amongst the various form of shrinkage, the autogenous shrinkage is the one deserving special attention because it occurs uniformly throughout the whole microstructure and may cause a complete failure of the structure. This is especially the case when high levels of paste content, low w/c ratios and massive concrete are used.

This research aims at developing a mineral shrinkage-compensating admixture for use in concrete with special considerations below: (1) it is mineral, expected to be more durable than organic shrinkage-reducing admixture; (2) it is a mixture, which can be used in the mixing plant and even on construction sites according to the engineering requirement; (3) it can be used to compensate the autogenous shrinkage; (4) it is made from industrial byproducts, yielding low costs of the MSA and a useful application of waste products.

Before carrying out experiments in the lab on MSA, the types of expanding agents in concrete are reviewed, starting from the hydroxide-based admixture. A computer model is established for simulating the hydration of periclase and quick lime in concrete, which is validated with experimental results in literature.

This thesis aims at developing MSA based on the ettringite formation, because it is relatively easier to regulate compared to the formation of brucite and portlandite. Effects of different compositions, ingredients, dosages, curing conditions, w/b ratios and aggregates on the performance of the MSA are investigated. Compressive strength and length changes of mortar samples are measured as key objectives. Chemical shrinkage and XRD analysis are used to evaluate the hydration of cement paste containing the MSA developed in this thesis.

It is shown that 10 m/m% of this new MSA can already successfully compensate the autogenous shrinkage of mortar samples. Higher dosages result in larger expansions. For dosages higher than 5 m/m%, there is an approximately linear relationship between the expansion and the dosages. Therefore, the actual amount of MSA used in practice can be very flexible according to the engineering requirements.

As an ingredient of MSA, the use of anhydrite is recommended instead of a pre-mixed anhydrite because of the higher shrinkage-compensating capacities. The shrinkage-compensating capacity is slightly influenced by the aggregate, the change of its ingredients, but strongly influenced by the w/b ratio in concrete and the curing conditions. The drying shrinkage of concrete containing this MSA is comparable to normal concrete. Therefore, appropriate sealing should be used to prevent the loss of moisture from the concrete in practice.

However, the increasing dosages of MSA in concrete are accompanied by a reduction in the compressive strength of the samples. For 5, and 10 m/m% replacement levels by this MSA, the

compressive strength is comparable to that of samples made from Portland cement. But, for 15 and 20 m/m% of replacement levels, the compressive strength is obviously reduced. Therefore, dosages between 5 and 10 m/m% MSA is preferable, which can compensate the autogenous shrinkage and avoid loss of strength.

The hydration of cement pastes containing various amounts of MSA is simulated with the 3-D cement hydration model developed in this thesis. Cement pastes containing higher dosages of MSA have a bigger fraction of ettringite crystals, which is confirmed with XRD analysis.

The sulfate content in binder with the replacement level of 15 m/m% clinker by this MSA is complying with the standards in Europe, United States and China, which is practically the maximum in practice. There is therefore a great possibility that this admixture can be successfully marketed and applied in construction.

9.2 Recommendations and future research

This thesis is designed to help understanding the reactivity and chemical reactions of slag in cement, and the microstructure development of the hydrating slag cement paste. The computer model developed can simulate the hydration process of AAS or slag-blended cement. However, the complexity in practice should be born in mind and the theories and models are schematic representations of the reality. It is a question how reliable these representations may be. Hypotheses are commonly used in models, which may or may not be correct. For example, the clinker phases in Portland cement are regarded to be pure, which is hardly the fact in plant clinker. The validity of hypotheses applies to the models developed in this thesis as well. Therefore, it is worthy to note the possible limitations of the models in this thesis.

Furthermore, models developed in this thesis are not expected to be comprehensive. On the contrary, they are regarded fundamental, i.e. they focus on the principle changes in the system, and represent the structure in the scale as fine as possible. On the one hand, the readers may use the models to investigate their own interests, for example, permeability and durability of hardened pasts. On the other hand, continuous effects can be made in future to clarify the hypotheses, to consolidate the theoretical backgrounds of the models and to broaden their applications.

Recipes of shrinkage-compensating admixture for concrete are developed in this thesis. They are tested in the lab with considerations to engineering requirements. However, these recipes are not tested on a real scale, yet. Only a few properties relevant to concrete technology are examined in this thesis. Prior to the real applications of the recipes designed in this thesis, additional tests are necessary.

In this section, a few recommendations for using the models and recipes developed in this thesis and possible future research are presented:

1. The role of activator in the chemical reaction of slag is not considered in the theoretical model, except when the activator is Portland cement/clinker. While the effect of activators on the chemical reaction may be minor when the dosage of activators is small, sometimes, large amounts of activators are used, for example, in supersulfated cement. In this case, the reaction of activators should be included in the models as well.
2. The alkali-binding capacity of C-S-H with various compositions and in combination with the presence of hydrotalcite is not completely understood, yet. The alkali-binding capacity of hydrotalcite requires more investigations as well. The findings in this thesis are not completely validated by experimental researches before, although they are findings based on measurements with real hydrating cement pastes. Further research on this aspect is interesting, and may be useful to help understanding the performance of slag cement concrete.
3. The simulated 3-D microstructure is straightforward, with which many properties can be calculated directly. However, to apply the models for specific objectives, the corresponding algorithms are necessary, for example, the percolation theory (Bentz, 1997), the coating

theory (Van Eijk, 2001) and normalized two-point correlation function (Bentz, 2006). To choose or develop the appropriate algorithms is important in this respect. In other words, theories to bridge the gap between microstructural properties and macro performance of concrete are essential for effective use of the models.

4. The reactivity of slag is a complex subject. A few factors are accounted for in this thesis, which are believed to be the most important ones. However, some other factors influence the slag reactivity as well, for example, the presence of crystalline minerals. To determine the reactivity of slag more accurately, a comprehensive consideration of these factors is recommended.
5. The principle of the model, i.e. phase distribution, transformation, and CA algorithms may be applied in other researches as well, for example, to predict the workability of mortar and concrete. In this case, particle packing, physical and chemical interactions between phases should be considered. The scale of the model should be altered as well, for example, be increased to include the aggregate as a part of the system.
6. The MSA developed in this thesis should be tested more comprehensively in future before it becomes deliverable to the market, for example, the soundness of cement with this admixture, its effect on the setting time and susceptibility to internal sulfate attack if cured at high temperatures during early ages. Combinations with the hydroxide-based SCC can also be of practical interest.

Bibliography

Ali, M. and Mullick, A. (1995). Volume stabilisation of high MgO cement: effect of curing conditions and fly ash addition, *Cement and Concrete Research* **28**(11): 1585–1594.

Allmann, V. R. (1970). Doppelschichtstrukturen mit brucitähnlichen Schichtionen $[Me(II)_{1-x}Me(III)_x(OH)_2]^{x+}$, *Chimia* **24**: 99–108.

Andersson, R. and Gram, H. E. (1987). Properties of alkali activated slag concrete, *Nordic Concrete Research* **6**(1): 7–18.

Anstice, D., Page, C. L. and Page, M. (2004). The pore solution phase of carbonated cement pastes, *Cement and Concrete Research* **35**(2): 377–388.

Atkins, M., Glasser, F. P. and Kindness, A. (1992). Cement hydrate phases: solubility at 25°C, *Cement and Concrete Research* **22**(2-3): 241–246.

Atkins, M., Glasser, F. P., Kindness, A., Bennett, D. G., Dawes, A. C. and Read, D. (1991). A thermodynamic model for blended cements, *Report DoE/HMIP/RR/92/005.*, University of Aberdeen, Department of Chemistry, Aberdeen, U.K.

Barlow, D. F. and Jackson, P. J. (1988). The release of alkalis from pulverised-fuel ashes and ground granulated blastfurnace slags in the presence of Portland cements, *Cement and Concrete Research* **18**(2): 235–248.

Baroghel-Bouny, V., Mounanga, P., Khelidj, A., Loukili, A. and Rafai, N. (2006). Autogenous deformations of cement pastes: Part II, w/c effects, micro-macro correlations, and threshold values, *Cement and Concrete Research* **36**(1): 123–136.

Battagin, A. F. (1992). Influence of degree of hydration of slag on slag cements, *Proc. 9^{th} ICCC*, Vol. III, National Council for Cement and Building Materials, New Delhi, India, pp. 166–172.

Bennett, D. G., Read, D., Atkins, M. and Glasser, F. P. (1992). A thermodynamic model for blended cements. 2. cement hydrate phases, thermodynamic values and modeling studies, *Journal of Nuclear Materials* **190**(2): 315–325.

Bentz, D. P. (1995). A three-dimensional cement hydration and microstructure program. i. hydration rate, heat of hydration, and chemical shrinkage, *Report NISTIR 5756*, National Institute of Standards and Technology, Gaithersburg, MD. U.S.

Bentz, D. P. (1997). Guide to using CEMHYD3D: a three-dimensional cement hydration and microstructure development modelling package, *Report NISTIR 5977*, NIST, Gaithersburg, MD. U.S.

Bentz, D. P. (2000). CEMHYD3D: a three-dimensional cement hydration and microstructure development modelling package, version 2.0, *Report NISTIR 6485*, NIST, Gaithersburg, MD. U.S.

Bentz, D. P. (2005). CEMHYD3D: a three-dimensional cement hydration and microstructure development modeling package, version 3.0, *Report NISTIR 7232*, NIST, Gaithersburg, MD. U.S.

Bentz, D. P. (2006). Quantitative comparison of real and CEMHYD3D model microstructures using correlation functions, *Cement and Concrete Research* **36**(2): 259–263.

Bentz, D. P. and Garboczi, E. J. (1991). A digitized simulation model for microstructural devel-

opment, *in* S. Mindess (ed.), *Advances in Cementitious Materials (Ceramic Transactions, Vol 16)*, Amer. Ceramic Society, Westerville, U.S., pp. 365–380.

Bentz, D. P. and Garboczi, E. J. (1992). Modelling the leaching of calcium hydroxide from cement paste: effects on pore space percolation and diffusivity, *Materials and Structures* **25**(9): 523–533.

Bentz, D. P., Garboczi, E. J., Haecker, C. J. and Jensen, O. M. (1999). Effects of cement particle size distribution on performance properties of Portland cement-based materials, *Cement and Concrete Research* **29**(10): 1663–1671.

Bentz, D. P. and Haecker, C. J. (1999). An argument for using coarse cements in high-performance concretes, *Cement and Concrete Research* **29**(4): 615–618.

Bentz, D. P. and Jensen, O. M. (2004). Mitigation strategies for autogenous shrinkage cracking, *Cement and Concrete Composites* **26**(6): 677–685.

Bentz, D. P., Waller, V. and de Larrard, F. (1998). Prediction of adiabatic temperature rise in conventional and high-performance concretes using a 3-D microstructural model, *Cement and Concrete Research* **28**(2): 285–297.

Berliner, R., Popovici, M., Herwig, K., Berliner, M., Jennings, H. M. and Thomas, J. J. (1998). Quasielastic neutron scattering study of the effect of water-to-cement ratio on the hydration kinetics of tricalcium silicate, *Cement and Concrete Research* **28**(2): 231–243.

Bérubé, M. A., Tremblay, C., Fournier, B., Thomas, M. D. and Stokes, D. B. (2004). Influence of lithium-based products proposed for counteracting ASR on the chemistry of pore solution and cement hydrates, *Cement and Concrete Research* **34**(9): 1645–1660.

Bezjak, A. and Jelenic, I. (1980). On the determination of rate constants for hydration processes in cement paste, *Cement and Concrete Research* **10**(4): 553–563.

Blezard, R. (1998). Reflections on the history of the chemistry of cement, *SCI Electronic Lecture Paper Series*, Society of Chemical Industry, London, U.K.

Brough, A. R. and Atkinson, A. (2002). Sodium silicate-based, alkali-activated slag mortars Part I. Strength, hydration and microstructure, *Cement and Concrete Research* **32**(6): 865–879.

Brouwers, H. J. H. (2004a). The work of Powers and Brownyard revisited: composition of Portland cement paste, *Report CE&M 2004W-006 / CME-001*, University of Twente, Enschede, The Netherlands.

Brouwers, H. J. H. (2004b). The work of Powers and Brownyard revisited: Part 1, *Cement and Concrete Research* **34**(9): 1697–1716.

Brouwers, H. J. H. (2005). The work of Powers and Brownyard revisited: Part 2, *Cement and Concrete Research* **35**(10): 1922–1936.

Brouwers, H. J. H. and Van Eijk, R. J. (2002). Fly ash reactivity: extension and application of a shrinking core model and thermodynamic approach, *Journal of Materials Science* **37**(10): 2129 –2141, Erratum, ibid, 3803.

Brouwers, H. J. H. and Van Eijk, R. J. (2003). Alkali concentrations of pore solution in hydrating OPC, *Cement and Concrete Research* **33**(2): 191–196.

Butler, J. N. (1998). *Ionic equilibrium. Solubility and pH calculations*, John Wiley & Sons, New York, U.S.

Cesareni, C. and Frigione, G. (1966). Some researches on the physical properties of hardened pastes of Portland cements containing granulated blast furnace slag, *Symposium on Structure of Portland Cement Paste and Concrete*, Highway Research Board, National Academy of Engineering, Washington D.C., U.S.

Chan, Y., Liu, C. and Lu, Y. (1998). Effects of slag and fly ash on the autogenous shrinkage of high performace concrete, *in* E. Tazawa (ed.), *Proceedings of International Workshop on Autogenous Shrinkage of Concrete*, Japan Concrete Institute, Hiroshima, Japan, pp. 213–220.

Chartschenko, I. and Stark, J. (1995). Über die Bedeutung der Nachbehandlung bei der Erhärtung von Quellzementen, *Wiss. Z. Hochsch. Archit. Bauwes. - Weimar* **41**: 167–173.

Chatterji, A. (2001). X-ray diffraction, *in* V. Ramachandran and J. Beaudoin (eds), *Handbook of Analytical Techniques in Concrete Science and Technology*, Noyes Publications / William Andrew Publishing, LLC, New York, U.S., chapter 8, pp. 275–332.

Chatterji, S. (1995). Mechanism of expansion of concrete due to the presence of dead-burnt CaO and MgO, *Cement and Concrete Research* **25**(1): 51–56.

Chatterji, S. and Jeffery, J. W. (1963). Studies of early stages of paste hydration of cement compounds II, *Journal of the American Ceramic Society* **46**(4): 187.

Chen, W. and Brouwers, H. J. H. (2007a). The hydration of slag, Part 1: reaction models for alkali-activated slag, *Journal of Materials Science* **42**(2): 428–443.

Chen, W. and Brouwers, H. J. H. (2007b). The hydration of slag, Part 2: reaction models for blended-cement, *Journal of Materials Science* **42**(2): 444–464.

Clark, D. E. and Zoitos, B. K. (1992). *Corrosion of glass, ceramics, and ceramic superconductors: principles, testing, characterization, and applications*, Noyes, Park Ridge, NJ., U.S.

Collins, F. and Sanjayan, J. G. (2000). Effect of pore size distribution on drying shrinking of alkali-activated slag concrete, *Cement and Concrete Research* **30**(9): 1401–1406.

Copeland, L. E., Kantro, D. L. and Verbeck, G. (1960). Chemistry of hydration of Portland cement, *Report Bull. 153*, Res. Lab. of Portland Cement Association, Washington, D.C., U.S.

Czernin, W. (1956). Über die Schrumpfung des erhärtenden Zementes, *Zement-Kalk-Gips* **9**: 525–530.

Daimon, M., Abo-El-Enein, S. A., Hosaka, G., Goto, S. and Kondo, R. (1977). Pore structure of calcium silicate hydrate in hydrated tricalcium silicate, *Journal of the American Ceramic Society* **60**(3-4): 110–114.

Damidot, D. and Glasser, F. P. (1995). Investigation of the CaO-Al_2O_3-SiO_2-H_2O system at 25°C by thermodynamic calculations, *Cement and Concrete Research* **25**(1): 22–28.

Daube, J. and Bakker, R. (1986). Portland blast-furnace slag cement: a review, *in* G. Frohnsdorff (ed.), *Blended Cements, ASTM STP 897*, ASTM, Philadelphia, Pennsylvania, U.S., pp. 1–14.

Dehwah, H., Malslehuddin, M. and Austin, S. (2002). Effect of cement alkalinity on pore solution chemistry and chloride-induced reinforcement corrosion, *ACI Materials Journal* **99**(3): 227–233.

Deja, J. (2003). Freezing and de-icing salt resistance of blast furnace slag concretes, *Cement and Concrete Composites* **25**(3): 357–361.

Deng, M. and Tang, M. (1994). Formation and expansion of ettringite crystals, *Cement and Concrete Research* **24**(1): 119–126.

Diamond, S. (1975). A review of alkali-silica reaction and expansion mechanisms 1. alkalies in cements and in concrete pore solutions, *Cement and Concrete Research* **5**(4): 329–345.

Diamond, S. (1981). Effect of two Danish flyashes on alkali contents of pore solutions of cement-flyash pastes, *Cement and Concrete Research* **11**(3): 383–394.

Domone, P. (2006). Self-compacting concrete: An analysis of 11 years of case studies, *Cement & Concrete Composites* **28**(2): 197–208.

Doremus (1979). Chemcial durability of glass, *Treatise on materials science and technology*, Vol. 17, Academic Press, New York, U.S., pp. 41–69.

Douglas, R. and El-Shamy, T. (1967). Reaction of glasses with aqueous solutions, *Journal of the American Ceramic Society* **50**(1): 1–8.

Du, C. (2006). A review of magnesium oxide in concrete, *Cement and Concrete World* **59**: 53–63.

Duan, X. and Evans, D. G. (2006). *Layered double hydroxides*, Springer, Berlin; New York.

Dubovoy, V., Gebler, S., Klieger, P. and Whiting, D. (1986). Effects of ground granulated blast-furnace slags on some properties of pastes, mortars, and concretes, *in* G. Frohnsdorff (ed.), *Blended Cements, ASTM STP 897*, ASTM, Philadelphia, Pennsylvania, U.S., pp. 29–48.

Duchesne, J. and Bérubé, M. A. (1994). The effectiveness of supplementary cementing materials in suppressing expansion due to ASR - another look at the reaction mechanisms, 2. pore solution chemistry, *Cement and Concrete Research* **24**(2): 221–230.

Duchesne, J. and Bérubé, M. A. (1995). Effect of supplementary cementing materials on the composition of cement hydration products, *Advanced Cement Based Materials* **2**(2): 43.

El-Shamy, T., Lewins, J. and Douglas, R. (1972). The dependence on the pH of the decomposition of glasses by aqueous solutions, *Glass Technology* **13**(3): 81–87.

Emanuelson, A. and Hansen, S. (1997). Distribution of iron among ferrite hydrates, *Cement and Concrete Research* **27**(8): 1167–1177.

Escalante-García, J. I. and Sharp, J. H. (1998). Effect of temperature on the hydration of the main clinker phases in Portland cements: Part II, Blended cements, *Cement and Concrete Research* **28**(9): 1259–1274.

Feldman, R. (1986). Pore structure, permeability and diffusivity as related to durability, *Proc. 8^{th} ICCC*, Vol. I, Rio de Janeiro, Brazil, pp. 336–356.

Feng, X., Garboczi, E. J., Bentz, D. P. and Stutzman, P. E. (2004). Estimation of the degree of hydration of blended cement pastes by a scanning electron microscope point-counting procedure, *Cement and Concrete Research* **34**(10): 1787–1793.

Fernández-Jiménez, A. (1997). Kinetic study of alkali-activated blast furnace slag, *in* H. Justnes (ed.), *Proc. 10^{th} ICCC*, Vol. 3, Amarkai AB and Congrex Göteborg A, Göteborg, Sweden, p. 3ii098.

Fernández-Jimenéz, A. and Puertas, F. (1997). Influence of the activator concentration on the kinetics of the alkaline activation process of a blastfurnace slag, *Materiales De Construccion* **246**: 31–42.

Fernández-Jimenéz, A. and Puertas, F. (2001). Alkaline activated slag cements. determination of reaction degree, *Materiales De Construccion* **261**: 53–66.

Flint, E. P., McMurdie, H. F. and Wells, L. S. (1941). Hydrothermal and X-ray studies of the garnet-hydrogarnet series and the relationship of the series to hydration products of Portland cement, *Journal of Research of the National Bureau of Standards* **26**(1): 13–33.

Frigione, G. (1986). Manufacture and characteristics of Portland blast-furnace slag cements, *in* G. Frohnsdorff (ed.), *Blended Cements, ASTM STP 897*, ASTM, Philadelphia, Pennsylvania, U.S., pp. 15–28.

Fujii, K. and Kondo, W. (1984). Heterogeneous equilibria of calcium silicate hydrate in water at 30°C, *J. Chem. Soc. Dalton Trans* **2**: 645–651.

Garboczi, E. J. and Bentz, D. P. (2001). The effect of statistical fluctuation, finite size error, and digital resolution on the phase percolation and transport properties of the NIST cement hydration model, *Cement and Concrete Research* **31**(10): 1501–1514.

Geiker, M. and Knudsen, T. (1982). Chemical shrinkage of Portland cement pastes, *Cement and Concrete Research* **12**(5): 603–610.

Glasser, F. P. (1991). Chemical, mineralogical, and microstructural changes occurring in hydrated slag-cement blends, *in* S. Skalny, J. P. Mindess (ed.), *Materials Science of Concrete II*, American Ceramic Society, Westerville, OH, U.S., pp. 41–81.

Glasser, F. P. (2003). The pore fluid in Portland cement: its composition and role, *in* G. Grieve, G. Owens (ed.), *Proc. 11^{th} ICCC*, Cement & Concrete Institute, Durban, South Africa, pp. 341–352.

Glasser, F. P., Kindness, A. and Stronach, S. A. (1999). Stability and solubility relationships in AFm phases: Part I. Chloride, sulfate and hydroxide, *Chemistry of Materials* **29**(6): 861.

Glukhovsky, V. (1959). *Soil silicates*, Gosstroiizdat Publish., Kiev, Ukraine. (in Russian).

Glukhovsky, V. D. (1980). High strengh slag-alkaline cements, *Proc. 7th ICCC*, Vol. III, Paris, France, pp. 164–168.

Gollop, R. S. and Taylor, H. F. W. (1996a). Microstructural and microanalytical studies of sulfate attack. IV. Reactions of a slag cement paste with sodium and magnesium sulfate solutions, *Cement and Concrete Research* **26**(7): 1013–1028.

Gollop, R. S. and Taylor, H. F. W. (1996b). Microstructural and microanalytical studies of sulfate attack. V. Comparison of different slag blends, *Cement and Concrete Research* **26**(7): 1029–1044.

Groves, G. W., Le Sueur, P. J. and Sinclair, W. (1986). Transmission electron microscopy and microanalytical studies of ion-beam-thinned sections of tricalcium silicate paste, *Journal of the American Ceramic Society* **69**(4): 353–356.

Gruskovnjak, A., Lothenbach, B., Holzer, L., Figi, R. and Winnefeld, F. (2006). Hydration of alkali-activated slag: comparison with ordinary Portland cement, *Advances in Cement Research* **18**(3): 119–128.

Häkkinen, T. (1993). The influence of slag content on the microstructure, permeability and mechanical properties of concrete Part 1 microstructural studies and basic mechanical properties, *Cement and Concrete Research* **23**(2): 407–421.

Harchand, K. S., Kumar, R., Chandra, K. and Vishwamittar (1984). Mössbauer and X-ray investigations of some Portland cements, *Cement and Concrete Research* **14**(2): 170–176.

Harrisson, A. M., Winter, N. B. and Taylor, H. F. W. (1987). Microstructure and microchemistry of slag cement paste, *Mat. Res. Soc. Symp. Proc.*, Vol. 85, Materials Research Society, Pittsburgh, PA, USA, pp. 199–208.

Hewlett, P. C. (1998). *Lea's chemistry of cement and concrete*, 4th edn, Arnold, London, U.K.

Hill, J. and Sharp, J. H. (2003). The mineralogy and microstructure of three composite cements with high replacement levels, *Cement and Concrete Composites* **24**(2): 191–199.

Hinrichs, W. and Odler, I. (1989). Investigation of the hydration of Portland blast furnace slag cement: Hydration kinetics, *Advances in Cement Research* **2**: 9–13.

Höglund, L. O. (1992). Some notes of ettringite formation in cementitous materials; influence of hydration and thermodynamic constraints for durability, *Cement and Concrete Research* **22**(2-3): 217–228.

Hong, S. Y. and Glasser, F. P. (1999). Alkali binding in cement pastes: Part I, The C-S-H phase, *Cement and Concrete Research* **29**(12): 1893–1903.

Hong, S. Y. and Glasser, F. P. (2002). Alkali sorption by C-S-H and C-A-S-H gels: Part II. Role of alumina, *Cement and Concrete Research* **32**(7): 1101–1111.

Hooton, R. D. and Emery, J. (1983). Glass content determination and strength development predictions for bitrified blast furnace slag, *in* V. M. Malhotra (ed.), *Proceedings of the 1st international conference on the use of fly ash, silica fume, slag and other mineral by-products in concrete*, Vol. II, American Concrete Institute, Montebello, Quebec, Canada, pp. 945–962.

Hori, A. and Morioka, M. (1998). Influence of expansive additives on autogenous shrinkage, *in* E. Tazawa (ed.), *Proceedings of International Workshop on Autogenous Shrinkage of Concrete*, Japan Concrete Institute, Hiroshima, Japan, pp. 177–184.

Jantzen, C. M. and Plodinec, M. J. (1984). Thermodynamic model of natural, medieval and nuclear waste glass durability, *Journal of Non-Crystalline Solids* **67**(1-3): 207–223.

Jennings, H. M. and Ghosh, S. N. (1983). The developing microstructure in Portland cement,

Advances in Cement Technology, Pergamon Press, New York, U.S., p. 349.

Jennings, H. M., Hsieh, J., Srinivasan, R., Jaiswal, S., Garci, M., Sohn, D., Hinners, C., Heppner, S. and Neubauer, C. (1996). Modelling and materials science of cement-based materials Part I: an overview, *in* H. M. Jennings (ed.), *The modelling of microstructure and its potential for studying transport properties and durability*, Kluwer Academic Publishers, Dordrecht, the Netherlands, pp. 29–62.

Jennings, H. M. and Johnson, S. K. (1986). Simulation of microstructure development during the hydration of a cement compound, *Journal of the American Ceramic Society* **69**(11): 790–795.

Jennings, H. M. and Tennis, P. D. (1994). Model for the developing microstructure in Portland cement pastes, *Journal of the American Ceramic Society* **77**(12): 3161.

Jiang, W., Silsbee, M. R. and Roy, D. M. (1997). Alkali activation reaction mechanism and its influence on microstructure of slag cement, *in* H. Justnes (ed.), *Proc. 10th ICCC*, Amarkai AB and Congrex Göteborg A, Göteborg, Sweden, p. 3ii100.

Jupe, A. C., Turrillas, X., Barnes, P., Colston, S. L., Hall, C., Hausemann, D. and Hanfland, M. (1996). Fast in situ X-ray-diffraction studies of chemical reactions: A synchrotron view of the hydration of tricalcium aluminate, *Physical Review B* **53**(22): 14697–14700.

Kalyoncu, R. (1998). Minerals yearbook: Slag—iron and steel, *Report*, U.S. Geological Survey, Reston, U.S.

Kantro, D., Weise, C. and Brunauer, S. (1966). Paste hydration of beta-dicalcium silicate, tricalcium silicate, and alite, *Symposium on Structure of Portland Cement Paste and Concrete*, Highway Research Board, Washington, D.C., U.S., pp. 309–327.

Kasselouris, V., Ftikos, C. and Parissakis, G. (1985). On the hydration of MgO in cement pastes hydrated up to eight years, *Cement and Concrete Research* **15**(5): 758–764.

Klein, A. and Troxell, G. (1958). Studies of calcium sulfoaluminate admixtures for expansive cement, *Proc., ASTM*, Vol. 58, pp. 986–1008.

Knudsen, T. and Geiker, M. (1985). Obtaining hydration data by measurement of chemical shrinkage with an archimeter, *Cement and Concrete Research* **15**(2): 381–382.

Kollek, J. J., Varma, S. P. and Zaris, C. (1986). Measurement of OH^- ion concentrations of pore fluids and expansion due to alkali-silica reaction in composite cement mortars, *Proc. 8th ICCC*, Vol. IV, Rio de Janeiro, Brazil, pp. 183–189.

Kondo, R. and Ohsawa, S. (1968). Studies on a method to determine the amount of granulated blastfurnace slag and the rate of hydration of slag in cement, *Proc. 5th ISCC*, Vol. 4, Cement Association of Japan, Tokyo, Japan, pp. 255–269.

Kramer, W. (2006). Cement consumption in the Netherlands since 1980, Private communication, ENCI, 's-Hertogenbosch, The Netherlands.

Krishnan, A. (2002). *Durability of concrete containing fly ash or slag exposed to low temperatures at early ages*, Master thesis, Purdue University, West Lafayette, IN, U.S.

Lacroux, É. (2006). Domestic deliveries by cement type in CEMBUREAU member countries in 2004, Private communication, CEMBUREAU, Brussels, Belgium.

Lafuma, H. (1952). Expansive cement, *Proc. 3rd ISCC*, Cement and Concrete Association, London, UK, pp. 581–596.

Larbi, J. A., Fraay, A. L. A. and Bijen, J. M. J. M. (1990). The chemistry of the pore fluid of silica fume-blended cement systems, *Cement and Concrete Research* **20**(4): 506–516.

Levenspiel, O. (1999). *Chemical reaction engineering*, 3rd edn, Wiley, New York, U.S.

Li, F. (2006). Private communication.

Li, Y. (2002). Autogenous shrinkage of cementitious materials: characteristics and mechanism, *Report*, Tongji University, Shanghai, China. (in Chinese).

Lide, D. R. (2003). *CRC Handbook of Chemistry and Physics*, 84^{th} edn, CRC press.

Locher, F., Richartz, W. and Sprung, S. (1976). Erstarren von Zement, *Zement-Kalk-Gips* **29**(10): 435–442.

Locher, F. W. (1960). Hydraulic properties and hydration of glasses of the system CaO-Al_2O_3-SiO_2, *Proc. 4^{th} ISCC*, Vol. 1, National Bureau of Standards, Washington D.C., U.S., pp. 267–276.

Longuet, P. (1976). La protection des armatures dans le béton armé élaboré avec des ciments de laitier, *Silicates Industriels* **7/8**: 321–328.

Longuet, P., Burglen, L. and Zelwer, A. (1973). La phase liquide du ciment hydraté, *Revue des Matériaux de Construction* **676**: 35–41.

Lossier, H. (1946). Cements with controlled expansions and their applications to pre-stressed concrete, *The Structural Engineer* **24**(10): 503–534.

Lothenbach, B. and Winnefeld, F. (2006). Thermodynamic modelling of the hydration of Portland cement, *Cement and Concrete Research* **36**(2): 209–226.

Lou, Z., Ye, Q., Chen, H., Wang, Y. and Shen, J. (1998). Hydration of MgO in clinker and its expansion property, *Guisuanyan Xuebao* **26**(4): 430–436. in Chinese.

Luke, K. and Glasser, F. P. (1987). Selective dissolution of hydrated blast furnace slag cements, *Cement and Concrete Research* **17**(2): 273–282.

Luke, K. and Glasser, F. P. (1988). Internal chemical evolution of the constitution of blended cements, *Cement and Concrete Research* **18**(4): 495–502.

Lumley, J. S., Gollop, R. S., Moir, G. K. and Taylor, H. F. W. (1996). Degree of reaction of the slag in some blends with Portland cements, *Cement and Concrete Research* **26**(1): 139–151.

Ma, B., Zhu, H., Bai, J., Dong, R. and Li, X. (2005). Effect of WHU expanding-agent on shrinkage of C80 self-compacting concrete, *in* Z. Yu, C. Shi, K. Henri and Y. Xie (eds), *SCC'2005-China - 1^{st} International Symposium on Design, Performance and Use of Self-Consolidating Concrete*, RILEM, Changsha, China, pp. 499–506.

Macphee, D. E., Atkins, M. and Glasser, F. P. (1989). Phase development and pore solution chemistry in ageing blast furnace slag-Portland cement blends, *Mat. Res. Soc. Symp. Proc.*, Vol. 127, Materials Research Society, Pittsburgh, PA, USA, pp. 475–480.

Maekawa, K., Chaube, R. and Kishi, T. (1996). Coupled mass transport, hydration and structure formation theory for durability design of concrete structures, *in* K. Sakai (ed.), *Integrated Design and Environmental Issues in Concrete Technology*, E & FN Spon, London, U.K., pp. 83–98.

Marchand, J., Bentz, D. P., Samson, E. and Maltais, Y. (2001). Influence of calcium hydroxide dissolution on the transport properties of hydrated cement systems, *Materials Science of Concrete: Calcium Hydroxide in Concrete, Workshop on the Role of Calcium Hydroxide in Concrete*, American Ceramic Society, Anna Maria Island, Florida, U.S., pp. 113–129.

Masuda, H., Higashitani, K. O. and Yoshida, H. (2006). *Powder technology handbook*, 3^{rd} edn, Taylor & Francis, Boca Raton, U.S.

Mehta, P. K. (1976). Scanning electron micrographic studies of ettringite formation, *Cement and Concrete Research* **6**(2): 169–182.

Mehta, P. K. and Wang, S. (1982). Expansion of ettringite by water adsorption, *Cement and Concrete Research* **12**(1): 121–122.

Mejlhede Jensen, O., Freiesleben Hansen, P., Lachowski, E. E. and Glasser, F. P. (1999). Clinker mineral hydration at reduced relative humidities, *Cement and Concrete Research* **29**(9): 1505–1512.

Mikhail, R. S. and Selim, S. A. (1966). Adsorption of organic vapors in relation to the pore

structure of hardended Portland cement pastes, *Symposium on structure of Portland cement paste and concrete*, Highway Research Board, Washington, D.C., U.S., pp. 123–134.

Mills, K. (1995). Structure of liquid slags, *Slag Atlas*, 2^{nd} edn, Verlag Stahleisen GmbH, Düsseldorf, Germany, pp. 1–8.

Mills, R. H. (1986). Chemical shrinkage and differential sorptions in mixtures of Portland cement and blast-furnace slag, *in* G. Frohnsdorff (ed.), *Blended cements*, ASTM Special Technical Publication, ASTM, Philadelphia, PA, U.S., pp. 49–61.

Mindess, S. and Young, J. F. (1981). *Concrete*, Prentice-Hall, Inc., Englewood Cliffs, NJ, U.S.

Mindess, S., Young, J. F. and Darwin, D. (2003). *Concrete*, 2^{nd} edn, Prentice Hall, Upper Saddle River, U.S.

Mounanga, P., Khelidj, A., Loukili, A. and Baroghel-Bouny, V. (2004). Predicting $Ca(OH)_2$ content and chemical shrinkage of hydrating cement pastes using analytical approach, *Cement and Concrete Research* **34**(2): 255–265.

Mysen, B. O. (1988). *Structure and properties of silicate melts*, Vol. 4 of *Developments in geochemistry*, Elsevier, Amsterdam; New York.

Nagataki, S. and Gomi, H. (1998). Expansive admixtures (mainly ettringite), *Cement & Concrete Composites* **20**(2-3): 163–170.

Narang, K. C. and Chopra, S. K. (1983). Studies on alkaline activation of BF, steel and alloy slags, silicates industrials, *Silicates Industriels* **9**: 175–182.

Navi, P. and Pignat, C. (1996). Simulation of effects of small inert grains on cement hydration and its contact surfaces, *in* H. M. Jennings (ed.), *The Modelling of Microstructure and Its Potential for Studying Transport Properties and Durability*, Kluwer Academic Publishers, Dordrecht, The Netherlands, pp. 227–240.

Neville, A. M. (2000). *Properties of Concrete*, 4^{th} edn, Prentice Hall/Pearson, Harlow, H.K.

Odler, I. (1980). Interaction between gypsum and the C-S-H phase formed in C_3S hydration, *Proc. 7^{th} ICCC*, Vol. IV, Paris, France, pp. 493–495.

Odler, I. (1998). Hydration, setting and hardening of portland cement, *in* P. Hewlett (ed.), *Lea's chemistry of cement and concrete*, 4th edn, Arnold, London, U.K., pp. 241–297.

Odler, I. and Abdul-Maula, S. (1987). Investigations on the relationship between porosity structure and strength of hydrated portland cement pastes III. Effect of clinker composition and gypsum addition, *Cement and Concrete Research* **17**(1): 22–30.

Odler, I. and Gasser, M. (1988). Mechanism of sulfate expansion in hydrated Portland cement, *Journal of the American Ceramic Society* **71**(11): 1015–1020.

Odler, I. and Rößler, M. (1985). Investigations on the relationship between porosity, structure and strength of hydrated Portland cement pastes. II. Effect of pore structure and of degree of hydration, *Cement and Concrete Research* **15**(3): 401–410.

Olbrich, E. and Frischat, G. H. (2001). Corrosion of granulated glassy blast furnace slags in aqueous solutions, *Glass Science and Technology* **74**(4): 86–96.

Osborne, G. J. (1999). Durability of Portland blast-furnace slag cement concrete, *Cement and Concrete Composites* **21**(1): 11–21.

Page, C. L. and Vennesland, O. (1983). Pore solution composition and chloride binding capacity of silica-fume cement pastes, *Materials and Structures* **16**(91): 19–25.

Pane, I. and Hansen, W. (2004). Investigation of blended cement hydration by isothermal calorimetry and thermal analysis, *Cement and Concrete Research* **35**(6): 1204–1209.

Panesar, D. and Chidiac, S. (2006). Chloride binding and its effects on the pore structure of concrete containing ggbfs, *Cement and Concrete Research* . In preparation.

Parrott, L. J., Geiker, M., Gutteridge, W. A. and Killoh, D. (1990). Monitoring Portland cement

hydration: Comparison of methods, *Cement and Concrete Research* **20**(6): 919.

Paul, A. (1977). Chemical durability of glasses: a thermodynamic approach, *Journal of Materials Science* **12**(11): 2246.

Persson, B. (2002). Self-desiccation and chloride migration, *Self-desiccation and Its Importance in Concrete Technology, Proceedings of the 3rd International Research Seminar*, Lund Institute of Technology, Lund, Sweden, pp. 175–194.

Pietersen, H. S. and Bijen, J. M. J. M. (1994). Fly ash and slag reactivity in cements - tem evidence and application of thermodynamic modelling, *Environmental Aspects of Construction with Waste Materials*, Elsevier, Amsterdam; London; New York; Tokyo, pp. 949–957.

Pignat, C., Navi, P. and Scrivener, K. L. (2005). Simulation of cement paste microstructure hydration, pore space characterization and permeability determination, *Materials and Structures* **38**: 459–466.

Pollitt, H. and Brown, A. W. (1968). The distribution of alkalis in Portland cement clinker, *Proc. 5th ISCC*, Cement Association of Japan, Tokyo, Japan, pp. 322–333.

Pöllmann, H. (2006). Private communication.

Pöllmann, H., Kuzel, H. J. and Wenda, R. (1989). Compounds with ettringite structure, *Neues Jahrbuch für Mineralogie-Abhandlungen* **160**: 133–158.

Powers, T. (1960). Physical properties of cement paste, *Proc. 4th ISCC*, Vol. 2, National Bureau of Standards, Washington, D.C. U.S., pp. 577–613.

Powers, T. C. and Brownyard, T. (1948). Studies of the physical properties of hardened Portland cement paste, *Report Bulletin 22*, Res. Lab. of Portland Cement Association, Skokie, IL, U.S. reprinted from J. Am. Concrete Inst. (Proc.), Vol. 43 (1947), p. 101-132, p. 249-336, p. 469-505, p. 549-602, p. 669-712, p. 845-880, p. 933-992.

Princigallo, A., Lura, P., Van Breugel, K. and Levita, G. (2003). Early development of properties in a cement paste: A numerical and experimental study, *Cement and Concrete Research* **33**(7): 1013–1020.

Reardon, E. J. (1992). Problems and approaches to the prediction of the chemical composition in cement/water systems, *Waste Management* **12**(2-3): 221.

Regourd, M. (1980). Structure and behaviour of slag Portland cement hydrates, *Proc. 7th ICCC*, Vol. I, Paris, France, pp. III – 2/10.

Reschke, T. (2000). *Der Einfluss der Granulometrie der Feinstoffe auf die Gefügeentwicklung und die Festigkeit von Beton*, PhD thesis, Bauhaus University, Weimar, Germany.

Richardson, I. G. (1997). The structure of C-S-H in hardened slag cement pastes, *in* H. Justnes (ed.), *Proc. 10th ICCC*, Vol. 2, Amarkai AB and Congrex Göteborg A, Göteborg, Sweden, p. 2ii068.

Richardson, I. G. (1999). The nature of C-S-H in hardened cements, *Cement and Concrete Research* **29**(8): 1131.

Richardson, I. G. (2000). The nature of the hydration products in hardened cement pastes, *Cement and Concrete Composites* **22**(2): 97.

Richardson, I. G., Brough, A. R., Groves, G. W. and Dobson, C. M. (1994). The characterization of hardened alkali-activated blast-furnace slag pastes and the nature of the calcium silicate hydrate (C-S-H) phase, *Cement and Concrete Research* **24**(5): 813.

Richardson, I. G. and Groves, G. W. (1992). Microstructure and microanalysis of hardened cement pastes involving ground granulated blast-furnace slag, *Journal of Materials Science* **27**(22): 6204–6212.

Richardson, J. M., Biernacki, J., Stutzman, P. E. and Bentz, D. P. (2002). Stoichiometry of slag hydration with calcium hydroxide, *Journal of the American Ceramic Society* **85**(4): 947.

Rodger, S. A. and Groves, G. W. (1989). Electron microscopy study of ordinary Portland cement and ordinary Portland cement-pulverized fuel ash blended pastes, *Journal of the American Ceramic Society* **72**(6): 1037–1039.

Rößler, M. and Odler, I. (1985). Investigations on the relationship between porosity, structure and strength of hydrated Portland cement pastes I, effect of porosity, *Cement and Concrete Research* **15**(2): 320–330.

Rothstein, D., Thomas, J. J., Christensen, B. J. and Jennings, H. M. (2002). Solubility behavior of Ca-, S-, Al-, and Si-bearing solid phases in Portland cement pore solutions as a function of hydration time, *Cement and Concrete Research* **32**(10): 1663–1671.

Sagüës, A. A., Moreno, E. I. and Andrade, C. (1997). Evolution of pH during in-situ leaching in small concrete cavities, *Cement and Concrete Research* **27**(11): 1747–1759.

Sato, K., Konish, E. and Fukaya, K. (1986). Hydration of blastfurnace slag particle, *Proc. 8^{th} ICCC*, Vol. 4, Rio de Janeiro, Brazil, pp. 98–103.

Schäfer, E. (2004). *Einfluss der Reaktionen verschiedener Zementbestandteile auf den Alkalihaushalt der Porenlösung des Zementsteins*, PhD thesis, Clausthal University of Technology, Clausthal-Zellerfeld, Germany.

Schäfer, E. and Meng, B. (2001). Influence of cement and addtitions on the quantity of alkalis availabe for an alkali-silica reaction, *Report*, VDZ, Düsseldorf, Germany.

Schilling, P. J., Roy, A. and Eaton, H. C. (1994). Microstructure, strength, and reaction products of ground granulated blast-furnace slag activated by highly concentrated naoh solution, *Journal of Material Research* **9**(1): 188–197.

Schwiete, H. E. and Ludwig, U. (1968). Crystal structures and properties of cement hydration products (hydrated calcium aluminates and ferrites, *Proc. 5^{th} ISCC*, Vol. 2, Cement Association of Japan, Tokyo, Japan, pp. 37–69.

Shi, C. (1996). Strength, pore structure and permeability of alkali-activated slag mortars, *Cement and Concrete Research* **26**(12): 1789–1799.

Shi, C. and Day, R. L. (1995). A calorimetric study of early hydration of alkali-slag cements, *Cement and Concrete Research* **25**(6): 1333–1346.

Shimada, Y. and Young, J. F. (2001). Structural changes during thermal dehydration of ettringite, *Advances in Cement and Concrete Research* **13**(2): 77–81.

Slag Cement Association (2002). Mitigating sulfate attack, Online resource, http://www. slagcement. org.

Smolczyk, H. G. (1980). Slag structure and identification of slags, *Proc. 7^{th} ICCC*, Vol. I, Paris, France, pp. III 1–III 3.

Song, S. and Jennings, H. M. (1999). Pore solution chemistry of alkali-activated ground granulated blast-furnace slag, *Cement and Concrete Research* **29**(2): 159–170.

Stade, H. (1989). On the reaction of C-S-H(di, poly) with alkali hydroxides, *Cement and Concrete Research* **19**(5): 802–810.

Stark, J. and Ludwig, H. (1997). Freeze-deicing salt resistance of concrete containing blast furnace slag cement, *Proc. Freeze-thaw Durability of Concrete*, E&FN Spon, Sainte-Foy, Canada and Lund, Sweden, pp. 107–120.

Stebbins, J., Oglesby, J. and Xu, Z. (1997). Disorder among network-modifier cations in silicate glasses: New constraints from triple-quantum ^{17}O NMR, *American Mineralogist* **82**: 1116–1124.

Steinour, Harold, H. (1944). The bleeding of Portland cement paste, mortar and concrete: Treated as a specialcase of sedimentation, *Report Bulltin 3*, Portland Cement Association. Reprinted from *Industrial and Engineering Chemistry*, Vol. 36, Pages 618-24, 840-7, 901-7 (1944).

Tanaka, H. and Totani, Y. (1983). Structure of hydrated glassy blastfurnace slag in concrete, *in* V. M. Malhotra (ed.), *1 International conference on the use of fly ash, silica fume, slag,m and other mineral by-products in concrete*, Vol. II, American Concrete Institute, Montebello, Quebec, Canada, pp. 963–977.

Taplin, J. (1959). A method for following the hydration reaction in Portland cement. paste, 1959. page 64. page 65, *Australian Journal of Applied Science* **10**: 329–345.

Taylor, H. (1985). The reactions of cement compounds with water, *in* P. Barret and L.-C. Dufour (eds), *Proceedings of the 10th International Symposium on the Reactivity of Solids*, Vol. A, Elsevier, Dijon, France, pp. 39–45.

Taylor, H. F. W. (1987a). Bound water in cement pastes and its significance for pore solution compositions, *in* J. Struble and P. Brown (eds), *Microstructural Development During Hydration of Cement, Mat. Res. Soc. Symp. Proc.*, Vol. 85, Materials Research Society, Pittsburgh, PA, USA, pp. 47–54.

Taylor, H. F. W. (1987b). A method for predicting alkali ion concentrations in cement pore solutions, *Advances in Cement Research* **1**(1): 5–16.

Taylor, H. F. W. (1990). *Cement chemistry*, 1st edn, Academic press, London, U.K.

Taylor, H. F. W. (1997). *Cement chemistry*, 2nd edn, Thomas Telford Publishing, London, U.K.

Taylor, H. F. W., Mohan, K. and Moir, G. K. (1985). Analytical study of pure and extended Portland cement pastes: II, Fly ash- and slag-cement pastes, *Journal of the American Ceramic Society* **68**(12): 685–690.

Taylor, H. F. W. and Newbury, D. E. (1984). An electron microprobe study of mature cement paste, *Cement and Concrete Research* **14**(4): 565–573.

Tazawa, E. (1998). *Proceedings of International Workshop on Autogenous Shrinkage of Concrete*, Japan Concrete Institute, Hiroshima, Japan.

Tazawa, E., Miyazawa, S. and Kasai, T. (1995). Chemical shrinkage and autogenous shrinkage of hydrating cement paste, *Cement and Concrete Research* **25**(2): 288.

Thomas, J. J., Chen, J. J. and Jennings, H. M. (2003). Ca-OH bonding in the C-S-H gel phase of tricalcium silicate and white Portland cement pastes measured by inelastic neutron scattering, *Chemistry of Materials* **15**(20): 3813–3817.

Tomosawa, F. (1997). Development of a kinetic model for hydration of cement, *in* H. Justnes (ed.), *Proc. 10th ICCC*, Vol. 2, Amarkai AB and Congrex Göteborg A, Göteborg, Sweden, p. 2ii051.

Uchikawa, H. (1986). Effect of blending components on hydration and structure formation, *Proc. 8th ICCC*, Vol. I, Rio de Janeiro, Brazil, pp. 250–280.

Uchikawa, H. and Uchida, S. (1986). Effect of character of glass phase in blending components on their reactivity in calcium hydroxide mixture, *Report*, Toyosu 1-1-7, Koto-ku, Japan.

U.S. Geological Survey (1996–2006). *Mineral Commodity Summaries*, U.S. Geolotical Survey, Reston, U.S. online resouces (http://minerals.usgs.gov/minerals/pubs/mcs/).

Van Breugel, K. (1997). *Simulation of hydration and formation of structure in hardening cement-based materials*, Vol. 9, 2nd edn, Delft University Press, Delft, the Netherlands.

Van Breugel, K. (2004). Modelling of cement-based systems—-the alchemy of cement chemistry, *Cement and Concrete Research* **34**: 1661–1668.

Van Eijk, R. J. (2001). *Hydration of cement mixtures containing contaminants*, PhD thesis, University of Twente, Enschede, The Netherlands.

Van Eijk, R. J. and Brouwers, H. J. H. (1998). Study of the relation between hydrated Portland cement composition and leaching resistance, *Cement and Concrete Research* **28**(6): 815–828.

Van Eijk, R. J. and Brouwers, H. J. H. (2001). Modelling the effects of waste components on

cement hydration, *Waste Management* **21**(3): 279–284.

Wang, S. D. (2000). Alkali-activated slag: Hydration process and development of microstructure, *Advances in Cement Research* **12**(4): 163–172.

Wang, S. D. and Scrivener, K. L. (1995). Hydration products of alkali activated slag cement, *Cement and Concrete Research* **25**(3): 561–571.

Wang, S. and Scrivener, K. L. (2003). ^{29}Si and ^{27}Al NMR study of alkali-activated slag, *Cement and Concrete Research* **33**(5): 769–774.

Wassing, W. (2003). Relationship between the chemical reactivity of granulated blastfurnace slags and the mortar standard compressive strength of the blastfurnace cements produced from them, *Cement International* **5**: 94–104.

Williams, D. A., Saak, A. W. and Jennings, H. M. (1999). The influence of mixing on the rheology of fresh cement paste, *Cement and Concrete Research* **29**(9): 1491–1496.

Wolhuter, C. W., Turkstra, J. and Morris, R. M. (1980). Effect of calcium chloride on the volume contraction, non-evaporable water content and bound chloride content of hydrated Portland cement and blast-furnace slag, *Cement and Concrete Research* **10**(4): 535–543.

Wolter, A., Frischat, G. H. and Olbrich, E. (2003). Investigation of granulated blast furnace slag (gbfs) reactivity by SNMS, *in* G. Grieve, G. Owens (ed.), *Proc. 11th ICCC*, Vol. 4, Cement & Concrete Institute, Durban, South Africa, pp. 1866–1877.

Wu, X., Roy, D. M. and Langton, C. A. (1983). Early stage hydration of slag-cement, *Cement and Concrete Research* **13**(2): 277–286.

Xanthos, M. (2005). *Functional Fillers for Plastics*, Wiley-VCH, Weinheim, Germany.

Xu, Y. (1997). The influence of sulphates on chloride binding and pore solution chemistry, *Cement and Concrete Research* **27**(12): 1841–1850.

Yamazaki, Y. and Sakakibara, Y. (1986). The mechanism of expansive pressure development with the hydration of CaO, *Proc. 8th ICCC*, Vol. IV, Rio de Janeiro, Brazil, pp. 395–400.

Yan, P., Peng, J. and Qin, X. (2002). Behaviour and the controlling factor of delayed ettringite formation in shrinkage-compensating massive concrete, *Magazine of Concrete Research* **54**(5): 315–319.

Ye, Q., Chen, H. X., Wang, Y. Q., Wang, S. X. and Lou, Z. G. (2004). Effect of MgO and gypsum content on long-term expansion of low heat Portland slag cement with slight expansion, *Cement & Concrete Composites* **26**(4): 331–337.

Young, J. F. (1988). Investigations of calcium silicate hydrate structure using silicon-29 nuclear magnetic resonance spectroscopy, *Journal of American Ceramic Society* **71**(3): 118–120.

Young, J. F. and Hansen, W. (1987). Volume relationship for C-S-H formation based on hydration stoichiometry, *in* J. Struble and P. Brown (eds), *Microstructural Development During Hydration of Cement, Mat. Res. Soc. Symp. Proc.*, Vol. 85, Materials Research Society, Pittsburgh, PA, USA, pp. 313–322.

Zachariasen, W. (1932). The atomic arrangement in glass, *J. Am. Chem. Soc* **54**(9): 3841–3851.

Zhang, X., Yang, Y. and Ong, C. K. (1999). A novel way of estimation of the apparent activation energy of cement hydration using microwave technique, *Journal of Materials Science* **34**(13): 3143–3147.

Zhou, H., Wu, X., Xu, Z. and Tang, M. (1993). Kinetic study on hydration of alkali-activated slag, *Cement and Concrete Research* **23**(6): 1253–1258.

List of symbols and abbreviations

Abbreviations

AAS	Alkali-activated slag, pp. 5
AEM	Analytical electron microscopy, pp. 76
AFm	Al_2O_3–Fe_2O_3–mono, pp. 21
AFt	Al_2O_3–Fe_2O_3–tri, pp. 29
AH	Tetracalcium aluminate hydrate, pp. 46
ASR	Alkali-silica reaction, pp. 8
ASTM	American Society for Testing and Materials, pp. 3
BET	Brunauer-Emmett-Teller method, pp. 18
BSE	Backscattered electron, pp. 52
C-S-H	Calcium silicate hydrate, pp. 8
CA	Cellular automation, pp. 34
CH	Calcium hydroxide, pp. 6
DSC	Differential scanning calorimetry, pp. 162
DTA	Differential thermal analysis, pp. 28
EDTA	ethylenediaminetetraacetic acid, pp. 19
EDX	Energy dispersive X-Ray, pp. 52
EMPA	Electron microprobe analysis, pp. 52
ESEM	Environmental scanning electron microscope, pp. 24
GGBFS	Ground granulated blastfurnace slag, pp. 3
HG	Hydrogarnet, pp. 46
HT	Hydrotalcite, pp. 46
ITZ	Interfacial transition zone, pp. 10
MIP	Mercury intrusion porosimetry, pp. 61
MSA	Mineral shrinkage-compensating admixture, pp. 159
MT	Million tons, pp. 1
NMR	Nuclear magnetic resonance, pp. 47
PSD	Particle size distribution, pp. 18
QXDA	Quantitative X-Ray diffraction analysis, pp. 5
RH	Relative humidity, pp. 12
SCC	Shrinkage-compensating cement, pp. 159
SCM	Supplementary cementitious materials, pp. 2
SEM	Scanning electron microscope, pp. 5
SSA	Specific surface area, pp. 18
ST	Strätlingite, pp. 46
TEM	Transmission electron microscopy, pp. 52

TGA	Thermogravimetric analysis, pp. 65	
XRD	X-Ray diffraction, pp. 52	
XRF	X-Ray fluorescence, pp. 19	
Roman		
$x_{\overline{S}}^{p}$	SO_3 content in Portland cement , pp. 183	[m/m%]
$x_{\overline{S}}^{MSA}$	SO_3 content in MSA , pp. 183	[m/m%]
$x_{\overline{S}}^{standard}$	Maximum SO_3 content in cement in standards , pp. 183	[m/m%]
A	Frequency factor, pp. 148	
$\hat{a}$, $\bar{a}$	C/S ratio in C-S-H , pp. 20	[–]
a	Slope coefficient , pp. 148	[–]
a_1, a_2	Slope coefficient , pp. 150	[–]
B	Time conversion factor , pp. 44	[hour/cycle^2]
$\hat{b}$	A/S ratio in C-S-H , pp. 46	[–]
b	Intercept , pp. 148	[–]
b_a	Alkali binding factor , pp. 93	[L]
C	Concentration , pp. 93	[mol/L]
C_0	Concentration at the reaction front , pp. 129	[mol/L]
C_∞	Concentration in the pore solution , pp. 129	[mol/L]
$cycles$	Number of hydration cycles , pp. 44	[cycle]
D	Diffusion coefficient , pp. 128	[m^2/s]
d	Particle size , pp. 18	[µm]
d_m	Mean particle size , pp. 18	[µm]
E_a	Activation energy , pp. 148	[kJ/mol]
F	Fraction of hydration products , pp. 93	[–]
F_1, F_2	Factors accounting for temperature in HYMOSTRUC , pp. 33	[–]
F_s	Empirical constant in calculation of SSA , pp. 18	[–]
f	Fraction of alkali , pp. 92	[–]
f^b	Fraction of bound alkalis , pp. 119	[–]
f_d	Mass fraction of particles having size d , pp. 18	[–]
f_e	Fraction of Fe^{3+} in four co-ordinations , pp. 217	[–]
g	Water content in hydration product , pp. 20	[–]
H	Water content in hydration product , pp. 56	[–]
HR	Relative hydration rate , pp. 136	[–]
J	Diffusion flux , pp. 128	[mol/s·m^2]
J_0	Diffusion flux at the reaction front , pp. 129	[mol/s·m^2]
J_0^{max}	Maximum flux of diffusion , pp. 129	[mol/s·m^2]
K	Equilibrium constant, pp. 212	
K^0	Activity product, pp. 95	
K_i	Rate constant in HYMOSTRUC , pp. 33	[µm/h or µm^2/h]
k_1, k_2, k_3	Characteristic parameters for the hydration degree of slag , pp. 104	[–]
k_T	Rate constant, pp. 148	
M	Molar mass , pp. 46	[g/mol]

M_a	Molality , pp. 98	[mol/g]
M_a^1	Molality of alkali in C-S-H , pp. 108	[mol/g]
M_a^2	Molality of alkali in hydrotalcite , pp. 108	[mol/g]
m	Mass , pp. 26	[g]
$m^{sl,r}$	Mass of reacted slag , pp. 68	[g]
m_{nw}	Mass of non-evaporable water , pp. 26	[g]
m_{gw}	Mass of gel water , pp. 26	[g]
NBO	Non-bridging oxygen, pp. 142	
NBO/T	Non-bridging oxygen per tetrahedrally-coordinated cation, pp. 142	
n	Moles , pp. 46	[mol]
n'_A	Moles of A available for C-S-H and C_4AH_{13} (C_2ASH_8) , pp. 47	[mol]
n'_C	Moles of C available for C-S-H and C_4AH_{13} (C_2ASH_8) , pp. 47	[mol]
n'_S	Moles of S available for C-S-H and C_2ASH_8 , pp. 47	[mol]
n^c_{CH}	Moles of CH consumed by slag reaction , pp. 68	[mol]
P	Dissolution probability , pp. 129	[–]
P^0	Base dissolution probability , pp. 44	[–]
PP	Compressive strength of Portland cement mortar cubes , pp. 211	[MPa]
p	Fraction of CH consumed by the slag reaction , pp. 73	[–]
R	Retained mass fraction , pp. 18	[–]
R_d	Distribution ratio , pp. 94	[L/g]
R_s	Sulfate-alkali ratio , pp. 92	[–]
r	Exponent of $\hat{a}$ for R_d^1 , pp. 109	[–]
S	Specific surface area , pp. 18	[m^2/kg]
SP	Compressive strength of slag cement mortar cubes , pp. 211	[MPa]
T	Temperature , pp. 148	[K]
t	Time , pp. 44	[hour]
V	Volume , pp. 58	[cm^3]
$V^{sl,r}$	Volume of reacted slag , pp. 75	[cm^3]
$V^{sl,ur}$	Volume of unreacted slag , pp. 75	[cm^3]
V_{gp}	Volume of gel pores , pp. 60	[cm^3]
V_{hcp}	Volume of hardened cement paste , pp. 75	[cm^3]
V_{hp}	Volume of hydration product , pp. 58	[cm^3]
V_H	Volume of water , pp. 58	[cm^3]
w/b	Water/binder mass ratio , pp. 60	[–]
w/c	Water/cement mass ratio , pp. 17	[–]
x	Mass fraction , pp. 19	[–]
x_p	Particle size , pp. 128	[m]
Y	Constant for R_d^1 , pp. 109	[L/g]
y	Molar fraction , pp. 52	[–]
$y_{NB}^{(1)}$	Total charge on network-breaking cations , pp. 217	[–]
$y_{NB}^{(2)}$	Total charge allowing for Al and Fe , pp. 217	[–]
z	Molar content , pp. 71	[mol/g]

z'_A	Molar content of A in slag for C-S-H and C_4AH_{13} , pp. 71	[mol/g]
z'_C	Molar content of C in slag for C-S-H and C_4AH_{13} , pp. 71	[mol/g]

Greek

α	Hydration degree , pp. 93	[–]
β'	Model parameter , pp. 151	[–]
β_1	Model parameter considering the pH of solution , pp. 150	[–]
β_2	Model parameter considering the NBO/T of glass in slag , pp. 150	[–]
β_h	Empirical constant in HYMOSTRUC , pp. 33	[–]
γ	Relative reaction degree of slag , pp. 68	[–]
γ_c	Activity coefficient , pp. 213	[–]
δ	Thickness of coating layer , pp. 129	[m]
$\Delta\delta_{in,x}$	Penetration depth in HYMOSTRUC , pp. 33	[µm/h]
δ_f	Distribution factor , pp. 96	[–]
Δ_t	Time increment in HYMOSTRUC , pp. 33	[h]
δ_x	Total thickness of product layer in HYMOSTRUC , pp. 33	[µm]
λ	Mass fraction of slag in blended cement , pp. 66	[–]
λ^0	Translational slag proportion , pp. 71	[–]
λ_h	Factors for the rate-controlling mechanism in HYMOSTRUC , pp. 33	[–]
λ_{MSA}	Maximum replacement level in Portland cement by MSA , pp. 183	[m/m%]
Π^0_{nuc}	Maximum nucleation probability of diffusing species , pp. 40	[–]
Π_{nuc}	Nucleation probability of diffusing species , pp. 40	[–]
ν	Specific volume , pp. 58	[cm^3/g]
ν_0	Specific volume of initial paste , pp. 60	[cm^3/g]
ρ	Density , pp. 18	[g/cm^3]
Φ	Porosity , pp. 60	[–]
Φ_{cp}	Capillary porosity , pp. 60	[–]
Φ_{gp}	Gel porosity , pp. 60	[–]
φ	Shape factor , pp. 35	[–]
χ	Potassium-sulfate ratio , pp. 92	[–]
Ψ_S	Chemical shrinkage , pp. 58	[cm^3/g]
Ω	Model parameter , pp. 129	[m]
$\Omega_1, \Omega_2, \Omega_3$	Reduction factors in HYMOSTRUC , pp. 33	[–]
ω	Molar volume , pp. 58	[cm^3/mol]

Superscripts

p	Portland cement, pp. 26
T	Total amount, pp. 69
b	Alkali bound in hydration products, pp. 93
c	Blended cement, pp. 75
clinker	Clinker, pp. 93
cr	Crystalline mineral, pp. 46
r	Alkali released by cement hydration, pp. 93
s	Alkali in pore solution, pp. 93
sl	Slag, pp. 46

sul	Sulfate, pp. 92	
Subscripts		
glass	Glass phase in slag, pp. 151	
gyp	Gypsum, pp. 74	
monoc	Monocarbonate, pp. 74	
T	Network formers, pp. 217	
w	Water, pp. 60	
w0	Initial water, pp. 60	
n_d	Width of distribution , pp. 18	[–]
Other		
$[I]^0$	Number of pixels in the initial microstructure , pp. 42	[–]
$[I]^i_j$	Number of pixels of species j in cycle i , pp. 40	[–]
$[I]_{dis}$	Number of pixels dissolved in one cycle , pp. 136	[–]
$[I]^{max}_{dis}$	Maximum number of pixels dissolved in all executed cycles , pp. 136	[–]
$[I]_{j,max}$	Scale factor for specie j , pp. 40	[–]
$\{i\}$	Activity of an ion , pp. 213	[mol/L]
ℓ	System resolution, pp. 35	
pH	pH value of solution, pp. 148	
R	Gas constant, 8.314×10^{-3} kJ/(mol·K), pp. 148	

Appendix A

Terminology of some minerals

Formula	Name	Formula	Name
A_3S_2	mullite	$KA_3\overline{S}_4H_6$	alunite
AH_3	gibbsite	CMS_2	dioside
C_2AS	gehlenite	$(Ca,Na)_2(Al,Mg,Fe^{2+})$	
C_2MS_2	akermanite	$[(Al,Si)SiO_7]$	melilite
C_2ASH_8	strätlingite	CS	wollastonite
C_2S	belite	C-S-H	calcium silicate hydrate
C_3A	aluminate	$C\overline{S}$	anhydrite
$C_3A(CaCl_2)\cdot 10H_2O$	Friedel's salt	$C\overline{S}H_{0.5}$	hemihydrate
$C_3A(CaCl_2)_{0.5}(CS)_{0.5}\cdot 10H_2O$	Kuzel's salt	$C\overline{S}H_2$	gypsum
C_3AH_6	hydrogarnet	CT	perowskite
C_3MS_2	merwinite	FH_3	iron hydroxide
C_3S	alite	K_2CS_2H	syngenite
C_3S_2	rankinite	$K\overline{S}$	arcanite
$C_3S\overline{S}\overline{C}H_{15}$	thaumasite	$KC_2\overline{S}_3$	Ca-langbeinite
$C_4A\overline{S}H_{12}$	monosulfate	$(K,Na)_3Na(SO_4)_2$	aphthitalite
C_4AF	ferrite	M	periclase
C_4AH_{13}	tetracalcium aluminate hydrate	$M_6A\overline{C}H_{12}$	hydrotalcite
		MA	spinelle
$C_6A\overline{S}_3H_{32}$	ettrintite	M_2S	forsterite
$C_7S_6\overline{C}\cdot 2H_2O$	scawtite	$M\overline{C}$	magnesite
CAS_2	anorthite	MS	enstatite
$C\overline{C}$	calcite	MH	brucite
CH	portlandite	$N_2\overline{S}$	thenardite
$CM\overline{C}_2$	dolomite	S(cr.)	quartz
CMS	monticellite		

Appendix B

Terminology in cement chemistry

Oxide	Symbol	Molar mass (g/mol)
Al_2O_3	A	102
B_2O_3	B	69.6
CaO	C	56.1
CO_2	$\overline{C}$	44
H_2O	H	18
Fe_2O_3	F	159.6
K_2O	K	94.2
MgO	M	40.3
Na_2O	N	62
SiO_2	S	60.1
SO_3	$\overline{S}$	80.1
TiO_2	T	79.9

Appendix C

Classifications of blastfurnace slag

According to ASTM C989-05, GGBFS is classified into three grades based on its performance in the "slag activity test". The three grades are: Grade 80, Grade 100 and Grade 120. Slag activity is determined by the following formula:

$$Slag\ activity\ index, \% = (SP/PP) \times 100 \tag{C.1}$$

in which: *SP* is average compressive strength of slag-reference cement mortar cubes at designated ages (MPa), *PP* is the average compressive strength of reference cement mortar cubes at designated ages (MPa). The requirements of ASTM C989-05 for each grade of GGBFS are listed below.

Table C.1: Slag activity index requirement of ASTM C989-05

Slag activity index	min, %	
	Average of last five consecutive samples	any individual sample
7 day index		
Grade 80		
Grade 100	75	70
Grade 120	95	90
28 day index		
Grade 80	75	70
Grade 100	95	90
Grade 120	115	110

Appendix D

Methods for non-alkali ion concentrations in pore solution of hydrating cement paste[3]

The alkali concentrations in hydrating Portland and slag cement pastes are predicted with the methods presented in Chapter 5. In this appendix, methods for predicting the non-alkali ion concentrations proposed by Van Eijk (2001) are introduced.

Theoretical background, after Butler (1998)

When substances are mixed and undergo a chemical change, a chemical reaction takes place. The chemical reaction can normally be expressed in the form of reaction formula, for example:

$$c\,C + a\,A \rightarrow C_cA_a \tag{D.1}$$

in which C and A are the cation and anion (or anion group) in the reactants and C_cA_c is the reaction product. However, few reactions can occur completely in the form from the left to the right of the reaction formula, i.e. all C and A are consumed and a homogenous product C_cA_a is formed. The reverse reaction may occur at the same time, as:

$$c\,C + a\,A \leftarrow C_cA_a \tag{D.2}$$

Under a certain reaction condition, a balance between the two forms of reaction is obtained, in which the rate of reaction in Eq. (D.1 equals that in Eq. (D.2), a state called "*equilibrium*". Hence, more commonly, the reaction is written as:

$$c\,C + a\,A \rightleftharpoons C_cA_a \tag{D.3}$$

Changes in temperature, or in the concentrations of reactants and products can alter the relative rates of forward or backward reactions, generating another state of equilibrium.

Equilibrium takes place when a sparingly soluble compound is in contact with water for a sufficiently long time. There is still solid compound remaining in the system, and parts of the compounds dissolve into the water, forming ions (forward reaction). Meanwhile, ions in the pore solution react to form the solid compound (reverse reaction).

When 1 mole of a compound C_cA_a dissolves in water, it produces c moles of compound C cations and a moles of A anions. When this compound is in equilibrium with the solution, an equilibrium constant, denoted K is defined by the equation:

$$K_{C_cA_a} = \frac{[C]^c \cdot [A]^a}{[C_cA_a]} \tag{D.4}$$

The concentration of solid compound C_cA_a is always unity. Hence, Eq. (D.4) is rewritten as:

$$K_{C_cA_a} = [C]^c \cdot [A]^a \tag{D.5}$$

For sparingly dissolved compound solution (low ion concentrations, e.g. <0.01 mol/L), the equilibrium constant K^0 has a fixed value, called "concentration product".

[3] Parts of this appendix are after Van Eijk (2001).

If the ion concentrations in the solution are high, the ions interact with each other and the concentration product of a salt is not constant. To account for the interactions among the ions, activity of an ion is used, instead of the concentration. The activity of an ion is defined as the product of its concentration and its activity coefficient:

$$i = [i] \cdot \gamma_{c_i} \tag{D.6}$$

in which i is the activity of ion i, $[i]$ is the concentration of ion i (mol/L), γ_{c_i} is the activity coefficient of ion i.

The equilibrium constant is now called "activity product" and reads:

$$K^0_{C_cA_a} = C^c \cdot A^a = [C]^c \cdot {\gamma_{c_C}}^c \cdot [A]^a \cdot {\gamma_{c_A}}^a \tag{D.7}$$

and thus, the concentration products read:

$$K_{C_cA_a} = \frac{K^0_{C_cA_a}}{{\gamma_{c_C}}^c \cdot {\gamma_{c_A}}^a} \tag{D.8}$$

The activity products K^0 are thermodynamic properties and can be found in many handbooks and literature (Butler, 1998; Lide, 2003; Reardon, 1992). The activity product is a function of temperature only. The activity coefficient can be calculated with the Debye-Hückel equation, the Davies equation or the Pitzer's equation. When the activity coefficient of each ion is known in a specific solution, the concentration product of a solid in this solution can be computed from its activity product according to Eq. (D.8).

In very dilute solutions activity coefficients are approximately unity and activity almost equals concentration. The activity of a solid is defined as unity and the activity of H_2O is proportional to the mole fraction of water in the solution and thus is very close to unity in most cases as well (Chatterji and Jeffery, 1963).

Set of equations

Van Eijk (2001) proposed methods for predicting the non-alkali ion concentrations in the pore solution of hydrating Portland cement paste. During the hydration process of Portland cement, the pore solution is saturated with respect to CH. This saturation state applies for both fresh and mature pastes, due to the presence of CH. Thus, the equilibrium equation for CH with water can always be employed, written as:

$$K_{CH} = [Ca^{2+}] \cdot [OH^-]^2 \tag{D.9}$$

in which K_{CH} is the equilibrium constant of CH; $[Ca^{2+}]$ etc. are the concentrations of the corresponding ions in the pore solution.

Two states are distinguished, depending on the presence of calcium sulfates in the paste or not.

State 1

During the early hydration ages (first few days), gypsum or some other calcium sulfate phases are present, and **State 1** applies. The concentration of sulfate, viz. $[SO_4^{2-}]$, is determined by the equilibrium of calcium sulfates with water. The gypsum equilibrium is used, since it is the most stable calcium sulfate compound and the other forms of calcium sulfate hydrates into gypsum when mixed with water. Taking the activity of pure water as unity, the activity of gypsum can be written as:

$$K_{gyp} = [Ca^{2+}] \cdot [SO_4^{2-}] \tag{D.10}$$

Finally, the charge balance needs to hold. This gives the following equation:

$$2[Ca^{2+}] + [Na^{+}] + [K^{+}] - [OH^{-}] - 2[SO_4^{2-}] = 0 \tag{D.11}$$

There are three equations (Eqs. (D.9)–(D.11)) in the system. Assuming that the total alkali concentration is computed with the methods in Chapter 5 and is thus known, and the numeric values for the concentration products are known from Eq. (D.8), there are also three unknowns: $[OH^{-}]$, $[Ca^{2+}]$ and $[SO_4^{2-}]$. Therefore, this system of equations be solved. In this case, from Eq. (D.9), the following equation is yielded

$$[Ca^{2+}] = \frac{K_{CH}}{[OH^{-}]^2} \tag{D.12}$$

and substituting Eq. (D.12 into (D.10) yields

$$[SO_4^{2-}] = \frac{K_{gyp}}{K_{CH}} \cdot [OH^{-}]^2 \tag{D.13}$$

Substituting Eq. (D.12) and (D.13) into Eq. (D.11) yields an equation which contains $[OH^{-}]$ as the only unknown (concentration of alkalis is known beforehand) as:

$$2K_{CH} \cdot [OH^{-}]^{-2} + [Na^{+}] + [K^{+}] - [OH^{-}] - \frac{2K_{gyp}}{K_{CH}} \cdot [OH^{-}]^2 = 0 \tag{D.14}$$

Then, $[OH^{-}]$ can be solved from Eq. (D.14). With the computed $[OH^{-}]$ and from Eq. (D.12), the $[Ca^{2+}]$ and can readily be solved.

Adding a second sulfate containing solid compound, e.g. an aluminum sulfate such as ettringite, gives one extra equilibrium, but also one extra unknown, namely $[Al(OH)_4^{-}]$, yielding again a solvable system. However, this extension of the system is not expected to have a significant influence on the predicted $[SO_4^{2-}]$, because $[OH^{-}]$ is high from the beginning of hydration and all aluminum sulfates are very slightly soluble. Therefore, these sulfates will not contribute to total concentrations in general and especially not to $[SO_4^{2-}$ because of the more soluble gypsum assumed present. Such additional equations would only be useful when A concentration ($[Al(OH)_4^{-}]$) is of interest. This is the same when accounting for the C-S-H equilibrium, which will only be relevant when computing S concentration ($[H_3SiO_4^{-}]$).

In conclusion, to find $[OH^{-}]$, $[Ca^{2+}]$ and $[SO_4^{2-}]$ and as long as gypsum is still present, the equilibria for CH and $C\overline{S}H_2$ and the charge balance have to be solved simultaneously.

State 2

When gypsum is fully consumed a new status in the pore solution is encountered, viz. **State 2**. Now the gypsum equilibrium (Eq. (D.10)) does not apply anymore, and other sulfate containing solids have to be taken into account, e.g. ettringite and monosulfate. Accounting for these phases is of essential importance with regard to the durability of cement paste. Because these solids form $[Al(OH)_4^{-}]$ ions, their presence implies a new variable in the system of equations: $[Al(OH)_4^{-}]$, now yielding four unknowns: $[OH^{-}]$, $[Ca^{2+}]$, $[SO_4^{2-}]$ and $[Al(OH)_4^{-}]$. This means that four equations are required, from which two are known already: the CH equilibrium (Eq. (D.9)) and the charge balance, including $[Al(OH)_4^{-}]$:

$$2 \cdot [Ca^{2+}] + [Na^{+}] + [K^{+}] - [OH^{-}] - 2 \cdot [SO_4^{2-}] - [Al(OH)_4^{-}] = 0 \tag{D.15}$$

Two additional equilibria are required to obtain a solvable system of equations and have to be selected from ettringite, monosulfate and C_4AH_{13}. Hydrogarnet is not considered here and the formation of the C_4AH_{13} is considered, because the C_4AH_{13} is more likely formed in the cement system (Taylor, 1997) and the formation of the hydrogarnet is less likely. Hydrogarnet is more

often observed in pastes cured at higher temperatures e.g. at 80°C (Jennings and Ghosh, 1983). Because thermodynamically the ettringite is much more stable than the monosulfate (Rothstein et al., 2002), its formation is taken here to account for the anion SO_4^{2-}. With the selected hydration product, to compute the $[OH^-]$, $[Ca^{2+}]$, and after gypsum is consumed, the equilibria for CH, ettringite and C_4AH_{13} and the charge balance have to be solved simultaneously. Again, the equilibrium equation (D.9) holds for the portlandite. The equation for the C_4AH_{13} is

$$K_{C_4AH_{13}} = [Ca^{2+}]^4 \cdot [Al(OH)_4^-]^2 \cdot [OH^-]^6 \tag{D.16}$$

and the equation for the ettringite is

$$K_{C_6A\bar{S}_3H_{32}} = [Ca^{2+}]^6 \cdot [Al(OH)_4^-]^2 [SO_4^{2-}]^3 \cdot [OH^-]^4 \tag{D.17}$$

Similarly from Eq. (D.9) the $[Ca^{2+}]$ can be solved from $[OH^-]$, and will further be substituted into Eq. (D.16) and (D.17), yielding:

$$[Al(OH)_4^-] = \left[\frac{K_{C_4AH_{13}}}{[Ca^{2+}]^4 \cdot [OH^-]^6}\right]^{1/2} = \frac{{K_{C_4AH_{13}}}^{1/2} \cdot [OH^-]}{{K_{CH}}^2} \tag{D.18}$$

and:

$$[SO_4^{2-}] = \left[\frac{K_{C_6A\bar{S}_3H_{32}}}{[Ca^{2+}]^6 \cdot [Al(OH)_4^-]^2 \cdot [OH^-]^4}\right]^{1/3} = \frac{{K_{C_6A\bar{S}_3H_{32}}}^{1/3} \cdot [OH^-]^2}{{K_{CH}}^2/3} \cdot {K_{C_4AH_{13}}}^{1/3} \tag{D.19}$$

in which Eq. (D.9) is already substituted. $[Al(OH)_4^-]$ (from Eq. (D.18) and $[SO_4^{2-}]$ (from Eq. (D.19) are substituted into Eq. (D.11), giving:

$$2K_{CH} \cdot [OH^-]^{-2} - \left(1 + \frac{{K_{C_4AH_{13}}}^{1/2}}{{K_{CH}}^2}\right) \cdot [OH^-] - 2 \cdot \frac{{K_{C_4AH_{13}}}^{1/3}}{{K_{CH}}^{2/3} \cdot {K_{C_4AH_{13}}}^{1/3}} \cdot [OH^-]^2 + [Na^+] + [K^+] = 0 \tag{D.20}$$

In Eq. (D.20), $[OH^-]$ is the only unknown and can thus be solved. With the computed $[OH^-]$, accordingly, the concentrations of other ions concerned can readily be solved from Eqs. (D.9), (D.16) and (D.17).

Table D.1: Dissolution equations for solid compounds

Solid	Reaction
C-S-H	$xCaO \cdot SiO_2 \cdot nH_2O + H_2O \rightarrow xCa^{2+} + H_3SiO_4^- + (2n-1)OH^-$
C_4AH_{13}	$Ca_4Al_2(OH)_{14} \cdot 3H_2O \rightarrow 4Ca^{2+} + 2Al(OH)_4^- + 6OH^- + 3H_2O$
Ettringite	$Ca_6Al_2(SO_4)_3(OH)_{12} \cdot 26H_2O \rightarrow 6Ca^{2+} + 2Al(OH)_4^- + 3SO_4^{2-} + 4OH^- + 26H_2O$
Gypsum	$CaSO_4 \cdot 2H_2O \rightarrow Ca^{2+} + SO_4^{2-} + 2H_2O$
Hydrogarnet	$Ca_3Al_2O_6 \cdot 6H_2O \rightarrow 3Ca^{2+} + 2Al(OH)_4^- + 4OH^-$
Monosulfate	$Ca_4Al_2O_6SO_4 \cdot 12H_2O \rightarrow 4Ca^{2+} + 2Al(OH)_4^- + SO_4^{2-} + 4OH^- + 6H_2O$
Brucite	$Mg(OH)2 \rightarrow Mg^{2+} + 2OH^-$
Portlandite	$Ca(OH)_2 \rightarrow Ca^{2+} + 2OH^-$
Hydrotalcite	$Mg_4Al_2(OH)_{14} \cdot 2H_2O \rightarrow 4Mg^{2+} + 2Al(OH)_4^- + 6OH^- + 3H_2O$
Strätlingite	$Ca_2Al_2SiO_7 \cdot 8H_2O \rightarrow 2Ca^{2+} + 2Al(OH)_4^- + H_3SiO_4^- + OH^- + 2H_2O$

Appendix E

Method for calculating the NBO/T value of glass

The (NBO/T) ratio can be calculated in the following manner (Mills, 1995):

1. Calculating the molar fractions of various constituents in the slag as in Eq. (3.46), e.g. y_S, y_A, y_C.
2. Since some molecules contain two cations e.g. Al_2O_3, P_2O_5, Fe_2O_3, multiply these molar contents by 2, e.g. $2y_A$, $2y_N$. Sum network formers (T) as:

$$y_T = y_S + 2y_A + 2y_F + y_T + 2y_P \tag{E.1}$$

3. Determine the fraction of Fe^{3+} in four co-ordinations (f_e) and that in six co-ordination ($1 - f_e$). In practice, $f_e = 0$ for most iron and steel making slags.
4. Determine the total charge on network-breaking cations e.g. $\sum z_i y_i$ as:

$$y_{NB}^{(1)} = 2(y_C + y_M + y_{FeO} + y_{MnO} + y_N + y_K) + 6(1 - f_e)y_F \tag{E.2}$$

5. Calculate $y_{NB}^{(2)}$ by allowing for the electrical charge balance of AlO_4^{4-}, FeO_4^{4-}:

$$y_{NB}^{(2)} = y_{NB}^{(1)} - 2y_A - 2f_e \cdot y_F \tag{E.3}$$

6.

$$(NBO/T) = y_{NB}^{(2)}/y_T \tag{E.4}$$

Summary

This thesis addresses theories and models for the hydration of slag cement, together with their technical applications. The use of slag cement in construction industry is growing rapidly because the blastfurnace slag is a by-product of the iron production and is normally cheaper than the Portland cement clinker. Furthermore, its use is encouraged due to the environmental benefits, like the use of secondary material and less CO_2 emission. The mechanical strength and durability of concrete made from slag cement normally are also superior to the concrete made from Portland cement.

However, the use of slag cement may be more complicated than that of Portland cement. At least three aspects should be considered concerning the use of slag cement in concrete (*Chapter 1*):

1. The reactivity of slag may vary from one slag to another to a great extent. Not all the slags produced in various blastfurnaces are suitable for use in concrete. The applicability of given slags as construction materials is thus important in an economic respect, mainly depending on the reactivity of the slags. As the reactivity of slag can be adjusted in the iron production process, practical suggestions about the oxide composition and the processing methods are valuable;
2. The long-term behavior of concrete made from slag cement is more complicated and important than that from Portland cement because of the latent hydraulic nature of slag itself. It might take years for slag to achieve hydration degrees comparable to those of the clinker phases from the Portland cement;
3. The microstructure of cement paste—the gluey part in concrete—is altered when slag is used to replace the Portland cement. The result microstructure has different properties, and thus changes the performance of concrete as well.

The first research presented in this thesis concerns an overview about the hydration and microstructure development of slag cement paste, based on the existing knowledge on the hydration of Portland and slag cement (*Chapter 2*).

Next, to reveal the chemistry of slag cement hydration, theories about the reaction of *pure slag* are established (*Chapter 3*). The reaction of pure slag is investigated with observations in experiments presented in the literature about the type of hydration products, their compositions, and properties of the reaction process. A stoichiometric approach is used to develop theoretical models that are able to predict both the compositions and the quantities of the hydration products.

Subsequently, models for the hydration of *slag-blended cement* are developed (*Chapter 4*). Interactions between the reaction of pure slag and those of clinker phases are investigated based on concepts like product equilibrium and CH consumption. Stoichiometric approaches are used for developing theoretical models that account for the degree of CH consumption, and types/ quantities of hydration products (such as C-S-H).

An extensive comparison between the model predictions (*Chapter 3* and *4*) and experimental data confirms the validity of these models.

The reactivity of slag is important in respect to the hydration of slag-blended cement. The reactivity of slag depends on many factors; a few of them could be predicted beforehand, for example, the alkalinity of pore solution. In this thesis, methods for predicting the alkali concentrations in the pore solution of hydrating Portland and slag cement pastes are established based on the measurements in a large series of of experiments presented in literature (*Chapter 5*). The methods are further used to predict the concentrations of other ions in the solution. The alkali concentrations predicted with these methods are used for determining the reactivity of slag in an alkaline environment for computer modeling of slag cement hydration.

Computer modeling of Portland cement hydration has been proven a useful tool in understanding the chemistry of cement hydration and predicting the long-term performance of concrete. At the University of Twente, CEMHYD3D, one of the most advanced 3-D computer models available, is used. It is first developed at NIST in the 1990's. In this thesis, the version developed by Van Eijk (2001) in the Netherlands is taken over. It is extended with the newest developments in cement chemistry and is subsequently modified with considerations to reaction kinetics (*Chapter 6*). The new model with the modifications can successfully eliminate the effects of system resolution on the model predictions, and is robust for a wide range of cements.

With the knowledge established in Chapter 3–5, the model CEMHYD3D for the Portland cement hydration, is further extended for modeling the slag cement hydration. Methods for predicting the reactivity of slag with respect to its oxide composition and the alkalinity of pore solution (predicted with the methods developed in Chapter 5) are proposed. The new computer model is thoroughly validated with experimental results from literature.

The autogenous shrinkage of concrete is important in respect to at least three types of concrete: high strength concrete, self-compacting concrete and massive concrete. Using binders exhibiting expansive volume change is one of the most effective methods for counteracting the autogenous shrinkage. In this thesis, a mineral shrinkage-compensating admixture (MSA) for Portland cement is developed based mainly on the controlled ettringite formation in concrete (*Chapter 8*). It is composed of some industrial by-products including slags, which is expected to keep the cost of this product low. Concrete made with this mineral shrinkage-compensating admixture is more durable compared to that made with some organic admixtures because all the ingredients are inorganic minerals. The computer model is used to design and predict the hydration of various ingredients in the new admixture, and the microstructure development of cement pastes containing this admixture. The properties of the simulated microstructure can be used to investigate the possible mechanism of expansion and to improve the performance of the admixture.

The main conclusions of the research presented in this thesis are summarized as follows (*Chapter 9*):

1. Reliable general stoichiometric models for the hydration of AAS and slag-blended cement are developed (*Chapter 3 and 4*).
2. The methods proposed by Taylor (1987b) and further developed ones by Brouwers and Van Eijk (2003) are very useful for predicting the alkali concentrations in hydrating Portland and slag-blended cement pastes. While for Portland cement the C-S-H is the main alkali adsorbent, for the slag cement, the alkali-binding capacity of hydrotalcite should be considered (*Chapter 5*).
3. It appears that most of the important factors on the cement hydration process are considered appropriately in the newly developed 3-D computer model CEMHYD3D (*Chapter 6*).
4. This new version of CEMHYD3D is extended with the slag cement hydration, accounting for the reactivity of slag in different conditions and using the new theories on slag cement hydration (*Chapter 7*).
5. The mineral shrinkage-compensating admixture (MSA) developed in this thesis can successfully compensate the autogenous shrinkage of concrete. Its industrial applications are feasible (*Chapter 8*).

Finally, together with the conclusions, a few recommendations for the further developments and the use of the models and the MSA are presented (*Chapter 9*).

Samenvatting

Dit proefschrift gaat in op theorieën en modellen voor de hydratie van hoogovencement, samen met hun technische toepassingen. Het gebruik van hoogovencement in de bouwnijverheid groeit snel omdat de hoogovenslakken een restproduct van de ruwijzerproductie zijn, en normaliter goedkoper zijn dan Portlandcementklinker. Voorts wordt het gebruik aangemoedigd wegens de milieuvoordelen, zoals het gebruik van dit secundaire materiaal en de lagere CO_2 emissie. De mechanische sterkte en duurzaamheid van beton met hoogovencement is beter dan van beton die van Portlandcement is gemaakt.

Nochtans, het gebruik van hoogovencement is meer gecompliceerd dan dat van Portlandcement. Minstens drie aspecten dienen wat betreft het gebruik van hoogovencement in beton (*Hoofdstuk 1*) te worden overwogen:

1. De reactiviteit van de diverse slakken kan erg variëren. Niet alle slakken die in hoogovens worden geproduceerd zijn geschikt voor gebruik in beton. De toepasselijkheid van bepaalde slakken als bouwmateriaal is belangrijk in economisch opzicht, en is hoofdzakelijk afhankelijk van de reactiviteit van de slak. Omdat de reactiviteit van slakken bij de ruwijzerproductie kan worden aangepast, zijn praktische suggesties over de oxidesamenstelling en de verwerkingsprocédés erg waardevol;
2. Het gedrag op lange termijn van beton dat van hoogovencement is gemaakt is ingewikkelder en belangrijker dan dat van Portlandcement wegens de latente hydraulische aard van de slakken zelf. Het vergt jaren voor slakken om hydratatiegraden te bereiken vergelijkbaar met die van de klinkerfasen van de Portlandcement;
3. De microstructuur van cement, de lijmcomponent van beton, veranderd wanneer de slakken worden gebruikt om de Portlandcementklinker te vervangen. De resulterende microstructuur heeft andere eigenschappen, en zo worden de prestaties van het beton eveneens veranderd.

Het eerste deel van deze thesis betreft een overzicht van de hydratatie en microstructuurontwikkeling van de cementpasta, gebaseerd op aanwezige kennis op het gebied van cementhydratatie van Portland- en hoogovencement (*Hoofdstuk 2*).

Daarna worden theorieën over de chemische reactie van *zuivere slakken* afgeleid (*Hoofdstuk 3*). De reactie van zuivere slakken wordt gemodelleerd gebruikmakend van observaties in experimenten uit de literatuur over de typen van hydratieproducten, hun samenstellingen, en eigenschappen gedurende het reactieproces. Een stoichiometrische benadering wordt gebruikt om theoretische modellen te ontwikkelen die zowel de samenstellingen als de hoeveelheden hydratieproducten kunnen voorspellen.

Vervolgens worden de modellen voor de hydratie van hoogovencement (slakken gemend met Portlandcementklinker) ontwikkeld (*Hoofdstuk 4*). De interactie tussen de reactie van zuivere slakken en die van klinkerfasen worden onderzocht gebaseerd op concepten zoals productevenwicht en de consumptie van CH. Stoichiometrische benaderingen worden gebruikt voor het ontwikkelen van theoretische modellen die de consumptiegraad van CH en de types/hoeveelheden hydratatieproducten (zoals C-S-H) voorspellen. Een uitgebreide vergelijking tussen de modelvoorspellingen (*Hoofdstuk 3 en 4*) en experimentele gegevens bevestigt de geldigheid van de ontwikkelde modellen.

De reactiviteit van slakken is belangrijk wat betreft de hydratatie van hoogovencement. De reactiviteit van slakken hangt van vele factoren af; enkelen van hen kunnen vooraf worden voorspeld zoals de alkaliniteit van porieoplossing. In deze thesis worden methoden ontwikkeld om de alkaliconcentraties in de porieoplossing van Portland- en hoogovencement te voorspellen, gebaseerd op metingen in een grote serie van experimenten uit literatuur (*Hoofdstuk 5*). Deze

methoden worden verder gebruikt om de concentraties van andere ionen in de oplossing te voorspellen. De alkaliconcentraties die met deze methoden kunnen worden voorspeld worden gebruikt voor het bepalen van de slakreactiviteit in de computer modellering van de hydratatie van hoogovencement.

De computermodellering van Portlandcementhydratatie heeft al bewezen een nuttig hulpmiddel te zijn voor het begrip van de chemie van cementhydratatie en het voorspellen van de prestaties op lange termijn van beton. Aan de Universiteit Twente wordt CEMHYD3D, één van de meest geavanceerde beschikbare 3-D computermodellen, gebruikt. Het is oorspronkelijk ontwikkeld bij NIST (VS) in de jaren '90. In deze thesis is de versie overgenomen die later door Van Eijk (2001) is ontwikkeld in Nederland. Deze is hier verder uitgebreid met de nieuwste inzichten in cementchemie, en op basis van reactiekinetische overwegingen gewijzigd (*Hoofdstuk 6*). Dit nieuwe model elimineert de effecten van de systeemresolutie op de modelvoorspellingen, en is robuust voor een breed scala van cementen.

Met de kennis die in de *Hoofdstukken 3-5* is bepaald, wordt CEMHYD3D, voor Portlandcementhydratatie, verder uitgebreid met de modellering van de hydratatie van hoogovencement. Er worden methoden voorgesteld om de reactiviteit van slakken met betrekking tot hun oxidesamenstelling en de alkaliniteit van de porieoplossing (met gebruik van methoden ontwikkeld in *Hoofdstuk 5*) te voorspellen. Het nieuwe computermodel is grondig gevalideerd met experimentele resultaten uit de literatuur.

De autogene krimp van beton is belangrijk voor minstens drie typen van beton: hoge sterkte beton, zelfverdichtend beton en bulkbeton. Het gebruiken van bindmiddelen die een expansieve volumeverandering bewerkstelligen is één van de meest efficiënte methoden om de autogene krimp tegen te gaan. In deze thesis wordt een mineraal krimpcompenserend additief (MSA) ontwikkeld voor Portlandcement dat is gebaseerd op gecontroleerde ettringietvorming (*Hoofdstuk 8*). Het is samengesteld uit industriële restproducten, waaronder slakken, om de kosten van dit product laag te houden. Alle ingrediënten zijn anorganische mineralen, die een duurzamer beton opleveren in vergelijking met organische additieven. Het computermodel is gebruikt om het MSA te ontwerpen, en om de hydratatie van de diverse ingrediënten in het additief en de microstructuurontwikkeling van de cementpasta te voorspellen. De eigenschappen van de gesimuleerde microstructuur kunnen worden gebruikt om het expansiemechanisme nader te onderzoeken en de prestaties van het additief te verbeteren.

De belangrijkste conclusies van het onderzoek dat in deze thesis wordt gepresenteerd kunnen worden samengevat als volgt (*Hoofdstuk 9*):

1. Betrouwbare en algemeen geldige stoichiometrische modellen voor de hydratiereacties van AAS en slakcement zijn ontwikkeld (*Hoofdstuk 3 en 4*).
2. De methoden die door Taylor (1987) worden voorgesteld, verder ontwikkeld door Brouwers en Van Eijk (2003), zijn zeer bruikbaar om de alkaliconcentraties in hydraterende Portland- en hoogovencementpasta te voorspellen. Terwijl voor Portlandcement C-S-H het de belangrijkste alkaliadsorbens is, voor slakkencement dient ook de alkalibindcapaciteit van hydrotalciet te worden meegenomen (*Hoofdstuk 5*).
3. Het blijkt dat de meeste factoren die van belang zijn voor de cementhydratatie kunnen worden meegenomen in het nieuw ontwikkelde 3-D computermodel CEMHYD3D (*Hoofdstuk 6*).
4. Deze nieuwe versie van CEMHYD3D is uitgebreid met de hydratatie van hoogovencement, en houdt rekening met de reactiviteit van de slakken door gebruik te maken van verschillende nieuwe theorieën op het gebied hoogovencementhydratatie (*Hoofdstuk 7*).
5. Het ontwikkelde minerale krimpcompenserende additief (MSA) is in staat de autogene krimp van beton met succes te compenseren. De industriële toepassing ervan is haalbaar (*Hoofdstuk 8*).

Ten slotte, samen met conclusies, worden een aantal aanbevelingen voor de verdere ontwikkeling en het gebruik van de modellen en het MSA voorgesteld (*Hoofdstuk 9*).

Relevant publications

Publications produced in this PhD project are listed below:

Journals

1. Chen, W. and Brouwers, H. J. H. 2007, The hydration of slag, Part 1: reaction models for alkali-activated slag, Journal of Materials Science, Vol. **42**(2), pp. 428–443.
2. Chen, W. and Brouwers, H. J. H. 2007, The hydration of slag, Part 2: reaction models for blended-cement, Journal of Materials Science, Vol. **42**(2), pp. 444–464.
3. Chen, W. and Brouwers, H. J. H. 2007, Alkali binding in hydrating cement paste, part I: Portland cement, Cement and Concrete Research, (Submitted).
4. Chen, W. and Brouwers, H. J. H. 2007, Alkali binding in hydrating cement paste, part II: slag cement, Cement and Concrete Research, (Submitted).
5. Chen, W. and Brouwers, H. J. H. 2007, Mitigating the effects of system resolution on computer simulation of Portland cement hydration, Cement and Concrete Composite, (Submitted).
6. Chen, W. and Brouwers, H. J. H. 2007, Three-dimensional computer modeling of the hydration and microstructure development of slag cement paste, Journal of Materials Science, (In preparation).
7. Chen, W. and Brouwers, H. J. H. 2007, An ettringite-based mineral shrinkage-compensating admixture for use in concrete, Materials and Structures, (In preparation).

Conferences

1. Chen, W. and Brouwers, H. J. H. 2006, "The reaction of slag in cement: theory and computer modelling", Proceedings of 16^{th} IBAUSIL, Weimar, Sep. 20–23, 2006, Volume 1, pp. 445–454, Bauhaus-University Weimar, Weimar, Germany.
2. Brouwers, H. J. H. and Chen, W. 2004, Reaction models for alkali-activated slags, Proceedings of 8^{th} CANMET/ACI International Conference on Fly Ash, Silica Fume, Slag, and Natural Pozzolans, Las Vegas, May 23–29, 2004, Paper SP-221-17, pp. 303–318, Ed. V.M. Malhotra, American Concrete Institute, Michigan, U.S.
3. Chen, W. and Brouwers, H. J. H. 2004, Hydration models for alkali-activated slag, Proceedings of 5^{th} International PhD Symposium in Civil Engineering, Delft, June 16–19, Vol. 1, pp. 449–458, Ed. J. Walraven, J. Blaauwendraad, T. Scarpas & B. Snider, A.A. Balkema Publishers, London, UK.

Curriculum Vitae

Wei Chen (in Chinese, 陈伟) was born in Wuhan, China on August 3, 1976. He finished his primary school and high school education in Huangpi county, Wuhan. In 1994, he started to study Civil Engineering in the Wuhan University of Technology and received his bachelor degree in 1998. In 1999, he followed a master program at the same university in Structural Engineering with the research subject "Structural damage diagnosis by using dynamic responses and artificial neural network". He received his Master of Science degree in 2002. Afterward, he came to The Netherlands in January 2003 and became a PhD student (in Dutch: *Assistent in Opleiding* or AIO) at the University of Twente under the supervision of dr.ir. H.J.H. Brouwers. His research interests include the chemistry of cement hydration, its computer modeling and applications, which are presented in this thesis.

During his spare time in The Netherlands, he likes playing basketball and card games with friends, disassembling and assembling his computer, and traveling around.

After his PhD study in The Netherlands, he intends to go back to China and pursues an academic career.

ISBN 90-365-2437-7